UNIVERSIDADE DE SÃO PAULO

INSTITUTO DE QUÍMICA

Programa de Pós-Graduação em Química

MUHAMMAD KHALID

Influence of Solvent Viscosity, Polarity and Polarizability on the Chemiluminescence Parameters of Inter and Intramolecular Electron Transfer Initiated Chemiexcitation Systems

Influência da Viscosidade, Polaridade e Polarizabilidade do Solvente sobre os Parâmetros de Quimiluminescência de Sistemas de Quimiexcitação Iniciadas por Transferência de Elétron Inter e Intramoleculares

Versão Corrigida da Tese

São Paulo

Date of submission to SPG:

04/08/2015

Ficha Catalográfica
Elaborada pela Divisão de Biblioteca e
Documentação do Conjunto das Químicas da USP.

Khalid, Muhammad
K45i Influence of solvent viscosity, polarity and polarizability on the chemiluminescence parameters of inter and intramolecular electron transfer initiated chemiexcitation systems / Muhammad Khalid. -- São Paulo, 2015.
189p.

Thesis (doctorate) – Institute of Chemistry of the University of São Paulo. Department of Fundamental Chemistry.
Orientador: Baader, Josef Wilhelm

1. Quimiluminescência : Físico-química : Orgânica 2. Solvente I. T. II. Baader, Josef Wilhelm, orientador.

547.135 CDD

MUHAMMAD KHALID

Influence of Solvent Viscosity, Polarity and Polarizability on the Chemiluminescence Parameters of Inter and Intramolecular Electron Transfer Initiated Chemiexcitation Systems

Influência da Viscosidade, Polaridade e Polarizabilidade do Solvente sobre os Parâmetros de Quimiluminescência de Sistemas de Quimiexcitação Iniciadas por Transferência de Elétron Inter e Intramoleculares

Thesis Submitted to the Instituto de Química, Universidade de São Paulo, for Ph.D. Degree in Chemistry.

Supervisor: Prof. Dr. Josef Wilhelm Baader

São Paulo

2015

“Anyone who has never made a mistake has never tried anything new."
(Albert Einstein)

This research is dedicated to my grandfather Umar Deen as well as my father Muhammad Shafi whose financial and moral support leads me to success.

Acknowledgements

All praises be to Almighty Allah (the most merciful, the most gracious and the most compassionate) who is the entire and only source of every knowledge, who guides me in the obscurity and helps me in difficulties, and his prophet Hazrat Muhammad Mustafa (Salallah-o-Alaihe Wasallim) whose teachings provide the spirit of learning the hidden and unconcealed facts of nature.

It is really difficult to acknowledge all the people who provided their unselfish assistance during any stage of my studies.

First and foremost, I would like to gratefully acknowledge my supervisor **Prof. Dr. Josef Wilhelm Baader** for his guidance, interesting discussions, genius ideas and support during my Ph.D studies. I have learned so much from him and he is an excellent mentor. Truly, I am lucky to have such a nice supervisor and do not have suitable words to thank him.

I would like to express my sincere feelings of gratitude and appreciation to **Prof. Dr. Ataualpa Albert Carmo Braga** who opened the door of computational lab for me in order to do theoretical study during my Ph.D research.

I am extremely grateful to Prof. Dr. Erick Leite Bastos , Prof. Dr. Cassius V. Stevani, Prof. Dr. Luiz Francisco M.L. Ciscatoa, Prof. Dr. Fernando Heering Bartoloni and Prof. Dr. Omar Abou El Seoud who always offered their encouraging attitude in the solution of issues confronted during my research work.

I would pay heartily thanks and appreciations to my friends and colleagues: Panda, Pooria, Sergio, Glalci, Luiz, Biff, Fernanda, Karina, Medi, Sandro and Suzana for their nice cooperation and continuous encouragement during my research career. Special thanks to Panda, Pooria and Sergio for their continuous guideline and valuable suggestions during my research work.

Thanks to all the IQ-USP postgraduate, chemical store staff and central analytical for their continuous favor and kind behavior.

I would also pay thanks and gratefulness to my friends Dr. Ana, Dr Antonio Bruno and Vitor from my computational lab for their nice cooperation and continuous encouragement during my theoretical study.

I am especially indebted to my teachers, Prof. Khalid Mateen, Prof. Muhammad Nawaz Ali, Prof. Amjad Pervez Bhutta, and Prof. Nadeem Raza who always offered their expert aptitudes whenever required.

I would like to extend my gratitude to my friends: Dr. Ajaz Hussain, Dr. Haq Nawaz, Dr. Bakhat Ali, Dr. Muhammad Aslam, Dr. Faiz Ahamed, Dr. Muhammad Imran and Dr. Ishtiaq Ahamed.

I would like to thank to all members of my family, especially my dear mother Jamila Begum who gave me excellent nature and profound prayers, my brothers Liaqat Ali, Muhammad Abid, Sajid, Majid, Tariq and the only sister Abida Perveen for their support and encouragement all the time. I would like to extend my special thanks to my elder brother Liaqat Ali who was strongly motivating for higher education.

Special thanks to all members of my uncle family particularly my uncle Allah Bakhsh and cousins; Hafiz KB, Ramzan Shahid, Saif Ul Rehman, Ubaid Ul Rehman and Asif for their continuous courage and care.

I am highly grateful to my father Muhammad Shafi who was motivating and supporting me all the time. I hope, he is happy now for making one of his dreams true.

I would like to express my special thanks to my eminent cousin Prof. Dr. Muhammad Bashir whose fruitful suggestions and friendly attitude gave me enough encouragement to do this job.

I am also grateful to my wife, Sumaira Khalid, for her selfless love and her support throughout the completion of my Ph.D. Also love for my son, Muhammad Umar Khalid who take birth during my PhD study and make me smile during tense hours of my research when I think about him.

Last but not least; I am most grateful to CAPES for providing the funds for my Ph.D. studies.

Resumo

Muhammad Khalid, S.P. **Influência da Viscosidade, Polaridade e Polarizabilidade do Solvente sobre os Parâmetros de Quimiluminescência de Sistemas de Quimiexcitação Iniciadas por Transferência de Elétron Inter e Intramoleculares**. 2015. 189p. Tese de Doutorado - Programa de Pós-Graduação em Química. Instituto de Química, Universidade de São Paulo, São Paulo.

Os peróxidos cíclicos: peróxido de difenoila (**1**), *spiro*-adamantil-1,2-dioxetanona (**2**) e 4-(3-*terc*-butildimetilsililoxifenil)-4-metoxispiro[1,2-dioxetano-3.2'-adamantano] (**3**) foram sintetizados, purificados e caracterizados e as suas propriedades cinéticas e de quimiluminescência (CL) determinadas. A influência da polaridade do solvente sobre os parâmetros de quimi-excitação da decomposição catalisada de **1** e **2**, e a decomposição induzida de **3** foi examinada em diversas misturas binárias de solventes com parâmetros de polaridade e polarizabilidade diferente, mas viscosidades semelhantes. Para solventes com baixa polaridade, os rendimentos quânticos singlete para a decomposição catalisada intermolecular do peróxido de difenoila (**1**) e 1,2-dioxetanona (**2**) aumentam em função da polaridade do meio, mostrando valores máximos em meios com polaridade intermediária, e diminuim para misturas altamente polares. Para a decomposição induzida de **3**, o rendimento quântico mostrou aumentar com o aumento da polaridade do solvente, inclusive para sistemas com alta polaridade. Nos sistemas binários de solventes estudados, os parâmetros de polarizabilidade mostraram-se contrários aos valores de polaridade, portanto, parece que um aumento da polarizability leva a uma diminuição nos rendimentos quânticos singlete para a decomposição catalisada do peróxido de difenoila (**1**) e a decomposição induzida de **3**, no entanto, um aumento nos rendimentos quânticos singlete para a 1,2-dioxetanona **2**.

Os três sistemas de CL também foram estudados em misturas binárias de solventes com diferentes viscosidades, mas com parâmetros de polaridade e

polarizabilidade semelhantes e os rendimentos quânticos singlete mostraram aumentar com o aumento da viscosidade do meio. Os dados foram analisados usando tanto o modelos colisional quando o modelo de volume livre. Surpreendentemente, o sistema altamente eficiente decomposição induzida intramolecular do 1,2-dioxetano **3** mostrou-se muito mais sensível aos efeitos da viscosidade do que os sistemas intermoleculares ineficientes, o que indica claramente que a decomposição induzida do 1,2-dioxetano deve ocorrer por um processo de retro-transferência de elétron intramolecular.

Além disso, os parâmetros de quimiluminescência destes sistemas foram estudados em vários solventes puros. Os rendimentos quânticos singlete obtidos foram correlacionados com parâmetros de viscosidade, polarizabilidade e polaridade usando análise de regressão linear múltipla.

Palavras-chave: quimiluminescência, parâmetros de solvente, viscosidade, polaridade, polarizabilidade, peróxidos cíclicos, rendimento quântico, modelo collisional, modelo de volume livre.

Abstract

Muhammad Khalid, S.P. **Influence of Solvent Viscosity, Polarity and Polarizability on the Chemiluminescence Parameters of Inter and Intramolecular Electron Transfer Initiated Chemiexcitation Systems**. 2015. 189p. Ph.D. Thesis – Programa de Pós-Graduação em Química. Instituto de Química, Universidade de São Paulo, São Paulo.

The cyclic peroxides: diphenoyl peroxide (**1**), *spiro*-adamantyl-1,2-dioxetanone (**2**) and 4-(3-tert-butyldimethylsilyloxyphenyl)-4-methoxyspiro[1.2-dioxetane-3.2'-adamantane] (**3**) synthesized, purified and characterized, also their kinetic and chemiluminescence (CL) properties were determined. The influence of solvent polarity on the chemiexcitation parameters of the catalyzed decomposition of **1** and **2**, as well as the induced decomposition of **3** were examined in several binary solvent mixtures with different polarity and polarizability parameters, but similar viscosities. For solvents with low polarity, singlet quantum yields for the intermolecular catalyzed decomposition of diphenoyl peroxide (**1**) and 1,2-dioxetanone (**2**) increase in function of medium polarity, showing maximum values in mediums of intermediate polarity, and decreasing in highly polar mixtures. For the induced decomposition of **3**, the quantum yield showed to increase with increasing solvent polarity, including high polar solvent systems. In the binary solvent systems studied, the polarizability parameter showed to be contrary to the polarity values, therefore, it might appear that an increase of polarizability leads to a decrease in the singlet quantum yields for catalyzed decomposition of diphenoyl peroxide (**1**) and the induced decomposition of **3**, however an increase in the singlet quantum yields for 1,2-dioxetanone **2**.

The three CL systems were also studied in binary solvent mixtures with different viscosities but similar polarity and polarizability parameters and singlet quantum yields showed an increase with increasing medium viscosity. Data were analyzed by using the collisional and the free volume models. The highly efficient intramolecular system induced 1,2-dioxetane **3** decomposition

showed to be much more sensible to viscosity effects than the inefficient intermolecular systems. This surprising fact indicates that, even showing a significant solvent-cage effect, the induced 1,2-dioxetane should occur by an intramolecular electron back transfer.

Moreover, chemiluminescence parameters of these systems were studied in several pure solvents. The obtained singlet quantum yields were correlated with viscosity, polarizability and polarity parameters by using multiple linear regression analysis.

Keywords: chemiluminescence, solvent parameters, viscosity, polarity, polarizability, cyclic peroxides, quantum yields, collisional model, free volume model.

Physical Constants and Abbreviations

ACT	Activator
ACN	Acetonitrile
CL	Chemiluminescence
CIEEL	Chemically Initiated Electron Exchange Luminescence
DPA	9,10-Diphenylanthracene
DPP	Diphenyl Peroxide
DPE	Diphenyl ether
DPM	Diphenylmethane
DMF	*N,N*-Dimethylformamide
DMSO	Dimethyl sulfoxide
DBP	Dibutyl phthalate
DMP	Dimethyl phthalate
DFT	Density Functional Theory
EBT	Electron Back Transfer
ET	Electron Transfer
Em	Emission
Ex	Excitation
ECL	Electrochemiluminescence
EA	Energy Acceptor
EDTA	Ethylenediaminetetraacetic Acid
η	Viscosity
f_{lum}	Calibration Factor
Φ_{lum}	Luminol Chemiluminescence Quantum Yield
Φ_{CL}	Chemiluminescence Quantum Yield
Φ_{FL}	Fluorescence Quantum Yield
Φ_S	Singlet Quantum Yield
Φ_S^{CAT}	Catalyzed Singlet Quantum Yield
Φ_S^{∞}	Infinite Singlet Quantum Yield
$\Delta G^{\neq}$	Activation Gibbs free energy
HEI	High Energy Intermediate
$\Delta H^{\neq}$	Activation Enthalpy
IC	Internal Conversion
ISC	Intersystem Crossing
k_D	Unimolecular Decomposition Rate Constant
k_{CAT}	Catalytic Decomposition Rate Constant
LDA	Lithium Diisopropylamide
LL	Lorentz-Lorenz Equation
LM	Lippert-Mataga Equation
PER	Perylene
Q_{lum}	Total Amount of Light Emitted
RUB	Rubrene
ρ	Rho (density)
$\Delta S^{\neq}$	Activation Entropy
THF	Tetrahydrofuran
TBAF	Tertabutylammonium Fluoride
TBDMS	*ter*t-Butyldimethylsilyl

Contents

1. Introduction

Luminescence is a general term indicating light-producing process. It can be differentiated three efficient luminescence processes: fluorescence (FL), bioluminescence (BL), and chemiluminescence (CL). In all cases, light is produced when molecules in an electronically excited state decay to a stable ground state.[1] Bioluminescence (BL), emission of visible light by living organisms, and CL, light emission caused by a chemical reaction is long-known phenomenon and has attracted the interest of researchers in different areas during decades.[2] BL has been described already by Aristoteles (284 – 322 AC).[1] The first clear-cut definition of CL has been given by E. Wiedemann[3] in 1888, "Das bei chemischen Prozessen auftretende Leuchten würde Chemilumineszenz genannt", which means: "The emission observed during chemical processes should be called chemiluminescence". This definition was based on the experimental observation made by B. Radziszewski in 1887 who verified that lophine (2,4,6-triphenylimidazole) does not emit light when heated in the absence of oxygen, however, obtained intense light emission upon its autoxidation.[4] H. O. Albrecht has described the first well-defined chemiluminescent system in 1928 the transition metal catalyzed oxidation of luminol (5-amino-2,3-dihydrophthalazin-1,4-dione) by hydrogen peroxide.[5]

A qualitative advance in mechanistic CL research was achieved in the late sixties and early seventies with the synthesis of the first 1,2-dioxetane[6,7] and 1,2-dioxetanone.[8]

1.2. Photophysical and photochemical processes

The absorption of light is the first step during a photochemical reaction as a result of excited molecule produced, which excited molecules decay to the ground state after the emission of light. The photo-physical processes involve the absorption and emission of light and the non-radiative deactivation. When emission takes place from first singlet excited state (S_1) to ground state (S_0) is called fluorescence and its life time is so short ($1ns$ to $1\mu s$). However, when emission takes place from T_1 to S_0 is known phosphorescence and its lifetime goes from $1ms$ to many seconds or even minutes. If the transition takes place between two electronic states with the same spin multiplicity is known internal conversion (IC), otherwise is known intersystem crossing (ISC). The photo-physical and photo-chemical processes in photochemistry can be explained by using the Jablonski diagram (Figure 1).[9-11]

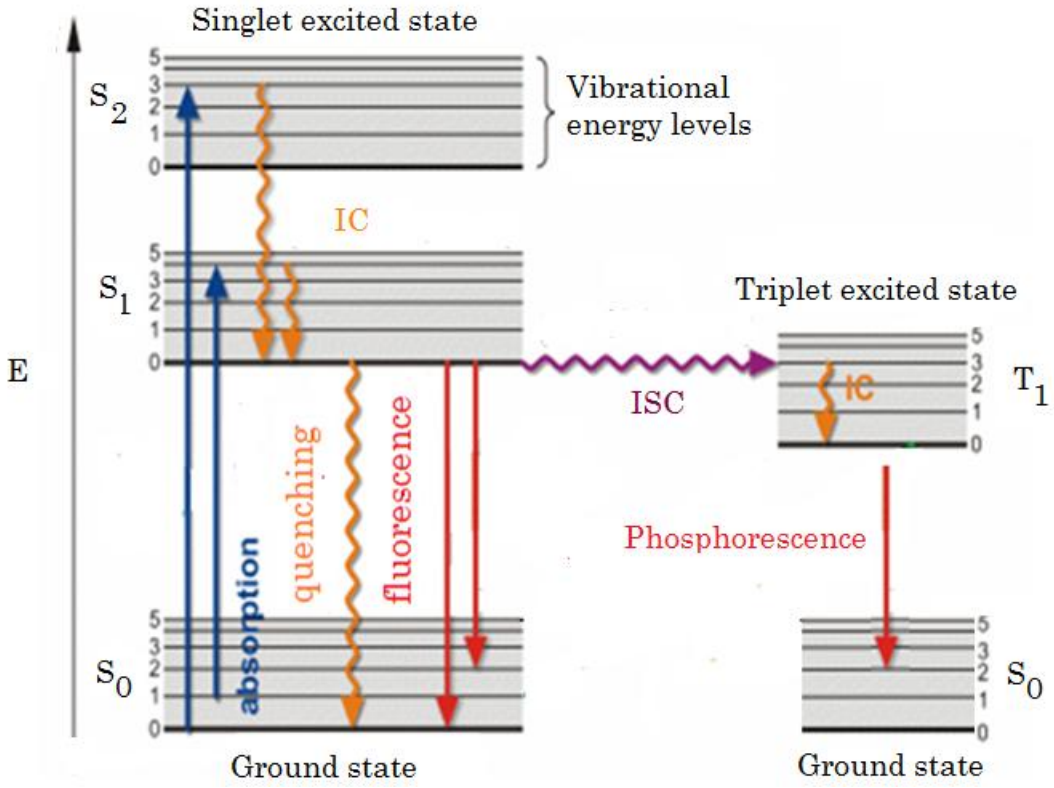

Figure 1: Jablonski diagram for photophysical and photochemical processes.[12-14]

1.3. Principles of chemiluminescence

CL is generally defined as the phenomenon of visible light emission occurring during the progress of a chemical reaction. There are three requirements for CL emission: (i) liberation of sufficient energy to form the product in its electronically excited state; (ii) a reaction pathway capable to transform the chemical energy into electronical excitation energy; and (iii) efficient release of photons by the molecules generated in the electronically excited state.[15-17]

Chemiluminescence and bioluminescence reactions usually involve organic peroxides as energy sources and reactions occur by cleavage of the weak O-O bond. Especially cyclic peroxides are prevalent in light emitting reactions because the relatively weak peroxide bond is easily cleaved and the resulting molecular reorganization liberates a large amount of energy. The chemiluminescent properties of dioxetanes as high energy peroxides are of particular interest for the generation of excited states without light. The formation of electronically excited products can be induced either thermally or by an electron-transfer mechanism originally discovered by Schuster for the diphenoyl peroxide[1819] and in the meantime abundantly documented for the α-peroxylactones [20] and appropriate dioxetanes. [21] This phenomenon of light emission derived from electron transfer chemistry is known as chemically initiated electron exchange luminescence (CIEEL).[2] However, the unimolecular decomposition of these cyclic peroxides leads to the formation of triplet electronic excited states, which are largely non-emissive species, making it a poor model for efficient CL and BL transformations.[22,23]

The successful chemiluminescence reaction follow some significant requirements:

A highly exothermic reaction to generate sufficient energy to form one of the products in its electronically excited state. Gibbs free energy (ΔG) can be used in order to know whether chemiluminescence reaction will take place or not:

$$\Delta G = \Delta H - T\Delta S \qquad \text{Equation 1}$$

Where: T, ΔH, ΔS, stand for temperature, enthalpy and entropy respectively.

The formation of electronically excited state can be taken place in the result of specific energy which denoted enthalpy. The activation energy can be needed to take place for any chemical reaction. The energy which is available in order to form the excited state must be the difference between activation energy and reaction energy. If the change in energy is similar or higher in comparision to the energy which is required for the formation of the excited state, the chemiluminescence reaction will be occured. It can be displayed by using following relationship.[24]

$$\text{Energy available} = \Delta H_A - \Delta H_E \geq \Delta E_{EX} \qquad \text{Equation 2}$$

Where: ΔH_A stands for activation energy, ΔH_E stands for reaction enthalphy, ΔE_{EX} stands for energy of excited state.[24]

Usually, the change in entropy is small in the case of unimolecular 1,2-dioxetane decomposition, therefore enthalpy and free energy are very similar in terms of magnitude. The energetic requirements can be considered in form of (kcal.mol^{-1}). The chemiluminescence reaction would proceed just in that case, when the reaction must be sufficiently exothermic (Equation 3).

$$\Delta G \geq \frac{hc}{\lambda_{ex}} = \frac{2.86 \times 10^4}{\lambda_{ex}} \qquad \text{Equation 3}$$

Where: λ_{ex} stands for the long wavelength limit for excitation of the luminescent molecules.

In all the luminescent reactions, the emission intensity depends on the efficiency of generating molecules in the excited state, which is known as a quantum yield (quantum efficiency) and the rate of the reaction.[25] For

chemiluminescence reactions, the intensity can be explained using the following equation.

$$I_{CL} = \Phi_{CL}\left(-\frac{dA}{dt}\right) \qquad \text{Equation 4}$$

Where: I_{CL} stands for CL emission intensity (photons/second), Φ_{CL} stands for chemiluminescence quantum yield and $(-\mathrm{d}A/\mathrm{d}t)$ stands for rate at which the CL precursor A is consumed.

The energetic parameters of chemiluminescence reactions can be explained by using potential energy diagrams. In a generic way, the chemiluminescent transformation includes the formation of excited state products from an exothermic reaction in one or more reaction steps. But it does not mean that every exothermic reaction leads to formation of excited state products. Just those reactions might be chemiluminescent in which the transition state has enough energy to make one of the products in its electronically excited state (Figure 2).

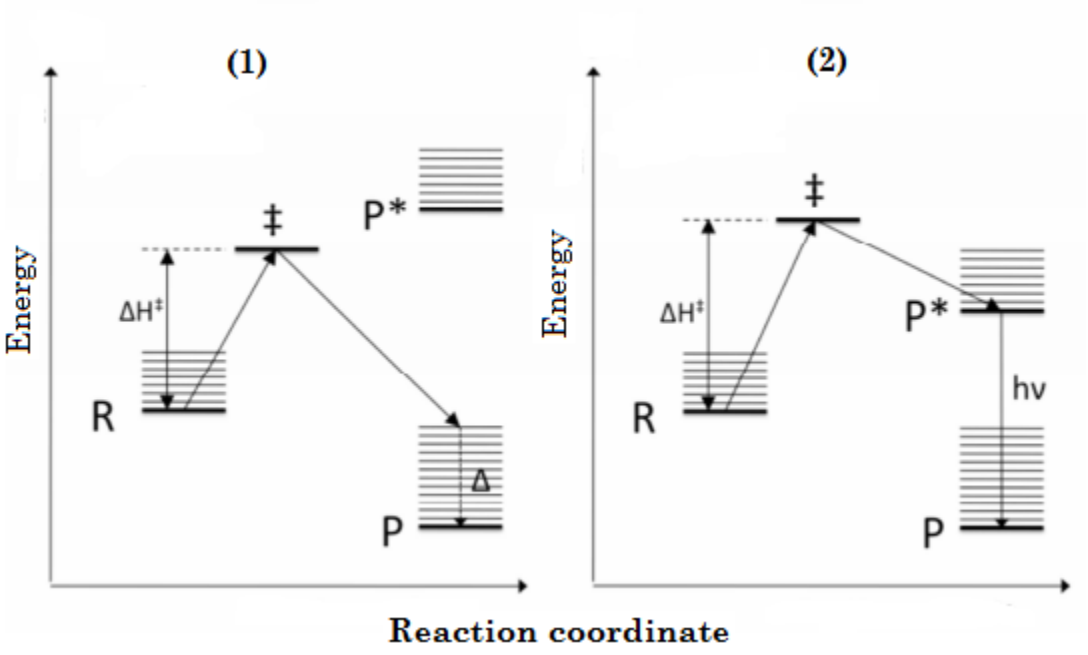

Figure 2: Potential energy diagrams for a non chemiluminescence reaction (1) and a chemiluminescence reaction (2).[26]

The energy requirement is one of the most significant factor for efficient chemiexcitation which means that the chemical reaction must be able to release enough energy for the excited state production. The reaction exothermicity has to be from 50 to 100 kcal mol^{-1} which is the excitation energy of most organic chromophores. Moreover, this energy must be liberated in a single step and electronic excitation-step must be instantaneous. Even though, the energy necessity is certainly important for the CL reaction to take place but it is not satisfactory parameter and the other parameters are known as geometric factors that conclude whether CL can take place in a given chemical reaction or not. These factors can generally be related to the Franck–Condon Principle (Figure 4) that will be discussed here; the absorption of light by a molecule takes place very fast (10^{-15} sec). It is too quick to allow any motions of atoms in the molecule itself or in the solvent molecules surrounding it. It is called as the Franck-Condon principle, and the molecule goes to the excited state after getting photon that is known Franck-Condon excited state and the energy level of the Franck-Condon excited state is higher as compared to equilibrium excited state. There are two reasons behind this statement; (i) the molecule may stay in a vibrational substate other than the lowest-energy vibrational level in the Franck-Condon excited. Some fraction of molecules comes to the vibrational level of the excited state which consists of lowest-energy as a result of one part of 'relaxation' of the Franck-Condon excited state, (ii) the properties of a molecule for excited state are different as compared to ground state. As a result, immediately after absorption of a photon, the excited-state molecule will not show an optimal interaction with the solvent molecules around it. The another attitude of 'relaxation' of the Franck-Condon excited state is, thus, that an excited-state molecule and the solvent molecules around it will accommodate their locations and directions in order to obtain a new alignment of solvent molecules, that is optimally accommodated to the properties of the excited-state molecule. This is

sometimes unlikely, and lower-energy, alignment of solute and solvent molecules than the one that characterized the Franck-Condon excited state. Because of these two reasons the equilibrium excited state attained after relaxation of excited state (Figure 4).

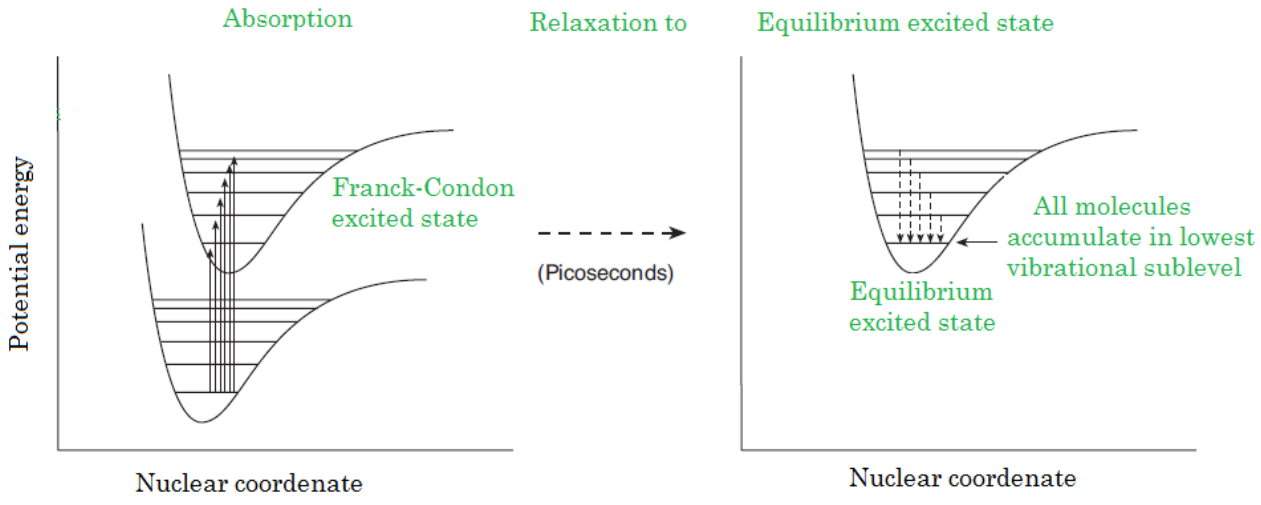

Figure 3: Relaxation of the Franck-Condon excited state to equilibrium excited state.[27,14]

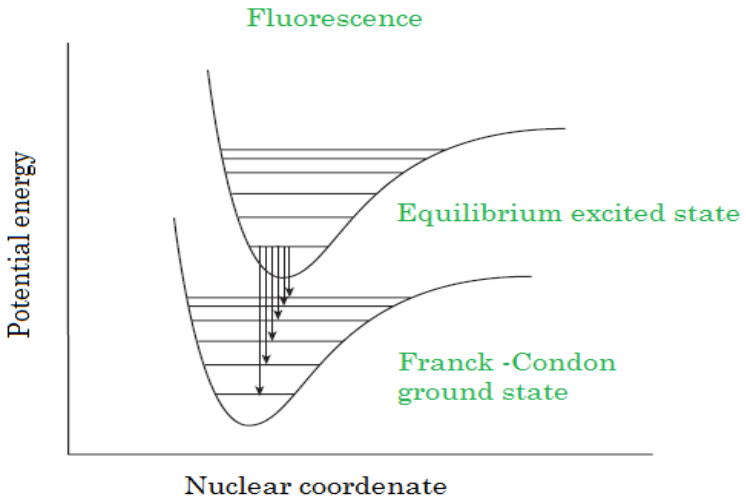

Figure 4: Potential energy diagram for the fluorescence according to the Franck-Condon principle.[14,28,29]

Generally, after absorption of a photon, a molecule will have time to reach the equilibrium excited state before emission of photon. However, the time scale of nuclear movements (10^{-13} to 10^{-12} s) is larger than the time scale of electronic transitions (10^{-16} to 10^{-14} s), so electronic transitions occur much faster than the rearrangement of atoms in the molecular structure[30] or in the surrounding solvent molecules. We can say that the newly 'deexcited' molecule comes back initially to a Franck-Condon ground state. A chemical reaction, in which the structure of the transition state or reactant is similar to the structure of the product's excited state, and dissimilar to the structure of the product's ground state, has a greater probability of forming excited states.[31]

Marcus Theory

The excited state formation process might be better rationalized using the Marcus Theory to electron-transfer (ET) reactions, where the geometric and energetic necessities can be calculated with the help of potential energy reaction coordinate diagrams. [32] In non-chemiluminescent exothermic reactions, the energy barrier for the production of the product P in the electronic ground state ($\Delta H^{\neq}$) is lower than the activation energy ($\Delta H^{\neq *}$) for the formation of the product in its electronically excited state (P*), thus the formation of P in its ground state is kinetically favorable. It is particularly valid if the structure of the ground state products is similar to the structure of the reactants [Figure 5(1)]. However, if the structure of the excited state products is similar to the structure of the reactants, a chemiluminescence reaction can take place, where $\Delta H^{\neq *}$ smaller than $\Delta H^{\neq}$ producing the excited state of the product more kinetically favorable, therefore, effective production of electronically excited states may be observed [Figure 5(2)].

In these cases, a highly exothermic reaction, leading to the formation of products in the ground state, can be kinetically less favorable than the cases reaction leading to production of electronically excited states, due to the fact that the structure of the transition state is more similar to the structure of excited state products than of the ground state products [Figure 5(2)].[26]

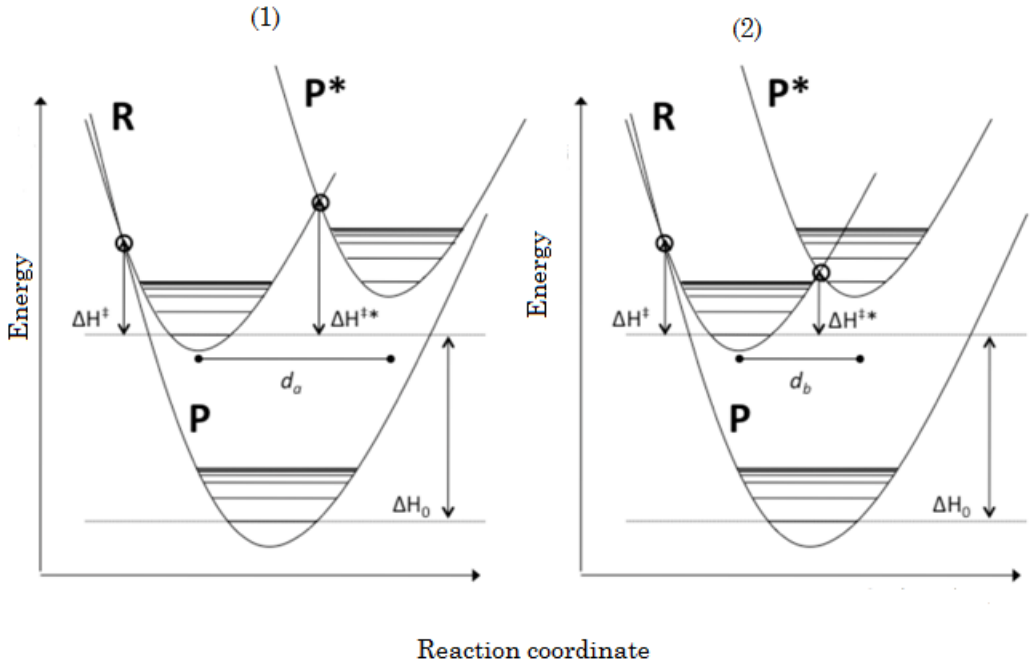

Figure 5: Diagram of reaction coordinates for a non-chemiluminescent exothermic reaction (1) and a chemiluminescent exothermic reaction (2), according to the Marcus Theory.[26]

1.4. The nature of the chemiluminescence reactions

The light emits by chemiluminescence reactions exactly the same way as does during the photoluminescent reactions except for the excitation phenomenon. During the photoluminescent reaction, the excited state is formed after absorption of light from external source. On the other hand, during the chemiluminescence reaction the energy can be produced within the system as the result of chemical reaction which is enough to make one of the products in

its electronically excited state, subsequently, the electronically excited state discharges light and comes back to the ground state product is called CL.[33]

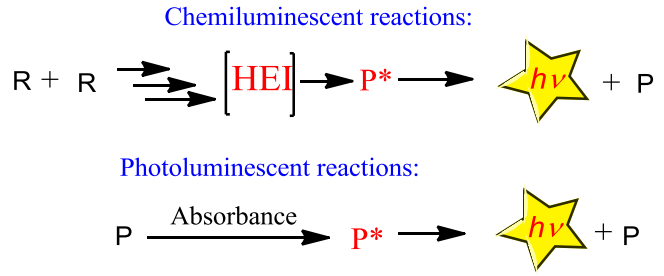

Scheme 1: General path ways for chemiluminescent and photoluminescent reactions.

1.5. General mechanisms for chemiluminescence

Generally, chemiluminescence reactions can be divided into three major steps; (i) production of a high-energy intermediate (HEI), in one or more chemical transformations of ground state reagents, (ii) unimolecular decomposition of the HEI or its interaction with other molecules, in a single elementary step which leads to formation of electronically excited state and (iii) the excited product emits light and directly goes to the ground-state product (P) or this excited product transfer energy to an energy acceptor (EA) after while, this EA is formed in its electronically excited state which will be responsible for the CL emission.

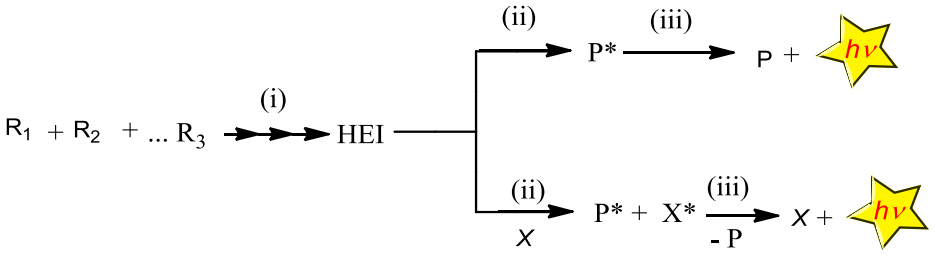

Scheme 2: General mechanism for generation of electronically excited states by chemical transformations.[2]

1.6. Classification of chemiluminescence reactions

There are two classes of chemiluminescence reactions; (i) direct chemiluminescence reactions and (ii) indirect chemiluminescence reactions.

1.6.1. Direct chemiluminescence reactions

The reaction where the oxidant and reactant interact each other, as a result, formation of electronically excited state, takes place and this excited product emits light and directly goes to the ground-state product (P) with the first order or pseudo first order rate constant as is called direct chemiluminescence reactions.

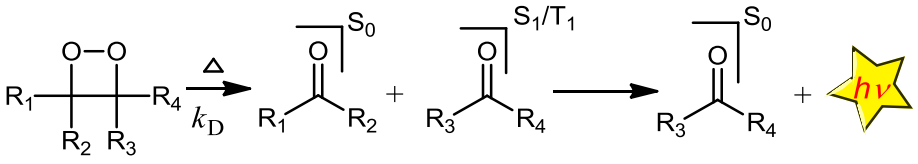

Scheme 3: General pathway for the direct chemiluminescence reactions.[2]

1.6.2. Indirect chemiluminescence reactions

The reaction where the oxidant and reactant interact each other as a result, formation of electronically excited state, takes place and subsequently, the formation of secondary electronically excited state takes place either by the result of energy transfer or electron transfer, consequently, this secondary electronically excited state emits light and goes to the ground-state product (P) is denoted indirect chemiluminescence reactions. This type of reactions is also called as sensitized or complex chemiluminescence reactions.

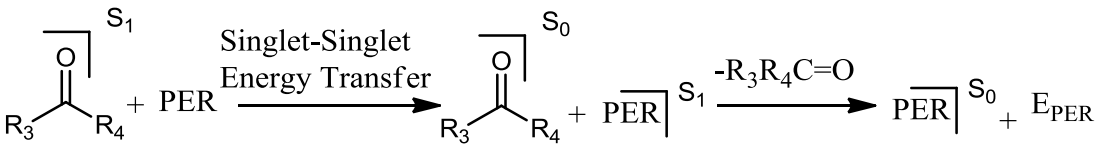

Scheme 4: General pathway for the indirect chemiluminescence reactions.[2]

1.7. General mechanism

In general, three mechanisms are proposed for the unimolecular 1,2-dioxetane decomposition: (1) the concerted mechanism by simultaneously way, (2) biradical mechanism and (3) an intermediate mechanism. However, two mechanisms are proposed out of three at extreme level for the unimolecular 1,2-dioxetane decomposition: the concerted mechanism [34, 35] in which the cleavages of the O-O and C-C bonds take place by simultaneously way and the biradical mechanism[36,37] in which, the peroxide bond is firstly ruptured and a 1,4-dioxy biradical is produced, leading to the production of a carbonyl compound in the singlet excited or the ground state. Moreover, an intersystem crossing (ISC) may happen and a 1,4-dioxy biradical may be produced in its triplet excited state.[38,39] As a result, a triplet excited carbonyl compound may be formed after breaking of the C-C bond (Scheme 1). Both mechanisms include changes in spin multiplicity, but ISC in the biradical mechanism is considered to be reversible while it appears to be irreversible in the concerted mechanism.[40] The biradical mechanism is adequate to describe the activation parameters of 1,2-dioxetane decomposition.[41] However, it has no ability to rationalize the singlet and triplet quantum yields. As a result, an intermediate mechanism is proposed, in which the cleavage of the O-O and C-C bond is concerted, but they do not behave in a simultaneous way.[42] This merged mechanism upholds the kinetic attitude of the biradical mechanism and has ability to describe the production of the electronically excited product in detail on the same basis of the concerted mechanism, So this intermediate mechanism is known as best mechanism to rationalize the activation parameters and excitation quantum yields of different 1,2-dioxetane derivatives.[43]

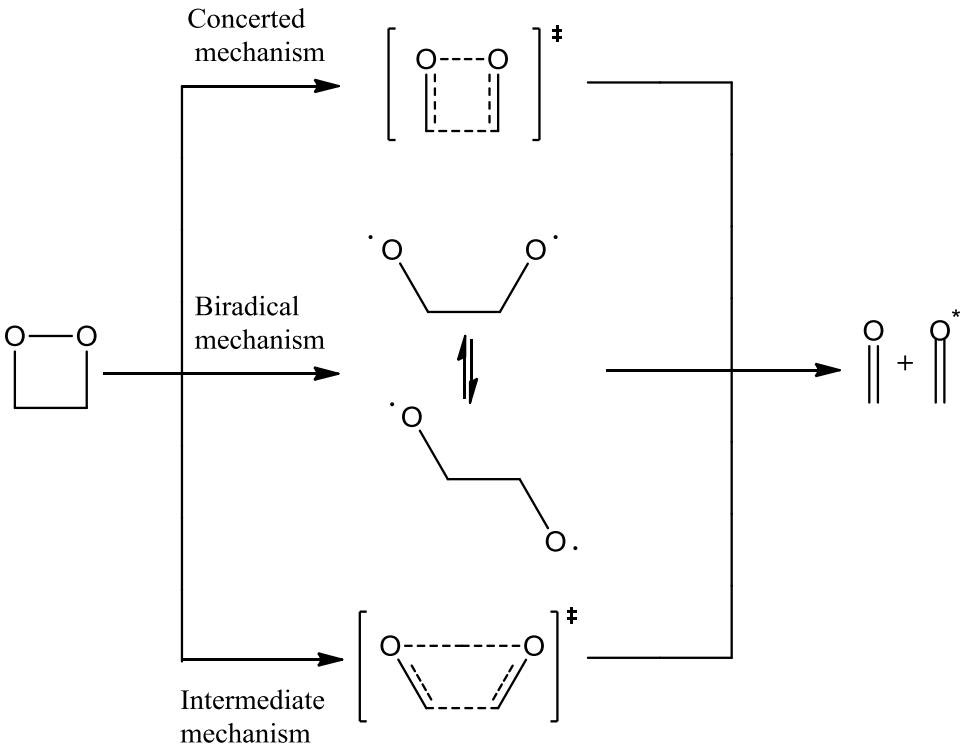

Scheme 5: Proposed mechanisms for unimolecular decomposition of 1,2-dioxetanes: concerted simultaneous, concerted biradical like and biradical.

1.8. Electrochemiluminescence

A method where a second entity has been oxidized or reduced subsequently, intermediates are generated that react with the suitable species which generate excited state and resulting emission of light is extensively utilized as an analytical tool.[44] The ion annihilation electrochemiluminescence (ECL) (Scheme 6) can be considered as the basis for the chemically initiated electron exchange luminescence (CIEEL) mechanism, understood to happen in the catalyzed decomposition of organic peroxides.[45] A radical cation and a radical anion are produced at the anode and cathode respectively by the ECL method. These radical ions can be diffused in solution and the initially involved species A and B are produced by annihilation (Scheme 6).[46] However, electronically excited states can also be produced by this ET process, during this annihilation process, enough energy can be released for chemiexcitation. When the electron

is moved from the former lowest unoccupied molecular orbital (LUMO) of the radical anion species A to the LUMO of the radical cation species B, this radical cation species B is produced in its excited state (Scheme 6). However, when the electron is moved from the former highest occupied molecular orbital (HOMO) of the radical anion species A to the HOMO of the radical cation species B the radical anion species A is produced in its excited state (Scheme 6).[46]

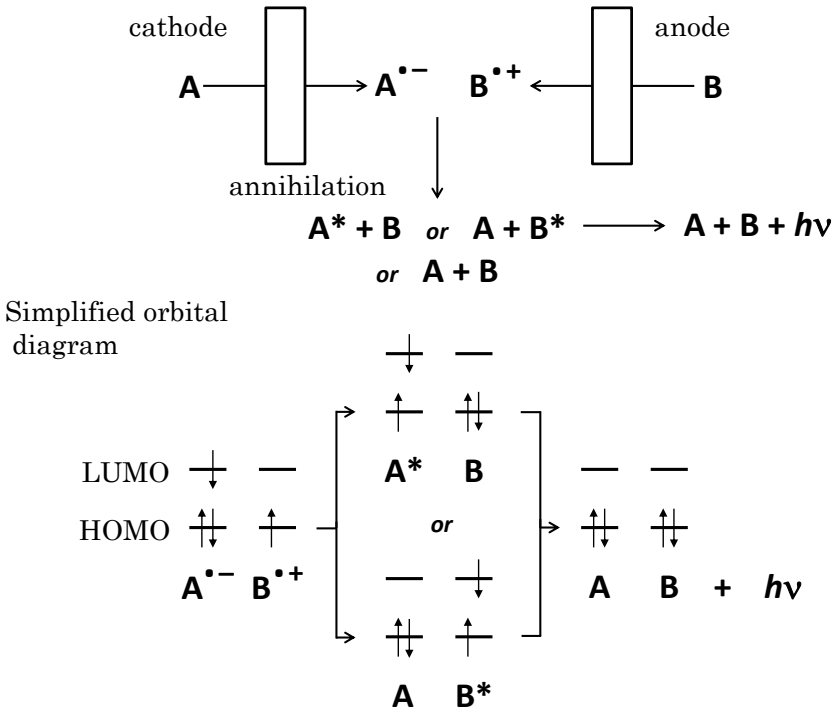

Scheme 6: General mechanism for excited state generation by ion annihilation ECL, where A and B can be the same or different species.

1.9. Catalyzed peroxide decomposition

1.9.1. Intermolecular electron transfer initiated peroxide decomposition

The mechanistic studies on CL peroxide provide the observation about the decomposition of certain peroxides catalyzed by polycondensed aromatic hydrocarbons[47,48] which lead to formation of the CIEEL mechanism. First time Schuster proposed this mechanism[49] which based on the study of cyclic and linear peroxides. Decay of light emission could help in the monitoring of decomposition rate of these peroxides and its decomposition rate increased in presence of polycondensed aromatic hydrocarbons of low oxidation potential and high fluorescence quantum yield (Φ_{FL}), these called activators (ACT) and emission intensities were enhanced. Rate constant and emission intensities were depended on the oxidation potential of the activator utilized, showing the ET in the rate limiting step.

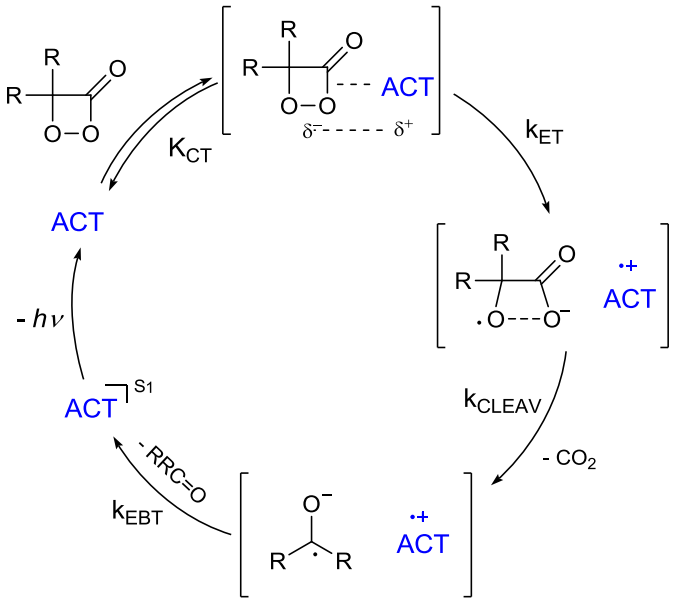

Scheme 7: Mechanism of the intermolecular electron transfer initiated peroxide decomposition.[43]

The CIEEL sequence is initiated by charge transfer complex formation between the peroxide and the activator, followed by electron transfer from the

activator to the peroxide, probably simultaneously with O-O bond cleavage.[50] Cleavage of the C-C bond and the formation of acetone leave a pair of radical ions, still in contact within the solvent cage (radical cation of the ACT and radical anion of CO_2). The electron back transfer between these two radical ions can release enough energy to form the ACT in its first singlet excited state (Scheme 7).

1.9.2. Intramolecular electron transfer initiated peroxide Decomposition

In 1982, it was demonstrated that CL from a 1,2-dioxetane bearing a phenolic substituent could be triggered in organic solvents by the addition of base. Deprotonation of a thermally stable 1,2-dioxetane carrying a phenolic substituent with a base can generate an unstable phenoxide-substituted 1,2-dioxetane[51] which decomposes rapidly to emit light by intramolecular CIEEL mechanism.[52] A 1,2-dioxetane bearing a protected phenolic group such as siloxyphenyl can also give a CIEEL-active phenoxide by deprotection (Scheme 8).[53,54] For the intramolecular CIEEL, an electron transfer from the phenoxide as a donor to the peroxidic bond induces decomposition of the 1,2-dioxetane ring so that the rate of decomposition of the intermediary dioxetane, which is observed as the rate of emission or its half-life time, depends directly on the ease of the electron transfer.[55] The half-life time of emission has been known to be varied by changing the phenolic substituent as an electron donor; a dioxetane bearing a *p*-phenoxy group emits light with far shorter half-life than the m-phenoxy analogue, though the chemiluminescent efficiency is extremely poor.[56,57] Moreover, in this case two pathways are possible. The high quantum yields obtained from efficient singlet excited states and this reaction was considered as an evidence for a fully intramolecular CIEEL mechanism (Route A, Scheme 8), in which the electron transfer (ET) and retro-transfer (RTE) of electrons occurred by intramolecular fashion. In route B, the separation of the radical-ion can not occur by diffusion, as if it occurred, would lead to decreased

formation of excited states, which explains the large difference in quantum yields obtained in CIEEL systems with intermolecular ET ($\Phi_S \approx 10^{-4}$ E mol^{-1})[51] or intramolecular ($\Phi_S \approx 1$ E mol^{-1})[58,59]. However, from studies about the influence of viscosity on the obtained quantum yields, Adam and colleagues postulated the occurrence of a retro-transfer of electron (RTE_{inter}) by intermolecular (Route B, Scheme 8). This conclusion was reached in terms of the yield of formation of excited states increases with increasing viscosity of the medium, since the ion-radical pair remains within the solvent cavity.[60]

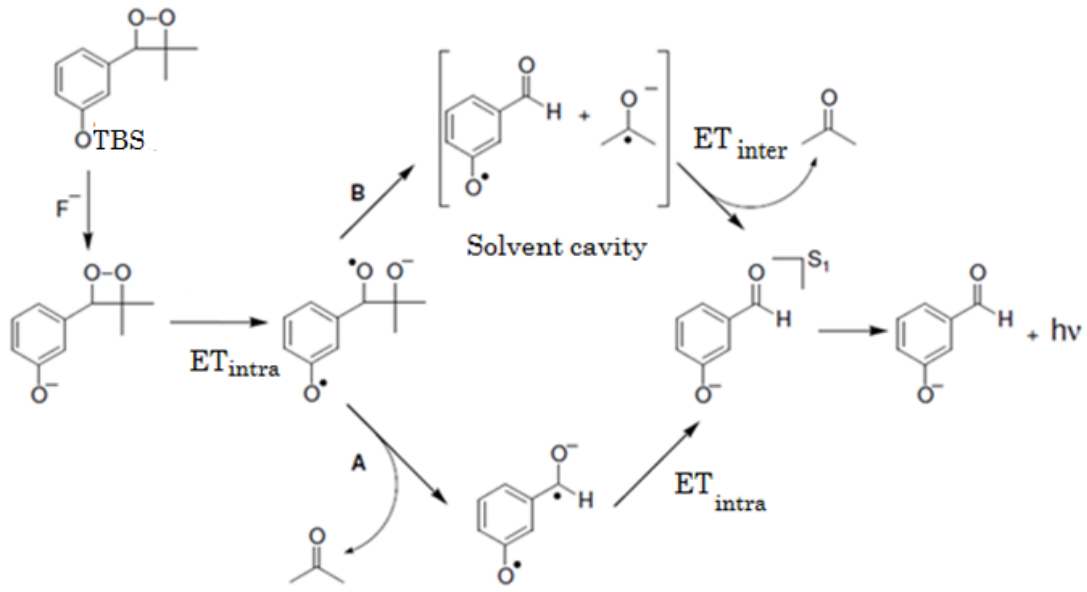

Scheme 8: Mechanism of the induced decomposition of the 1,2-dioxetane according to intramolecular CIEEL, indicating the possible occurrence of an intramolecular (A) and an intermolecular (B) electron back transfer.

2. Objectives of study

The aim of the present study is to clarify the mechanisms involved in the generation of electronically excited states during electron transfer initiated peroxide decomposition, leading to high singlet excitation quantum yields.

In order to achieve this objective, the influence of solvent polarity and polarizability on the kinetic data and quantum yields for the intermolecular catalyzed decomposition of cyclic peroxides as well as the intramolecular induced 1,2-dioxetane decomposition are verified using different pure aprotic solvents and binary solvent mixtures.

Furthermore, the influence of the medium viscosity on the chemiexcitation quantum yields of intermolecular as well as intramolecular CL system is investigated using solvents which possess similar polarity parameters but different viscosity. Data analysis is performed applying the known physico-chemical approaches: collisional model and free-volume model.

The obtained result should allow to identify conditions which lead to efficient chemiexcitation and to compare the efficiency of inter and intramolecular CL systems. Finally, a general model for efficient chemiexcitation might be outlined.

3. Experimental part

3.1. Reagents and solvents

Potassium iodide (KI, Synth) is used to prepare the potassium iodide solution for the ozone test. Aluminium oxide (Al_2O_3) was activated at 100 °C at 1 mmHg for 10 h in a vacuum oven and used for treatment of dibutyl phthalate ester solvent. Molecular sieves 4Å (Sigma-Aldrich) were activated in a vacuum oven at 1 mmHg and 90 °C for 12 h and used to dry solvents and for maintenance of anhydrous solvents. Sodium hydroxide (NaOH, Synth), potassium hydroxide (KOH, synth), phosphorus pentoxide (P_2O_5, Synth) and ethylenediaminetetraacetic acid (EDTA, Synth) were used for treatment of solvents. Magnesium sulfate ($MgSO_4$) was activated at 180 °C for 24 h in a vacuum oven at 1 mmHg and used as a drying reagent. A solution of hydrogen peroxide (H_2O_2, 60% w/w) in water, from Solvay Peroxidos do Brasil, was used for preparing stock solutions of H_2O_2.

Reichardt's Dye, perylene, rubrene and 9, l0-diphenylanthracene (DPA) were obtained from Aldrich and used without further purification. **Trimethyl phosphite** was refluxed in the presence of sodium metal for 4 h, after that, it was distilled under argon gas. **Dichloromethane** was stirred with EDTA for over night, refluxed for 2 h and it was distilled, after while, phosphoras penta oxide was added in dichloromethane, filtered and was redistilled. **Methanol** (Synth) (100 mL) was refluxed with magnesium (5 g) and iodine (0.5 g), until the color has disappeared; the volume was completed to 1 L with methanol, refluxed again for 4 h and distilled. **Toluene** (Synth) was stirred in the presence of EDTA for over night, distilled after filtration, refluxed in the presence of sodium metal for 2 h, redistilled and stored at 4 Å molecular sieve. **Ethyl acetate** (EtOAc, Sigma-Aldrich) was dried over $CaCl_2$ for one day, filtered, stirred for 40 min over NaOH (pellets; 40 gL^{-1}) at 0 °C, distilled (bp = 77 °C) after refiltration, placed for one day over 4 Å molecular sieves and again distilled over a Vigreux column (length of about 1.5 m) under a nitrogen

atmosphere. The distilled solvent was stored over molecular sieves 4 Å. **Butyl acetate** (Synth) was treated for one day over $CaCl_2$, stirred for 40 min in the presence of NaOH (pellets; 40 gdm^{-3}) at 0 °C, distilled after filtration, kept for one day over 4 Å molecular sieves and distilled over a Vigreux column (length of about 1.5 m) under a nitrogen atmosphere. The distilled solvent was stored over molecular sieves 4 Å. **Acetonitrile** (Synth) was stirred with EDTA for overnight, after filteration it was dried for 1 h over CaH_2. It was filtered again, distilled and stored over 3 Å molecular sieves . **1-methyl-2-Pyrrolidinone** (Synth) was stirred in the presence of P_2O_5 for 6 h by mechanically, after filtration it was distilled under reduced pressure and stored over 4 Å molecular sieves. ***N,N*-Dimethyl formamide** (Synth) was stirred in the presence of EDTA and $MgSO_4$ (1:1) for overnight, distilled under reduced pressure after filtration, first 5-10% of *N,N*-dimethyl formamide was discarded and stored over 4 Å molecular sieves. **Acetone** (Synth) was stirred in the presence of $CaSO_4$ just for 2 h and distilled after filtration and also stored at 3 Å molecular sieve. **Dimethyl sulfoxide** (Synth) was stirred in the presence of EDTA and $MgSO_4$ (1:1) for overnight, distilled under reduced pressure after filtration, first 5-10% of dimethyl sulfoxide was discarded, the distillate was stored over 4 Å molecular sieves. **Tetrahydrofuran** (THF, Synth) was refluxed and distilled two times in the presence of sodium metal wire, after while, benzophenone was added , refluxed until the strong blue color has been appeared and all the time before using, solvent was distilled from the blue mixture (indicating the presence of benzophenone radical anion and subsequent absence of water) and stored under nitrogen atmosphere and molecular sieve 4 Å. **Dibutyl phthalate** (Sigma-Aldrich) was stirred in the presence of EDTA as well as $MgSO_4$ for overnight and after filtration it was passed by activated neutral aluminium oxide (Al_2O_3). The filtered solvent was stored over molecular sieves 4 Å. Its distillation was not possible due to the high boiling point having at atmospheric pressure (284 °C), even it was impossible to distill at reduced pressure distillation aparatus. **Dimethyl**

phthalate (Sigma-Aldrich) was treated in the same way as dibutyl phthalate. **Ethyl ether (Synth) and di-n-butyl ether** (Synth) were refluxed with 40 ml of H_2SO_4 (98%), 1 L of each solvent and then distilled, After that, the distilled ether stirred in the presence of $MgSO_4$ for overnight, refluxed in the presence of sodium wires after filtration for 4 h, again distilled and stored over 4 Å molecular sieves. **n-Pentane** was stirred with EDTA and distilled after filtration. It was refluxed in the presence of sodium wires for 4 h and again distilled. **n-Hexane** was stirred with EDTA and distilled after filtration. It was refluxed in the presence of sodium metal and again distilled. **Diisopropylamine** was refluxed in the presence of CaH_2 then distilled under an inert atmosphere and stored over molecular sieve 4 Å. ***t*-Butyl alcohol** refluxed in the presence of CaH_2 then distilled and stored over 4 Å molecular sieve. **Diphenylmethane** was refluxed in the presence of metallic sodium, and then distilled under reduced pressure (140 °C, 35 mm Hg) and stored over molecular sieve 4 Å. The pure liquid should be colorless, specifically the absence of acidic impurities was verified with solvatochrom probe E_T (30).[87] Short test: If this solvent is pure then color will be blue after desollving Reichardt's Dye otherwise yellow because of acidic impurities. **Tetrabutylammonium fluoride** (TBAF) was used in the kinetic experiments, commercially solution in THF from Aldrich chemical company. **Isopropanol** refluxed in the presence of CaH_2 then distilled and stored over 4 Å molecular sieves. **Diphenyl ether** was stirred in the presence of $MgSO_4$ for 6 h, after filtration, it was distilled under reduced pressure (110 °C, 35 mm Hg) and stored over 4 Å molecular sieves.[61]

3.2. Instrumentation

3.2.1 Nuclear magnetic resonance spectroscopy

Nuclear magnetic resonance spectra were recorded on a Bruker DRX 500 (500 MHz) NMR spectrometer. Chemical shifts (δ) of the spectra were obtained as reported in parts per million (ppm). Tetramethylsilane was used as an internal standard and deuterated chloroform ($CDCl_3$) as a solvent.

3.2.2. UV-VIS: UV-visible spectra were obtained on a Varian Cary 50 Bio-spectrophotometer which possesses a cell holder for 18 cuvets, thermostated by a Varian Cary PCB 150 bath at 25.0 ± 0.5 °C.

3.2.3. Viscometer: The viscosities of pure solvents and their mixtures were measured by using a Brookfield LVD VII Rheometer (CP40 cone, 0.8° angle, 0.5 mL final volume, 3.4 cm radius) with thermostated by a VWR Scientific Products bath at 36.0 ± 0.5 °C.

3.2.4. Density meter: Density (ρ) of pure sovents and their mixtures was measured using density meter (DMA4500 digital density meter, Anton Paar, Graz). Each measurement was performed at least two times in order to get reliable data. As a precaution, it was washed by acetone and dried with fan of an Anton Paar after every measurement.

3.2.5. Refractometer: Refractive indices of pure solvents and their binary mixtures were determined using an ABBE refractometer (Model: 60/ED, Prism Melt: 6, Prism index: 1.76142 and wavelength: 589.6nm (sodium)) with thermostated by a Fisher scientific model (9001) bath at 25.0 ± 0.5 °C. Each measurement was performed at least two times in order to ensure reproducibility. It was washed by acetone and dried before doing every new measurement.

3.2.6. Fluorescence spectrophotometer: Kinetic emission intensity experiments were performed on a Hitachi F-4500, fluorescence spectrophotometer equipped with a magnetic stirring system and thermostated at 25.0 ± 0.5 °C or 36.0 ± 0.5 °C by a Lauda Brinkmann bath

E100. The sensitivity of the apparatus was regulated by varying the parameters of the photomultiplier voltage and emission slit.

3.2.7. Ozonator: An ozonater (Gerador de ozônio Modelo O & L 3.0 RM) has been used to produce ozone (68 mg-O_3/L) utilized as a reagent in the preparation of diphenoyl peroxide.

3.3. Preparation of cyclic peroxides

3.3.1. Preparation of diphenoyl peroxide (1)

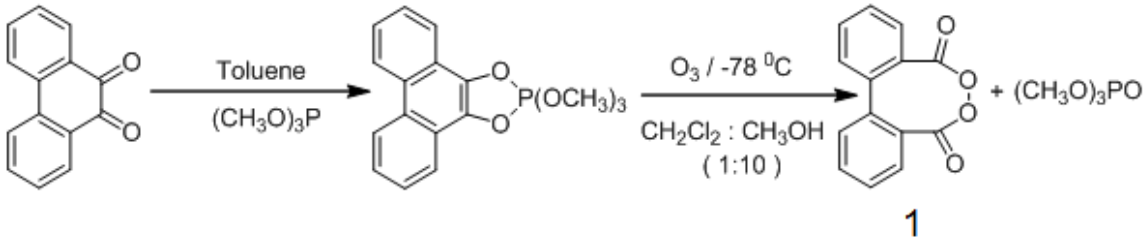

1

In a 125 ml round bottom flask containing a small magnetic bar, 1.21 g (5.8 mmol) of the recrystallized phenanthrene quinone was mixed with dry toluene (60 mL), resulting in a pale yellow suspension containing a considerable amount of solid phenanthrene quinine, as this compound showed to be not completely soluble in the solvent, even after stirring. After that 0.75 mL (6.4 mmol) of trimethyl phosphite was added to the reaction mixture by means of a Hamilton syringe. Within 30 min, the pale yellow suspension turned into a yellow colored transparent orange homogeneous solution. The reaction mixture was vigorously magnetically stirred and always maintaining the reaction mixture under an inert gas (argon) atmosphere. Then the solvent was evaporated under vacuum at room temperature. The residue was dissolved in hexane (3 mL) and the solution cooled down to 0 °C in an ice bath for 30 min. During this time, orange colored oil separated on the bottom of the flask; then the clear yellow hexane solution was taken out by pipette. The concentrated oil was dried in current of inert gas and roughly weighted to get 1.01 g (the oil

still contained small quantities of solvent). Solution of quinine-phosphite (1.01 g) adduct (I) in dry methylene chloride (3 mL) was cooled to -78 °C by a dry ice ethanol bath and then diluted with methanol (30 mL, precooled to -78 °C). This solution was immediately treated with ozone (68 mg-O_3/L) during 2 h, by using an ozonater (Gerador de ozônio modelo O&L 3.0 RM). The solution turned brown initially, the color was discharged toward the end of the reaction. The peroxide precipitates out of the solution in this solvent mixture. At the end of the reaction, the mixture was kept for 30 min at -78 °C and the peroxide was filtered and dried in a current of argon at 22 °C (1 h). This crude peroxide was pale yellow. This crude peroxide was dissolved in 3 mL of methylene chloride and the solution was diluted with 4 mL of methanol and placed in ice bath for 2 h; during this time precipitation of white crystals occurred. Then the solvent was taken out from flask with the help of glass pipette, in the presence of argon gas. A colorless to pale yellow substance was obtained which was dried in a current of inert gas (argon) for 3 h at 0 °C. The purified peroxide was preserved in freezer.[62]

Yield: 20 %.

NMR ^{1}H ($CDCl_3$), 500 MHz 25 °C: δ = 7.38 (d, *J*= 7.93, 1H) ppm; δ = 7.62 (td, J_{ortho} = 7.53 and J_{meta} = 1.0 Hz, 1H) ppm; δ = 7.69 (td, J_{ortho} = 7.73 and J_{meta} = 1.39 Hz, 1H) ppm; δ = 7.75 (dd, J_{ortho} = 7.73 and J_{meta} = 1.19 Hz, 1H) ppm.

NMR ^{13}C ($CDCl_3$), 500 MHz 25 °C: δ = 128.3, δ = 129.3, δ = 130.6, δ = 132.7, δ = 136.2, δ = 171.3 (C=O) ppm.

(**CAUTION!** This peroxide explodes at 70 °C)

During handling of pure solid diphenoyl peroxide(a quantity lower than 100 mg) contained in a 100 mL RB flask at room temperature, using a metallic spatula for weighting, this peroxide exploded with a sound how listened like bomb blasting, furthermore a lot of foam is being observed during the

explosion. After the incident, a protective sheet is used during handling of diphenoyl peroxide the entire time, additionally, immediately after recrystallization and drying, the solid peroxide is dissolved in the desired solvent and only stock solutions with concentrations lower than 1 molar are utilized.

3.3.2. Preparation of *spiro*-adamantyl *α*-peroxy lactone (2)

The 2-adamantanecarboxylic acid was obtained before in the group.

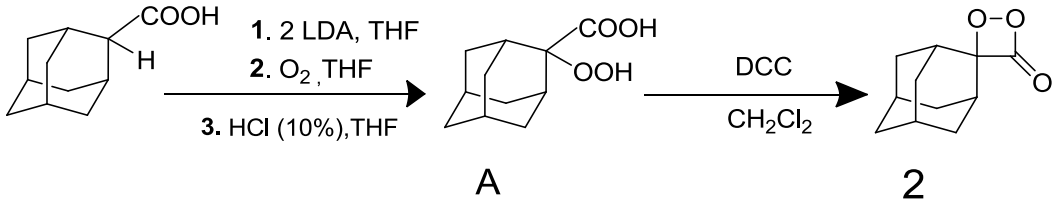

A 250 mL triple-necked round-bottomed flask was containing 1.12 mL (8 mmol) of dry diisopropylamine and 20 mL of dry THF, in the presence of argon gas. The system has been cooled with an acetone/dry ice bath at −78 °C and 21 mL (8.2 mmol) of a 0.9 mol L^{-1} n-BuLi solution in hexanes were slowly added by means of a Hamilton syringe. The temperature was allowed to increase to 0 °C, maintained constant for 20 min, and then lowered again to −20 °C. The 2-adamantanecarboxylic acid (0.61 g, 3.4 mmol) dissolved in 5 mL of dry THF was slowly added and the solution allowed to reach room temperature under magnetically stirring. Diisopropylamine and THF were eliminate under vacuum (room temperature, 5 mm Hg) and the white solid obtained was dissolved in 40 mL of dry THF and slowly transfered within 3 h, by a cannula, to another round-bottomed flask which already contained 50 mL of dry THF saturated with oxygen gas, was vigorously magnetically stirred and kept in a dry ice/acetone bath at −78 °C. After 1 h of additional stirring at −78 °C, 6 mL of a 10% aqueous solution of HCl was added to the system which was still under argon atmosphere. The temperature was allowed to raise up to −20 °C and the reaction mixture extracted with Et_2O. The combined organic

layers were dried with $MgSO_4$ for 10 min at 4 °C, filtered and concentrated under vacuum in a water/ice bath. The crude peroxidic product was purified by crystallization The intermediate peroxide [A] was obtained as a colorless solid. (190 mg, 0.9 mmol, 27 % yield)

A twin-necked round-bottomed flask was charged with 190 mg (0.9 mmol) of the intermediate peroxide [A] dissolved in 10 mL of CH_2Cl_2, the temperature was kept at −40 °C during this step using an acetone/dry ice bath, and 185 mg (1.74 mmol) of dicyclohexylcarbodiimide (DCC) dissolved in 5 mL of CH_2Cl_2 was slowly added. The reaction mixture was vigorously magnetically stirred during 5 h, while the temperature was maintained at −40 °C, and the reaction mixture was subject to TLC analysis during this time. The urea derivative produced during the reaction, insoluble in the solvent used, was removed by filtration through a column packed with florisil (3 g) at −45 °C. The solvent was evaporated under reduced pressure at a temperature which was not higher than −20 °C, obtained a slightly yellow solid. For purification, the product was recrystallized four or five times from *n*-pentane by dissolution at temperatures not higher than 20 °C and slow crystallization at -50 °C. As with the intermediate peroxide, after crystallization the mother liquor was removed carefully from the round-bottom flask by a glass pipette at low temperature under argon athmosphere. The pure compound consists in light-yellow colored cubic crystals.

Yield: 8%.

Caution! Always try to work at room temperature or below, with the smallest possible amounts. Do not expose solid peroxides to mechanic stress and or high temperature.

3.3.3. Preparation of 4-(3-tert-butyldimethylsilyloxyphenyl)-4-methoxyspiro[1.2-dioxetane-3.2-adamantane] (3)

The 1,2-dioxetane derivative (**3**)[73] was kindly provided by Dr. Luiz Francisco Monteiro Leite Ciscato (UFABC) and its identity and purity verified by the ^{1}H-NMR and ^{13}C-NMR spectra.

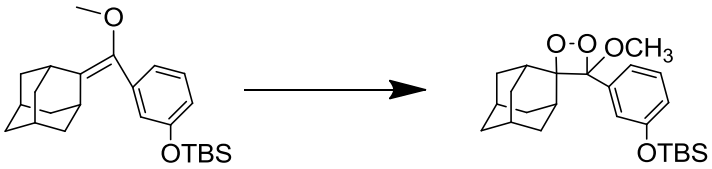

B 3

NMR ^{1}H (CDCl$_3$), 500 MHz 25 °C**:** δ = 0.22[s, 6H, Si(CH$_3$)$_2$], 1.00[s, 9H, C(CH$_3$)$_3$], 1.00 -2.29(m, 12, adamantane), 2.29(s, 1H, adamantane, 3.04(s 1H, adamantane), 3.26(s, 3H, OCH$_3$), 7.28-7.31(m, 4H ArH) ppm.

NMR ^{13}C (CDCl$_3$), 500 MHz 25 °C**:** δ = -4.4, 18.24, 25.68, 25.68, 26.08, 31.54, 32.80, 36.46, 38.84, 49.92, 76.78, 77.04, 77.28. 95.53, 112.07, 119.44, 121.07, 124.03, 125.54, 129.44, 136.16, 138.76, 155.86 ppm.

3.4. Kinetic chemiluminescence assays

3.4.1. Iodometric assay for the determination of cyclic peroxides (1 & 2) concentrations in the stock solution

A iodometric assay was used to determine the concentration of cyclic peroxides. First of all, the cyclic peroxide stock solution was diluted 10 times with methanol. 3 mL of a KI solution (0.05 mol L^{-1}) in acetate buffer solution (0.1 mol L^{-1} and pH 3.8) and 10 μL HRP solution (1 mg/mL in H_2O) were added to three quartz cuvette. After that, baseline of the mixture was recorded by one of three cuvette. After measuring the base line, 10 μL of the diluted solution of cyclic peroxide was mixed in each cuvette and absorbance at 353 nm (ε_{353} = 25,500 mol L^{-1} cm^{-1}) was measured until the value remained unchanged. The measurements were performed three times, taken the average of three

absorbance values and used in dilution formulas to know the exact concentrations of cyclic peroxides.

3.4.2. Kinetic chemiluminescence assays for cyclic peroxides (1 & 2)

The kinetic measurements were performed in a quartz cuvette of capacity 3.0 mL containing final volume of 2.0 mL with magnetic stirring. The ACT solution was added to the cuvette, which was placed in the cell holder of the spectro-fluorimeter with magnetic stirring. The data acquisition was initiated, followed by addition of peroxide stock solution by a micro syringe to the quartz cuvette. The peroxide stock solutions were maintained at -78 °C in a dry ice chamber during the experiments, in order to avoid the thermal peroxide decomposition. The solutions were warmed-up to 0 °C just before their use in the assay in order to allow volume measurement with the micro syringe. The kinetics generally showed mono exponential emission intensity decay curves, after the initial mixing time of the cyclic peroxide solutions with ACT solution as well as reaction temperature readjustment. Light emission time profiles were fitted with a first-order exponential decay equation to determine the initial emission intensities (I_0, in Einstein s^{-1}) and the observed rate constants (k_{obs}, in s^{-1}).

$$I_t = I_0 e^{-k_{obs} t} \qquad \text{Equation 5}$$

3.4.3. Iodometric assay for the determination of 1,2-dioxetane 3 concentrations in the stock solution

The 1,2-dioxetane concentration was determined by an iodometric assay, using an absorption cuvette with 3.0 mL of a 0.05 mol L^{-1} potassium iodide solution in 0.1 mol L^{-1} HOAc / OAc^- buffer (pH = 3.8), containing 10 µL of 1 mg mL^{-1} aqueous solution of HRP-VI (hydrogen-peroxidase oxidoreductase, EC 1.11.1.7, type VI-A, from horseradish) and 5 µL 1,2-dioxetane stock solution (in THF) in

order to get an absorbance between 0.5 and 0.8 at 353 nm (ε_{353} = 2.55 × 10^4 L mol^{-1} cm^{-1} for I_3^-

3.4.4. Kinetic chemiluminescence assays for 1,2-dioxetane (3)

The kinetic measurements were performed in a quartz cuvette of capacity 3.0 mL containing final volume of 2.0 mL with magnetic stirring. The required solvent was added in the cuvette, which was placed in the cell holder of the spectrofluorimeter with magnetic stirring and allowed to reach the desired temperature. Afterwards, the 1,2-dioxetane stock solution was injected by a micro syringe to quartz cuvette containing the solvent. The data acquisition was initiated followed by addition of TBAF stock solution (in ethyl acetate). The equipment baseline was discounted for all kinetic assays. The emission intensity was always shown to be maximum at acquisition time 0 and showed a first-order decay, which was followed during at least 4 half-lives. The observed rate constants (k_{obs}) were obtained by fitting the intensity versus time curves using a mono exponential decay function.

3.5. Determination of the activation parameters

Kinetic CL assays for peroxides: 1, 2 and 3 were performed exactly same way as discussed above. Temperature range from 36 to 70 °C used to determine the activation parameters for the thermolysis of diphenyol peroxide (1.0 mmol L^{-1}) using perylene as an activator and the thermolysis of *spiro*-adamantyl-1,2-dioxetanone (0.075 mmol L^{-1}) employing rubrene as an ACT in toluene, however, a temperature range from 30 to 48 °C in THF and from 35 to 60 °C in acetonitrile solvent has been used for the thermolysis of *spiro*-adamantyl-substituted dioxetane (0.01 mmol L^{-1}) with [TBAF] = 2.5 mmol L^{-1}. All the values of the rate constant and initial emission intensity have been obtained from the curves of first order decay.

3.5.1. Determination of the activation enthalpy ($\Delta H^{\neq}$)

The values for ΔH have been determined from slop obtained from a $\ln\left(\frac{k}{T}\right)$ *vs.* $\frac{1}{T}$ plot.[12,14]

$$k = \frac{k_B T}{h} e^{-\frac{\Delta G^{\neq}}{RT}} \qquad \text{Equation 6}$$

$$\Delta G^{\neq} = \Delta H^{\neq} - T\Delta S^{\neq} \qquad \text{Equation 7}$$

$$\frac{k}{T} = \frac{k_B}{h} e^{-\frac{(\Delta H^{\neq} - T\Delta S^{\neq})}{RT}} \qquad \text{Equation 8}$$

$$\ln\left(\frac{k}{T}\right) = \ln\left(\frac{k_B}{h}\right) + \frac{\Delta S^{\neq}}{R} - \frac{\Delta H^{\neq}}{R}\frac{1}{T}$$

(-ΔH/R) =slope

k_B = Boltzmann constant (1.381X10^{-23} J K^{-1});

h = Planck constant (6.626 X10^{-34} J s);

R = Universal gas constant (1.987 cal mol^{-1} K^{-1});

T = Temperature in Kelvin;

$\Delta G^{\neq}$ =Gibbs free energy;

3.5.2. Determination of the activation entropy ($\Delta S^{\neq}$)

The values for $\Delta S^{\neq}$ can be determined from slop which obtained from a $T * \ln\left(\frac{k}{T}\right)$ *vs.*T plot.[12,14]

$$T*\ln\left(\frac{k}{T}\right) = T[\ln\left(\frac{k_B}{h}\right) + \frac{\Delta S^{\neq}}{R}] - \frac{\Delta H^{\neq}}{R} \qquad \text{Equation 9}$$

$$\ln\left(\frac{k_B}{h}\right) + \frac{\Delta S^{\neq}}{R} = slope$$

Knowing $\Delta G^{\neq}$ from equation 11, and knowing E_a from an Arrhenius plot, can also get a good estimate of $\Delta S^{\neq}$ using an equation 10, without doing an Eyring plot.

$$\Delta S^{\neq} = [((E_a - RT) - \Delta G^{\neq})/T] \qquad \text{Equation 10}$$

3.5.3. Determination of the activation Gibbs free energy ($\Delta G^{\neq}$)

The Gibbs free energy of the system is a state function because it is defined in terms of thermodynamic properties that are state functions.[12] The change in the Gibbs free energy of the system that occurs during a reaction is therefore, equal to the change in the enthalpy of the system minus the change in the product of the temperature times the entropy of the system.

Knowing $\Delta H^{\neq}$ and $\Delta S^{\neq}$ from an Eyring plot and can get a good estimate of $\Delta G^{\neq}$.

$$\Delta G^{\neq} = \Delta H^{\neq} - T\Delta S^{\neq} \qquad \text{Equation 11}$$

3.6. Fluorometer calibration and quantum yield determination

Kinetic emission intensity experiments were performed on a Hitachi F-4500, fluorescence spectrophotometer equipped with a magnetic stirring system and thermostated at 25.0 ± 0.5 °C by a Lauda Brinkmann bath E100. All the kinetic experiments were performed in a quartz cuvette of capacity 3.0mL containing final volume of 2.0 mL with magnetic stirring. A 3.0 mL quartz cell containing 1.85 mL of the luminol stock solution was placed in the fluorimeter and data acquisition was initiated, followed by addition of 75 μL of the hydrogen peroxide (0.3%) stock solution and 75 μL of the diluted hemin solution (absorbance 0.2), when an intense CL emission was observed. After the emission intensity approached background level, 75 μL of the concentrated hemin solution (absorbance 0.6) were added and the procedure was repeated until no more considerable light emission could be observed upon hemin addition; normally the second addition of the concentrated hemin solution only leaded to very low light emission. The whole experiment was repeated at least five times in order to get reliable results. The calibration factor is calculated from the integral of total light emission in the luminol assay (Q_{lum}), the

luminol CL quantum yield (Φ_{lum} = 0.0114 ± 0.0006 E mol^{-1}) and the number of moles of luminol (n_{lum}) utilized in the standard assay (Table 1).

$$f_{lum} = \frac{\Phi_{lum}\, n_{lum}}{Q_{lum}} \; [E\,a.u.^{-1}] \qquad \text{Equation 12}$$

Where: f_{lum} = calibration factor; Φ_{lum} = luminol CL quantum yield; n_{lum} = number of moles of luminol used in the standard assay; Q_{lum} = total amount of light emitted by the luminol reaction.

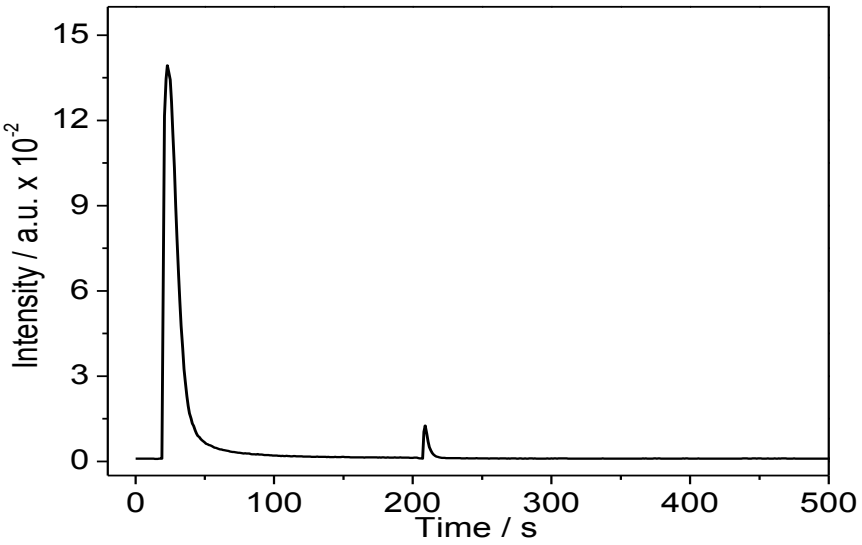

Figure 6*:* Time versus emission intensity decay for the calibration of the photomultiplier with [luminol] = 2.3 10^{-5} mol L^{-1} and H_2O_2 = 0.30%.

Table 1: Correction factors obtained from the photomultiplier calibration procedure of the fluorimeter Hitachi F-4500 in different conditions of the instrument.

$n_{luminol}$ (mol)	Emission slit (nm)	Voltage (V)	F_{CF} (E / a. u.)
2.3×10^{-5}	1	400	1.1×10^{-13}
1.63×10^{-7}	2.5	700	8.77×10^{-16}
1.63×10^{-8}	5	950	9.92×10^{-18}
1.63×10^{-7}	5	700	3.10×10^{-16}
1.63×10^{-7}	10	700	1.11×10^{-16}
1.63×10^{-9}	20	950	3.47×10^{-19}

The quantity of emitted photons is determined by the area under the emission curve and calibration of the detection instrument is necessary in order to determine reliable quantum yields in CL reactions.[43]

3.6.1. Determination of the chemiluminescence quantum yield (Φ_{CL})

The CL quantum yield (Φ_{CL}) can be defined as the relation between the number of photons emitted by a certain chemical reaction (in Einstein) per number of moles of limiting reactant (Equation 13).

$$\Phi_{CL} = \frac{\text{Number of photons emitted}}{\text{moles of limiting reagent}} \qquad \text{Equation 13}$$

3.6.2. Determination of the singlet chemiexcitation quantum yield (Φ_S)

Absolute singlet chemiexcitation quantum yields (Φ_S) were determined from the calibrated CL quantum yields (Φ_{CL} in E mol^{-1}) and fluorescence quantum yields of ACT (Φ_{FL}) were taken from literature. It can be explained by equation (Equation 14).

$$\Phi_S = \frac{\Phi_{CL}}{\Phi_{FL}} \qquad \text{Equation 14}$$

3.6.3. Determination of the catalyzed singlet quantum yield ($\boldsymbol{\Phi_S^{CAT}}$)

In order to calculate catalyzed singlet quantum yield, the singlet chemiexcitation quantum yield (Φ_S) is divided by the fractioning factor (χ_{CAT}), which is the fraction of the initial diphenoyl peroxide concentration which is reacting by catalyzed pathway (Equation 15).

$$\Phi_S^{CAT} = \frac{\Phi_S}{\chi_{CAT}} \qquad \text{Equation 15}$$

The fractioning factor (χ_{CAT}) is defined as the ratio between the calalyzed pathway and all reaction pathways consuming the peroxide and it can be calculated from the rate constants k_{CAT} and k_D as well as the [ACT] utilized (Equation 16).

$$\chi_{CAT} = \frac{k_{CAT}[ACT]}{k_D + k_{CAT}[ACT]} x100 \qquad \text{Equation 16}$$

3.6.4. Determination of the infinite singlet quantum yield ($\boldsymbol{\Phi_S^{\infty}}$)

In the case of the catalyzed 1,2-dioxetanone decomposition, where observed rate constants do not depend on the [ACT], the singlet quantum yields of the chemiexcitation step can be considered as the infinite quantum yields at an infinite concentration of the rubrene activator and determined from the double-reciprocal plots of singlet quantum yield (Φ_S) and the [ACT] (Equation 17), which show linear correlation.[63]

$$\frac{1}{\Phi_S} = \frac{1}{\Phi_S^{\infty}} + \left[\frac{k_D}{k_{CAT}\Phi_S^{\infty}}\right]\frac{1}{[ACT]} \qquad \text{Equation 17}$$

3.6.5. Determination of the fluorescence quantum yield (Φ_{FL})

The fluorescence quantum yield (Φ_{FL}) can be determined by dividing the number of absorbed photons by the number of emitted photons (Equation 21), utilizing an appropriate fluorescence standard (Equation 18).[64]

$$\Phi_{FL} = \frac{\text{No. of emitted photons}}{\text{No. of absorbed photons}} \qquad \text{Equation 18}$$

$$\Phi_{FL} = \left(\frac{A_s}{A_U}\right)\left(\frac{I_U}{I_S}\right)\left(\frac{n_u}{n_s}\right)^2 \Phi_{FL(s)} \qquad \text{Equation 19}$$

Where: n_s, n_u stand for refractive indices for standard and unknown solvents respectively; $\Phi_{FL(s)}$, Φ_{FL} stand for the quantum yield of standard and unknown compound; A_s, A_u stand for the absorbance of standard and unknown compound and I_u, I_s stand for the area under the curve of fluorescence spectrum of unknown and standard compound respectively.

First, the baseline of the desired solvent was recorded, after measuring the base line, the phenolate ester stock solution was added by means of a micro syringe to the solvent contained in the quartz cell placed in the thermostated cell holder of the UV-visible -spectrophotometer for measuring the absorbance of the phenolate ester. After that, the TBAF stock solution was also added by means of a micro syringe to this quartz cell which contained already solution of phenolate ester. The maximum absorbance of the solution has been observed at the 316 nm wavelength but 320 nm wavelength used for excitation wavelength. The same compound was used as a standard in toluene solvent which consists of quantum efficiency equal to (Φ_{FL} = 0.22)[65] and a correction for the refractive indices have been done for all the solvents which are used for this study (Equation 19) (Tables 2, 3).

Table 2: Measured fluorescence quantum yield of emitter in pure solvents

Solvent	λ_{ex}	Φ_{FL}	Solvent	λ_{ex}	Φ_{FL}
anisole	320	0.29	Acetone	320	0.23
diphenyl ether	320	0.22	DMSO	320	0.26
butyl acetate	320	0.27	DMF	320	0.23
ethyl acetate	320	0.23	ACN	320	0.21
THF	320	0.26	/	/	/

[Phenolate ester] = 0.014 mmol L^{-1}; [TBAF] = 0.2 mmol L^{-1} in THF; conditions = λ_{ex} = 320; Ex slit =10 nm; Em slit = 10 nm; voltage=700V; at 25 °C.

Table 3: Measured and calculated fluorescence quantum yields of emitter in binary solvent mixtures.

Solvent	Φ_{FL}(Exp)	Φ_{FL}(calcu)	Solvent	Φ_{FL}(Exp)	Φ_{FL}(calcu)
Butyl	0.24	0.24	Toluene	0.26	0.26
20% DMF	0.21	0.22	20%Ethyl	0.25	0.25
40% DMF	0.20	0.20	40%Ethyl	0.24	0.24
60% DMF	0.20	0.19	60%Ethyl	0.24	0.22
80% DMF	0.19	0.18	80%Ethyl	0.21	0.21
100%DMF	0.17	0.17	100%Ethyl	0.20	0.20
100%TOL	0.26	0.26	20%Buty	0.240	0.250
20% DMF	0.23	0.24	40%butyl	0.240	0.249
40% DMF	0.21	0.22	60%butyl	0.236	0.244
60% DMF	0.22	0.20	80%butyl	0.235	0.237
80% DMF	0.175	0.18	100%butyl	0.230	0.230

Exp. = experimental; calcu = calculated; [Phenolate ester] = 0.014 mmol L^{-1}; [TBAF] = 0.2 mmol L^{-1} in THF; conditions = λ_{ex} = 320; Ex slit =10 nm; Em slit = 10 nm; voltage=700V; at 25 °C.

3.7. Determination of solvents parameters

3.7.1. Determination of the solvent polarity parameter [E_T (30)] of the solvent systems

In 1963, Dimroth *et al.* highlighted that the electronic transition energies E_T which can be defined by using equation 20 and now a days this parameter is known as $E_T(30)$ parameter [66] which is utilized as an empirical parameter for solvent polarity.

The solvent polarity parameter $E_T(30)$ of the pure solvents and binary solvent mixture like ethyl acetate–toluene, butyl acetate–toluene and acetone–toluene were obtained at 25.0 ± 0.5°C, using Reichardt's pyridinium-N-phenolate betaine dye. A stock solution of Reichardt's pyridinium-N-phenolate betaine dye was prepared in ethanol. About 2.0 mL of ethanol solution was evaporated as a result betaine dye remained in flask was mixed in desired solvent, in order to verify the polarity of desired solvent and transferred to a cuvette and spectra was performed. The final concentration of the dye was approximately 0.05 mmol L^{-1} and all measurements were performed duplicate in order to get reliable result. The values of the wavelength with the maxium absorbance (λ_{max}) were used in equation 20 to get the E_T (30) (Table 4).[67]

$$E_T\,(30)\left(\frac{\text{kcal}}{\text{mol}}\right) = h\,.\,C\,.\,\bar{\upsilon}_{max}\,.\,N_A = (2.8591\,.\,10^{-3})\,\bar{\upsilon}_{max}\,(\text{cm}^{-1}) = \; 28591/\lambda_{max}(\text{nm})$$

So

$$E_T\,(30)\left(\frac{\text{kcal}}{\text{mol}}\right) = \; 28591/\lambda_{max}(\text{nm}) \qquad \text{Equation 20}$$

Where: $\bar{\upsilon}_{max}$ stands for the wave number and λ_{max} stands for the maximum wavelength and h, c, and N_A stand for Planck constant, the speed of light and Avogadro constant, respectively.

Table 4: $E_T(30)$ values for pure solvents and binary solvent mixtures.

%Solvent A	% Solvent B	$E_T(30)$	%Solvent A	% Solvent B	$E_T(30)$
100% TOL	00% EA	33.22	80% TOL	20% ACE	36.20
80% TOL	20% EA	35.63	60% TOL	40% ACE	40.00
60% TOL	40% EA	36.28	40% TOL	60% ACE	40.30
40% TOL	60% EA	37.37	20% TOL	80% ACE	41.60
20% TOL	80% EA	38.56	100% THF	0% ACE	37.70
0% TOL	100% EA	39.38	80% THF	20% ACE	38.60
80% TOL	20% BUTY	35.50	60% THF	40% ACE	39.50
60% TOL	40% BUTY	36.00	40% THF	60% ACE	40.40
40% TOL	60% BUTY	36.50	20% THF	80% ACE	41.30
20% TOL	80% BUTY	37.30	0% THF	100% ACE	42.20
0% TOL	100% BUTY	38.80	100% EA	00% ACE	38.50
100% TOL	00% ACN	34.44	80% EA	20% ACE	41.44
95% TOL	5% ACN	39.70	60% EA	40% ACE	42.00
90% TOL	10% ACN	40.80	40% EA	60% ACE	42.17
80% TOL	20% ACN	41.44	20% EA	80% ACE	42.29
70% TOL	30% ACN	42.61	00% EA	100% ACE	43.20
60% TOL	40% ACN	43.06	100% TOL	0% DMF	34.30
50% TOL	50% ACN	43.80	80% TOL	20% DMF	39.78
40% TOL	60% ACN	44.00	60% TOL	40% DMF	40.78
30% TOL	70% ACN	44.50	40% TOL	60% DMF	41.86
20% TOL	80% ACN	45.24	20% TOL	80% DMF	42.86
80% BUTY	20% DMF	41.26	00% TOL	100% DMF	43.58
60% BUTY	40% DMF	41.86	80% EA	20% DMF	41.10
40% BUTY	60% DMF	42.42	60% EA	40% DMF	41.36
20% BUTY	80% DMF	42.80	40% EA	60% DMF	42.38
0% BUTY	100% DMF	43.58	20% EA	80% DMF	42.52

TOL = toluene; EA = ethyl acetate; BUTY = butyl acetate; ACN = acetonitrile; ACE = acetone; DMF = *N,N*-dimethyl formamide and pyrro = 1-methyl-2-pyrrolidinone.

Precautions

Precautions were taken to avoid evaporation and contamination by humidity. The Reichardt dye [2,6-diphenyl-4-(2,4,6-triphenylpyridinium-1-yl)-phenolate] was used as received from Sigma. Binary solvent mixtures were prepared gravimetrically. The concentration of the dye in all solvents was 0.05 mmol L^{-1}. The solutions in each individual solvent and binary solvent mixture were prepared just before use.

3.7.2. Determination of the refractive index (n_D) of the solvent systems

The law of refraction was mathematically formulated first by Snell in 984.[68] The refractive index (n) of a medium is denoted following equation.

$$n = \frac{c}{v} \qquad \text{Equation 21}$$

3.7.3. Determination of the polarizability using the Lorentz-Lorenz (LL) equation

Refractive indices of pure solvents and binary solvent mixtures were measured using an ABBE refractometer [model: 60/ED, prism melt: 6, prism index: 1.76142 and wavelength: 589.6nm (sodium)] (Table 5).

The Lorentz-Lorenz (LL) equation

The values of these refractive indices were used in the Lorentz-Lorenz (LL) equation 22 to get the polarizability (P) values (Table 5).[69]

$$P = (n^2 - 1)/(n^2 + 2) \qquad \text{Equation 22}$$

Table 5: Refractive indices and polarizability for pure solvents and binary solvent mixtures.

%Solv.A	% Solv. B	*n*	π*	%Sol. A	% Sol. B	*n*	π*
100% TOL	00% THF	1.497	0.29	40% DPE	60% DMSO	1.520	0.30
80% TOL	20% THF	1.473	0.28	20% DPE	80% DMSO	1.500	0.29
60% TOL	40% THF	1.458	0.27	0% DPE	100% DMSO	1.479	0.28
40% TOL	60% THF	1.443	0.26	80% TOL	20% BUTY	1.470	0.28
20% TOL	80% THF	1.428	0.25	60% TOL	40% BUTY	1.440	0.26
0% TOL	100% THF	1.400	0.24	40% TOL	60% BUTY	1.430	0.26
80% TOL	20% EA	1.460	0.27	20% TOL	80% BUTY	1.410	0.25
60% TOL	40% EA	1.440	0.26	0% TOL	100% BUTY	1.390	0.24
40% TOL	60% EA	1.420	0.25	80% TOL	20% DMF	1.477	0.28
20% TOL	80% EA	1.390	0.24	60% TOL	40% DMF	1.468	0.28
0% TOL	100% EA	1.370	0.23	40% TOL	60% DMF	1.457	0.27
80% TOL	20% ACN	1.475	0.28	20% TOL	80% DMF	1.445	0.27
60% TOL	40% ACN	1.460	0.27	0% TOL	100% DMF	1.430	0.26
40% TOL	60% ACN	1.430	0.26	80% TOL	20% ACE	1.470	0.27
20% TOL	80% ACN	1.400	0.25	60% TOL	40% ACE	1.440	0.26
0% TOL	100% ACN	1.340	0.21	40% TOL	60% ACE	1.420	0.25
100%DPE	0% DMSO	1.580	0.33`	20% TOL	80% ACE	1.390	0.24
80% DPE	20% DMSO	1.540	0.31	0% TOL	100% ACE	1.360	0.22
60% DPE	40% DMSO	1.530	0.31	100% THF	00% ACE	1.400	0.33

Solv.= solvent; *n*= refractive indices; π*= polarizability; TOL = toluene; EA = ethyl acetate; BUTY = butyl acetate; THF = tetrahydrofuran; ACN = acetonitrile; ACE = acetone; DMF = *N,N*-dimethyl formamide and DMSO = dimethyl sulfoxide.

3.7.4. Determination of low and high frequency polarizability using the Lippert-Mataga Equation (LM).

This model does not consist of any sort of chemical interactions. There are considered just physical interactions like formation of charge transfer states or hydrogen bonding, sometimes deviations were found from the general concept of this theory. However, explanation of this model will be done step by step here.

The Lippert- Mataga equation has been described by the following relationship.[13]

$$\overline{\nu_A} - \overline{\nu_F} = \frac{2}{hc}\left(\frac{\varepsilon - 1}{2\varepsilon + 2} - \frac{n^2 - 1}{2n^2 + 1}\right)\frac{(\mu_E - \mu_G)^2}{a^3} + \text{constant} \qquad \text{Equation 23}$$

Where: h, c, a, $\overline{\nu_A}$ ν_F μ_E, μ_G are Planck constant, the speed of light, the radius for the cavity the wave numbers for the absorption and emission, dipole moments for excited state and ground state, respectively.

The refractive index (n) is known as a high-frequency response which depends on the motion of electrons within the solvent molecules.
In contrast, the dielectric constant (ε_r) is recognized as a static property and depends on electronic movement as well as the motion of solvent molecules the latter being solvent reorganization around the excited state.
Reorientation of the electrons in the medium system occurs instantaneously, that's why this component recognized as a **high frequency polarizability f(n)** which is a function of the refractive index and showed by below equation 24.

$$f(n) = \frac{n^2 - 1}{2n^2 + 1} \qquad \text{Equation 24}$$

The polarizability of the medium also depends on the dielectric constant (ε) which involves the influence of molecular orientation of the solvent molecules. Due to the slower timescale for molecular reorientation, recognized as a **low frequency polarizability** of the medium and displayed by equation 25.

$$f(\varepsilon) = \frac{\varepsilon - 1}{2\varepsilon + 2} \qquad \text{Equation 25}$$

The difference between these two terms is known as orientation polarizability for solvent (equation 26).

$$\Delta f = \frac{\varepsilon - 1}{2\varepsilon + 2} - \frac{n^2 - 1}{2n^2 + 1} \qquad \text{Equation 26}$$

Table 6: Low, high frequency polarizability and orientation polarizability for solvents

Solvents	ε	n	L.F.P. $f(\varepsilon) = \frac{\varepsilon - 1}{2\varepsilon + 2}$	H.F.P. $f(n) = \frac{n^2 - 1}{2n^2 + 1}$	O.P. (Δf)
toluene	2.43	1.497	0.24	0.23	0.02
n-dibutyl ether	3.18	1.398	0.30	0.19	0.10
diphenyl ether	3.69	1.581	0.32	0.25	0.07
dibenzyl ether	3.86	1.562	0.33	0.24	0.08
diethyl ether	4.42	1.352	0.35	0.18	0.17
anisole	4.45	1.517	0.35	0.23	0.12
chloroform	4.89	1.446	0.36	0.21	0.15
n-butyl acetate	5.01	1.394	0.36	0.19	0.17
ethyl acetate	6.03	1.372	0.39	0.19	0.19
di-n-butyl phthalate	6.44	1.493	0.39	0.23	0.17
THF	7.47	1.406	0.41	0.20	0.21
methyl phthalate	8.66	1.515	0.42	0.23	0.19
acetone	21.36	1.359	0.47	0.18	0.29
PYRR	32.58	1.469	0.48	0.22	0.26
ACN	35.94	1.344	0.48	0.18	0.31
DMF	37.04	1.430	0.48	0.21	0.28
DMSO	46.71	1.479	0.48	0.22	0.26

ε = dielecrtic constant; n = refractive indices; L.F.P.= low frequency polarizability; H.F.P.= high frequency polarizability; O.P.= orientation polarizability; PYRR=1-methyl-2-pyrrolidinone

The part inside the large parentheses as showed in equation 23 is the orientation polarizability which is generally shown by Δf (equation 26). The first part (ε–1)/(2ε + 1) indicates reorientation for the dipoles of solvent as well as the electronic redistribution in the solvent systems (equation 25). The second part (n^2 – 1)/(2n^2 + 1) of equation just due to the redistribution for electrons (equation 24). The difference of above both parts of equation is due to the reorientation of the medium molecules and known as orientation polarizability. The polarizability of the medium is a consequence of the movements of electrons of the solvent as well as the dipole moment by the solvent molecules.

Table 7: Polarizability for binary solvent mixtures.

solvent	n	H.F.P. $f(n) = \frac{n^2-1}{2n^2+1}$	solvent	n	H.F.P. $f(n) = \frac{n^2-1}{2n^2+1}$
TOL	1.50	0.226	P	1.48	0.220
A	1.47	0.218	Q	1.47	0.217
B	1.44	0.209	R	1.46	0.214
C	1.43	0.205	S	1.45	0.210
D	1.41	0.199	T	1.43	0.205
E	1.43	0.192	U	1.48	0.217
F	1.46	0.215	V	1.46	0.215
G	1.44	0.209	W	1.43	0.205
H	1.42	0.202	X	1.40	0.195
I	1.39	0.192	Y	1.34	0.173
J	1.37	0.185	Z	1.58	0.249
K	1.47	0.218	AA	1.54	0.238
L	1.44	0.209	BB	1.53	0.236
M	1.42	0.202	CC	1.52	0.233
N	1.39	0.192	DD	1.50	0.227
O	1.36	0.181	EE	1.48	0.221

n = refractive indice; H.F.P.= high frequency polarizability; Toluene (TOL) containing A: 20% butyl acetate, B: 40% butyl acetate, C: 60% butyl acetate, D: 80% butyl acetate, E: 100% butyl acetate; F: 20% Ethyl acetate, G: 40% ethyl acetate, H: 60% ethyl acetate, I: 80% ethyl acetate, J: 100% ethyl acetate; K: 20% acetone, L: 40% acetone, M: 60% acetone, N: 80% acetone, O: 100% acetone; P: 20% DMF, Q: 40% DMF, R: 60% DMF, S: 80% DMF, T: 100% DMF; U: 20% ACN, V: 40% ACN, W: 60% ACN, X: 80% ACN, Y: 100% ACN; Z: diphenyl ether (DPE) containing AA: 20% DMSO, BB: 40% DMSO, CC: 60% DMSO, DD: 80% DMSO, EE: 100% DMSO.

3.7.5. Calculation of the dielectric constants (ε_r) for binary solvent systems

Dielectric constant values for toluene-acetone and tetrahydrofuran-acetone systems were calculated using a molar fraction formula (equation 27) because these systems are ideal systems which follow raoult's law (Figure 7).

$$\epsilon = \varepsilon_1 x_1 + \epsilon_2 x_2 \qquad \text{Equation 27}$$

3.7.6. Determination of density (ρ) of the solvent systems

The density of a substance is its mass per unit volume. Density (ρ) of pure sovents and their mixtures were measured using density meter (Tables 8a, 8b).[12,14]

$$\rho = \frac{m}{v} \qquad \text{Equation 28}$$

Where: ρ is the density, m is the mass, and v is the volume.

Table 8a: Density (ρ) of pure sovents and their binary mixtures

X_1(TOL)	X_2(ACE)	Density
1.00	0.00	0.862
0.93	0.07	0.852
0.85	0.15	0.846
0.77	0.23	0.839
0.68	0.32	0.833
0.59	0.41	0.824
0.49	0.51	0.821
0.38	0.62	0.809
0.27	0.73	0.801
0.14	0.86	0.795
0.00	1.00	0.784

X_1(ACE)	X_2(THF)	Density
1.00	0.00	0.785
0.91	0.09	0.798
0.82	0.18	0.805
0.72	0.28	0.815
0.63	0.37	0.828
0.53	0.47	0.836
0.43	0.57	0.845
0.33	0.67	0.852
0.22	0.78	0.862
0.11	0.89	0.872
0.00	1.00	0.883

X_1(BUTY)	X_2(DMF)	Density
1.00	0.00	0.876
0.84	0.16	0.885
0.70	0.30	0.891
0.58	0.42	0.898
0.47	0.53	0.905
0.37	0.63	0.911
0.28	0.72	0.918
0.20	0.80	0.925
0.13	0.87	0.935
0.06	0.94	0.936
0.00	1.00	0.944

X_1(TOL)	X_2(DMF)	Density
1.00	0.00	0.862
0.87	0.13	0.875
0.74	0.26	0.882
0.63	0.37	0.889
0.52	0.48	0.897
0.42	0.58	0.904
0.33	0.67	0.911
0.24	0.76	0.919
0.15	0.85	0.926
0.07	0.93	0.935
0.00	1.00	0.944

TOL = toluene; EA = ethyl acetate; BUTY = butyl acetate; THF = tetrahydrofuran; ACN = acetonitrile; ACE = acetone; DMF = *N,N*-dimethyl formamide.

Table 8b: Density (ρ) of pure sovents and their binary mixtures

X_1(EA)	X_2(ACN)	Density	X_1(TOL)	X_2(ACN)	Density
0.00	1.00	0.777	0.00	1.00	0.777
0.05	0.95	0.790	0.05	0.95	0.788
0.12	0.88	0.780	0.11	0.89	0.795
0.19	0.81	0.820	0.18	0.82	0.804
0.26	0.74	0.830	0.25	0.75	0.814
0.35	0.65	0.840	0.33	0.67	0.822
0.44	0.56	0.850	0.43	0.57	0.823
0.55	0.45	0.860	0.54	0.46	0.838
0.68	0.32	0.870	0.67	0.33	0.845
0.82	0.18	0.880	0.82	0.18	0.852
1.00	0.00	0.890	1.00	0.00	0.864

TOL = toluene; EA = ethyl acetate; BUTY = butyl acetate; THF = tetrahydrofuran; ACN = acetonitrile; ACE = acetone; DMF = *N,N*-dimethyl formamide.

The experimantal and calculated values have been used in the following graphes in order to indicate deviations and interactions between solute and solvents.

These two solvent systems: acetone- tetrahydrofuran (A) and acetone-toluene (B) are ideal solutions.

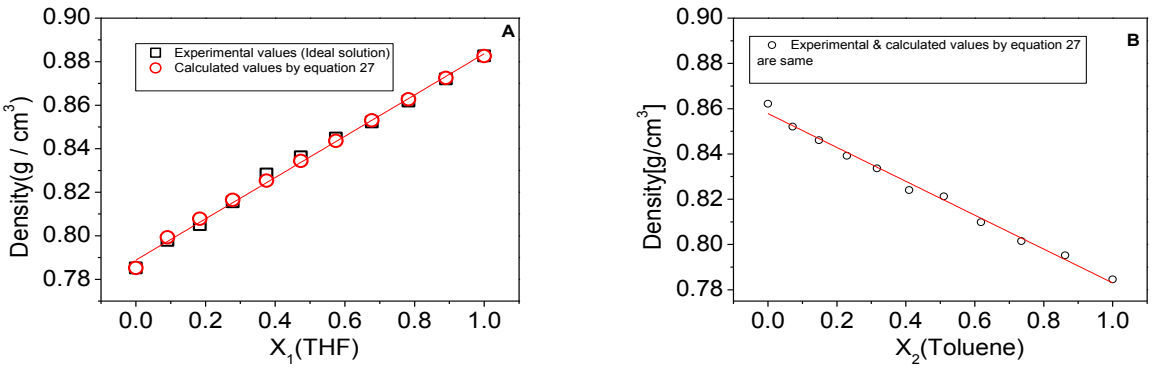

Figure 7*:* Density of binary solvent mixture for (A) acetone and tetrahydrofuran versus mole fraction (x_1) of tetrahydrofuran; (B) acetone and toluene versus mole fraction (x_1) of toluene at 25 °C.

Following solvent mixtures showing a positive deviation from Raoult's Law, is called non-ideal behavior (Figure 8).

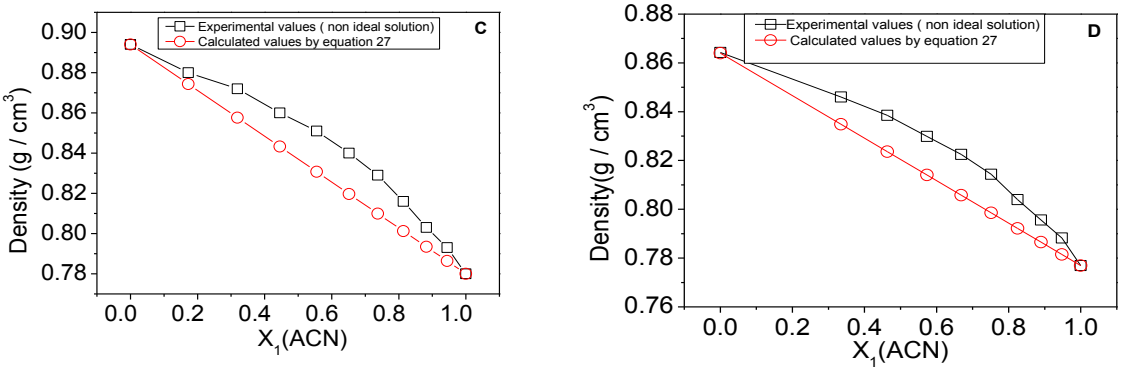

Figure 8*:* Density of binary solvent mixture for (C) ethyl acetate and acetonitrile versus mole fraction (x_1) of acetonitrile; (D) toluene and acetonitrile versus mole fraction (x_1) of acetonitrile at 25°C.

Following solvent mixtures showing a negative deviation from Raoult's Law, is known also non ideal behavior (Figure 9).

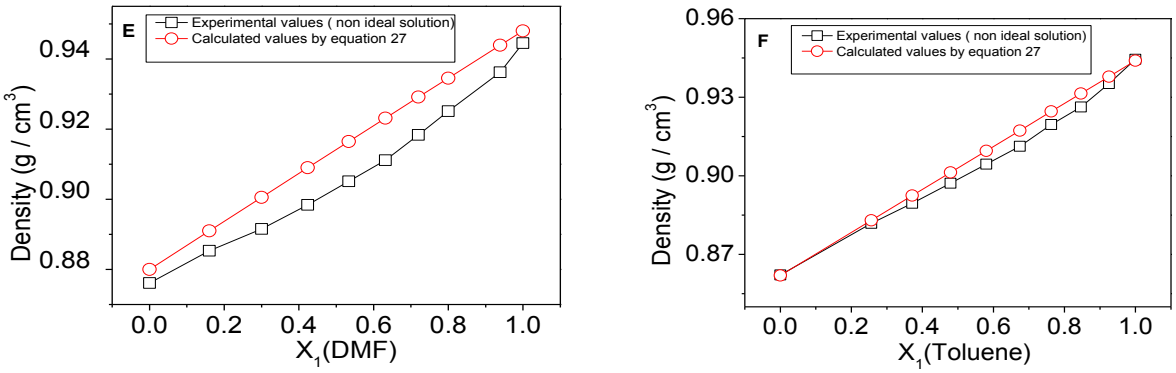

Figure 9*:* Density of binary solvent mixtures of (E) butyl acetate and *N,N*-dimethyl formamide versus mole fraction (x_1) of DMF; (F) toluene and *N,N* -dimethyl formamide versus mole fraction (x_1) of toluene at 25 °C.

3.7.7. Determination of viscosity (η) of the solvent systems

The viscosities of pure solvents and their binary mixtures were measured using a Brookfield LVD VII Rheometer (CP40 cone, 0.8° angle, 0.5 mL final volume, 3.4 cm radius). The desired solvent is placed by means of a micro syringe on the bottom plate containing final volume of 0.5 mL with the instrument head in the upper position. Always the solvent sample has been avoided from air bubbles which can affect the results and removed excess solvent from around the cone or plate by using the paper. The required temperature has been adjusted on thermostated by a VWR scientific products bath which was 36.0 ± 0.5°C and did not start the measurement of solvent until the temperature has been stabilized at set point. The Rheometer keyboard corresponding Rheometer functions have been used in order to continue next process to get results. Each measurement was performed at least two times, in order to get reliable data. As a precaution, the plate was washed by acetone and dried after every measurement.

3.8. Mathematically adjustments

The kinetic emission curves were fitted mathematically to exponential decay using the following equation 29.

$$y = Ae^{\left(\frac{-x}{t_1}\right)} \qquad \text{Equation 29}$$

The standard deviation measurements were calculated using equation 30.

$$\sigma_x^2 = (\partial x/\partial a)^2\,\sigma_a^2 + (\partial x/\partial b)^2\,\sigma_b^2 + \cdots (\partial x/\partial n)^2\,\sigma_n^2 \qquad \text{Equation 30}$$

The standard deviation is the root mean square fluctuations of each data that was collected from the average value. This finding has better representation of

the true variations that occur in any experiment and therefore is more widely used in statistical analysis.

The standard deviation values have been calculated using equation 31 for the collisional model.

$$\partial\frac{A}{B} = \left(\frac{\partial A}{A} + \frac{\partial B}{B}\right)\left(\frac{A}{B}\right)$$

$$\partial\frac{1}{B} = \left(\frac{0}{1} + \frac{\partial B}{B}\right)\frac{1}{B} = \frac{\partial B}{B^2} \qquad \text{Equation 31}$$

The standard deviation values have been determined using equation 31 for the free volume model.

$$\ln(A \pm \Delta A) = \ln(A) \pm \left|\frac{1}{A}\right| \Delta A \qquad \text{Equation 32}$$

4. Results

4.1. Synthesis of the cyclic peroxides

4.1.1. Synthesis of the diphenoyl peroxide (1)

The diphenoyl peroxide was prepared from phenanthrene quinone followed by the method described in the literature[70,71] which involves the transformation of an adduct of the quinone with trimethylphosphite which is transformed to the diphenoyl peroxide via ozonolysis (Scheme 9).

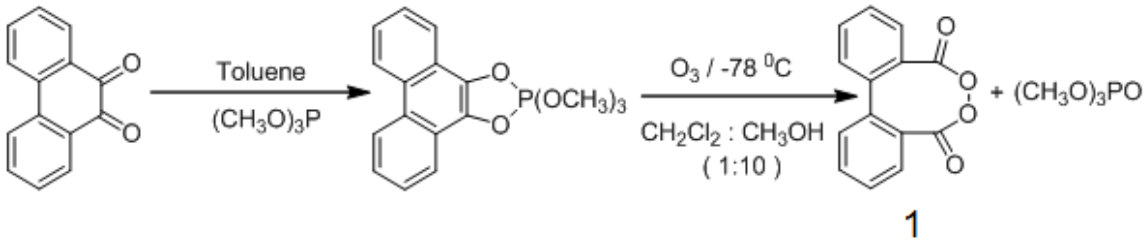

Scheme 9: Synthetic route for obtaining diphenoyl peroxide via ozonolysis.

The recrystallized phenanthrene quinone were mixed with dry toluene resulting in a pale yellow suspension, After that trimethyl phosphite were added to the reaction mixture and the pale yellow suspension turned into a yellow colored transparent orange homogeneous solution. Then, the solvent was evaporated under vacuum at room temperature. Solution of quinine-phosphite adduct were added in dry methylene chloride and methanol with the ratio of solvent mixtures 1:10, respectively. In fact, solvents affect on the composition of peroxide yield. The ratio of solvent mixtures 1:10 with respect to methylene chloride and methanol is very adequate for an efficient preparation of diphenoyl peroxide. This solution was immediately treated with ozone. The peroxide precipitates out of the solution in this solvent mixture. Then, the solvent was taken out in the presence of argon gas. A pale yellow colorless substance was obtained which was dried in a current of inert gas (argon) at 0 ˚C. The purified peroxide was preserved in freezer.

Obtained = 20 % yield.

We took the ^{1}H-NMR and ^{13}C-NMR spectra in order to know its identity and purity, as a result, following values have been got which are in good agreement with literature.

NMR ^{1}H ($CDCl_3$), 500 MHz 25 °C: δ = 7.38 (d, *J*= 7.93, 1H) ppm; δ = 7.62 (td, J_{ortho} = 7.53 and J_{meta} = 1.0 Hz, 1H) ppm; δ = 7.69 (td, J_{ortho} = 7.73 and J_{meta} = 1.39 Hz, 1H) ppm; δ = 7.75 (dd, J_{ortho} = 7.73 and J_{meta} = 1.19 Hz, 1H) ppm.

NMR ^{13}C ($CDCl_3$), 500 MHz 25 °C: δ = 128.3, δ = 129.3, δ = 130.6, δ = 132.7, δ = 136.2, δ = 171.3 (C=O) ppm.

4.1.2. Synthesis of *spiro*-adamantyl *α*-peroxy lactone (2)

The 2-adamantanecarboxylic acid was provided in the group. The *α*-hydroperoxy adamantanecarboxylic acid obtained by *α*-lithiation of 2-adamantanecarboxylic acid and autoxidation took place at low-temperature (Scheme 10) The 2-adamantanecarboxylic acid has been utilized to get the enolate dianion using two equivalents of lithium diisopropylamide (LDA) and temperature was very low. The solvent THF and diisopropylamine removed by vacuum distillation. Removal of the amine before oxygenation is very important in order to obtain the successful preparation, to avoid electron transfer catalyzed decomposition of the peroxide by the electron rich amine.[72]

For an efficient preparation of *α*-hydroperoxyacids, it is necessary to slowly add the enolate dianion dissolved in THF to oxygen saturated THF at about –70 °C. Oxygen bubbling into a solution of the dianion at low temperature does not lead to *α*-hydroperoxyacid formation. The α-hydroperoxyacid derivatives can be isolated by aqueous work-up at low temperature.

The last reaction step has been started by proton transfer from the carboxylic acid to DCC, subsequently, the carboxylate group attacked as a nucleophilic to the protonated DCC molecule. The proton transfered from the *α*-hydroperoxy group to the DCC nitrogen atom by intramolecular fashion. Consequently, this group becomes good leaving group. Subsequently, the

cyclization reaction took place by intramolecular nucleophilic addition of the peroxy anion onto the derivatized carboxyl carbon therefore, the elimanation of *N*,*N*-dicyclohexylurea and 1,2-dioxetanone formation took place. the resulting urea derivative is unable to soluble in CH_2Cl_2, at the low temperatures which used for reaction, the reaction mixture filtered over florisil at −45 °C in oreder to remove the urea derivative and the solvent evaporated at temperature less than −20 °C, leading to a slightly yellow solid. This peroxide further purified by low temperature recrystallization from *n*-pentane, obtained as slightly yellow cubic crystals (8% yields). Peroxides **2** analyzed by TLC using a specially developed low-temperature method (Scheme 10).

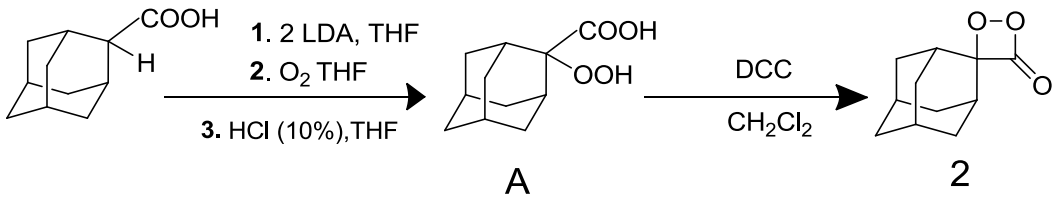

Scheme 10: *spiro*-adamantyl α-peroxy lactone obtained from the 2-adamantanecarboxylic acid

4.1.3. Synthesis of 4-(3-tert-butyldimethylsilyloxyphenyl)-4-methoxyspiro[1.2-dioxetane-3.2'-adamantane](3)

I am highly grateful to Dr.Luiz Francisco Monteiro Leite Ciscato (UFABC) because he provided this compound to me for the CL study. We took the ^{1}H-NMR and ^{13}C-NMR spectra in order to know its identity and purity, as a result following values have been got which are in good agreement with literature.[73]

NMR ^{1}H ($CDCl_3$), 500 MHz 25 °C**:** δ = 0.22[s, 6H, $Si(CH_3)_2$], 1.00[s, 9H, $C(CH_3)_3$], 1.00 -2.29(m, 12, adamantane), 2.29(s, 1H, adamantane, 3.04(s 1H, adamantane), 3.26(s, 3H, OCH_3), 7.28-7.31(m, 4H ArH) ppm.

NMR ^{13}C ($CDCl_3$), 500 MHz 25 °C**:** δ = -4.4, 18.24, 25.68, 25.68, 26.08, 31.54, 32.80, 36.46, 38.84, 49.92, 76.78, 77.04, 77.28. 95.53, 112.07, 119.44, 121.07, 124.03, 125.54, 129.44, 136.16, 138.76, 155.86 ppm.

4.2. Kinetic studies with diphenoyl peroxide

4.2.1. Kinetic study of diphenoyl peroxide using perylene as an activator

The decomposition of diphenoyl peroxide (1.0 mmol L^{-1}) catalyzed by perylene (0.5 to 3.0 mmol L^{-1}) in ethyl acetate and first order decay curves of the emission intensity were obtained (Figure 10).

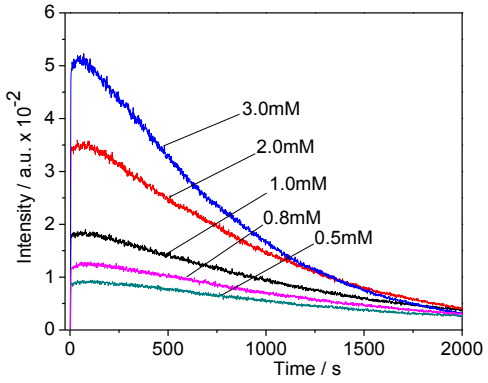

Figure 10: Emission intensity decay versus time in the reaction of diphenoyl peroxide(1.0 mmol L^{-1}) with different concentrations of perylene (PER); ethyl acetate at 36 °C; conditions: emission slit = 5 nm and photomultiplier voltage = 950 V.

The emission intensity was always maximam at acquisition time zero and displayed a first order kinetic decay and the CL light intensity decay has been recorded for at least three half-life times for all experiments. The observed rate constants (k_{obs}) have been got through fitting the intensity contrast time curves by employing a mono exponential decay function (Table 9).

The magnitude of the observed rate constants (k_{obs}) increases with the increase of polarity of solvent (Figure 11). Moreover, the magnitude of the observed rate constants (k_{obs}) also increased with the increasing the concentrations of perylene as an ACT (Figure 11, 13).

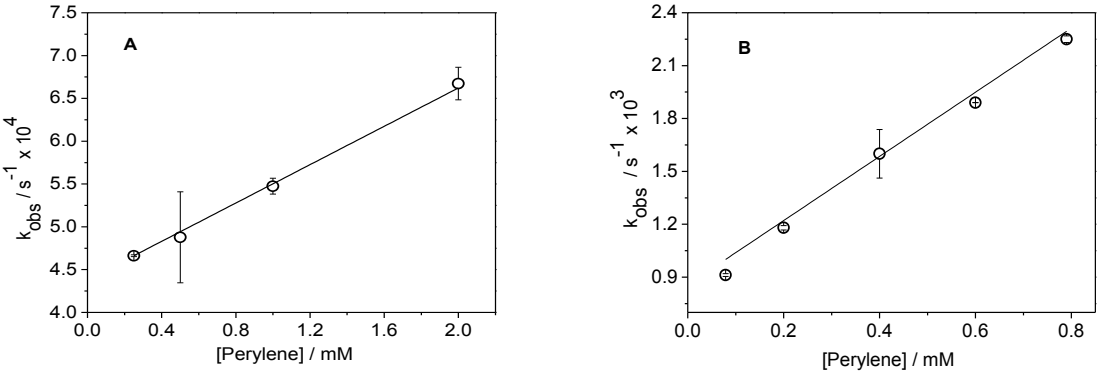

Figure 11: Dependence of the observed rate constants (k_{obs}) on the concentrations of perylene (PER), in butyl acetate (A) and acetonitrile (B), at 36 °C.

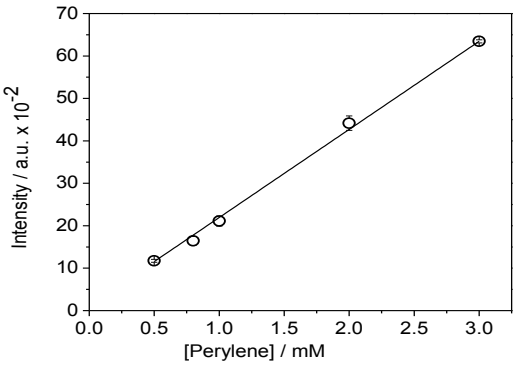

Figure 12: Correlation of the initial intensities (I_0) with the perylene concentration; ethyl acetate, at 36 °C.

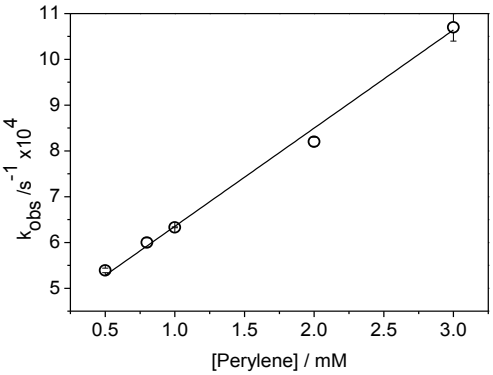

Figure 13: Correlation of the observed rate constants (k_{obs}) with the perylene concentration; ethyl acetate at 36 °C.

The areas under the emission intensity curves correspond to the total amount of light emission by the specific reaction and is therefore, proportional to the CL quantum yield (Φ_{CL}). In order to obtain this quantum yield, the emission intensity registered in arbitrary units (a.u. s^{-1}) was transformed into absolute light units (Einstein s^{-1}) through calibration of the photomultiplier tube (PMT) with the luminol standard (*see* Experimental for details)[43]

Table 9: Initial emission intensities (I_o), observed rate constants (k_{obs}), area under emission curve (area) and percentage of catalyzed decomposition for the reaction of diphenoyl peroxide with perylene in ethyl acetate.

[PER] / mM	I_o / a.u. × 10^{-2}	k_{obs} / s^{-1} × 10^4	Area / a.u. × 10^{-6}	P^{CAT} / %
0.5	11.70 ± 0.01	5.4 ± 0.1	2.2 ± 0.2	19
0.8	16.40 ± 0.03	6.0 ± 0.4	2.7 ± 0.2	28
1.0	21.0 ± 0.1	6.8 ± 0.3	3.09 ± 0.17	32
2.0	44.0 ± 0.1	8.8 ± 0.2	5.03 ± 0.29	49
3.0	63.40 ± 0.03	10.7 ± 0.3	5.95 ± 0.22	59

Conditions: emission slit = 5 nm and photomultiplier voltage = 950 V.

As outlined above (Introduction) the CL quantum yields can be determined from the integrated kinetic emission intensity curves (in Einstein units) in relation to the number of mols of limiting reagent. The CL quantum yields (Φ_{CL}), divided by the fluorescence quantum yield of the ACT (Φ_{FL}^{ACT}), result the singlet chemiexcitation quantum yield (Φ_S), corresponding to the number of excited ACT molecules formed in the reaction per limiting reactant molecule. As the reaction of DPP with the ACT is always composed by the catalytic pathway and the unimolecular decomposition of the peroxide, the singlet quantum yield of the catalytic pathway (Φ_S^{CAT}) can be calculated from Φ_S by considering the fractioning factor (P^{CAT}) for the catalyzed decomposition (Equation 33).

$$P^{CAT} = \frac{k_{CAT}[ACT]}{k_D + k_{CAT}[ACT]} \text{ x } 100 \qquad \text{Equation 33}$$

Table 10: Chemiluminescence (Φ_{CL}) and chemiexcitation quantum yields (Φ_S and Φ_S^{CAT}) for the decomposition of diphenoyl peroxide in the presence of perylene in ethyl acetate.

[PER] / mM	Φ_{CL} (E mol^{-1}) ×10^5	Φ_S (E mol^{-1}) ×10^5	Φ_S^{CAT} (Emol^{-1}) ×10^4
0.5	1.8 ± 0.1	2.1 ± 0.2	1.1 ± 0.1
0.8	2.3 ± 0.2	2.7 ± 0.2	0.97 ± 0.08
1.0	2.6 ± 0.1	3.01 ± 0.16	0.94 ± 0.05
2.0	4.3 ± 0.2	4.9 ± 0.2	1.0 ± 0.1
3.0	5.1 ± 0.2	5.8 ± 0.2	0.98 ± 0.04

Conditions: emission slit = 5 nm and photomultiplier voltage = 950 V.

The CL and singlet quantum yields for the reaction of DPP with perylene increase with increasing ACT concentrations; as expected, the Φ_S^{CAT} showed to be independent of [ACT] and in the order of 1.0 10^{-4} E mol^{-1} (Table 10).

Absolute singlet quantum yields (Φ_S) have been caculated from the calibrated chemiluminescence quantum yields (Φ_{CL} in E mol^{-1}) and fluorescence quantum yields (Φ_{FL}) of rubrene (Φ_{FL} = 0.98) and of perylene (Φ_{FL} = 0.87 in high polar solvent)[74] as well as (Φ_{FL} = 0.89 in low polar solvent like toluene).[75-77] The difference between fluorescence quantum yields (Φ_{FL}) of perylene in low polar and high polar solvent is less than 3%. These quantum yields do not change for the low polar and high polar solvents, therefore, the fluorescence quantum yields of perylene (Φ_{FL} = 0.87) and rubrene (Φ_{FL} = 0.98) were used for all of the systems.

4.2.2. Kinetic study of the perylene catalyzed decomposition of diphenoyl peroxide using pure solvents

The experiments were performed to study the solvent influence on the CL parameters of the decomposition of diphenoyl peroxide with perylene (PER) as an activator using some selected solvents on the basis of different polarity and same viscosity values.

Table 11: Observed rate constants (k_{obs}), area under emission curve (area) and chemiexcitation parameters (Φ_S and Φ_S^{CAT}) for the decomposition of diphenoyl peroxide in the presence of perylene.

Solvents	[PER] / mM	k_{obs} / s^{-1} x 10^4	Area / a.u. x 10^{-6}	Φ_S (E mol^{-1}) x 10^5	Φ_S^{CAT} (E mol^{-1}) x 10^5
dibutyl ether	0.6	2.6 ± 0.3	5.7 ± 0.1	1.63 ± 0.01	4.53 ± 0.04
	0.7	2.7 ± 0.1	6.9 ± 0.1	1.96 ± 0.03	4.95 ± 0.01
	0.8	2.9 ± 0.1	7.4 ± 0.2	2.1 ± 0.1	4.92 ± 0.01
	0.9	3.0 ± 0.1	8.7 ± 0.1	2.49 ± 0.05	5.44 ± 0.01
diethyl ether	0.5	2.06 ± 0.60	0.82 ± 0.04	0.23 ± 0.01	1.23 ± 0.02
	0.6	2.1 ± 0.6	0.84 ± 0.11	0.24 ± 0.03	1.06 ± 0.02
	0.7	2.2 ± 0.2	0.91 ± 0.02	0.26 ± 0.01	1.05 ± 0.02
	0.8	2.3 ± 0.5	0.95 ± 0.04	0.27 ± 0.01	0.90 ± 0.02
anisole	0.2	8.95 ± 0.05	2.70 ± 0.02	1.67 ± 0.01	12.0 ± 0.1
	0.3	9.6 ± 0.1	2.4 ± 0.2	2.4 ± 0.2	12.0 ± 1.0
	0.4	10.3 ± 0.2	3.02 ± 0.03	2.95 ± 0.03	12.1 ± 0.1
	0.5	10.8 ± 0.1	3.8 ± 0.2	3.7 ± 0.2	12.9 ± 0.1
	0.6	11.7 ± 0.7	4.3 ± 0.3	4.2 ± 0.3	13.0 ± 1.0
BUTY	0.25	4.45 ± 0.01	0.9 ± 0.1	0.9 ± 0. 1	15.5 ± 0.4
	0.5	4.8 ± 0.9	1.9 ± 0.2	1.9 ± 0.2	16.7 ± 0.3
	1.0	5.5 ± 0.1	3.1 ± 0.1	3.0 ± 0.1	15.1 ± 0.1
	2.0	6.5 ± 0.1	4.7 ± 0.1	4.6 ± 0.1	14.0 ± 0.1
THF	0.25	5.71 ± 0.03	1.75 ± 0.03	1.70 ± 0.03	21.3 ± 0.1
	1.0	7.1 ± 0.2	3.6 ± 0.4	3.5 ± 0.4	14.0 ± 2.0
	2.0	8 .9 ± 0.1	7.31 ± 0.01	7.15 ± 0.01	20.4 ± 0.1
	3.0	10.7 ± 0.2	8.91 ± 0.03	8.72 ± 0.03	20.0 ± 0.1
DBP	0.1	11.2 ± 0.1	1.72 ± 0.01	1.68 ± 0.01	19.4 ± 0.1
	0.2	12.3 ± 0.3	3.0 ± 0.2	2.94 ± 0.17	18.4 ± 0.1
	0.4	14.2 ± 0.4	5.1 ± 0.3	4.93 ± 0.28	18.0 ± 0.1
	0.5	15.2 ± 0.1	5.70 ± 0.02	5.56 ± 0.02	18.0 ± 0.1
acetone	0.4	6.8 ± 0.4	2.9 ± 0.2	3.5 ± 0.2	16.3 ± 0.1
	0.5	7.07 ± 0.04	3.6 ± 0.1	4.4 ± 0.1	17.0 ± 0.1
	0.6	7.5 ± 0.1	4.1 ± 0.2	5.0 ± 0.3	17.1 ± 0.2
	0.7	7.8 ± 0.3	4.5 ± 0.2	5.5 ± 0.3	17.0 ± 0.1
	0.8	8.1 ± 0.1	4.9 ± 0.2	5.9 ± 0.2	17.0 ± 0.5

[DPP]= 1.0 mmol L^{-1}; conditions: emission slit = 5 nm and photomultiplier voltage = 950 V; BUTY = butyl acetate; DMP = dimethyl phthalate; DBP = di-n-butyl phthalate.

Table 12: Observed rate constants (k_{obs}), area under emission curve (area) and chemiexcitation parameters (Φ_S and Φ_S^{CAT}) for the decomposition of diphenoyl peroxide in the presence of perylene

Solvents	[PER] / mM	k_{obs} / s^{-1} × 10^4	Area / a.u.×10^{-6}	Φ_S (E mol^{-1})x 10^5	Φ_S^{CAT} (E mol^{-1}) x 10^5
Pyrrolidinone	0.2	6.8 ± 0.3	3.8 ± 0.4	3.7 ± 0.4	21.8 ± 0.3
	0.4	7.77 ± 0.02	6.5 ± 0.1	6.4 ± 0.1	21.8 ± 0.2
	0.6	8.81 ± 0.01	8.9 ± 0.2	8.7 ± 0.2	22.6 ± 0.4
	0.65	9.11 ± 0.01	9.8 ± 0.5	9.6 ± 0.2	23.7 ± 0.1
DMF	0.07	5.2 ± 0.5	0.9 ± 0.1	0.9 ± 0.1	3.10 ± 0.01
	0.2	10.5 ± 0.2	2.1 ± 0.5	2.2 ± 0.4	3.6 ± 0.2
	0.4	15.2 ± 0.8	4.2 ± 0.1	4.1 ± 0.2	5.75 ± 0.02
	0.7	20.5 ± 0.5	5.9 ± 0.1	5.7 ± 0.1	7.08 ± 0.01
ACN	0.079	9.1 ± 0.1	0.42 ± 0.01	0.41 ± 0.01	2.7 ± 0.1
	0.2	11. 8 ± 0.1	0.87 ± 0.02	0.85 ± 0.01	2.67 ± 0.03
	0.4	16.0 ± 0.9	1.27 ± 0.03	1.23 ± 0.02	2.6 ± 0.1
	0.6	18.90 ± 0.01	1.64 ± 0.04	1.59 ± 0.03	2.8 ± 0.1
	0.79	22.50 ± 0.01	1.85 ± 0.02	1.80 ± 0.02	2.8 ± 0.1

[DPP] = 1.0 mmol L^{-1}; conditions: emission slit = 5 nm and photomultiplier voltage = 950 V.

The first-order rate constant k_{obs} of CL decay in diphenoyl peroxide is linearly dependent on the concentration of ACT leading to the determination of the catalytic rate constant (k_{CAT}). The area under the curve increases with increasing the concentration of ACT which shows the quantity of emitted photons. Chemiexcitation (Φ_S and Φ_S^{CAT}) for the decomposition of diphenoyl peroxide increase with increasing the concentration of perylene (PER).

$$k_{obs} = k_D + k_{CAT}\,[ACT] \qquad \text{Equation 34}$$

The rate equation describing the process comprises the unimolecular and bimolecular path, where k_{obs} is the observed first-order rate constant which consists of the contribution of unimolecular decomposition rate constant (k_D) and the contribution of the catalytic decomposition rate constant (k_{CAT}) (Equation 34). It is explained here that how to get unimolecular decomposition (k_D) and the catalytic decomposition rate constant (k_{CAT}). The graph made by

correlation of the observed rate constants (k_{obs}) with the perylene concentration (Figure 13), cosequently, intercept which is known as unimolecular decomposition rate constant (k_D) and obtained slope which is called as catalytic decomposition rate constant (k_{CAT}). The values of unimolecular decomposition rate constant (k_D) and catalytic decomposition rate constant (k_{CAT}) have been shown in discussion part.

4.2.3. Kinetic study of the catalyzed decomposition of diphenoyl peroxide with perylene as activator using binary solvent mixtures

The selected binary solvent mixture systems have same viscosity parameters however, have different polarity and polarizability parameters which is an essential need for investigating influence of solvent's polarity on chemiexcitation systems initiated by intermolecular electron transfer systems. The perylene catalyzed decomposition of diphenoyl peroxide system has been studied in binary mixture of toluene and acetone which have similar viscosity but different polarity parameters.

Table 13: Observed rate constants (k_{obs}), CL quantum yields (Φ_{CL}) and singlet quantum yields (Φ_S) for the decomposition of diphenoyl peroxide (**1**) using perylene as a catalyst at 36 °C.

%solvent	$E_T(30)$	k_{obs} / s^{-1} x10^3	Φ_{CL} (E mol^{-1}) x10^6	Φ_S (E mol^{-1}) x10^6
toluene	34.2	2.29 ± 0.05	5.3 ± 0.5	6.1 ± 0.7
20% acetone	36.2	2.20 ± 0.08	6.12 ± 0.57	7.03 ± 0.66
40% acetone	38.2	2.28 ± 0.05	8.02 ± 0.31	9.2 ± 0.4
60% acetone	40.0	2.34 ± 0.12	9.33 ± 0.27	10.7 ± 0.3
80% acetone	41.6	2.37 ± 0.38	10.4 ± 0.6	11.9 ± 0.7
acetone	42 .2	2.39 ± 0.11	11.8 ± 0.3	13.5 ± 0.4

[DPP]= 1.0 mmol L^{-1}; [PER] = 0.7 mmol L^{-1}; conditions: emission slit = 5 nm and photomultiplier voltage = 950 V.

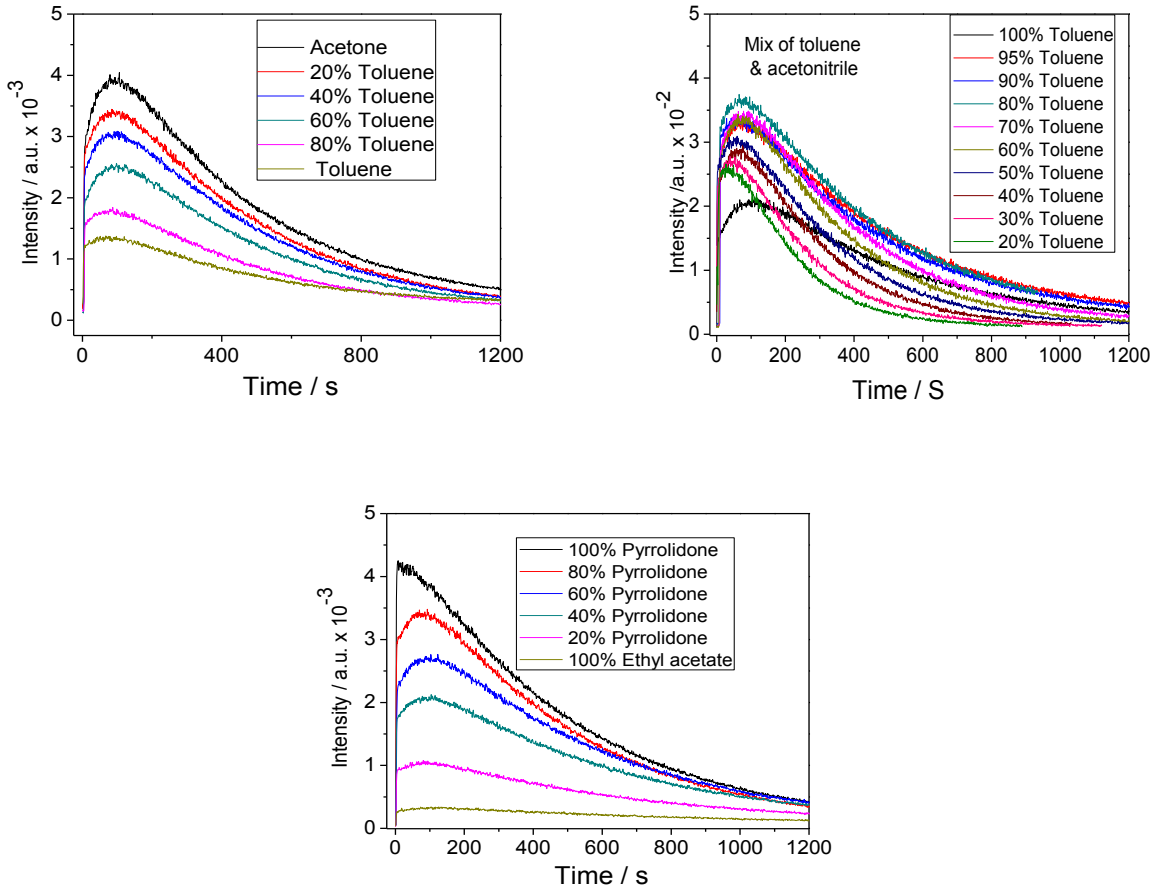

Figure 14: Emission intensity decay versus time in the reaction of diphenoyl peroxide(1.0 mmol L^{-1}) with perylene (PER) as an activator at 36 °C; in binay solvent mixtures; conditions: emission slit = 5 nm and photomultiplier voltage = 950 V.

The observed rate constants showed to be insentive to the percentage of acetone in toluene with a variation of less than 10% between the pure solvents and a mean value of $2.31 \pm 0.13\ 10^{-3}\ s^{-1}$ (Table 13).

The same system has been studied in binary mixture of toluene and acetonitrile which has also similar viscosities but different polarity parameters in order to confirm the polarity effect of solvents on quantum yields.

Table 14: Observed rate constants (k_{obs}), area (a.u.) and singlet quantum yields (Φ_S) for the decomposition of diphenoyl peroxide (**1**) using perylene as a catalyst, at 36 °C; in toluene /acetonitrile mixtures.

Solvent system	$E_T(30)$	k_{obs} / s^{-1} x 10^3	Área / a.u. x 10^{-5}	Φ_S(E mol^{-1}) x 10^5
100 % TOL	34.2	1.90 ± 0.1	1.50 ± 0.15	2.4 ± 0.2
95% TOL	39.7	2.24 ± 0.19	1.95 ± 0.05	3.1 ± 0.2
90% TOL	40.8	2.28 ± 0.11	2.01 ± 0.01	3.2 ± 0.1
80% TOL	41.4	2.62 ± 0.47	2.1 ± 0.1	3.3 ± 0.1
70% TOL	42.6	2.79 ± 0.12	1.73 ± 0.01	2.73 ± 0.01
60% TOL	43.06	3.16 ± 0.14	1.5 ± 0.1	2.4 ± 0.1
50% TOL	43.8	3.48 ± 0.13	1.30 ± 0.03	2.06 ± 0.04
40% TOL	44.0	3.9 ± 0.1	1.05 ± 0.01	1.66 ± 0.01
30% TOL	44.5	4.6 ± 0.2	0.89 ± 0.01	1.40 ± 0.01
20% TOL	45.24	5.37 ± 1.5	0.71 ± 0.02	1.11 ± 0.02

[DPP]= 1.0 mmol L^{-1}; [PER] = 3.0 mmol L^{-1}; conditions: emission slit = 5 nm and photomultiplier voltage = 950 V.

The observed rate constants (k_{obs}) increased with increase the polarity of solvent, it is raised by a factor of around 2.8 from toluene to acetonitrile (ACN) (Table 14).

The perylene catalyzed decomposition of diphenoyl peroxide has also been studied in binary mixture of ethyl acetate and 1-methyl-2-pyrrolidinone which have different viscosity and different polarity parameters in order to know which parameter acts as a major by using mulitple linear regression function.

The observed rate constants (k_{obs}) increased from 1.3 to 2.2 10^{-3} s^{-1} from pure ethylacetate to pure 1-methyl-2-pyrrolidinone, an increase by a factor of 1.7 (Table15).

Table 15: Observed rate constants (k_{obs}), intensity (a.u.) and singlet quantum yields (Φs) for the decomposition of diphenoyl peroxide (**1**) using perylene as a catalyst at 36 °C.

Solvent system	η (cP)	$E_T(30)$	k_{obs} / s^{-1} x 10^3	Φ_S (E mol^{-1}) x 10^5
ethyl acetate	0.42	38.1	1.3 ± 0.9	0.50 ± 0.01
20% pyrrolidinone	2.97	38.89	1.6 ± 0.2	0.93 ± 0.04
40% pyrrolidinone	5.5	39.67	1.7 ± 0.1	1.68 ± 0.02
60% pyrrolidinone	8.0	40.45	1.8 ± 0.5	2.03 ± 0.04
80% pyrrolidinone	10.5	41.23	2.2 ± 0.6	2.30 ± 0.03
pyrrolidinone	13.0	42.2	2.2 ± 0.1	2.41 ± 0.02

[DPP]= 1.0 mmol L^{-1}; [PER] = 0.4 mmol L^{-1}; conditions: emission slit = 5 nm and photomultiplier voltage = 950 V.

Table 16: Catalytic rate constants (k_{CAT}) and unimolecular decomposition rate constants (k_D) and catalyzed singlet quantum yields (Φ_S^{CAT}) for the decomposition of diphenoyl peroxide (**1**) using perylene as catalyst at 36 °C.

Solvent (A)	Solvent (B)	$E_T(30)$	k_{CAT} / L mol^{-1} s^{-1}	k_D/ s^{-1} x 10^{-3}	Φ_S^{CAT} (E mol^{-1}) x 10^4
100% TOL	0% EA	34.2	0.44 ± 0.01	1.53 ± 0.01	0.53 ± 0.01
80% TOL	20% EA	35.6	0.43 ± 0.08	1.35 ± 0.01	0.6 ± 0.1
60% TOL	40% EA	36.3	0.39 ± 0.01	1.17 ± 0.01	0.66 ± 0.02
40% TOL	60 % EA	37.4	0.38 ± 0.01	1.00 ± 0.04	0.7 ± 0.1
20% TOL	80% EA	38.2	0.35 ± 0.02	1.0 ± 0.3	0.84 ± 0.02
100% EA	0% ACE	38.5	0.19 ± 0.01	0.5 ± 0.1	1.0 ± 0.2
80% EA	20% ACE	39.0	0.150 ± 0.001	0.60 ± 0.01	1.1 ± 0.1
40% EA	60% ACE	40.7	0.20 ± 0.01	0.81 ± 0.01	2.3 ± 0.2
20% EA	80% ACE	41.4	0.35 ± 0.02	0.87 ± 0.01	1.9 ± 0.1
0% EA	100% ACE	42.2	0.35 ± 0.03	0.53 ± 0.02	1.7 ± 0.1

TOL = toluene; EA = ethyl acetate; ACE = acetone; [DPP] = 1.0 mmol L^{-1}; conditions: emission slit = 5 nm and photomultiplier voltage = 950 V.

The same system has been studied in binary mixture of toluene/ethyl acetate and ethyl acetate/acetone which have same viscosity and different polarity parameters.

The results in these studies indicate that the catalytic rate constant (k_{CAT}) is higher in toluene as compared to ethyl acetate by a factor of around 2.3. The unimolecular rate constant (k_D) also increased with increasing proportion of toluene, having a factor of around 3 for the values in pure solvents (Table 16). The magnitude of the catalytic decomposition rate constant (k_{CAT}) increased with increasing the polarity; for varying the polarity parameter [E_T(30] from E_T(30) = 39 (20% acetone) to E_T(30) = 41.4 (80% acetone) indicate increase in the magnitude by a factor of almost 2.4.

4.2.4. Kinetic studies of the catalyzed decomposition of diphenoyl peroxide using rubrene as an activator

The catalyzed decomposition of diphenoyl peroxide (1.0 mmol L^{-1}) is studied by utilizing rubrene as an activator. The concentrations of the activator [RUB] have been used in the range of 0.4 to 0.75 mmol L^{-1} in anhydrous ethyl acetate.

Table 17: Initial emission intensities (I_o), observed rate constants (k_{obs}) , area under emission curve (area) and percentage of catalyst for the decomposition of diphenoyl peroxide using rubrene as an activator.

[RUB] / mM	I_o / a.u. x10^{-2}	k_{obs} / s^{-1} x 10^4	Area / a.u. x 10^{-6}	P^{CAT}/ %
0.4	36.1 ± 0.1	27.1 ± 0.1	1.3 ± 0.1	63
0.5	43.7 ± 0.8	31.60 ± 0.01	1.4 ± 0.1	68
0.6	54.4 ± 0.4	36.5 ± 0.2	1.5 ± 0.1	72
0.75	73.2 ± 0.9	41.60 ± 0.01	1.76 ± 0.03	76

Conditions: emission slit = 2.5 nm and photomultiplier voltage = 700 V.

Table 18: Chemiluminescence quantum yields (Φ_{CL}) and chemiexcitation (Φ_S and Φ_S^{CAT}) for the decomposition of diphenoyl peroxide in the presence of rubrene.

[RUB] / mM	Φ_{CL} (E mol$^{-1)}$ x10^5	Φ_S (E mol^{-1}) x10^5	Φ_S^{CAT} (E mol^{-1}) x10^4
0.4	29.8 ± 0.1	30.4 ± 0.1	4.83 ± 0.04
0.5	33.1 ± 0.2	33.8 ± 0.2	4.96 ± 0.04
0.6	38.8 ± 0.1	39.6 ± 0.1	5.52 ± 0.03
0.75	42.0 ± 0.1	42.9 ± 0.1	5.63 ± 0.04

Conditions: emission slit = 2.5 nm and photomultiplier voltage = 700 V.

Time-profiles for the emission intensity decay in the reaction of diphenoyl peroxide with different concentrations of rubrene (RUB) (Figure 15) Initial intensity increases with increasing the concentration of rubrene (RUB) (Figure 16). The value of the observed rate constant k_{obs} changes with changing the concentration of rubrene (RUB) and a linear dependence is found between the concentration of (RUB) and k_{obs} (Figure 17). Chemiluminescence quantum yields (Φ_{CL}) increase with increasing the concentration of rubrene (RUB) (Figure 18).

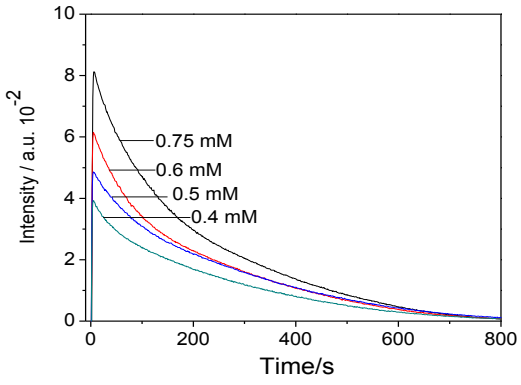

Figure 15: Time versus emission intensity decay in the reaction of diphenoyl peroxide with different concentrations of rubrene (RUB); ethyl acetate at 26 °C.

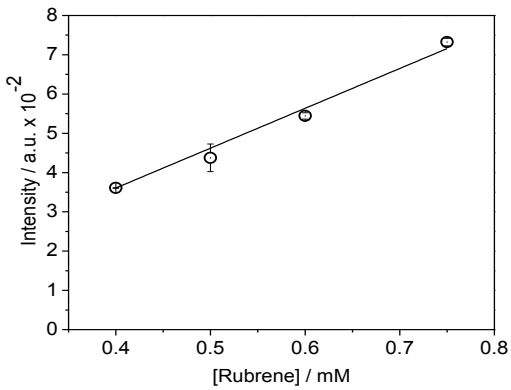

Figure 16: The initial intensity (I_0) depends on the concentrations of rubrene (RUB); ethyl acetate at 26 °C.

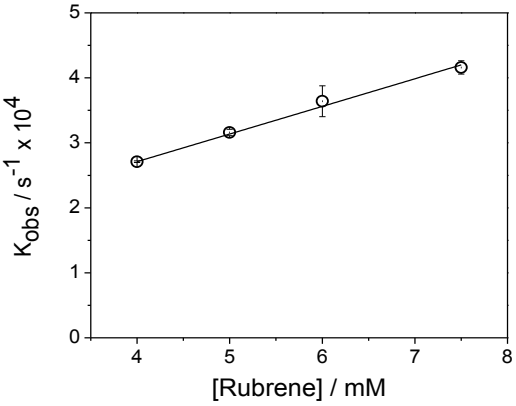

Figure 17: The observed rate constants (k_{obs}) depends on the concentrations of rubrene (RUB); ethyl acetate at 26 °C.

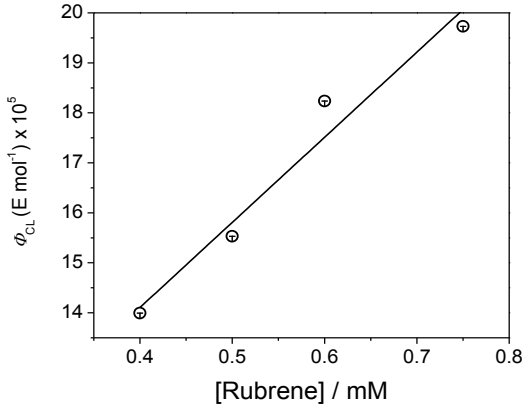

Figure 18: The chemiluminescence quantum yield (Φ_{CL}) increases with increasing the concentration of rubrene (RUB); ethyl acetate at 26 °C.

4.2.5. Kinetic study of the rubrene catalyzed decomposition of diphenoyl peroxide using pure solvents

The catalyzed decomposition of diphenoyl peroxide (1.0 mmol L^{-1}) is studied by using rubrene as an activator with different concentration in different pure solvents.

Table 19a: Observed rate constants (k_{obs}), area under emission curve (area) and chemiexcitation (Φ_S and Φ_S^{CAT}) for the decomposition of diphenoyl peroxide using rubrene as an activator.

Solvent	[RUB] / mM	k_{obs} / s^{-1} x 10^4	Area / a.u.x10^{-5}	Φ_S (E mol^{-1}) x10^4	Φ_S^{CAT} (E mol^{-1}) x10^3
anisole	0.05	15.6 ± 0.3	5.5 ± 0.4	2.9 ± 0.2	4.4 ± 0.2
	0.1	17.9 ± 0.5	8.7 ± 0.5	4.5 ± 0.3	5.8 ± 0.2
	0.2	22.0 ± 0.2	12.8 ± 1.0	6.6 ± 0.7	4.4 ± 0.2
	0.3	25.3 ± 0.3	18.30 ± 0.04	9.48 ± 0.02	4.2 ± 0.2
BUTY	0.04	8.9 ± 0.2	2.0 ± 0.3	1.1 ± 0.1	0.67 ± 0.03
	0.05	9.4 ± 0.1	2.6 ± 0.4	1.3 ± 0.2	0.70 ± 0.02
	0.1	11.0 ± 0.1	4.5 ± 0.4	2.3 ± 0.2	0.72 ± 0.06
	0.2	14.4 ± 0.6	6.8 ± 0.4	3.5 ± 0.2	0.71 ± 0.04
THF	0.2	9.39 ± 0.01	2.60 ± 0.01	1.35 ± 0.01	0.61 ± 0.03
	0.3	10.7 ± 0.1	3.97 ± 0.04	2.06 ± 0.02	0.68 ± 0.01
	0.4	11.60 ± 0.01	4.71 ± 0.02	2.45 ± 0.01	0.66 ± 0.01
	0.5	12.6 ± 0.1	5.91 ± 0.04	3.07 ± 0.01	0.72 ± 0.01
DMP	0.05	30.5 ± 0.2	5.61 ± 0.02	2.91 ± 0.01	12.8 ± 0.1
	0.06	32.0 ± 0.1	7.18 ± 0.02	3.73 ± 0.01	12.73 ± 0.04
	0.07	34.1 ± 0.1	9.50 ± 02	4.94 ± 0.01	14.48 ± 0.04
	0.09	36.8 ± 0.4	13.10 ± 0.03	6.82 ± 0.01	14.54 ± 0.01
	0.1	39.2 ± 0.6	15.7 ± 0.4	8.1 ± 0.2	16.7 ± 0. 1

[DPP] = 1.0 mmol L^{-1}; RUB = rubrene; BUTY = butyl acetate; THF = tetrahydrofuran; DMP = dimethyl phthalate; conditions: emission slit = 2.5 nm and photomultiplier voltage = 700 V.

Table 19b Observed rate constants (k_{obs}), area under emission curve (area) and chemiexcitation parameters (Φ_S and Φ_S^{CAT}) for the decomposition of diphenoyl peroxide using rubrene as an activator.

Solvent	[RUB] / mM	k_{obs} / s^{-1} x 10^4	Area / a.u. x10^{-5}	Φ_S (E mol^{-1}) x10^4	Φ_S ^{CAT} (E mol^{-1}) x10^3
DBP	0.025	20.7 ± 0.1	3.6 ± 0.1	1.9 ± 0.1	2.14 ± 0.02
	0.05	23.4 ± 0.7	6.5 ± 0.1	3.39 ± 0.06	2.12 ± 0.04
	0.1	27.8 ± 0.1	10.8 ± 0.3	5.6 ± 0.2	2.0 ± 0.1
	0.2	32.6 ± 0.3	18.3 ± 0.3	9.5 ± 0.2	2.16 ± 0.04
	0.3	36.2 ± 1	22.7 ± 0.4	11.7 ± 0.2	2.14 ± 0.02
aetone	0.007	6.7 ± 0.3	11.10 ± 0.02	0.23 ± 0.01	2.0 ± 0.1
	0.03	8.9 ± 0.2	36.4 ± 0.7	0.76 ± 0.01	1.88 ± 0.01
	0.05	10.1 ± 0.2	53.2 ± 3.4	1.11 ± 0.04	2.2 ± 0.1
	0.07	13.1 ± 0.2	67.5 ± 1.4	1.41 ± 0.02	2.39 ± 0.02
Pyrro	0.03	13.1 ± 0.1	5.7 ± 0.1	2.80 ± 0.04	11.3 ± 0.2
	0.05	14.10 ± 0.02	10.8 ± 1.0	4.3 ± 0.6	12.8 ± 1.8
	0.1	15.4 ± 0.6	18.7 ± 0.8	9.8 ± 0.4	10.1 ± 0.4
	0.2	18.3 ± 0.5	29.2 ± 0.4	14.2 ± 0.2	9.08 ± 0.04
	0.3	20.4 ± 0.1	37.70 ± 0.01	18.4 ± 0.1	8.04 ± 0.02
ACN	0.005	23.9 ± 0.3	6.80 ± 0.02	0.087 ± 0.002	0.34 ± 0.01
	0.006	24.0 ± 0.2	8.5 ± 0.1	0.11 ± 0.01	0.36 ± 0.01
	0.007	24.1 ± 0.2	9.63 ± 0.21	0.124 ± 0.03	0.35 ± 0.04
	0.008	24.3 ± 0.3	11.5 ± 0.1	0.15 ± 0.01	0.37 ± 0.02
	0.01	24.5 ± 0.1	13.70 ± 0.03	0.177 ± 0.001	0.35 ± 0.01

[DPP] = 1.0 mmol L^{-1}; RUB = rubrene; DBP = dibutyl phthalate; Pyrro = 1-methyl-2-pyrrolidinone; ACN = acetonitrile; conditions: emission slit = 2.5 nm and photomultiplier voltage = 700 V.

The observed rate constant increase with increasing the concentration of rubren (RUB), the area under the curve also increases with increasing the concentration of activator which shows the quantity of emitted photons. Chemiexcitation (Φ_S) for the decomposition of diphenoyl peroxide increase with increasing the concentration of rubrene (RUB), however, the catalyzed singlet quantum yield showed indpependent relationship to the concentration of rubrene (RUB) Table 19).

Table 20: Catalytic rate constants (k_{CAT}) and unimolecular decomposition rate constants (k_D) and catalyzed singlet quantum yields (Φ_S^{CAT}) for the decomposition of diphenoyl peroxide (**1**) using rubrene as catalyst at 25 °C.

solvent	ε_r	η (cP)	k_{CAT} / L mol^{-1} s^{-1}	k_D / s^{-1} x 10^3	Φ_S^{CAT} (E mol^{-1}) x 10^4
ANI	4.45	1.06	3.9 ± 0.2	1.30 ± 0.03	47.0 ± 2.0
BUTY	5.01	0.7	3.3 ± 0.2	0.70 ± 0.02	7.0 ± 0.4
EA	6.03	0.4	4.3 ± 0.2	1.0 ± 0.1	5.23 ± 0.04
THF	7.47	0,5	1.10 ± 0.01	0.72 ± 0.02	6.3 ± 0.4
DBP	6.44	16.6	6.7 ± 0.2	1.90 ± 0.04	21.0 ± 0.1
ACN	35.94	0.37	12.0 ± 1.0	2.30 ± 0.01	3.5 ± 0.2

[DPP] = 1.0 mmol L^{-1}; ε_r = dielectric constant; η = viscosity; ANI = anisole; BUTY = butyl acetate; EA = ethyl acetate; THF = tetrahydrofuran; DBP = dibutyl phthalate; ACN = acetonitrile.

The magnitude of the catalytic decomposition rate constant (k_{CAT}) increases with the increase of the dielectric constant (ε_r). However, k_{CAT} also appears to increase with the solvent viscosity (η), which is not necessarily expected (Table 20).

4.2.6. Kinetic studies of the catalyzed decomposition of diphenoyl peroxide using viscous binary solvent mixture

The solvent systems which utilized for this study consists of binary mixtures of toluene-diphenyl ether, toluene-dipheny methane and ethyl acetate-dibutyl phthalate which possesses similar physicochemical properties, except viscosity According to CIEEL mechanism, the electron transfer step must occur within the solvent cage. As these steps involve formation of charge and with an electron transfer that are responsible for formation of the excited state, it is expected that the viscosity and polarity must exert some influence on the yield of formation of excited states.

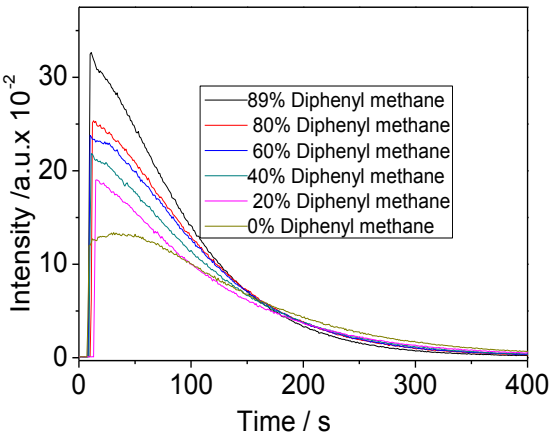

Figure 19: Time versus emission intensity decay in the reaction of diphenoyl peroxide (1.0 mmol L^{-1}) with rubrene (1 mmol L^{-1}) in the mixture of toluene and diphenyl ether at 25 °C.

In order to verify the influence of viscosity over an intermolecular CIEEL system, we selected to study the decomposition of the diphenoyl peroxide catalyzed with rubrene (1 mmol L^{-1}) in pure toluene and diphenylmethane and thieir mixtures, having different viscosities but have same polarity parameters.

Table 21: The observed rate constants (k_{obs}) and quantum yields depending on the viscosity of the mixture toluene / diphenyl methane on the decomposition of the diphenoyl peroxide (1.0 mmol L^{-1}) with rubrene as ACT at 25 °C.

% $CH_2\phi_2$	η (cP)	k_{obs} / s^{-1} x 10^3	Φ_S (E mol^{-1}) x10^4
0	0.52	8.5 ± 0.3	2.11 ± 0.06
20	0.82	9.3 ± 0.1	2.20 ± 0.06
40	1.05	10.1 ± 0.2	2.37 ± 0.08
60	1.37	10.2 ± 0.3	2.55 ± 0.06
80	2.17	11.0 ± 0.4	2.71 ± 0.03
89	2.57	13.0 ± 1.0	2.98 ± 0.01

Conditions: emission slit = 2.5 nm and photomultiplier voltage = 700 V.

The obtained results show that the observed rate constants (k_{obs}) change with viscosity for the diphenoyl peroxide system a slight increase by a factor of 1.5 is observed for higher viscosity medium.

The same system has also been studied in the binary mixtures of diphenyl ether and toluene which have similar polarity but different viscosity parameter.

Table 22: The observed rate constants (k_{obs}) and quantum yields depending on the viscosity of the mixture toluene / diphenyl ether on the decomposition of the diphenoyl peroxide (1.0 mmol L^{-1}) with rubrene (1.0 mmol L-1) as ACT at 36 °C.

% $o\phi_2$	η (cP)	k_{obs} / s^{-1} x 10^3	Φ_S (E mol^{-1}) x 10^4
0	0.52	3.3 ± 0.6	1.06 ± 0.01
25	0.74	4.9 ± 0.1	1.19 ± 0.02
50	1.1	6.3 ± 0.2	1.27 ± 0.01
75	1.6	7.3 ± 0.3	1.38 ± 0.06
95	2.1	6.5 ± 0.5	2.26 ± 0.18

Conditions: emission slit = 2.5 nm and photomultiplier voltage = 700 V

The observed rate constants (k_{obs}) raised with raising the viscosity of solvent for above system a slight increase by a factor of 2 is observed for higher viscosity mediums.

The same system has also been studied in mixtures of ethyl acetate / dibutyl phthalate which have similar polarity but different viscosity parameter.

Table 23: The rate constants (k_{CAT} and k_D), and quantum yields depending on the viscosity of the mixture ethyl acetate / dibutyl phthalate on the decomposition of the diphenoyl peroxide (1.0 mmol L^{-1}) perylene as ACT at 36 °C.

% DBP	η (cP)	k_{CAT} / L mol^{-1} s^{-1}	k_D / s^{-1} x 10^3	Φ_S^{CAT} x10^4 (Emol^{-1})
0	0.42	0.21 ± 0.01	0.45 ± 0.01	1.0 ± 0.2
20	0.61	0.285 ± 0.001	0.67 ± 0.01	1.1 ± 0.1
40	0.94	0.32 ± 0.01	0.87 ± 0.04	1.4 ± 0.2
60	1.67	0.40 ± 0.01	0.90 ± 0.05	1.48 ± 0.02
80	3.11	0.68 ± 0.01	1.01 ± 0.01	1.7 ± 0.4
100	9.63	0.95 ± 0.02	1.0 ± 0.1	1.8 ± 0.2

Conditions: emission slit = 5 nm and photomultiplier voltage = 950 V.

The catalytic decomposition rate constant (k_{CAT}) increases with the increase of the solvent viscosity (η) and the unimolecular rate constant (k_D) also increases with increasing the solvent viscosity (η) which is unexpected (Table 23). The experiments were made in only two experimental conditions; in pure ethyl acetate and pure dibutyl phthalate in order to better verify the behavior of solvent viscosity. The results are similar to those obtained above, there was an increase in the observed rate constant in parallel with the increase in emission intensity, which led to obtaining only a slight increase in the values of the Φ_S in more viscous medium (Table 24).

Table 24: Observed rate constants (k_{obs}), area under emission curve (area) and chemiexcitation (Φ_S) for the decomposition of diphenoyl peroxide (1.0 mmol L^{-1}) with perylene as ACT at 36 °C.

%DBP	η (cP)	k_{obs} / s^{-1} x 10^4	Area / a.u. x 10^{-6}	Φ_S (E mol^{-1}) x 10^5
0	0.36	5.5 ± 0.1	2.2 ± 0.2	2.1 ± 0.2
100	16.0	15.2 ± 0.8	4.9 ± 0.1	4.2 ± 0.1

Conditions: emission slit = 5 nm and photomultiplier voltage = 950 V.

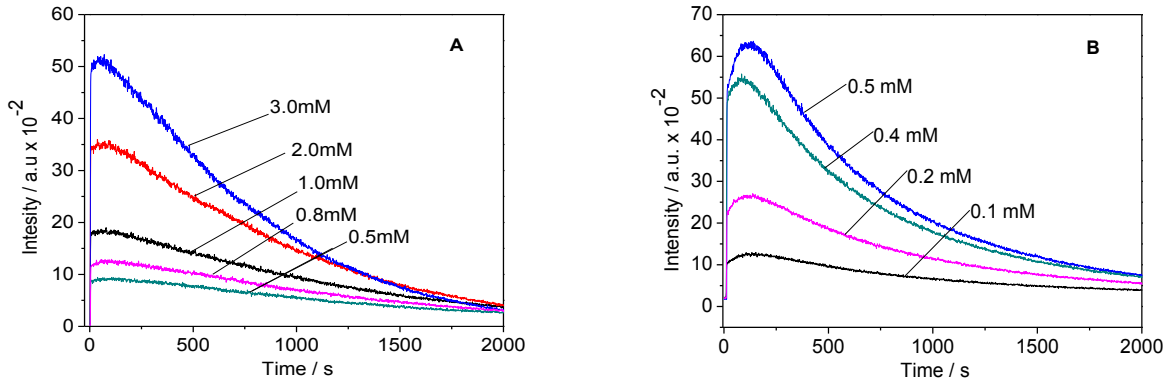

Figure 20: Time versus emission intensity decay in the reaction of diphenoyl peroxide with different concentrations of perylene (PER); ethyl acetate(A); dibutyl phthalate(B) at 36 °C.

Table 25: Initial emission intensities (I_o), observed rate constants (k_{obs}) and area under emission curve (area) for the decomposition of diphenoyl peroxide (1.0 mmol L^{-1}) in the dry ethyl acetate using perylene as activator at 36 °C.

[PER] / mM	I_o/ a.u. $\times 10^{-2}$	k_{obs} / s^{-1} $\times 10^{4}$	Area / a.u.$\times 10^{-6}$
0.5	1.17 ± 0.01	5.4 ± 0.1	2.2 ± 0.2
0.8	1.64 ± 0.03	6.0 ± 0.4	2.7 ± 0.2
1.0	2.1 ± 0.1	6.8 ± 0.03	3.09 ± 0.17
2.0	4.4 ± 0.1	8.8 ± 0.2	5.03 ± 0.29
3.0	6.34 ± 0.03	10.7 ± 0.3	5.95 ± 0.22

Conditions: emission slit = 5 nm and photomultiplier voltage = 950 V.

Table 26: Initial emission intensities (I_o), observed rate constants (k_{obs}) and area under emission curve (area) for the decomposition of diphenoyl peroxide (1.0 mmol L^{-1}) in the pure dibutyl phthalate using perylene as activator at 36 °C.

[PER] / mM	I_o/ a.u. $\times 10^{-2}$	k_{obs} / s^{-1} $\times 10^{3}$	Area / a.u. $\times 10^{-6}$
0.1	12.08 ± 0.01	1.12 ± 0.01	1.08 ± 0.01
0.2	28.44 ± 0.01	1.23 ± 0.03	2.3 ± 0.1
0.4	58.8 ± 0.2	1.42 ± 0.04	4.13 ± 0.02
0.5	75.0 ± 0.2	1.52 ± 0.01	4.9 ± 0.1

Conditions: emission slit = 5 nm and photomultiplier voltage = 950 V.

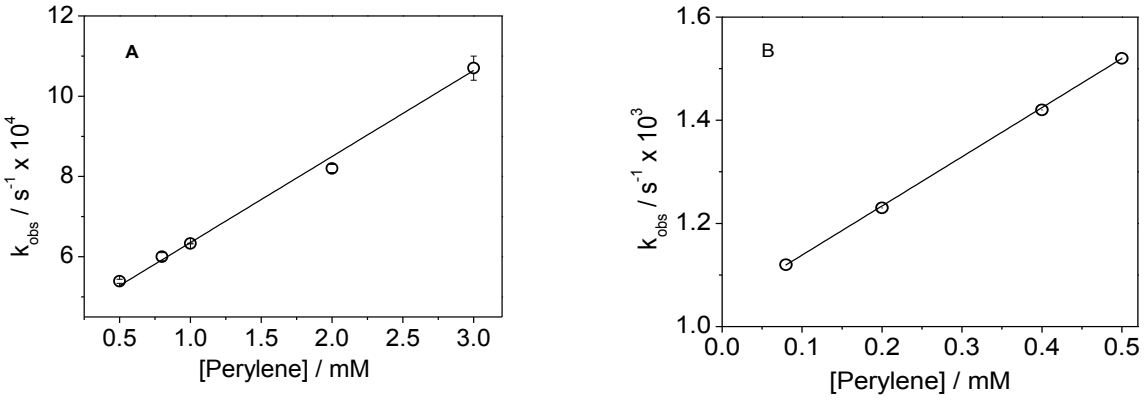

Figure 21: The observed rate constants (k_{obs}) depend on the concentrations of perylene (PER); ethyl acetate(A); dibutyl phthalate(B) at 36 °C.

Table 27: Chemiexcitation quantum yields (Φ_S), percentage of catalyst and catalyzed singlet quantum yields (Φ_S^{CAT}) for the decomposition of diphenoyl peroxide with different concentration of perylene at 36 °C in pure ethyl acetate.

[PER] / mM	Φ_S (E mol^{-1}) ×10^5	P^{CAT} / %	Φ_S^{CAT} (E mol^{-1})×10^4
0.5	2.1 ± 0.2	19	1.1 ± 0.1
0.8	2.7 ± 0.2	28	0.97 ± 0.08
1.0	3.0 ± 0.2	32	0.94 ± 0.05
2.0	4.9 ± 0.2	49	1.0 ± 0.1
3.0	5.8 ± 0.2	59	0.98 ± 0.04

Conditions: emission slit = 5 nm and photomultiplier voltage = 950 V; PER = perylene.

Table 28: Chemiexcitation quantum yields (Φ_S), percentage of catalyst and catalyzed singlet quantum yields (Φ_S^{CAT}) for the decomposition of diphenoyl peroxide with different concentration of perylene at 36 °C in pure butyl phthalate.

[PER] / mM	Φ_S (E mol^{-1}) ×10^5	P^{CAT} / %	Φ_S^{CAT} (E mol^{-1}) ×10^4
0.1	0.91 ± 0.01	9	1.931 ± 0.004
0.2	1.96 ± 0.04	16	1.84 ± 0.03
0.4	3.50 ± 0.02	28	1.81 ± 0.01
0.5	4.2 ± 0.1	32	1.73 ± 0.03

Conditions: emission slit = 5 nm and photomultiplier voltage = 950 V.

4.3. Kinetic studies of rubrene catalyzed decomposition *spiro*-adamantyl *a*-peroxy lactone (2)

The catalyzed decomposition of *spiro*-adamantyl-1,2-dioxetanone (0.075 mmol L^{-1}) has been studied by using rubrene as an activator and concentration range was used from 0.05 to 0.3 mmol L^{-1} in ethyl acetate and from 0.3 to 0.5 mmol L^{-1} in acetone solvent at 25 °C (Figure 22).

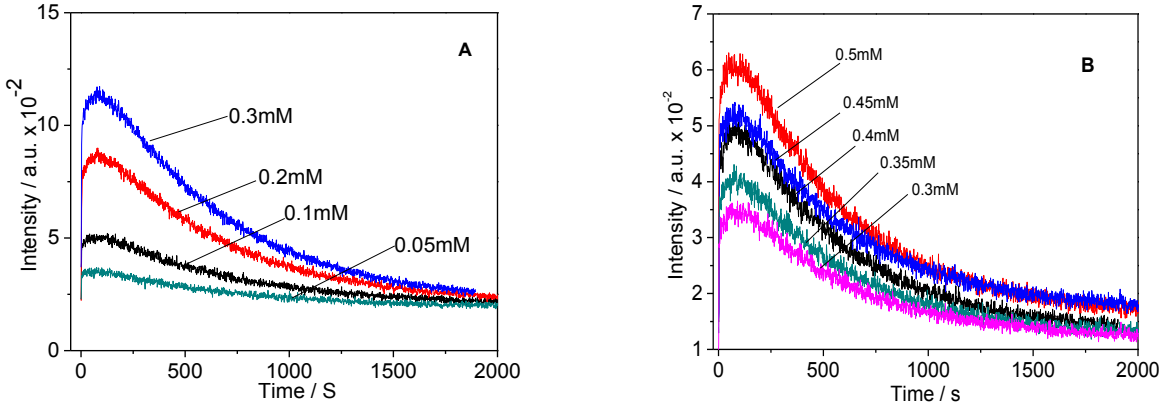

Figure 22: Time versus emission intensity decay for the reaction of *spiro*-adamantyl-1,2-dioxetanone with different concentrations of rubrene (RUB) in ethyl acetate (A); acetone (B) at 25 °C; conditions: emission slit = 20 nm and photomultiplier voltage = 950 V.

First order decay curves were obtained from the decomposition of *spiro*-adamantyl-1,2-dioxetanone with various concentrations of the activator and rate constants (k_{obs}), initial intensities (I_0) and the areas have been obtained from curve.

The observed rate constants (k_{obs}) do not depend on the concentration of activator (Figure 23).

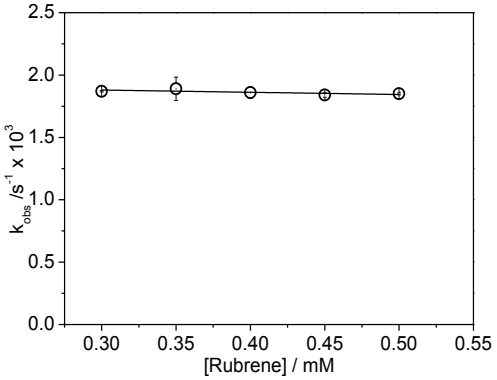

Figure 23: The relationship between the observed rate constants (k_{obs}) and the concentrations of rubrene (RUB) in acetone at 25 °C.

Table 29: Observed rate constants (k_{obs}), initial intensity (I_0) and chemiexcitation (Φ_{CL} and Φ_S) for the decomposition of *spiro*-adamantyl-1,2-dioxetanone using rubrene as an activator.

Solvent	[RUb] / mM	k_{obs} / s^{-1} × 10^3	I_o / a.u. ×10^{-2}	Φ_{CL} (E mol^{-1}) ×10^3	Φ_S (E mol^{-1})×10^3
BUTY	0.1	1.57 ± 0.09	2.1 ± 0.1	1.42 ± 0.02	1.45 ± 0.02
	0.2	1.56 ± 0.01	4.4 ± 0.4	2.05 ± 0.01	2.09 ± 0.02
	0.3	1.61 ± 0.03	9.1 ± 0.2	2.4 ± 0.3	2.4 ± 0.3
	0.4	1.61 ± 0.02	11.9 ± 0.3	3.3 ± 0.2	3.4 ± 0.2
EA	0.05	1.52 ± 0.16	1.93 ± 0.03	1.21 ± 0.01	1.24 ± 0.02
	0.1	1.54 ± 0.22	4.3 ± 0.8	1.6 ± 0.6	1.6 ± 0.6
	0.2	1.56 ± 0.02	8.27 ± 0.03	2.1 ± 0.2	2.2 ± 0.2
	0.3	1.59 ± 0.16	11.5 ± 0.4	2.6 ± 0.5	2.6 ± 0.5
ACE	0.3	1.87 ± 0.04	3.05 ± 0.02	0.93 ± 0.01	0.94 ± 0.01
	0.35	1.89 ± 0.09	3.58 ± 0.02	1.0 ± 0.5	1.0 ± 0.5
	0.4	1.86 ± 0.05	4.3 ± 0.2	1.3 ± 0.4	1.3 ± 0.4
	0.45	1.84 ± 0.02	4.5 ± 0.3	1.4 ± 0.3	1.4 ± 0.3
	0.5	1.85 ± 0.01	5.6 ± 0.3	1.5 ± 0.7	1.5 ± 0.7
	[RUB] / mM	**k_{obs} / s^{-1} × 10**	**I_o / a.u. ×10^{-2}**	**Φ_{CL} (E mol^{-1}) ×10^6**	**Φ_S (E mol^{-1}) ×10^6**
DMSO	0.3	5.2 ± 0.1	2.8 ± 0.1	7.16 ± 0.01	7.18 ± 0.01
	0.35	5.20 ± 0.01	4.4 ± 0.2	9.4 ± 0.5	9.5 ± 0.5
	0.4	5.10 ± 0.01	6.2 ± 0.2	12.3 ± 0.3	12.7 ± 0.3
	0.45	5.10 ± 0.01	6.3 ± 0.1	26.4 ± 0.3	26.8 ± 0.3

BUTY = butyl acetate; EA = ethyl acetate; ACE = acetone; conditions: emission slit = 20 nm and photomultiplier voltage = 950 V.

The [ACT] has no effect on k_{obs} for the decomposition of *spiro*-adamantyl-1,2-dioxetanone, however, k_{obs} has been increased by two order of magnitude from butyl acetate to DMSO. It is concluded that k_{obs} increased with increasing of polarity of solvent. Moreover, the values of I_0 and Φ_{CL} increase significantly in the presence of the fluorescent dye; i.e., the [ACT] affects the emission intensity and the total amount of light emission (Table 29).

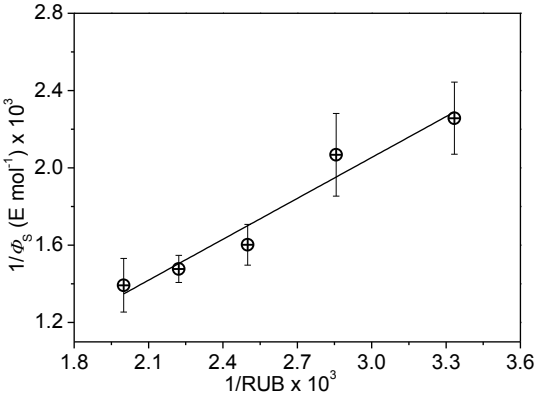

Figure 24: Double-reciprocal plots of the singlet quantum yields (Φ_S) and the activator concentration for the RUB-catalyzed decomposition of *spiro*-adamantyl-1,2-dioxetanone in acetone at 25 °C.

$$\frac{1}{\Phi_s} = \frac{1}{\Phi_s^{\infty}} + \left[\frac{k_D}{k_{CAT}\Phi_S^{\infty}}\right]\frac{1}{[ACT]} \qquad \text{Equation 35}$$

Table 30: Singlet quantum yields (Φ_S), infinite quantum yields (Φ_S^{∞}) and kinetic data for the decomposition of *spiro*-adamantyl-1,2-dioxetanone (**2**) using rubrene as a catalyst in pure solvents.

Solv.	η (cP)	$E_T(30)$	k_{obs} / s^{-1} x 10^3	Φ_S (E mol^{-1}) x 10^{3} [a]	k_{CAT} / k_D / L mol^{-1} x 10^{-3}	k_{CAT} / L mol^{-1} s^{-1}	Φ_S^{∞} (E mol^{-1}) x 10^{3} [b]
TOL	0.56	34	1.7 ± 0.1	2.9 ± 0.1	9.6 ± 0.8	16.61 ± 0.01	1.9 ± 0.7
DPE	2.13	35	2.04 ± 0.01	6.03 ± 0.08	5.6 ± 0.1	11.4 ± 0.1	4.8 ± 11.1
EA	0.45	38.1	1.6 ± 1.2	2.6 ± 0.5	15.5 ± 0.4	24.64 ± 0.01	1.3 ± 1.0
BUT	0.68	38.5	1.6 ± 0.1	3.4 ± 0.3	6.3 ± 0.1	10.14 ± 0.02	1.7 ± 5.0

[a] [rubrene] = 0.2 mmol for TOL = toluene, DPE = diphenyl ether; [a] [rubrene] = 0.3 mmol L^{-1} for EA = ethyl acetate, BUT = butyl acetate; [b] [rubrene] = 0.05 to 0.2 mmol L^{-1} for TOL, DPE and EA; [rubrene] = 0.1 to 0.3 mmol L^{-1} for BUT; conditions: emission slit = 20 nm and photomultiplier voltage = 950 V.

In this case, the unimolecular decomposition is predominant ($k_D \gg k_{CAT}$[ACT]) and the bimolecular rate constant did not determined graphically from the ACT concentration and k_{obs}, the chemiexcitation quantum yield is considered infinite quantum yield (Φ_S^{∞}) at an infinite concentration of the rubrene activator. It has been calculated from the double-reciprocal plots of singlet quantum yield Φ_S and the ACT concentration (Equation 35). which show linear correlation (Figure 24). The intercept and slope of the linear relationship between 1/[ACT] and $1/\Phi_S$ were equal to $1/\Phi_S^{\infty}$ and $\left[\frac{k_D}{k_{CAT}\Phi_S^{\infty}}\right]$. The parameter Φ_S^{∞} does not depend on the concentration of rubrene and the quantum yield has been calculated by hypothetically, where all peroxide interacts with rubrene and consequently they are decomposed by the activated pathway. In fact, the parameters Φ_S^{CAT} and Φ_S^{∞} are analogous and comparable, they do not depend on the ACT concentration and in both cases, and the yields are calculated in a hypothetically way, where all peroxides are decomposed by the activated pathway.

4.3.1. Kinetic study of the rubrene catalyzed of peroxide 2 using binary solvent mixtures

The catalyzed decomposition of *spiro*-adamantyl-1,2-dioxetanone (0.075 mmol L^{-1}) has been studied by using rubrene as an activator with one concentration in binary mixture solvent systems like the concentrations of an activator 0.3, 0.5, 0.05, 0.03, 0.03 mmol L^{-1} were used in toluene- acetone, toluene- ethyl acetate, diphenylether-DMSO, ethyl acetate-acetonitrile and toluene-acetonitrile at 25 ˚C respectively (Table 31).

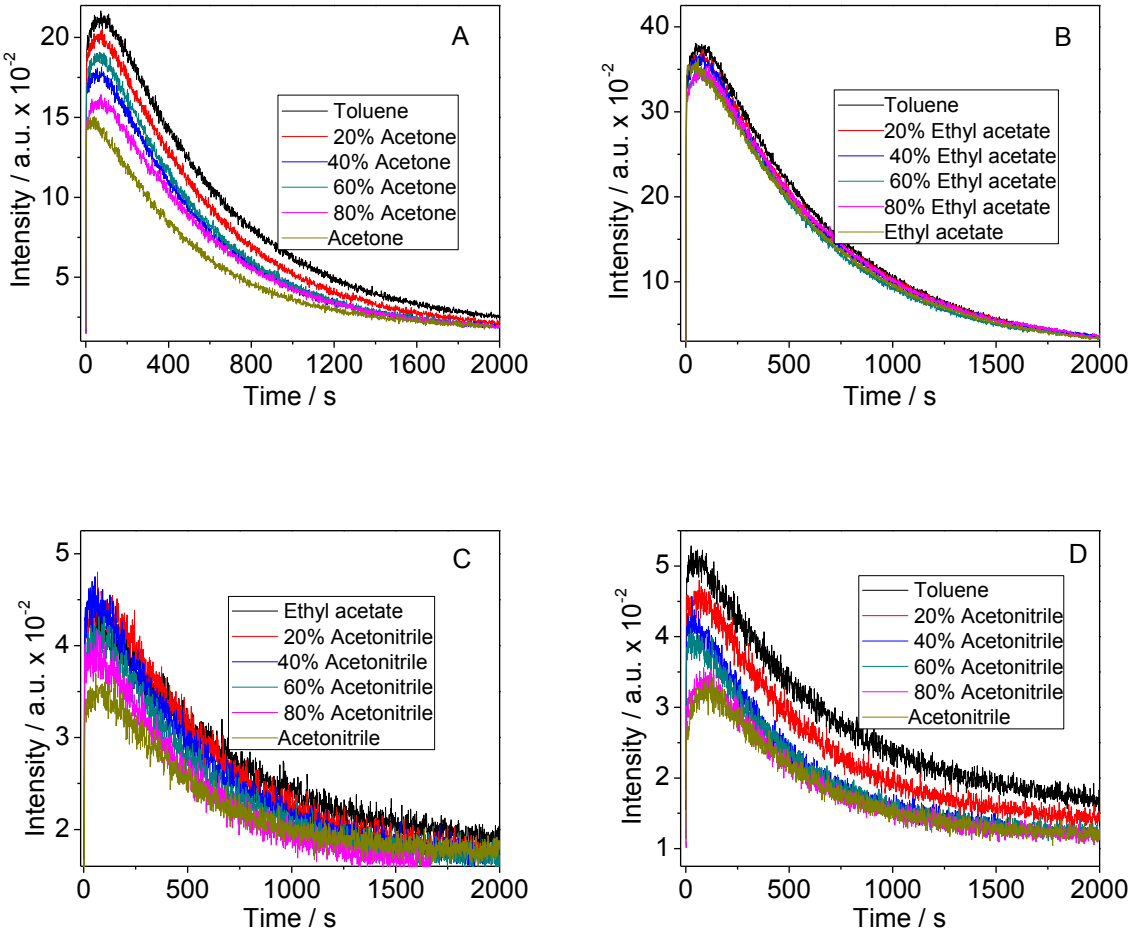

Figure 25: Emission intensity decay versus time curves for the reaction of *spiro*-adamantyl-1,2-dioxetanone (0.075 mmol L^{-1}) with rubrene (RUB) activator: A = 0.3 mmol L^{-1}; B = 0.5 mmol L^{-1}; C = 0.03 mmol L^{-1}; D = 0.03 mmol L^{-1} at 25 ˚C; conditions: emission slit = 20 nm and photomultiplier voltage = 950 V.

The obtained results display that observed rate constants (k_{obs}) increased with increasing the polarity of mediums, however, singlet quantum yields (Φ_S) for the decomposition of *spiro*-adamantyl-1,2-dioxetanone decreased with increasing the polarity of mediums (Table 31).

Table 31: Observed rate constants (k_{obs}), area under the emission curve (area) and chemiexcitation (Φ_S) for the decomposition of *spiro*-adamantyl-1,2-dioxetanone using rubrene as an activator.

% Solvent	k_{obs} / s^{-1} $\times 10^3$	Area / a.u. $\times 10^6$	Φ_S (Emol^{-1}) $\times 10^3$
ACE	2.00 ± 0.05	1.1 ± 0.1	2.6 ± 0.1
20%TOL	1.96 ± 0.05	1.3 ± 0.1	3.0 ± 0.2
40%TOL	1.93 ± 0.06	1.34 ± 0.02	3.19 ± 0.04
60%TOL	1.90 ± 0.03	1.4 ± 0.1	3.36 ± 0.02
80%TOL	1.78 ± 0.02	1.5 ± 0.1	3.7 ± 0.2
TOL	1.71 ± 0.04	1.58 ± 0.1	3. ± 0.3
EA	1.72 ± 0.01	2.69 ± 0.02	6.43 ± 0.05
20%TOL	1.62 ± 0.05	2.8 ± 0.1	6.8 ± 0.3
40%TOL	1.71 ± 0.06	2.8 ± 0.2	6.7 ± 0.4
60%TOL	1.70 ± 0.02	2.78 ± 0.03	6.7 ± 0.1
80%TOL	1.61 ± 0 .07	2.75 ± 0.04	6.6 ± 0.1
TOL	1.62 ± 0.03	2.8 ± 0.3	6.8 ± 0.8
% Solvent	**k_{obs} / s^{-1} $\times 10^3$**	**Area a.u.x10^5**	**Φ_S (E mol^{-1}) x 10^4**
ACN	2.29 ± 0.13	4.6 ± 0.1	1.63 ± 0.03
20%EA	2.03 ± 0.05	4.8 ± 0.1	1.70 ± 0.04
40%EA	2.02 ± 0.04	4.9 ± 0.2	1.72 ± 0.05
60%EA	1.92 ± 0.25	5.10 ± 0.04	1.79 ± 0.01
80%EA	1.87 ± 0 .01	5.2 ± 0.1	1.82 ± 0.02
EA	1.46 ± 0.01	5.5 ± 0.1	1.93 ± 0.03
ACN	2.29 ± 0.12	3.4 ± 0.1	1.22 ± 0.03
20 %TOL	2.16 ± 0.07	3.7 ± 0.3	1.3 ± 0.1
40%TOL	2.12 ± 0.03	3.8 ± 0.8	1.4 ± 0.3
60%TOL	2.11 ± 0.12	4.3 ± 0.7	1.6 ± 0.3
80%TOL	1.93 ± 0 .01	4.9 ± 0.5	1.8 ± 0.2
TOL	1.68 ± 0.01	5.9 ± 0.2	2.1 ± 0.1

[**2**] = 0.075 mmol L^{-1} at 25.0 °C; conditions: emission slit = 20 nm and photomultiplier voltage = 950 V; ACE = acetone; TOL = toluene; DPE = diphenylether; EA = ethyl acetate.

4.3.2. Kinetic study of the rubrene catalyzed decomposition of *spiro*-adamantyl-1,2-dioxetanone (2) using viscous binary solvent mixtures

The studies have been done in order to determine the influence of solvent viscosity on the chemiluminescence parameters of the decomposition of *spiro*-adamantyl-1,2-dioxetanone using rubrene (RUB) as an activator (Tables 32-34). The CL quantum yields (Φ_{CL}), the kinetic data and the singlet quantum yields (Φ_S) have been studied in the mixtures of ethyl acetate-dibutyl phthalate, toluene-diphenyl methane and toluene-diphenyl ether by varying the amount of the viscous solvent.

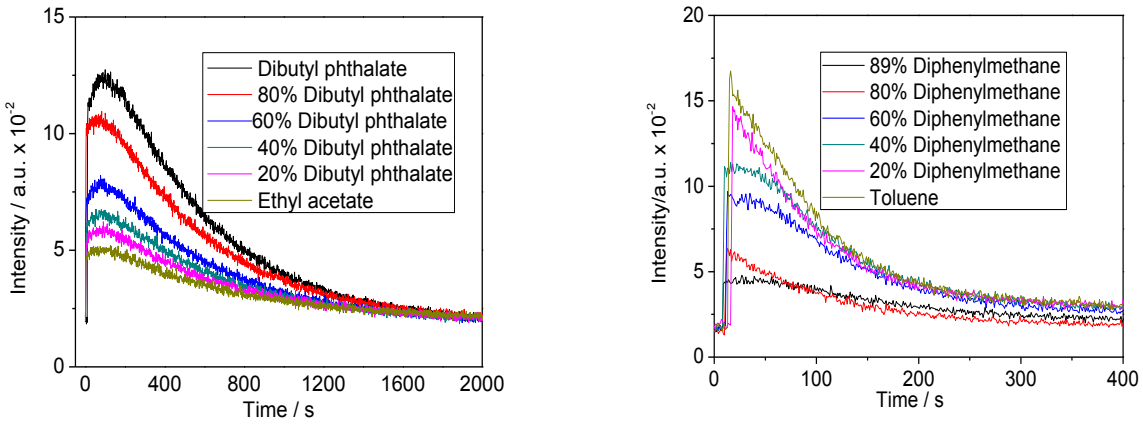

Figure 26: Time versus emission intensity decay for the reaction of *spiro*-adamantyl-1,2-dioxetanone with rubrene (RUB) activator at 25 °C.

The rubrene catalyzed decomposition of *spiro*-adamantyl-1,2-dioxetanone has been studied in the mixtures of ethyl acetate/dibutyl phthalate which have similar polarity but different viscosity parameters.

Table 32: The observed rate decay constant (k_{obs}), area under the emission curve and singlet quantum yields (Φ_S) for the decomposition of *spiro*-adamantyl-1,2-dioxetanone in the mixtures of ethyl acetate and dibutyl phthalate.

% DBP	η (cP)	k_{obs} / s^{-1} x10^3	Area/ a.u.x10^{-5}	Φ_S (E mol^{-1}) x10^3
0	0.42	1.54 ± 0.02	6.3 ± 0.5	1.49 ± 0.12
20	0.61	1.61 ± 0.06	6.6 ± 0.8	1.6 ± 0.2
40	0.94	1.63 ± 0.01	7.3 ± 0.2	1.73 ± 0.05
60	1.67	1.72 ± 0.02	8.3 ± 0.5	1.98 ± 0.12
80	3.11	1.79 ± 0.03	9.3 ± 0.3	2.21 ± 0.07
100	9.63	1.91 ± 0.02	11.4 ± 0.1	2.73 ± 0.02

[**2**] = 0.075 mmol L^{-1}; [RUB] = 0.1 mmol L^{-1}; at 25.0 °C; conditions: emission slit = 20 nm and photomultiplier voltage = 950 V.

The system **2** has also been studied in the mixtures of toluene and diphenyl methane which have similar polarity but different viscosity parameter.

Table 33: The observed rate decay constant (k_{obs}), area under emission curve (area) and singlet quantum yields (Φ_S) for the decomposition of *spiro*-adamantyl-1,2-dioxetanone using rubrene as a catalyst in the mixtures of toluene and diphenyl methane.

% DPM	η (cP)	k_{obs}/s^{-1} × 10^3	area /a.u. × 10^{-5}	Φ_S (E mol^{-1}) × 10^5
0	0.52	7.0 ± 1.0	1.46 ± 0.01	2.62 ± 0.02
20	0.82	9.0 ± 2.0	2.23 ± 0.03	4.01 ± 0.04
40	1.05	10.1 ± 0.4	2.8 ± 0.5	4.9 ± 0.9
60	1.37	11.2 ± 0.2	2.8 ± 0.2	5.0 ± 0.4
80	2.17	11.0 ± 1.0	3.0 ± 0.2	5.4 ± 0.4
89	2.57	12.7 ± 0.1	3.4 ± 0.3	6.2 ± 0.6

[**2**] = 0.075 mmol L^{-1}**;** [RUB] = 1.0 mmol L^{-1}; at 25.0 °C; conditions: emission slit = 20 nm and photomultiplier voltage = 950 V.

The system 2 has also been studied in binary mixtures of diphenyl ether and toluene which have similar polarity but different viscosity parameter.

Table 34: The observed rate decay constant (k_{obs}), area under emission curve (area), singlet quantum yields (Φ_S) for the decomposition of *spiro*-adamantyl-1,2-dioxetanone using rubrene as a catalyst in the mixtures of toluene and diphenyl ether.

% DPE	η (cP)	k_{obs} / $s^{-1} \times 10^3$	Area/a.u. $\times 10^{-5}$	Φ_S (E mol^{-1}) $\times 10^4$
0	0.52	1.66 ± 0.01	5.1 ± 0.1	5.7 ± 0.1
25	0.74	1.69 ± 0.02	5.9 ± 0.2	6.6 ± 0.2
50	1.10	1.84 ± 0.01	6.6 ± 0.4	7.5 ± 0.4
75	1.6	1.9 ± 0.1	7.7 ± 0.1	8.6 ± 0.1
100	2.2	2.01 ± 0.05	9.6 ± 1.3	11.4 ± 1.4

[**2**] = 0.075 mmol L^{-1}; [RUB] = 0.05 mmol L^{-1}; at 36.0 °C; conditions: emission slit = 20 nm and photomultiplier voltage = 950 V.

The magnitude of the observed rate constant (k_{obs}) just slightly increased with the increasing of amount of viscous solvent (η) like in the mixtures of ethyl acetate-dibutyl phthalate, toluene-diphenyl methane and toluene-diphenyl ether systems.

The experiments were carried out in only two experimental conditions in pure toluene and diphenyl ether in order to better verify the behavior of the system **2** (Table 35). The tendency of results are similar as obtained above.

Table 35: Observed rate decay constant (k_{obs}), area under emission curve, CL quantum yields (Φ_{CL}), singlet quantum yields (Φ_S) for the decomposition of *spiro*-adamantyl-1,2-dioxetanone using rubrene as a catalyst in pure toluene and diphenyl ether.

%DPE	η (cP)	k_{obs} / s^{-1} $\times 10^3$	Area/a.u. $\times 10^{-5}$	Φ_{CL} (E mol^{-1}) $\times 10^4$	Φ_S (E mol^{-1}) $\times 10^4$
TOL	0.52	1.7 ± 0.1	7.9 ± 0.4	18.5 ± 1.1	18.9 ± 0.5
DPE	2.1	2.01 ± 0.01	14.0 ± 0.3	32.8 ± 0.6	33.4 ± 0.4

[**2**] = 0.075 mmol L^{-1}; at 36.0 °C; conditions: emission slit = 20 nm and photomultiplier voltage = 950 V.

In order to better understand the behavior of this system, specifically the surprising observed rate constant higher speed in higher viscosity media, we

studied the effect of a low-viscosity solvent (toluene) and a high viscosity (diphenyl ether) on the observed rate decay constant (k_{obs}) and CL quantum yields, consequently which led to obtaining the values of the Φ_S^{∞}, k_{CAT}/k_D and k_{CAT}. Moreover, for this aim, the kinetics of the emission system was studied using different concentrations of activator (Figures 27, 28). The values of I_0, area and k_{obs} obtained from each concentration of rubrene in the decomposition of peroxide in toluene and diphenyl ether (Tables 36,37).

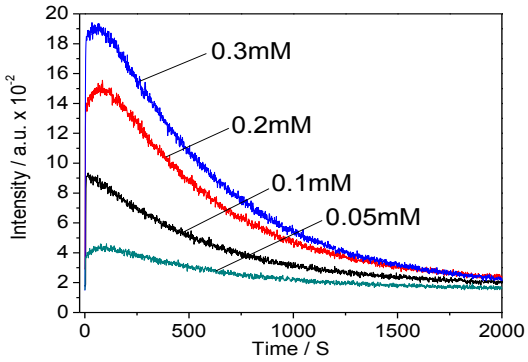

Figure 27: Time versus emission intensity decay for the reaction of *spiro*-adamantyl-1,2-dioxetanone with different concentrations of rubrene (RUB) in toluene at 25 °C.

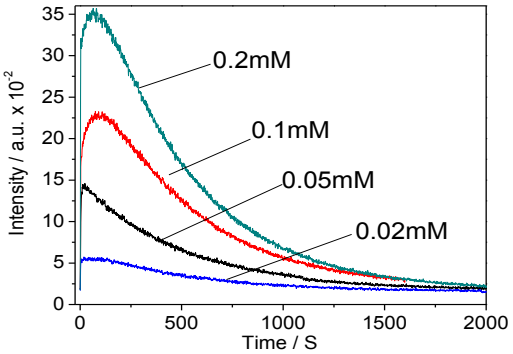

Figure 28: Time versus emission intensity decay for the reaction of *spiro*-adamantyl-1,2-dioxetanone with different concentrations of rubrene (RUB) in diphenyl ether at 25 °C.

Table 36: Observed rate decay constant (k_{obs}), intial intensity (I_0) ,area under emission curve (area), CL quantum yields (Φ_{CL}) and singlet quantum yields (Φ_S) for the decomposition of *spiro*-adamantyl-1,2-dioxetanone using rubrene as a catalyst in the pure toluene.

[RUB] / mM	k_{obs} / s^{-1} × 10^3	I_o / a.u. ×10^{-2}	Area / a.u. × 10^{-5}	Φ_{CL} (E mol^{-1})×10^4	Φ_S (E mol^{-1})×10^4
0.05	1.66 ± 0.01	3.52 ± 0.02	5.8 ± 0.3	13.6 ± 0.6	13.7 ± 0.6
0.1	1.73 ± 0.06	7.8 ± 0.2	7.9 ± 0.4	18.5 ± 1.1	19.1± 1.2
0.2	1.74 ± 0.06	16.3 ± 0.6	12.4 ± 0.4	29.1± 0.9	29.6 ± 0.9
0.3	1.70 ± 0.03	23.1 ± 1.4	16.2 ± 1.1	38.1 ± 2.8	39.5 ± 2.9

[**2**] = 0.075 mmol L^{-1}; at 36.0 °C; conditions: emission slit = 20 nm and photomultiplier voltage = 950 V.

Table 37: Observed rate decay constant (k_{obs}), intial intensity (I_0) ,area under emission curve (area), CL quantum yields (Φ_{CL}) and singlet quantum yields (Φ_S) for the decomposition of *spiro*-adamantyl-1,2-dioxetanone using rubrene as a catalyst in the pure diphenyl ether.

[RUB] / mM	k_{obs} / s^{-1} × 10^3	I_o / a.u.×10^{-2}	Area / a.u.× 10^{-5}	Φ_{CL} (E mol^{-1})×10^4	Φ_S (E mol^{-1}) × 10^4
0.02	1.90 ± 0.03	0.6 ± 0.1	5.3 ± 0.2	12.49 ± 0.44	12.74 ± 0.45
0.05	2.00 ± 0.05	1.2 ± 0.1	9.6 ± 1.2	22.46 ± 2.90	22.92 ± 3.1
0.1	2.04 ± 0.01	2.30 ± 0.01	14.0 ± 0.3	32.8 ± 0.7	33.4 ± 0.8
0.2	2.1 ± 0.1	4.8 ± 0.2	25.3 ± 2.0	59.1 ± 4.7	60.3 ± 4.8

[**2**] = 0.075 mmol L^{-1}; at 36.0 °C; conditions: emission slit = 20 nm and photomultiplier voltage = 950 V.

Table 38: Singlet quantum yields (Φ_S), k_{CAT} / k_D, k_{obs} and k_{CAT} for the decomposition of *spiro*-adamantyl-1,2-dioxetanone using rubrene as a catalyst in the pure diphenyl ether and toluene.

Solvent	Φ_S (E mol^{-1})x10^{-4}	$\Phi_S{}^{\infty}$ (E mol^{-1}) x 10^{-3}	k_{CAT} / k_D / M^{-1} x 10^{-3}	k_{obs} / s^{-1} x 10^3	k_{CAT}/ M^{-1} s^{-1}
TOL	18.9 ± 1.1	1.9 ± 0.5	9.6 ± 0.8	1.7 ± 0.1	16.61 ± 0.01
DPE	33.4 ± 0.9	4.8 ± 1.1	5.6 ± 0.1	2.04 ± 0.01	11.4 ± 0.1

[**2**] = 0.075 mmol L^{-1}; [RUB] = 0.1 mmol L^{-1}; at 36.0 °C; conditions: emission slit = 20 nm and photomultiplier voltage = 950 V; DPE=diphenyl ether.

4.4. Kinetic studies of *spiro*-adamantyl-substituted 1,2-dioxetane (3)

The decomposition of *spiro*-adamantyl-substituted 1,2-dioxetane is studied by using solution of tetrabutyl ammonium fluoride (TBAF). The concentrations of the substituted 1,2-dioxetane and solution of tetrabutylammonium fluoride (TBAF) are used 0.01 mmol L^{-1} and 2.5 mmol L^{-1} respectively.

4.4.1. Kinetic study of *spiro*-adamantyl-substituted 1,2- dioxetane (3) using pure solvents

The decomposition of *spiro*-adamantyl-substituted 1,2-dioxetane has been studied by using solution of tetrabutyl ammonium fluoride (TBAF) in pure solvents. Time-profiles for the emission intensity decay in the reaction of 1,2-dioxetane in following solvents at 25 °C (Figure 29).

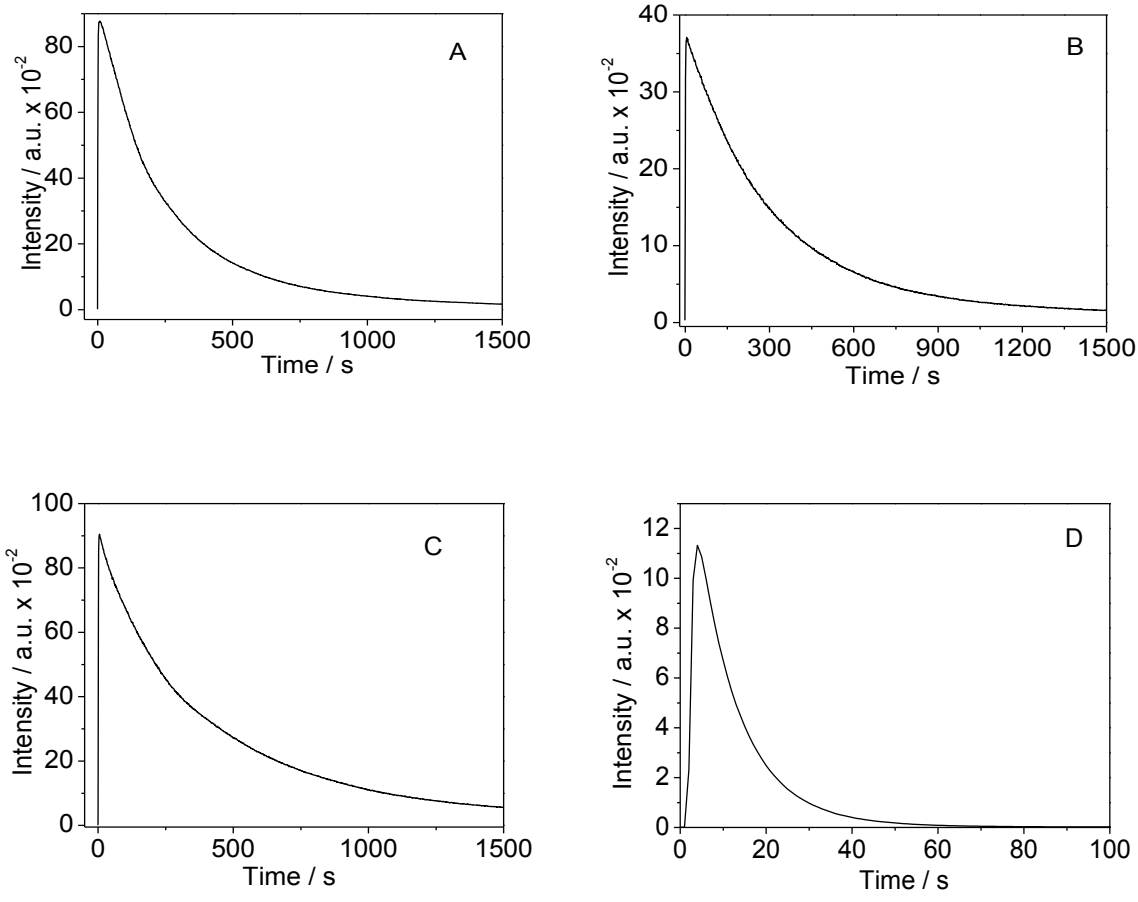

Figure 29: Emission intensity decay versus time curves for the reaction of *spiro*-adamantyl-substituted-1,2-dioxetane (0.01 mmol L^{-1}); with TBAF (2.5 mmol L^{-1}) in A = anisole; B = butyl acetate C = THF; D = ACN; at 25 °C.

Table 39: Observed rate constants (k_{obs}) and singlet quantum yields (Φ_S) for the decomposition of *spiro*-adamantyl-1,2-dioxetane **3** at 25 °C.

Solvent	ε_r / $E_T(30)$	η (cP)	k_{obs} / s^{-1} /10^3	Φ_S (E mol^{-1})
ANI	4.45 / 37.1	1.056	4.01 ± 0.02	0.38 ± 0.01
BUTY	5.01 / 38.5	0.685	3.2 ± 0.2	0.25 ± 0.01
EA	6.03 / 38.1	0.423	4.7 ± 0.1	0.44 ± 0.02
THF	7.47 / 37.4	0.456	2.4 ± 0.1	0.54 ± 0.02
ACN	35.94 /45.6	0.369	52.0 ± 4.0	0.43 ± 0.05
DMSO	46.7 / 45.1	1.987	140 ± 10	0.97 ± 0.02

ANI = anisole; BUTY = butyl acetate; EA = ethyl acetate; ACN = acetonitrile; DMSO = dimethyl sulfoxide.

The magnitude of quantum yields increase with increasing the magnitude of dielectric constant (ε_r) as well as with $E_T(30)$. The magnitude of the observed rate constant (k_{obs}) also increases with increasing the magnitude of dielectric constant (ε_r) as well as with $E_T(30)$ (Table 39).

4.4.2. Kinetic study of *spiro*-adamantyl-substituted 1,2-dioxetane (3) using binary solvent mixtures

To verify the effect of solvent polarity on the parameters of CL induced decomposition of *spiro*-adamantyl-substituted 1,2-dioxetane **3**, a number of solvents have been used for these studies that have different polarity and polarizability parameters with same viscosity, moreover, just aprotic solvents are used to avoid formation of hydrogen bonds as happened by protic solvents like water and methanol and also a considerable decrease in the quantum yields obtained. The preliminary choice of solvents was based on the following criteria: (i) availability; (ii) the possibility of obtaining a high degree of purity required for use in these experiments; (iii) ease of purification; (iv) probability of no interference occurs in the reaction and the emission process; (v) to avoid precipitation of the reagent TBAF deprotection as with aromatic and aliphatic hydrocarbons supposedly and (vi) the possibility of reuse of solvent recovery.

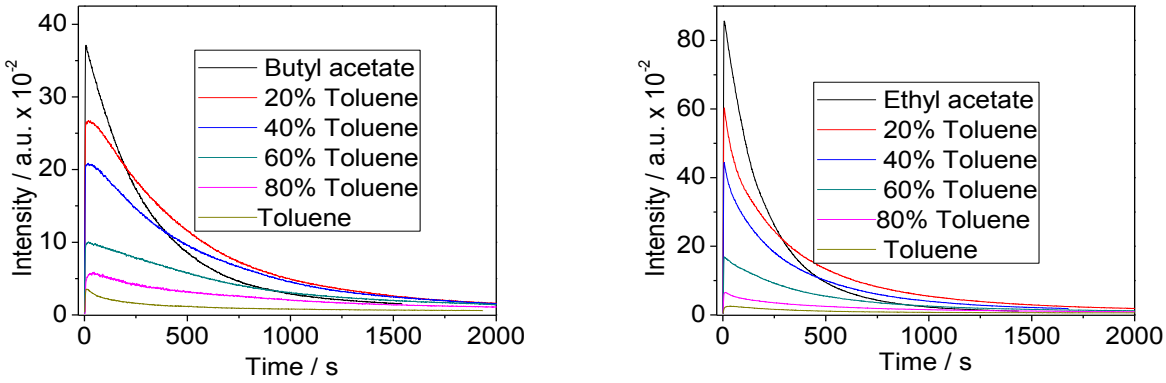

Figure 30: Emission intensity decay versus time curves for the reaction of *spiro*-adamantyl-substituted-1,2-dioxetane (0.01 mmol L^{-1}) with TBAF (2.5 mmol L^{-1}) at 25 °C; conditions: emission slit = 2.5 nm and photomultiplier voltage = 700V.

The compound (**3**) was studied in the mixtures of toluene-butyl acetate and toluene-ethyl acetate. These both binary solvent mixtures have similar viscosity parameter but different polarity parameter.

Table 40: Observed rate constants (k_{obs}) and singlet quantum yields (Φ_S) for the decomposition of **3** at 25 °C.

Solv.Sys	% Solv.	$E_T(30)$	k_{obs} / s^{-1} × 10^3	Φ_S (E mol^{-1})
	A	33.9	3.1 ± 0.2	0.033 ± 0.004
	B	35.5	1.3 ± 0.2	0.077 ± 0.003
	C	36.0	1.5 ± 0.3	0.12 ± 0.02
1	D	36.5	1.8 ± 0.1	0.17 ± 0.01
	E	37.3	2.01 ± 0.1	0.21 ± 0.01
	F	38.8	3.2 ± 0.3	0.25 ± 0.01
	G	34.22	3.1 ± 0.2	0.034 ± 0.004
	H	35.63	2.0 ± 0.2	0.08 ± 0.01
2	I	36.28	2.6 ± 0.3	0.16 ± 0.01
	J	37.37	3.0 ± 0.3	0.30 ± 0.01
	K	38.56	3.3 ± 0.2	0.37 ± 0.02
	L	39.38	4.7 ± 0.1	0.44 ± 0.02

Solv. Sys.= solvent systems; **1** = toluene-butyl acetate system: A = 0% butyl acetate; B = 20% butyl acetate; C = 40% butyl acetate; D = 60% butyl acetate; E = 80% butyl acetate; F = 100%

butyl acetate and **2** = toluene-ethyl acetate system; G = 0% ethyl acetate; H = 20% ethyl acetate; I = 40% ethyl acetate; J = 60% ethyl acetate; K = 80% ethyl acetate; L = 100% ethyl acetate.

The magnitude of the observed rate constant (k_{obs}) increases with increasing the polarity of solvent (Table 40).

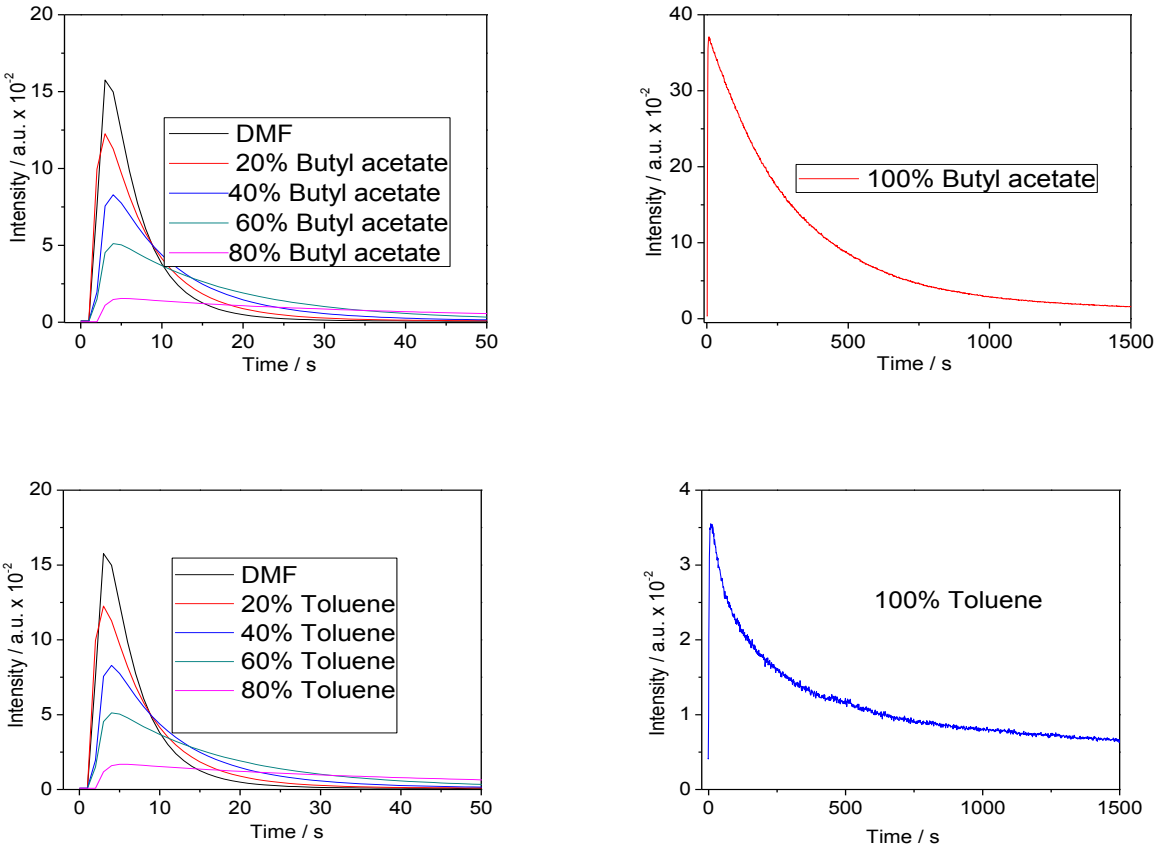

Figure 31: Emission intensity decay versus time curves for the reaction of *spiro*-adamantyl-substituted-1,2-dioxetane (0.01 mmol L^{-1}) with TBAF (2.5 mmol L^{-1}) at 25 °C; conditions for all binary solvent mixtures and pure DMF: emission slit = 1 nm and photomultiplier voltage = 400V; conditions for pure solvent butyl acetate and toluene: emission slit = 2.5 nm and photomultiplier voltage = 700V.

The compound (**3**) was also studied in the mixtures of toluene-DMF and butyl acetate-DMF. These both binary solvent mixtures have similar viscosity parameter but different polarity parameter.

Table 41: Observed rate constants (k_{obs}) and singlet quantum yields (Φ_S) for the decomposition of *spiro*-adamantyl-1,2-dioxetane **3** at 25 °C.

Syst.	% Solv.	$E_T(30)$	k_{obs} / $s^{-1} \times 10^2$	Φ_S (E mol^{-1})
	A	38.8	0.32 ± 0.03	0.08 ± 0.01
	B	41.26	2.35 ± 0.09	0.17 ± 0.01
	C	41.86	7.05 ± 0.01	0.236 ± 0.002
1	D	42.42	11.2 ± 0.3	0.26 ± 0.02
	E	42.8	16.0 ± 1.0	0.28 ± 0.02
	F	43.58	21.0 ± 2.0	0.35 ± 0.01
	G	34.3	0.31 ± 0.02	0.037 ± 0.001
	H	39.78	1.1 ± 0.1	0.16 ± 0.01
2	I	40.78	3.4 ± 0.4	0.24 ± 0.01
	J	41.86	8.2 ± 0.3	0.267 ± 0.001
	K	42.86	9.3 ± 1.0	0.31 ± 0.03
	L	43.58	21.0 ± 2.0	0.35 ± 0.03

Solv. Syst.= solvent systems**; 1**= butyl acetate-*N,N*-dimethyl formamide system; A = 0% *N,N*-dimethyl formamide system; B = 20% *N,N*-dimethyl formamide system; C = 40% *N,N*-dimethyl formamide system; D = 60% *N,N*-dimethyl formamide system; E = 80% *N,N*-dimethyl formamide system; F = 100% *N,N*-dimethyl formide system and **2** = toluene- *N,N*-dimethyl formide system; G = 0% *N,N*-dimethyl formamide system;H = 20% *N,N*-dimethyl formamide system; I = 40% *N,N*-dimethyl formamide system; J = 60% *N,N*-dimethyl formamide system; K = 80% *N,N*-dimethyl formamide system; L = 100% *N,N*-dimethyl formamide system.

The observed rate constant (k_{obs}) increased with increasing the polarity, for varying the polarity parameter $E_T(30)$, from $E_T(30)$ = 5.01 (100% butyl acetate) to $E_T(30)$ = 37.0 (100% *N,N*-dimethyl formamide) indicated significant increase in the magnitude of the observed rate constant (k_{obs}) by a factor of almost 65.4 for system 1. The tendency of increasing for the observed rate constants (k_{obs}) has been obtained from system **2** are very similar as obtained for system 1 (Table 41).

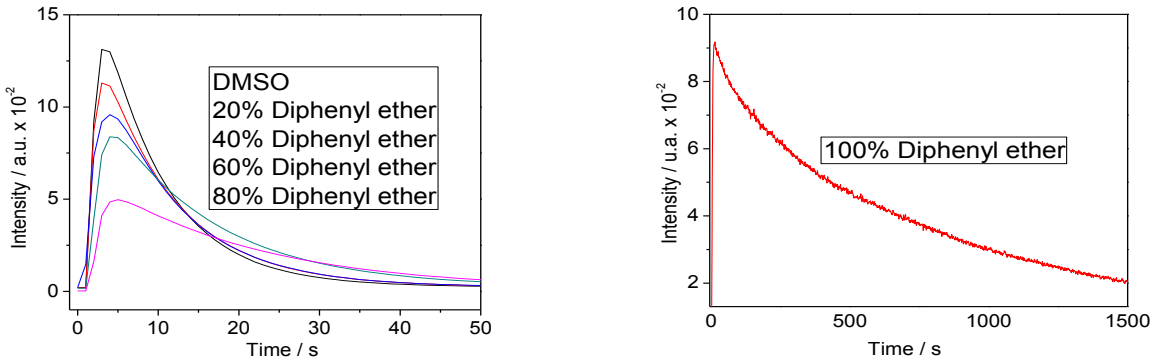

Figure 32: Emission intensity decay versus time curves for the reaction of *spiro*-adamantyl-substituted-1,2-dioxetane (0.01 mmol L^{-1}) with TBAF (2.5 mmol L^{-1}) at 25 °C; conditions for all binary solvent mixtures and pure DMSO: emission slit = 1 nm and photomultiplier voltage = 400V; conditions for pure diphenyl ether: emission slit = 2.5 nm and photomultiplier voltage = 700V.

The compound (**3**) was also studied in the mixtures of diphenyl ether–DMSO. These both solvents have similar viscosity parameter but different polarity parameter.

Table 42: Observed rate constants (k_{obs}) and singlet quantum yields (Φ_S) for the decomposition of *spiro*-adamantyl-1,2-dioxetane **3** at 25 °C.

Solvent	$E_T(30)$	k_{obs} / $s^{-1} \times 10^2$	Φ_S (E mol^{-1})
DPE	35.5	0.11 ± 0.01	0.32 ± 0.01
20% DMSO	37.8	3.9 ± 0.1	0.71 ± 0.05
40%DMSO	39.9	7.01 ± 0.3	0.87 ± 0.02
60%DMSO	42.1	10.5 ± 0.3	0.93 ± 0.02
80%DMSO	43.6	12.0 ± 2.0	0.946 ± 0.002
DMSO	45.1	14.0 ± 1.0	0.97 ± 0.02

Conditions: emission slit = 2.5 nm and photomultiplier voltage = 700V; DPE = diphenyl ether; DMSO = dimethyl sulfoxide.

The compound (**3**) was also studied in the mixtures of THF–acetone. These both solvents have similar viscosity parameter but different polarity parameter.

Table 43: Observed rate constants (k_{obs}) and singlet quantum yields (Φ_S) for the decomposition of *spiro*-adamantyl-1,2-dioxetane **3** at 25 °C.

Solvent	(π^*)	$E_T(30)$	k_{obs} / s^{-1} × 10^3	Φ_S (E mol^{-1})
100% THF	0.25	37.7	2.4 ± 0.1	0.54 ± 0.02
20 % acetone	0.24	38.6	3.2 ± 0.2	0.75 ± 0.03
40 % acetone	0.23	39.5	3.6 ± 0.1	0.80 ± 0.05
60 % acetone	0.23	40.4	3.5 ± 0.1	0.86 ± 0.04
80 % acetone	0.23	41.3	3.6 ± 0.2	0.92 ± 0.03
100% acetone	0.22	42.2	9.0 ± 3.0	0.96 ± 0.05

Conditions: emission slit = 2.5 nm and photomultiplier voltage = 700V.

The compound (**3**) was also studied in the mixtures of toluene–acetone, because both solvents have similar viscosity parameter but different polarizability parameter.

Table 44: Observed rate constants (k_{obs}) and singlet quantum yields (Φ_S) for the decomposition of *spiro*-adamantyl-1,2-dioxetane **3** at 25 °C.

% Solvent	(π^*)	k_{obs} / s^{-1} × 10^3	Φ_S (E mol^{-1})
100% toluene	0.29	3.1 ± 0.2	0.033 ± 0.004
80% toluene	0.27	1.3 ± 0.1	0.39 ± 0.04
60% toluene	0.26	2.26 ± 0.01	0.80 ± 0.03
40% toluene	0.25	2.65 ± 0.01	0.86 ± 0.01
100% acetone	0.22	1.7 ± 0.1	0.96 ± 0.05

Conditions: emission slit = 2.5 nm and photomultiplier voltage = 700V.

Table 45: Observed rate constants (k_{obs}) and singlet quantum yields (Φ_S) for the decomposition of *spiro*-adamantyl-1,2-dioxetane **3** with polarity parameter $E_T(30)$ at 25 °C in binary mixtures of toluene/ butyl acetate/ ethyl acetate/ acetone and DMSO.

% A	% B	$E_T(30)$	k_{obs} / s^{-1} × 10^3	Φ_S (E mol^{-1})
100% TOL	0% BUTY	34.0	3.1 ± 0.2	0.033 ± 0.004
80% TOL	20% BUTY	35.5	1.3 ± 0.2	0.077 ± 0.003
80% TOL	20% EA	35.63	2.0 ± 0.2	0.08 ± 0.01
60% TOL	40% BUTY	36.0	1.5 ± 0.3	0.17 ± 0.01
40% TOL	60% EA	37.37	3.0 ± 0.3	0.30 ± 0.01
0% TOL	100% EA	39.38	4.7 ± 0.1	0.44 ± 0.02
40% TOL	60% ACE	40.4	3.5 ± 0.1	0.86 ± 0.03
0% TOL	100% ACE	42.2	1.7 ± 0.1	0.96 ± 0.05
0% TOL	100% DMSO	45.1	14.0 ± 1.0	0.97 ± 0.02

Conditions: emission slit = 2.5 nm and photomultiplier voltage = 700V.

The observed rate constant (k_{obs}) increased with increasing the polarity. It is indicated that significant increase in the magnitude of the observed rate constant (k_{obs}) has been observed in all the cases (Tables 43-45).

4.4.3. Kinetic study of *spiro*-adamantyl-substituted 1,2-dioxetane (3) using viscous binary solvent mixture

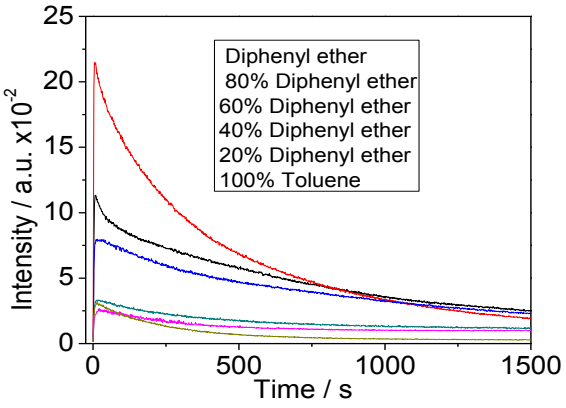

Figure 33: Time versus emission intensity decay in the reaction of the *spiro*-adamantyl-substituted 1,2-dioxetane **3** (0.01 mmol L^{-1}) with TBAF (2.5 mmol L^{-1}) in the mixture of toluene

and diphenyl ether at 36 °C; conditions: emission slit = 2.5 nm and photomultiplier voltage = 700V.

Table 46: Viscosity influence of solvents on the decomposition of the *spiro*-adamantyl-substituted 1,2- dioxetane (3).

%DPE	η / cP	k_{obs} / s^{-1} × 10^3	Φ_S (E mol^{-1})
0	0.52	3.1 ± 0.1	0.0395 ± 0.0001
20	0.64	2.4 ± 0.1	0.0433 ± 0.0001
40	0.92	2.20 ± 0.02	0.072 ± 0.001
60	1.29	1.8 ± 0.3	0.14 ± 0.01
80	1.80	2.0 ± 0.3	0.227 ± 0.001
100	2.2	2.3 ± 0.2	0.350 ± 0.001

[dioxetane] = 0.01 mmol L^{-1}; [TBAF] = 2.5 mmol L^{-1} in the mixtures of toluene (TOL) and diphenyl ether (DPE) at 36 °C.

Experiments were carried out for the study of CL emission of the *spiro*-adamantyl-substituted 1,2-dioxetane (**3**) with solution of tetrabutyl ammonium fluoride (TBAF), the kinetic parameters (k_{obs}) and the singlet quantum yield (Φ_S) are shown in Table 46. The viscosity of the solvent has no effect on fluorescence quantum yields (Φ_{FL}) of the emitter. The fluorescence quantum yields (Φ_{FL}) of emitter have been determined in binary mixture of benzene and diphenyl methane and over the entire range of concentration the fluorescence quantum yields (Φ_{FL}) of emitter remained constant values = 0.22 ± 0.02.[116]
The fluorescence quantum yields (Φ_{FL}) of emitter have also been determined in diphenyl ether and toluene, the fluorescence quantum yields (Φ_{FL}) of emitter (0.22) are same as reported in benzene and diphenyl methane because solvent parameters of these solvents are same as consist of benzene and diphenyl methane. The data presented in Table 46 which reflect that an increase in viscosity (η) results in a regular enhancement of the chemiexcitation yield (Φ_S).

4.5. Determination of activation parameters for cyclic peroxides

4.5.1. Determination of activation parameters for peroxide (1)

The various kinetics of light emission were performed to determine the activation parameters for the thermolysis of diphenyol peroxide and by keeping constant the concentration of diphenyol peroxide in a temperature range from 36 to 70 °C using perylene (0.1mmol L^{-1}) as an activator in less polar aprotic solvent like toluene and butyl acetate as well as high polar aprotic solvent like acetone. The values of the rate constant and initial emission intensity were obtained from the curves of first order decay.

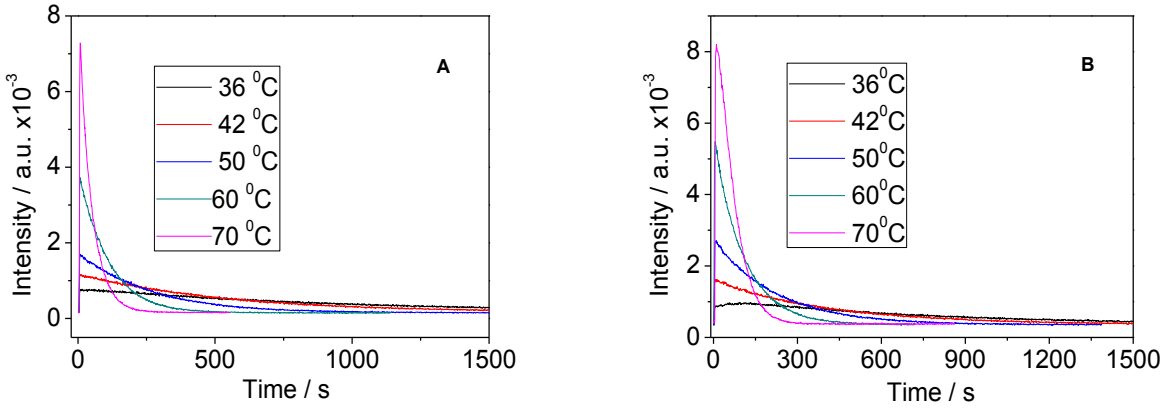

Figure 34: Kinetic curves of the emission intensity at various temperatures for the catalyzed decomposition of the diphenyol peroxide with perylene as an activator in butyl acetate (A); acetone (B).

Table 47: The observed rate constants (k_{obs}) and initial intensity (I_0) at different temperatures for the decomposition of the diphenyol peroxide using perylene (0.1mmol L^{-1})as an activator.

	Butyl acetate		Toluene		Acetone	
T/K	**k_{obs} /s^{-1}**	**I_0 / a.u.**	**k_{obs} /s^{-1}**	**I_0 / a.u.**	**k_{obs} /s^{-1}**	**I_0 / a.u.**
309	1.1 x 10^{-3}	643	2.1 x 10^{-3}	1939	1.4 x 10^{-3}	743
315	19 x 10^{-3}	1035	3.17 x 10^{-3}	3214	2.4 x 10^{-3}	1226
323	3.9 x 10^{-3}	1632	5.84 x 10^{-3}	5718	4.5 x 10^{-3}	2384
333	9.7 x 10^{-3}	3955	9.36 x 10^{-3}	8527	9.4 x 10^{-3}	5176
343	21.6 x 10^{-3}	7911	/	/	17.3 x 10^{-3}	12220

[DPP] = 0.1 mmol L^{-1} in butyl acetate and acetone; [DPP] = 0.2 mmol L^{-1} in toluene.

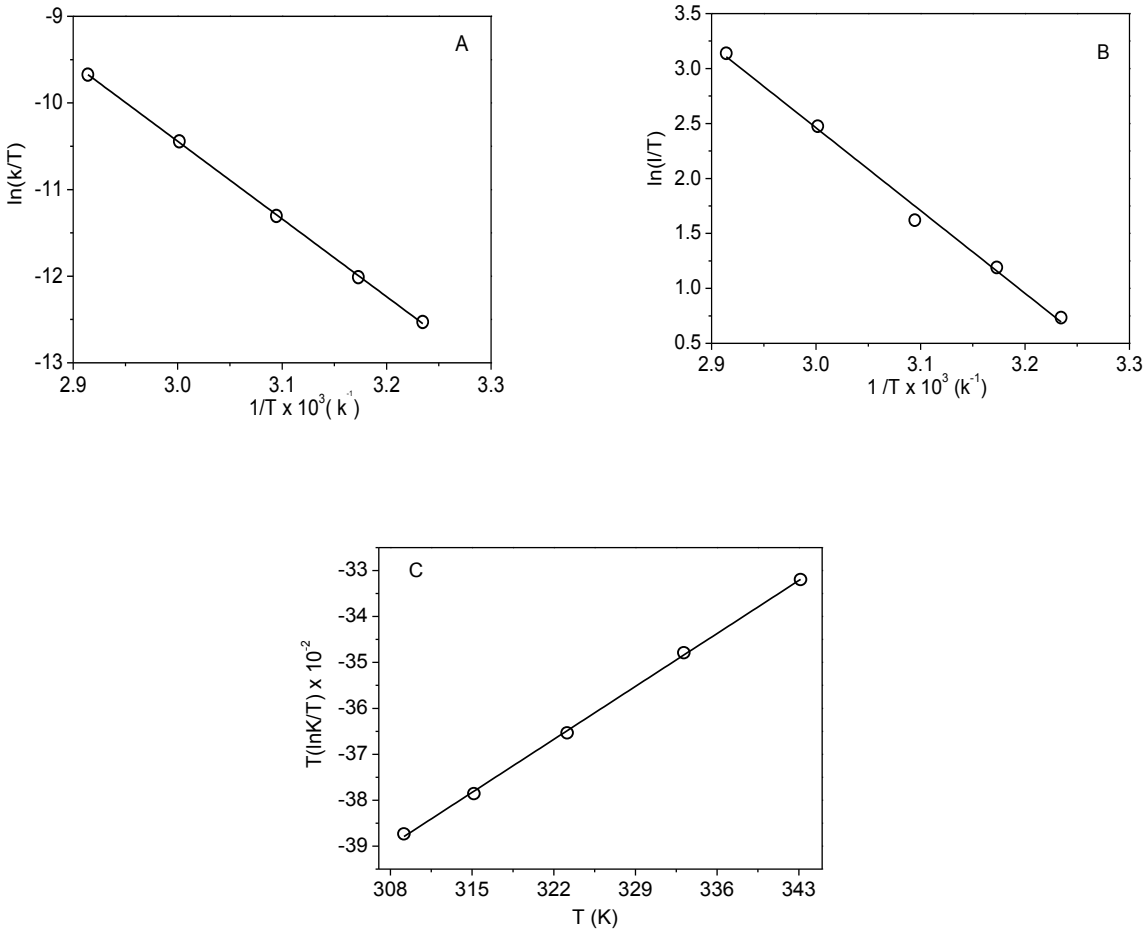

Figure 35: Determination of activation parameters: A = enthalpy ($\Delta H^{\neq}$); B = the enthalpy of the chemiluminescence reaction ($\Delta H_{Cl}^{\neq}$); C = entropy ($\Delta S^{\neq}$) for the catalyzed decomposition of the diphenyol peroxide in butyl acetate.

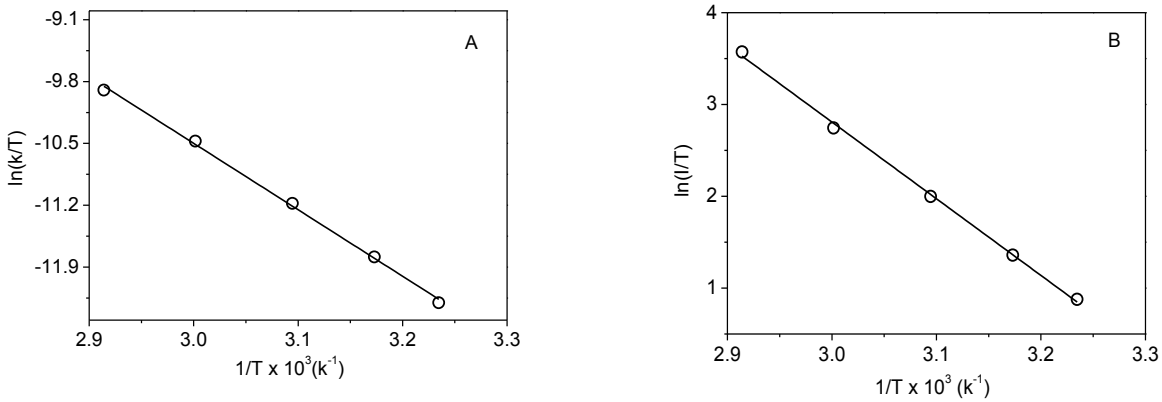

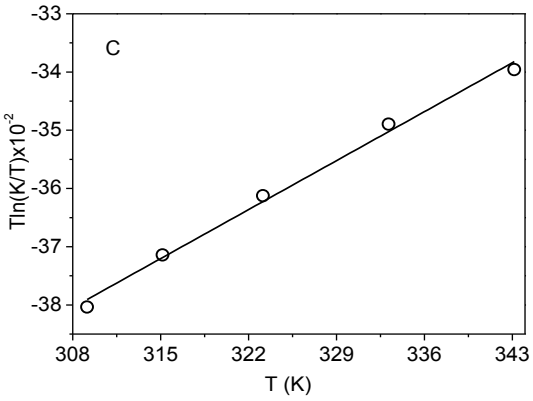

Figure 36: Determination of activation parameters: A = enthalpy (ΔH≠); B = the enthalpy of the chemiluminescence reaction ($\Delta H_{Cl}^{\neq}$); C = entropy (ΔS≠) for the catalyzed decomposition of the diphenyol peroxide in acetone.

The enthalpy of the chemiluminescence reaction ($\Delta H_{Cl}^{\neq}$) by using the Eyring equation have been determined by constructing the graph ($\ln(I_0/T)$) versus 1/T (Figures 35, 36).

Table 48: Activation parameters for the catalyzed decomposition of diphenyol peroxide.

solvent	**$\Delta H^{\neq}$**	**$\Delta S^{\neq}$**	**$\Delta H_{CL}^{\neq}$**	**$\Delta G^{\neq}$**
acetone	15.0	-23.4	17.0	22.2
toluene	15.0	-22.2	15.0	21.6
butyl acetate	18.0	-15.0	15.0	21.1

$\Delta H^{\neq}$ (Kcal mol^{-1}); $\Delta S^{\neq}$ (cal K^{-1}mol^{-1}); $\Delta H^{\neq}_{CL}$ (Kcal mol^{-1}); $\Delta G^{\neq}$ (Kcal mol^{-1}) at 298.15 K.

Comparing the activation parameters of the catalyzed decomposition of the diphenyol in toluene and butyl acetate to the acetone. This result indicates that the affect of polarity solvent is less pronounced.

4.5.2. Determination of activation parameters for peroxide (2)

The kinetics of light emission have been done in order to determine the activation parameters for the thermolysis of *spiro*-adamantyl-1,2-dioxetanone and by keeping constant the concentration of spiro-adamantyl-1,2-dioxetanone (0.075 mmol L^{-1}) in a temperature range from 36 to 70 °C employing rubrene(0.4 mmol L^{-1}) as an activator in toluene. The values of the rate constant and initial emission intensity have been obtained from the curves of first order decay.

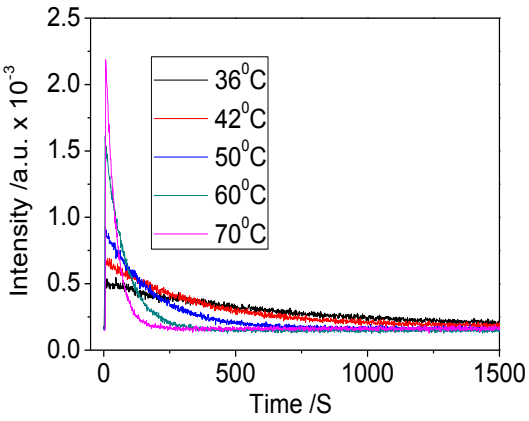

Figure 37: Kinetic curves of the emission intensity at various temperatures for the catalyzed decomposition of the *spiro*-adamantyl-1,2-dioxetanone (0.075 mmol L^{-1}) in toluene.

Table 49: The observed rate constants (k_{obs}) and initial intensity (I_0) at different temperatures for the decomposition of the *spiro*-adamantyl-1,2-dioxetanone in toluene.

T/K	k_{obs}/s^{-1}	I_0 / a.u.
309	1.6×10^{-3}	280
315	2.8×10^{-3}	561
323	5.7×10^{-3}	1123
333	1.3×10^{-2}	2246
343	2.6×10^{-2}	4896

[2] = 0.075 mmol L^{-1}; [RUB] = 0.4 mmol L^{-1} .

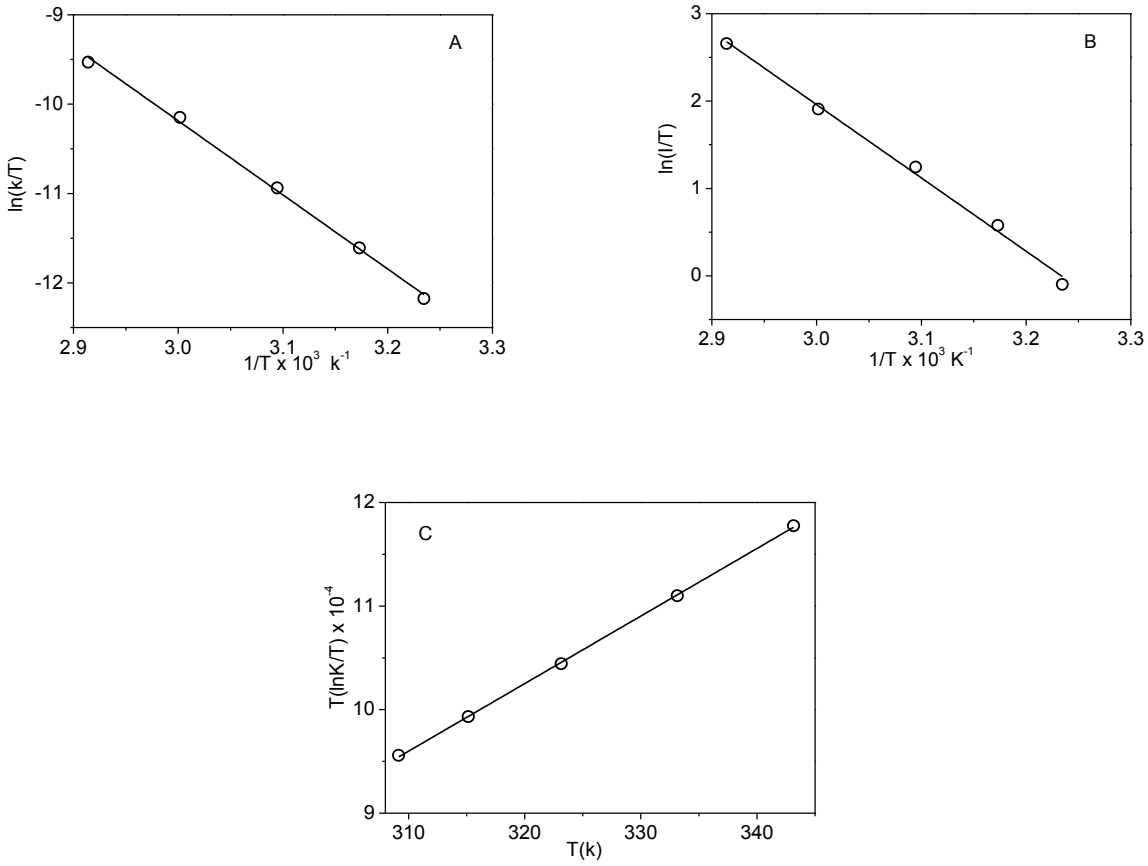

Figure 38: Determination of activation parameters: A= enthalpy ($\Delta H^{\neq}$); B = the enthalpy of the chemiluminescence reaction ($\Delta H^{\neq}_{CL}$), C = entropy ($\Delta S^{\neq}$) for the catalyzed decomposition of the *spiro*-adamantyl-1,2-dioxetanone in toluene.

The enthalpy of the chemiluminescence reaction ($\Delta H^{\neq}_{CL}$) has been determined by same way as determined for peroxide **1**. The activation parameters for the thermal decomposition of *spiro*-adamantyl-1,2-dioxetanone were determined with constant concentrations of rubrene by measuring the emission intensity decay at different temperatures obtaining an Eyring plot with excellent linear correlation.

Table 50: Activation parameters for the catalyzed decomposition of *spiro*-adamantyl-1,2-dioxetanone.

solvent	**$\Delta H^{\neq}$**	**$\Delta S^{\neq}$**	**$\Delta H_{CL}^{\neq}$**	**$\Delta G^{\neq}$**
TOL	16.7	-17.0	16.7	22.1

$\Delta H^{\neq}$ (Kcal mol^{-1}); $\Delta S^{\neq}$ (cal K^{-1}mol^{-1}); $\Delta H^{\neq}_{CL}$ (Kcal mol^{-1}); $\Delta G^{\neq}$ (Kcal mol^{-1}) at 298.15 K.

4.5.3. Determination of activation parameters for peroxide (3)

The various kinetics of light emission were performed to determine the activation parameters for the thermolysis of *spiro*-adamantyl-substituted 1,2-dioxetane (**3**) and by keeping constant the concentration of *spiro*-adamantyl-substituted 1,2-dioxetane (0.01 mmol L^{-1}) in a temperature range from 30 to 48 °C in tetrahydrofuran and temperature range from 35 to 60 °C in acetonitrile solvent. The values of the rate constant and initial emission intensity have been obtained from the curves of first order decay.

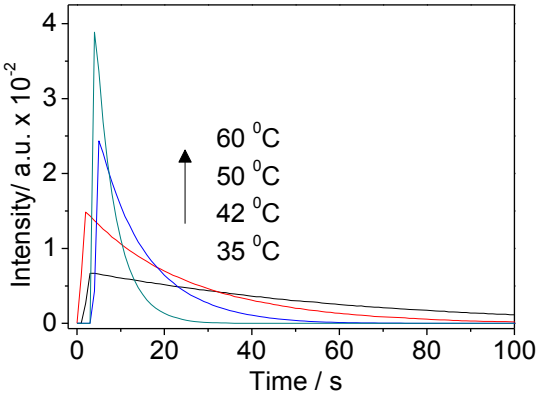

Figure 39: Kinetic curves of the emission intensity at various temperatures for the thermolysis of the *spiro*-adamantyl-substituted 1,2-dioxetane (0.01 mmol L^{-1}) with TBAF (2.5 mmol L^{-1}) in acetonitrile solvent.

Table 51: The observed rate constants (k_{obs}) and initial intensity (I_0) at different temperatures for the decomposition of the *spiro*-adamantyl-substituted 1,2-dioxetane with TBAF.

acetonitrile			THF		
T/K	**k_{obs} /s^{-1}**	**I_0 / a.u.**	**T/K**	**k_{obs} /s^{-1}**	**I_0 / a.u.**
308	1.84 x 10^{-2}	75	309	1.7 x 10^{-3}	1304
315	4.12 x 10^{-2}	159	315	3.3 x 10^{-3}	2793
323	8.88 x 10^{-2}	381	321	9.3 x 10^{-3}	7481
333	21.54 x 10^{-2}	972	/	/	/

[3] = 0.01 mmol L^{-1}; [TBAF] = 2.5 mmol L^{-1}.

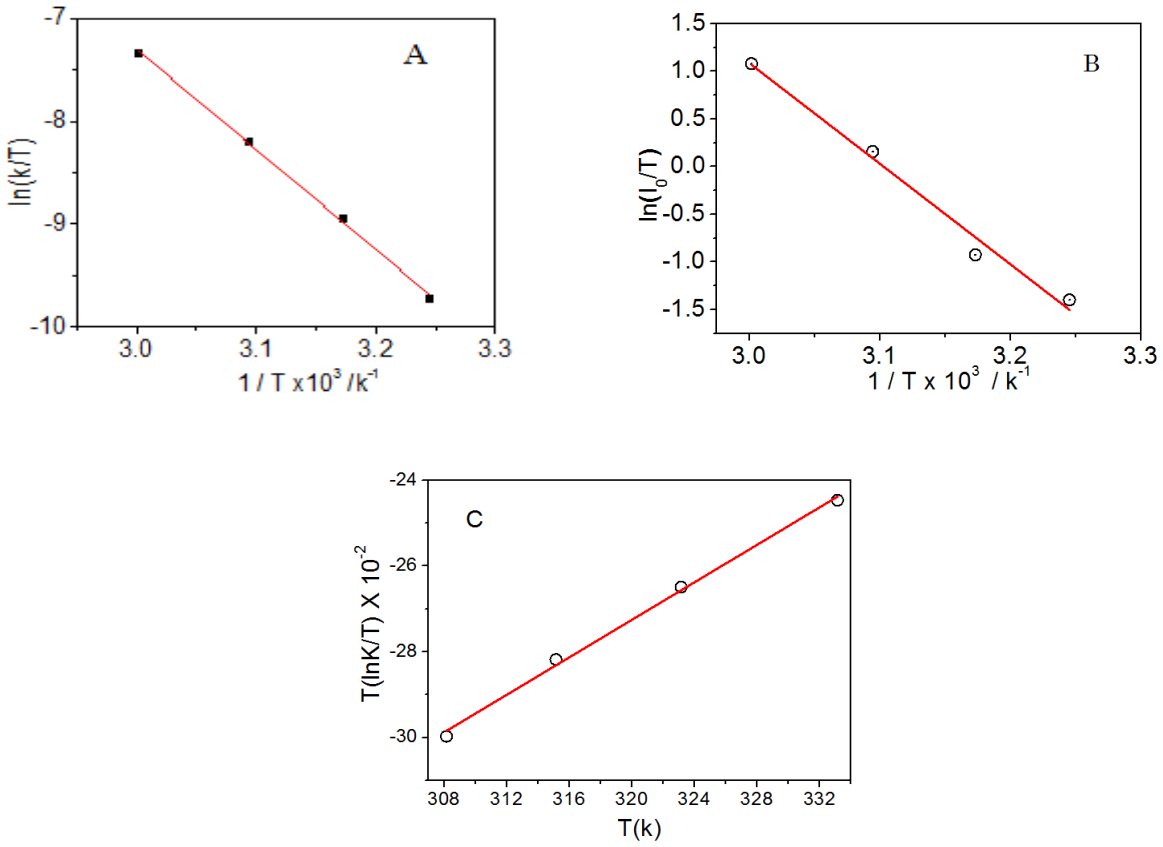

Figure 40: Determination of activation parameters: A= enthalpy ($\Delta H^{\neq}$); B = the enthalpy of the chemiluminescence reaction ($\Delta H^{\neq}_{CL}$); C=entropy ($\Delta S^{\neq}$) for the decomposition of the *spiro*-adamantyl-substituted dioxetane in acetonitrile solvent.

Table 52: Activation parameters for the induced decomposition of *spiro*-adamantyl-1,2-dioxetane.

solvent	$\Delta H^{\neq}$	$\Delta S^{\neq}$	$\Delta H_{CL}^{\neq}$	$\Delta G^{\neq}$
THF	27.2	-8.2	28.2	29.7
ACN	19.3	-3.8	21.0	20.4

$\Delta H^{\neq}$ (Kcal mol^{-1}); $\Delta S^{\neq}$ (cal $K^{-1}mol^{-1}$); $\Delta H^{\neq}_{CL}$ (Kcal mol^{-1}); $\Delta G^{\neq}$ (Kcal mol^{-1}) at 298.15 K.

5. Discussion

For mechanistic studies of this work needed to synthesise the cyclic peroxides: diphenoyl peroxide (**1**), *spiro*-adamantyl-1,2-dioxetanone (**2**) and *spiro*-adamantyl-1,2-dioxetane (**3**) following literature procedures.[78 - 81] The most difficult preparation is that of 1,2-dioxetanone, which could only be achieved by four groups who synthesized this class of compounds and performed kinetic studies with 1,2-dioxetanones.[82-84] The compound **2** has only been prepared by Adam's group and us all over the world.[80, 85] The cyclic peroxides were characterized by ^{1}H and ^{13}C NMR spectroscopy at low-temperature.[80]

The influence of solvent on the chemiluminescence parameters of the catalyzed decomposition of diphenoyl peroxide and *spiro*-adamantyl *a*-peroxy lactone as well as the induced decomposition of *spiro*-adamantyl-substituted dioxetane (**3**) was studied. The results obtained from the emission kinetics in the catalyzed decomposition of diphenoyl peroxide (**1**) and *spiro*-adamantyl-1,2-dioxetanone (**2**) with the activators the perylene and rubrene as well as decomposition of *spiro*-adamantyl-1,2-dioxetane (**3**) using tetra-butyl ammonium fluoride (TBAF) as deprotecting reagent in several solvents show that there is a considerable effect of the solvent on the kinetic data and quantum yields. The influence of the polarity of solvents on chemical reactions has been extensively studied. The term "solvent polarity" is complicated to define. A simple description about models for electrostatic solvation of ions and molecules considers the solvent as a medium with its own physical properties such as dielectric constant (ε_r), the permanent dipole moment (μ) and the refractive index (n_D), or any other medium constant which describes the macroscopic properties. However, the interactions between solute and solvent in microscopic properties occur in a medium that consists of individual molecules interacting with the solvent and solute. It is well known that solvents can have a strong influence on the position of chemical equilibria, on reaction rates, as well as on the position and intensity of spectral absorption

bands. Therefore, the selection of a proper solvent for the reaction under study is paramount importance for the success of this reaction. The effects can be explained in terms of solvent polarity [86 - 90] is much better described by molecular microscopic empirical solvent parameters derived from suitable solvent-dependent reference processes. In this case, the individual solvent molecules surrounding the ions or dipoles of the reference solute are arranged to a loose or tight solvation shell. The $E_T(30)$ values, empirically derived from solvatochromic measurements which are simply defined as the molar transition energies (kcal mol^{-1}) of the standard betaine dye[91,92] measured in solvents of different polarity at room temperature (25 °C).

5.1. Selection of solvents

The effect of solvent polarity on the catalyzed or induced decomposition of the peroxides **1**, **2** and **3** has been studied using several suitable solvent systems. These systems have a variation of the polarity in the largest possible range without significant variation in the viscosity parameters of the solvent system (Table 53).

Table 53: Binary solvent systems choosen, with their dielectric constant (ε_r), polarity $E_T(30)$ and viscosity (η) parameters for solvents.

# of binary solvent system	Solvent	ε_r	$E_T(30)$	η
1	toluene	2.4	33.9	0.5
	ethyl acetate	6.0	38.1	0.4
2	toluene	2.4	33.9	0.5
	butyl acetate	5.0	38.5	0.7
3	toluene	2.4	33.9	0.5
	acetone	21.0	42.2	0.3
4	ethyl acetate	6.0	38.1	0.42
	acetone	21.0	42.2	0.31
5	ethyl acetate	6.0	38.1	0.4
	acetonitrile	36	45.6	0.4
6	butyl acetate	5.0	38.5	0.7
	N, N-dimethyl formamide	36	43.2	0.8
7	toluene	2.4	33.9	0.5
	N, N-dimethyl formamide	36.0	43.2	0.8
8	acetone	21	42.2	0.3
	tetrahydrofuran	7.0	37.4	0.4
9	diphenyl ether	4.0	35.5	2.2
	dimethyl sulfoxide	47	45.1	2.0
10	toluene	2.4	33.9	0.5
	acetonitrile	36	45.6	0.4

According to the literature, for example, the pair of solvents benzene / diphenylmethane leading to values of about 0.004 to λ_S parameter, but these values can be found with large discrepancy in different literature sources. The accurate polarity parameters of these solvents were compiled (Table 54) in order to get accurate value for λ_S parameter of a large number of organic solvents [93] the solvent reorganization energy (λ_S) was calculated by using following formula.

$$\lambda_S = \frac{1}{n^2} - \frac{1}{\varepsilon} \qquad \text{Equation 36}$$

A series of aprotic polar solvents were selected to be utilized in the determination of their influence on chemiluminescent parameters (rate constants and quantum yields) for the above proposed systems in order to cover a polarity range between ε = 1.94 for *n*-heptane up to ε = 46.71 for dimethylsulfoxide, also covering a range of the empirical polarity parameter, $E_T(30)$, of 33.0 to 45.6, a solvent reorganization energy range of λ_S = 0.24 to 0.80, as well as a polarizability variation between 1.00 and 0.24 (Table 54). The suitable polar aprotic solvents have been evaluated with respect to their polarizability parameters like π*, which is an empirical polarizability parameter obtained from the refractive indices of these solvents. This approach has been used to verify the influence of solvent polarizability on the efficiency of the chemiexcitation in the final back-electron transfer step. The individual solvents such as anisole, butyl acetate and tetrahydrofuran and binary mixture solvent systems like ethyl acetate/dibutyl phthalate, toluene/diphenyl ether and toluene/diphenyl methane etc. have been used in order to investigate the influence of solvent viscosity on quantum yields. In these cases, the solvent reorganization energy (λ_S) is very similar which indicates that the polarity difference between the binary solvent mixtures is negligible.

Table 54: Polarity, polarizability and viscosity parameters for selected solvents

Solvente	n[a]	ε_r[b]	$E_T(30)$[c]	π^*[d]	π^*OMe[e]	λ_S[f]	η[g]
n-heptane	1.388	1.94	30.9[h]	/	0.15	0.0036	0.387
cyclohexane	1.426	2.024	30.9[h]	0.00	0.00	-0.0023	0.894
n-dibutyl ether	1.398	3.18	33.0[h]	0.24	0.18	0.1972	0.637
tetralin	1.541	2.773	33.5	/	/	0.0605	/
toluene	1.497	2.43	33.9	0.54	0.49	0.0347	0.560
diethyl ether	1.352	4.42	34.5	0.27	0.24	0.3208	0.224
1-methylnaphthalene	1.618	2.915	35.3h	/	0.78	0.0389	/
diphenyl ether	1.581	3.686	35.3	0.66	/	0.1288	2.130[i]
1,4-dioxan	1.422	2.27	36.0	0.55	0.49	0.0540	1.177
dibenzyl ether	1.562	3.86	36.3	0.80	0.80	0.1508	/
ethyl phenyl ether	1.507	4.22	36.6	0.69	0.65	0.2034	1.197
anisole	1.517	4.45	37.1	0.73	0.70	0.2098	1.056
tetrahydrofuran	1.406	7.47	37.4	0.58	0.55	0.3720	0.456
ethyl acetate	1.372	6.03	38.1	0.55	0.45	0.3654	0.423
ethyl benzoate	1.505	6.13	38.1	0.74	0.68	0.2784	/
n-butyl acetate	1.394	5.01	38.5	0.46	/	0.3150	0.685
chloroform	1.446	4.89	39.1	0.58	0.69	0.2738	0.537
di-n-butyl phthalate	1.493	6.44	39.5	/	/	0.2933	16.6
1,4-dichlorobutane	1.454	9.65	39.5	/	0.66	0.3693	/
glycerol triacetate	1.428	7.01	40.4	/	0.63	0.3477	/
acetophenone	1.534	18.18	40.6	0.90	0.81	0.3700	0.695
dimethyl phthalate	1.515	8.66	40.7	/	/	0.3202	14.4
dichloromethane	1.424	9.02	40.7	0.82	0.73	0.3823	0.413
1,2-dichloroethane	1.445	10.74	41.3	0.81	0.73	0.3858	0.779
acetone	1.359	21.36	42.2	0.71	0.62	0.4946	0.306
1-methyl-2-pyrrolidinone	1.469	32.58	42.2	0.92	0.92	0.4327	13
N, N-dimethyl formamide	1.430	37.04	43.2	0.88	0.88	0.4620	0.794
dimethyl sulfoxide	1.479	46.71	45.1	1.00	1.00	0.4357	1.987
acetonitrile	1.344	35.94	45.6	0.75	0.66	0.5258	0.369

a: refration index, 20 °C and 589.6 nm (Na-D). b: relative permittivity (ancient dielectric constant, 20 °C). c: Reichardt's empiric solvent parameter, 20 °C, (kcal/mol).[93,94] d: solvent polarizability parameter obtained from the solvatochromic shift of several aromatic probes A-C_6H_4-D, containing electron donating (D) and attracting (A) substituents using cyclohexane ($\pi^* = 0,0$) and dimethylsulfoxido ($\pi^* = 1,0$) as standards, 20 °C.[93,95] e: solvent polarizability parameter obtained similarly to the parameter π^*, however, using the solavatochromic shift of 4-methoxynitrobenzene.[96] g: absolute viscosity in cp (g/(cm s) x 10^2), 25 °C.[97] h: determined at 25 °C, utilizing the betaina $E_T(30)$.[98] i: determined at 25 °C, utilizing a Rheometer Brookfield model LV.D VIII.[98] j: obtained from the cinematic viscosity values at 20 °C in mm^2/s (www.glymes.com) using: absolute viscosity = cinematic viscosity x density.[97]

Activation parameters for the decomposition of cyclic peroxides.

The activation parameters for the catalyzed decomposition of diphenoyl peroxide (**1**), *spiro*-adamantyl-1,2-dioxetanone (**2**) and the induced decomposition of *spiro*-adamantyl-1,2-dioxetane (**3**) with TBAF were determined by measuring the emission intensity decay in different temperature ranges.

Table 55: Activation parameters for catalyzed decomposition of cyclic peroxides.

Peroxides	solvent	$\Delta H^{\neq}$	$\Delta S^{\neq}$	$\Delta H^{\neq}_{CL}$	$\Delta G^{\neq}$
1	acetone	15.0	-23.4	17.0	22.2
	toluene	15.0	-22.2	15.0	21.6
2	toluene	16.7	-17.0	16.7	22.0
3	THF	27.2	-8.20	28.2	29.7
	ACN	19.3	-3.80	21.0	20.4

$\Delta H^{\neq}$ (Kcal mol^{-1}); $\Delta S^{\neq}$ (cal $K^{-1}mol^{-1}$); $\Delta H^{\neq}_{CL}$ (Kcal mol^{-1}); $\Delta G^{\neq}$ (Kcal mol^{-1}) at 298.15 K.

The activation enthalpy values for **1** showed to be very similar in both solvents which indicates a transition state of the rate-limiting step with little charge separation, as this is apparently stabilized in the same way independent of solvent polarity. The chemiluminescence activation enthalpy value in toluene is similar to the decomposition activation enthalpy, which means that the transition states for excited and ground-state product formation posses the similar energy. However, in acetone the CL activation enthalpy is slightly higher, indicating that the transition state for formation of electronically

excited states has a higher energy than the unimolecular decomposition pathway, not leading to CL emission (Table 55).

The activation enthalpy values and the chemiluminescence activation enthalpy values of **2** in toluene are the same and this observation indicates that the transition states for unimolecular decomposition pathway and the chemiluminescent pathway of the *spiro*-adamantyl-1,2-dioxetanone (**2**) have almost the same energy (Table 55). Moreover, the similarity of the free activation energy values for **1** and **2** indicates a very similar kinetic behavior of both cyclic peroxides in toluene as solvent (Table 55).

On the other hand, the chemiluminescent activation enthalpy values for the induced decomposition of *spiro*-adamantyl-1,2-dioxetane (**3**) are considerable different in the two polar solvents studied and the values obtained in the more polar solvent acetonitrile are much lower than that measured in THF (Table 55). This fact indicates a higher charge separation of the transition state of the rate-limiting step as compared to the reagent state. Additionally, the CL activation enthalpy is slightly higher than the decomposistion enthalpy, which may indicate a different, higher energy, pathway for excited state formation.

The higher negative activation entropy value obtained for the catalyzed decomposition of **1** and **2** is in agreement with the assumption that the rate-limiting step of the CL pathway involves the bimolecular interaction of the peroxide with the ACT (Schemes 12, 13). The much lower negative entropy values for the induced decomposition of **3** is in agreement with the assumption that the rate-limiting step in this case should be the intramolecular electron transfer from the phenolate to the peroxidic ring (Scheme 16).[99] The negative values, even so low, might be due to the need of a specific conformation for the occurrence of the electron transfer process.

5.2. Kinetic study on the catalyzed diphenoyl peroxide decomposition

The chemiluminescent decomposition of diphenoyl peroxide by perylene or rubrene (Activators) is initiated by rate-limiting electron transfer from this

activator to the antibonding σ* orbital of the O-O bond in diphenoyl peroxide, followed by fast O-O bond cleavage, generating a radical anion from the former peroxide and the activator radical cation. Decarboxylation takes place rapidly and ring closure of this species produces benzocoumarin radical anion, which is a powerful reducing agent and annihilation with in the cage can produce the singlet excited state of activator which results in chemiluminescence emission. Diffusion of the radical ions out of the solvent cage leads only to ground-state product formation and no light emission is observed [100] (Scheme 11). The CIEEL mechanism was used to explain the catalyzed decomposition of diphenoyl peroxide. However, the quantum yield of the diphenoyl peroxide / perylene was much lower than previously reported.[100,51] So, this investigation raised questions about the genuineness of the CIEEL mechanism. Now, this CIEEL mechanism for diphenoyl peroxide remains a topic for discussion due to the low quantum yields.

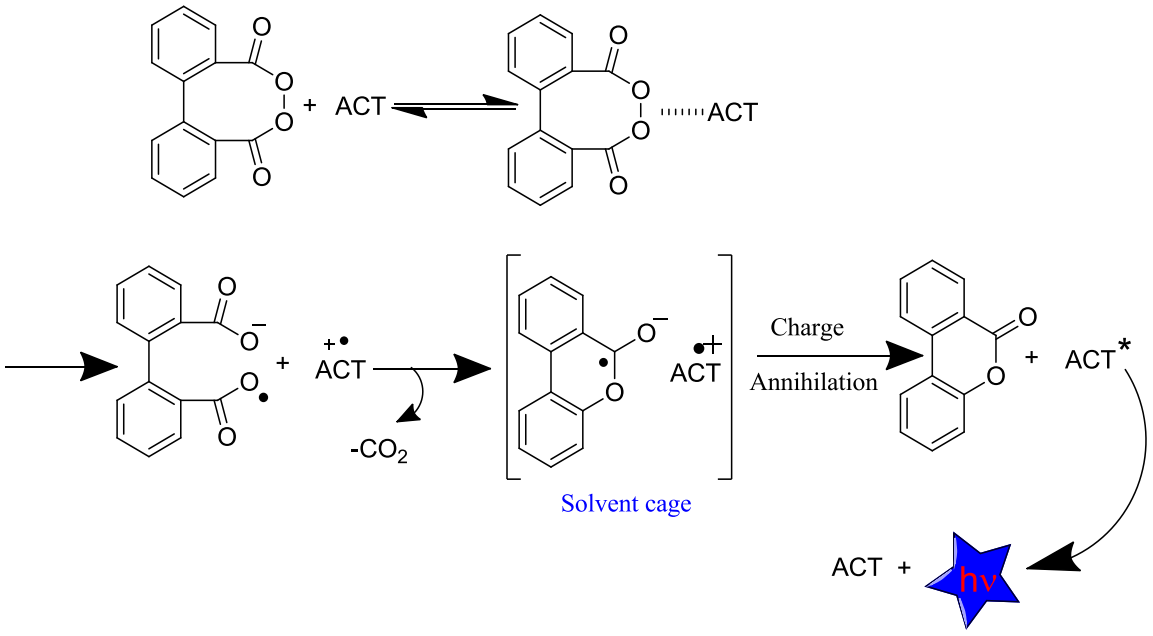

Scheme 11: CIEEL mechanism for the catalyzed decomposition of diphenoyl peroxide.

In order to contribute to a better understanding of the mechanism of the intermolecular CIEEL mechanism, the influence of the solvent polarity on the CL parameters of the catalyzed decomposition of diphenoyl peroxide was

studied using several polar nonprotic solvents, most of them with similar viscosity.

Table 56a: Chemiluminescence parameters for the perylene and rubrene catalyzed decomposition of the diphenoyl peroxide in solvents of different polarity.

Solvent	ε_r / $E_T(30)$	η (cP)	ACT	k_{CAT} / L mol^{-1} s^{-1}	k_D / s^{-1} x 10^3	Φ_S^{CAT} x 10^4 (E mol^{-1})
dibutyl ether	3.18 / 33.0	0.637	**PER**	0.15 ± 0.05	0.16 ± 0.03	0.49 ± 0.04
			RUB	2.00 ± 0.01	2.40 ± 0.02	4.2 ± 0.4
anisole	4.45 / 37.1	1.056	**PER**	0.62 ± 0.03	0.77 ± 0.01	1.24 ± 0.04
			RUB	3.9 ± 0.2	1.30 ± 0.03	47.0 ± 2.0
ethyl acetate	6.03 / 38.1	0.423	**PER**	0.21 ± 0.01	0.45 ± 0.01	1.1 ± 0.1
			RUB	4.3 ± 0.2	1.0 ± 0.1	5.23 ± 0.04
butyl acetate	5.01 / 38.5	0.685	**PER**	0.11 ± 0.01	0.438 ± 0.002	1.5 ± 0.1
			RUB	3.3 ± 0.2	0.70 ± 0.02	7.0 ± 0.4
dibutyl phthalate	6.44 / 39.5	16.6	**PER**	0.95 ± 0.02	1.00 ± 0.01	1.9 ± 0.1
			RUB	6.7 ± 0.2	1.90 ± 0.04	21.0 ± 0.1
DMF	37.04 / 43.2	0.794	**PER**	2.4 ± 0.1	0.39 ± 0.05	0.50 ± 0.06
			RUB	5.8 ± 0.2	0.90 ± 0.01	3.8 ± 2.0
ACN	35.94 / 45.6	0.369	**PER**	1.85 ± 0.01	0.78 ± 0.01	0.27 ± 0.08
			RUB	12.0 ± 1.0	2.30 ± 0.01	3.5 ± 0.2

ACN= acetonitrile; DMF= *N,N*-dimethyl formamide.

Table 56b: Chemiluminescence parameters for the perylene catalyzed decomposition of the diphenoyl peroxide in solvents of different polarity.

Solvent	ε_r / $E_T(30)$	η (cP)	ACT	k_{CAT} / L mol^{-1} s^{-1}	k_D / s^{-1} x 10^3	Φ_S^{CAT} x 10^4 (E mol^{-1})
toluene	2.3 / 34	0.56	**PER**	0.44 ± 0.01	1.53 ± 0.01	0.52 ± 0.05
diethyl ether	4.4 / 34.5	0.22	**PER**	0.08 ± 0.03	0.2 ± 0.1	0.11 ± 0.05
THF	7.5 / 37.4	0.46	**PER**	0.25 ± 0.01	0.4 ± 0.1	1.9 ± 0.2
acetone	21 / 42.0	0.42	**PER**	0.35 ± 0.03	0.53 ± 0.02	1.70 ± 0.01
PYRR	33 / 42.2	13.0	**PER**	0.53 ± 0.01	0.50 ± 0.01	2.24 ± 0.02

PYRR =1-methyl-2-pyrrolidinone.

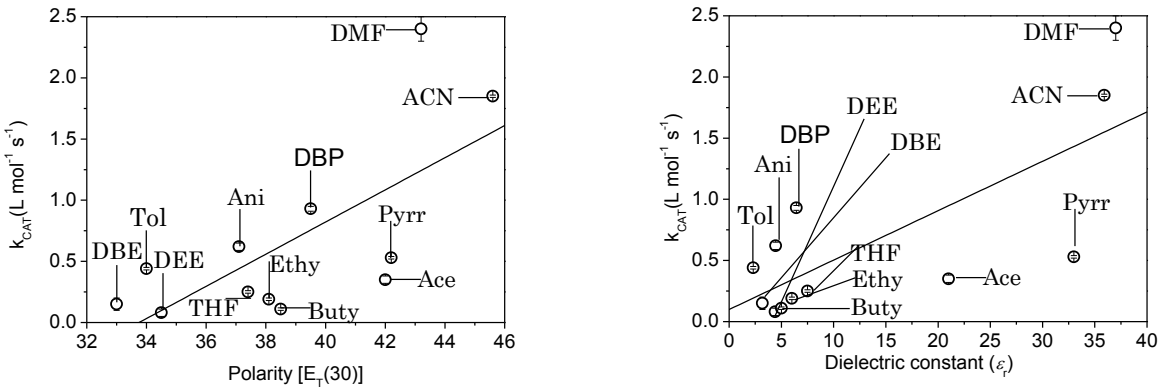

Figure 41: Dependence of the catalytic rate constants (k_{CAT}) for perylene catalyzed decomposition of diphenoyl peroxide on the solvent polarity constants $E_T(30)$ and dielectric constant (ε_r) at 36 °C. Tol = toluene; DBE = dibutyl ether; DEE = diethyl ether; Ani = anisole; Buty = butyl acetate; DBP = dibutyl phthalate; Ethy = ethyl acetate; THF = tetrahydrofuran; Ace = acetone; Pyrr =1-methyl-2-pyrrolidinone; ACN = acetonitrile; DMF = *N,N*-dimethyl formamide.

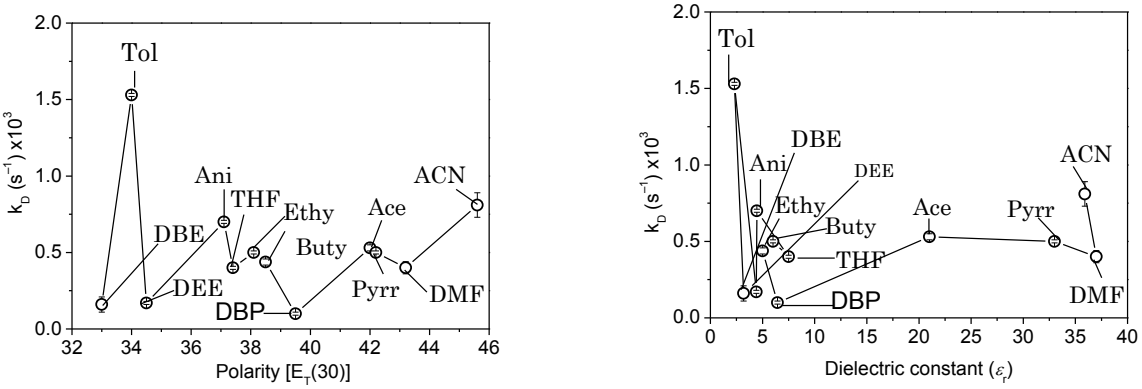

Figure 42: Dependence of the unimolecular rate constants (k_D) for perylene catalyzed decomposition of diphenoyl peroxide on the solvent polarity constants $E_T(30)$ and dielectric constant (ε_r) at 36 °C. Tol = toluene; DBE = dibutyl ether; DEE = diethyl ether; Ani = anisole; Buty = butyl acetate; DBP = dibutyl phthalat; Ethy = ethyl acetate; THF = tetrahydrofuran; Ace = acetone; Pyrr =1-methyl-2-pyrrolidinone; ACN = acetonitrile; DMF = *N,N*-dimethyl formamide.

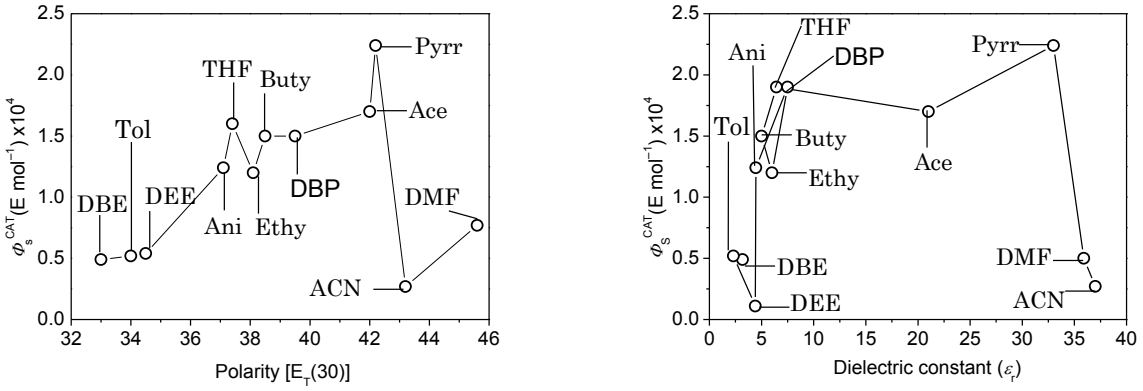

Figure 43: Dependence of the catalyzed singlet quantum yield (Φ_S^{CAT}) for perylene catalyzed decomposition of diphenoyl peroxide on the solvent polarity constants $E_T(30)$ and dielectric constant (ε_r) at 36 °C. Tol = toluene; DBE = dibutyl ether; DEE = diethyl ether; Ani = anisole; Buty = butyl acetate; DBP = dibutyl phthalate; Ethy = ethyl acetate; THF = tetrahydrofuran; Ace = acetone; Pyrr =1-methyl-2-pyrrolidinone; ACN = acetonitrile; DMF = *N,N*-dimethyl formamide.

The results obtained from these studies (Table 56) indicate that the magnitude of the catalytic decomposition rate constant (k_{CAT}) shows a slight increase with increasing polarity. However, k_{CAT} remarkably increased with high polar aprotic solvents i.e. ACN and DMF (Figure 41). Additionally, it appears that k_{CAT} slightly change with the solvent viscosity (η) as can be seen from a coparison of the values for ethyl acetate and butyl acetate to dibutyl phthalate (Table 56). The values of unimolecular rate constants (k_D) remained constant for all solvents except in TOL. Furthermore, values are higher for rubrene as activator, which is unexpected (Table 56a).

Catalyzed singlet quantum yields (Φ_S^{CAT}) for the decomposition of diphenoyl peroxide are significantly higher in medium polar aprotic solvents as compared to higher polar aprotic solvents (acetonitrile and *N,N*-dimethyl formamide) and lower polar aprotic solvents (toluene, dibutyl ether and diethyl ether) (Table 56, Figure 43).

Rubrene and perylene are used as activators for the decomposition of diphenoyl peroxide in order to compare the effects of thses activators on kinetic data and the catalyzed singlet quantum yield (Φ_S^{CAT}). The obtained results from these comparision studies (Table 56) indicate that catalyzed singlet quantum yields (Φ_S^{CAT}) are higher for rubrene as compared to perylene as activator, because in the case of rubrene the energy liberated upon electron back transfer has been shown to be higher (for a discussion of this subject see Ref. 63).

5.2.1. Influence of solvent polarity [$E_T(30)$] and polarizability (π^*) parameters on the Φ_S and Φ_S^{CAT} of 1 using binary solvent mixtures.

We selected some of the solvents which possess very similar physicochemical parameters with the exception of the polarity parameter. This fact opened the possibility to utilize binary solvent mixtures and the following binary mixtures were selected: (i) toluene-ethyl acetate, (ii) toluene-acetone, (iii) ethyl acetate-acetone and toluene-acetonitrile. In each of the pairs, the solvents showed similar physicochemical parameters, however, cover a wide range of polarity values, therefore, they are utilized to study the influence of polarity parameters on singlet chemiexcitation quantum yields (Φ_S) for the induced decomposition of diphenoyl peroxide. Moreover, the aprotic solvents are used to avoid complications in interpreting the results introduced by the formation of hydrogen bonds in protic solvents leading also to a considerable decrease in quantum yields.[101]

Table 57: Chemiluminescence parameters for the perylene catalyzed decomposition of the diphenoyl peroxide in binary solvent mixtures of toluene and acetone.

Solvent system	$E_T(30)$	(π*)	Φ_S (E mol^{-1}) ×10^6
100% toluene	34.2	0.29	6.1 ± 0.7
20% acetone	36.2	0.28	7.0 ± 0.7
40% acetone	38.2	0.26	9.2 ± 0.4
60% acetone	40.0	0.25	10.7 ± 0.3
80% acetone	41.6	0.24	11.9 ± 0.7
100% acetone	42 .2	0.22	13.5 ± 0.4

$E_T(30)$ and π* of binary solvent mixture obtained by using Reichardt's dye and refractive indices respectively.

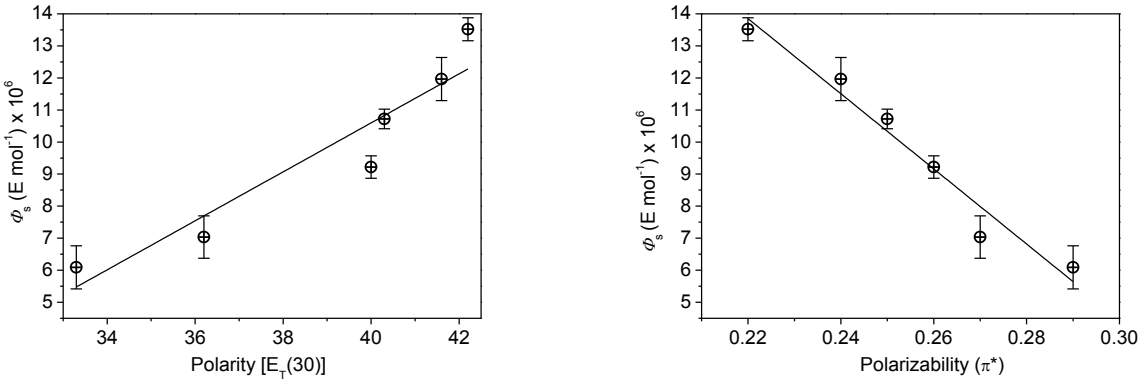

Figure 44: Dependence of the singlet quantum yield (Φ_S) for perylene catalyzed decomposition of diphenoyl peroxide on the solvent polarity constant [$E_T(30)$] and polarizability (π*) using mixtures of toluene and acetone at 36 ºC.

The experiments were carried out in mixtures of toluene and acetone that have similar viscosity parameters (η = 0.56 and 0.42, respectively) but completely different polarity [$E_T(30)$]and polarizability (π*) parameters. Interestingly, the polarity and polarizability values are contrarily for these two solvents, that is, acetone is more polar than toluene, however, toluene is more polarizable as compared to acetone (Table 57). The singlet quantum yields increase with increasing solvent polarity; for varying the polarity parameter $E_T(30)$ from

$E_T(30)$ = 36.2 (20% acetone) to $E_T(30)$ =41.6 (80% acetone) indicated increase in the singlet quantum yields (Φ_S) by a factor of 1.7. Moreover, comparing the values for the pure toluene [$E_T(30)$ = 34.2] with pure acetone [$E_T(30)$ = 42.2] reflected an increase in singlet quantum yields (Φ_S) by a factor of ca. 2.2 (Table 57). This experimental data show a continuous increase of the singlet quantum yields (Φ_S) with an increasing of the polarity of solvent system (mixtures of toluene and acetone). Consequentely, as the polarizability parameter shows the opposite trend to the polarity in this system, the singlet quantum yields decreased with increasing the polarizability (π^*) of the solvent system (Figure 44).

The solvent systems toluene-acetonitrile, toluene-ethyl acetate and ethyl acetate-acetone also possess similar viscosity parameters but completely different polarity parameters [$E_T(30)$] values. For the system toluene–acetonitrile, the quantum yields increased with increasing solvent polarity; from $E_T(30)$ = 34 (toluene) to $E_T(30)$ = 38 (20% acetonitrile). However, there is an important point where the polarity of the mixture is $E_T(30)$ = 38 (20% acetonitrile), at this point the quantum yields show a maximum value and for higher polarity values, the quantum yield start to decrease with increasing solvent polarity (Table 58, Figure 45).

For the system toluene–ethyl acetate, the catalyzed singlet quantum yields (Φ_S^{CAT}) increased with increasing polarity; for varying the polarity parameter from $E_T(30)$ = 35.63 (20% ethyl acetate) to $E_T(30)$ = 38.56 (80% ethyl acetate) a slight increase in the catalyzed singlet quantum yields (Φ_S^{CAT}) by a factor of almost 1.3 is observed. Moreover, comparing the values for pure toluene [$E_T(30)$ = 34.22] with pure ethyl acetate [$E_T(30)$ = 39.38], the increase in the catalyzed singlet quantum yields (Φ_S^{CAT}) is by a factor of ca. 2 (Table 59). This experimental data show a continuous increase of the catalyzed singlet quantum yields (Φ_S^{CAT}) with the increase of polarity of toluene–ethyl acetate mixtures.

Table 58: Singlet quantum yields for the perylene (3.0 mmol L^{-1}) catalyzed decomposition of the diphenoyl peroxide in binary solvent mixtures of toluene and acetonitrile.

Solvent system	$E_T(30)$	Φ_S (E mol^{-1}) x 10^5
100% toluene	34.2	2.4 ± 0.2
95% toluene	39.7	3.1 ± 0.2
90% toluene	40.8	3.2 ± 0.1
80% toluene	41.4	3.3 ± 0.1
70% toluene	42.6	2.73 ± 0.01
60% toluene	43.06	2.4 ± 0.1
50% toluene	43.8	2.06 ± 0.04
40% toluene	44.0	1.66 ± 0.01
30% toluene	44.5	1.40 ± 0.01
20% toluene	45.2	1.11 ± 0.02

$E_T(30)$ of binary solvent mixture obtained by using Reichardt's dye.

Table 59: Catalyzed singlet quantum yields (Φ_S^{CAT}) for the perylene catalyzed decomposition of the diphenoyl peroxide in binary solvent mixtures of toluene-ethyl acetate and ethyl acetate-acetone.

Solvent (A)	Solvent (B)	$E_T(30)$	Φ_S^{CAT} (E mol^{-1}) x10^4
100% TOL	0% EA	34.2	0.53 ± 0.01
80% TOL	20% EA	35.6	0.6 ± 0.1
60% TOL	40% EA	36.3	0.66 ± 0.02
40% TOL	60 % EA	37.4	0.7 ± 0.1
20% TOL	80% EA	38.2	0.84 ± 0.02
100% EA	0% ACE	38.5	1.0 ± 0.2
80% EA	20% ACE	39.0	1.1 ± 0.1
40% EA	60% ACE	40.7	2.3 ± 0.2
20% EA	80% ACE	41.4	1.9 ± 0.1
0% EA	100% ACE	42.2	1.7 ± 0.1

TOL = toluene; EA = ethyl acetate; ACE = acetone; $E_T(30)$ of binary solvent mixture obtained by using Reichardt's dye.

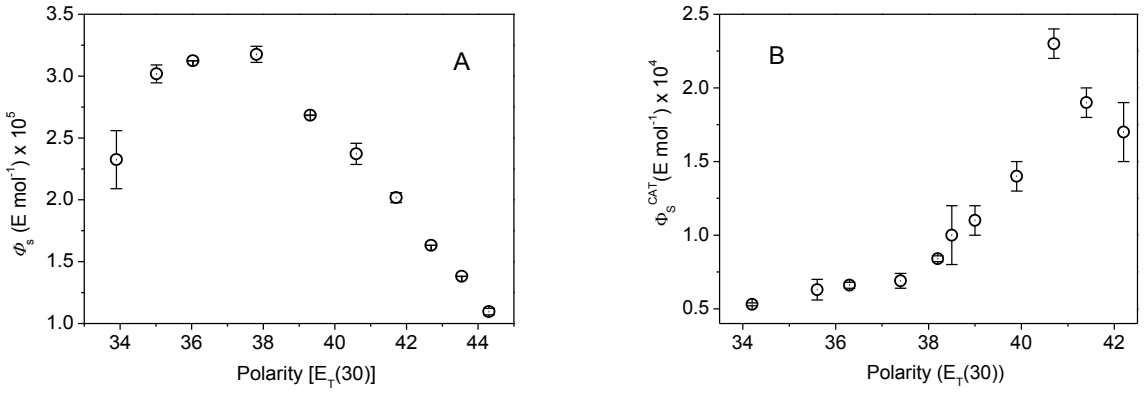

Figure 45: Dependence of the quantum yields for perylene catalyzed decomposition of diphenoyl peroxide on the solvent polarity constant [$E_T(30)$] using mixtures of toluene-acetonitrile (**A**) and toluene-ethyl acetate, ethyl acetate-acetone (**B**) at 36 °C.

For ethyl acetate–acetone mixtures, the quantum yields increased with increasing solvent polarity from $E_T(30)$ = 39 (20% acetone) to $E_T(30)$ = 40.7 (60% acetone) (Table 59). However, after this polarity point $E_T(30)$ = 40.7 (60% acetone) the quantum yields again started to decrease with increasing polarity (Figure 45).

In fact, polar solvents are considered to stabilize the initially produced radical ion pair in the intra as well as intermolecular systems. Solvation by polar solvents initially keeps these species together, however, an increase in solvent polarity can lead to the separation of the ion pair and as a result the excitation quantum yields will be lowered (Scheme 12). A very important and significant point is that chemiexcitation can only occur if the radical ion pair initially formed stays together in the same "solvent cage", permitting excited state formation by electron back transfer (EBT). If these species escape from the solvent cage then the highly reactive radical species will not have a sufficient long lifetime to be able to meet another opposite radical species for electron back transfer. In this way, these "cage-escaped" species will be "lost" for chemiexcitation and subsequently, only ground state products will be formed (Scheme 12).

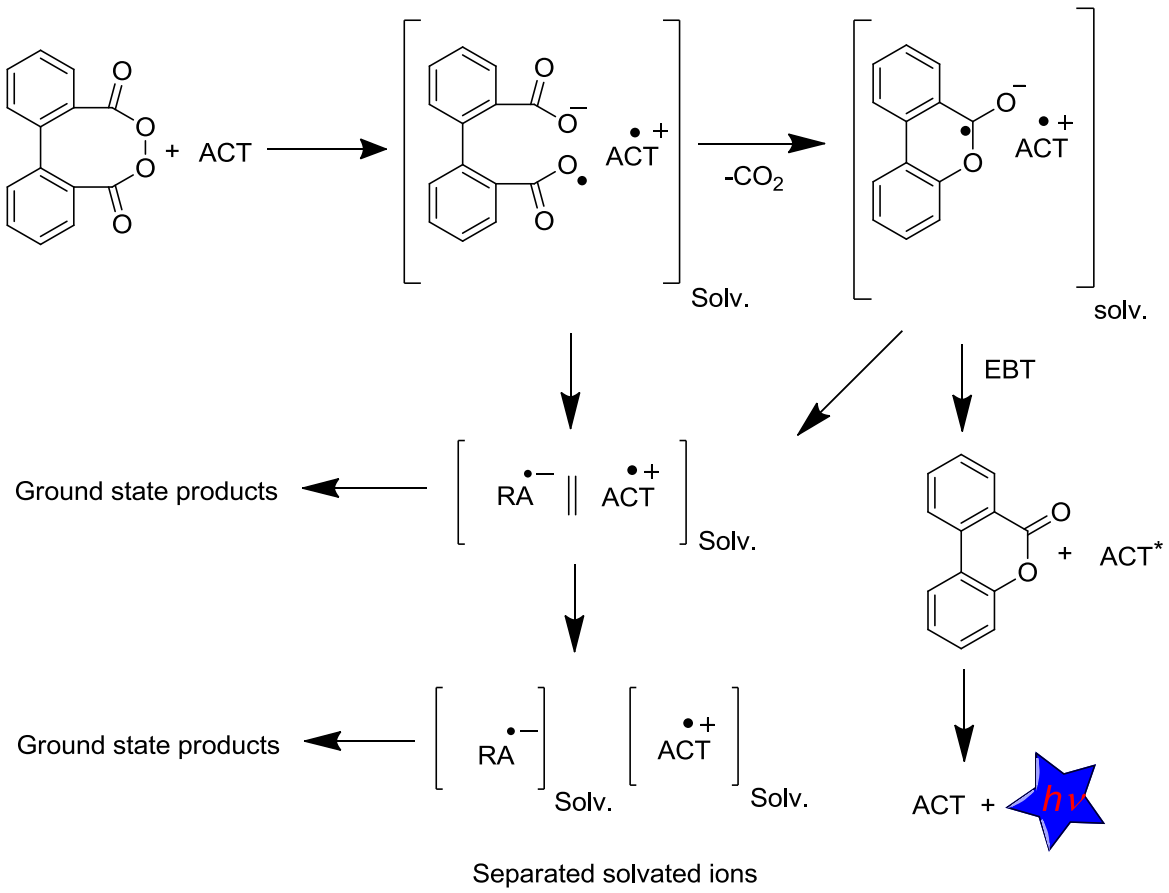

Scheme 12: Solvation process for the catalyzed decomposition of diphenoyl peroxide (**1**).

On the basis of these observations, it is expected that the reaction rates and the quantum yields increased with high polar solvent, however, it can be expected that the quantum yield start to decrease with increasing the solvent polarity due to the formation of solvent separated ion pairs and solvated íons, a process which will decrease the probability of excited state formation by electron back transfer (Scheme 12). Our studies on the solvent polarity influence on the singlet quantum yields in the catalyzed decomposition of diphenoyl peroxide show that this expected behavior can in fact occur in a certain medium polarity range.

5.3. Kinetic study on the catalyzed decomposition of *spiro*-adamantyl *a*-peroxylactone (2)

spiro-Adamantyl *a*-peroxy lactone **2** is the most stable derivative of this class of compounds which can be synthesized and appropriately purified by recrystallization. The kinetic data obtained for the catalyzed decomposition of this derivative are more reliable than results obtained for other, less stable, derivatives.

In the course of the mechanistic studies on the CL of *spiro*-adamantyl-1,2-dioxetanone usually can be catalyzed by polycondensed aromatic hydrocarbons has led to the formulation of the Chemically Initiated Electron Exchange Luminescence (CIEEL) mechanism. The decomposition rates of the dioxetanone monitored by the decay of light emission increased in the presence of polycondensed aromatic hydrocarbons of low oxidation potential and high fluorescence quantum yield (Φ_{FL}) the so-called activators (ACT) and the emission intensities were strongly enhanced. Furthermore, the rate constants and emission intensities were shown to depend on the oxidation potential of the activator utilized, indicating the occurrence of an electron transfer process in the rate-limiting step.

The chemiluminescent decomposition of *spiro*-adamantyl-1,2-dioxetanone by rubrene is initiated by charge transfer complex formation between the dioxetanone and the rubrene, followed by rate-limiting electron transfer from this activator to the antibonding σ* orbital of the O-O bond in *spiro*-adamantyl-1,2-dioxetanone and the most probable O-O bond cleavaged at the same time. A radical anion from the dioxetanone and the rubrene radical cation produced. Cleavage of the C-C bond and the formation of carbon dioxide left a pair of radical ions still in contact within the solvent cage (radical cation of the rubrene and radical anion of *spiro*-adamantanone). The electron back transfer between these two radical ions within the cage can be released enough energy to form the rubrene in its first singlet-excited state which results in chemiluminescence emission (Scheme 13).

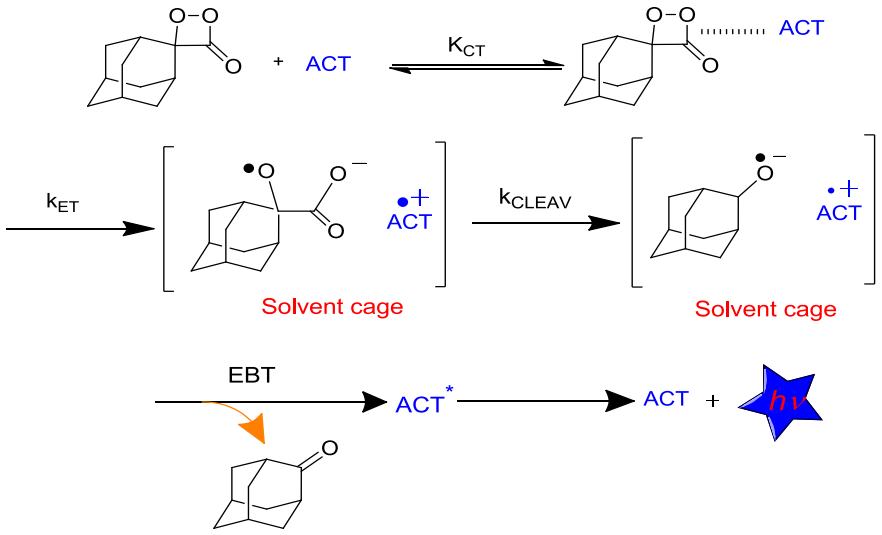

Scheme 13: CIEEL mechanism for the catalyzed decomposition of *spiro*-adamantyl-1,2-dioxetanone (**2**).

Solvation by polar solvents initially keeps these species together, however, the separation of the ion pair by highly polar solvents can occur, resulting in lower chemiexcitation quantum yields (Scheme 13). The CIEEL mechanism was first proposed in an attempt to rationalize the fact that easily oxidizable aromatic hydrocarbons (activators) catalyzed decomposition of 1,2-dioxetanones and the catalyzed rate constant (k_{CAT}) was proportional to the oxidation potential of activator. Contrary to these observations, the variation of the observed rate constant (k_{obs}) with the different concentration of activator could not be observed in the study of *spiro*-adamantyl-1,2-dioxetanone, i.e., it was not possible to obtain the catalyzed rate constants (k_{CAT}). Although it was possible to note the dependence of the emission intensity with the concentration and the nature of the activator used: the more easily oxidizable activator showed a higher emission intensity and the emission intensity also increases with increasing the concentration of activator.

The interaction between the ACT and the peroxide is based on the following kinetic scheme.

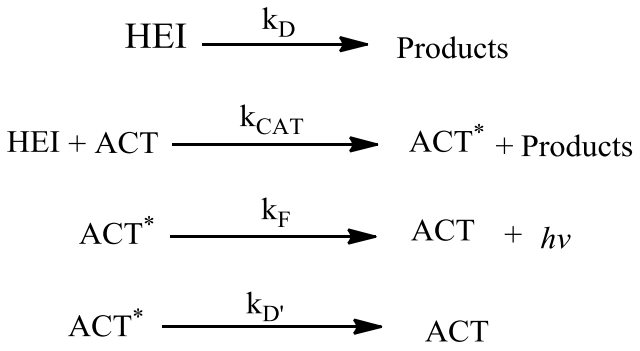

Scheme 14: Simplified kinetic scheme showing the reaction steps leading to light emission from the interaction of 1,2-dioxetanone (HEI) with an activator (ACT) and asterisk represents the excited state.

Applying the steady-state approximation to this kinetic scheme it is possible to deduce the relationship between the singlet quantum yields (Φ_S) and the singlet quantum yields at infinite concentration of activator (infinite singlet quantum yield Φ_S^{∞}).[63]

$$\frac{1}{\Phi_s} = \frac{1}{\Phi_s^{\infty}} + \left[\frac{k_D}{k_{CAT}\Phi_s^{\infty}}\right]\frac{1}{[ACT]}$$

Scheme 15: The relationship by steady state approximation for the interaction of the activator with 1,2-dioxetanone.[102]

The intercept and slop of the linear relationship between 1/[ACT] and $1/\Phi_S$ are equal to $1/\Phi_S^{\infty}$ and $\left[\frac{k_D}{k_{CAT}\,\Phi_S^{\infty}}\right]$. From the linear coefficient of the above equation, we obtained the infinite singlet quantum yield at the infinite concentration of activator. This yield have been obtained when the whole peroxide present in the system interacts with the activator. The k_{CAT}/k_D relation has also been obtained from the slope, where k_D is the constant for unimolecular decomposition of the peroxide, while k_{CAT} is the rate constant of its interaction with the activator. In this work, it was not possible to obtain the value of k_{CAT} directly for the catalyzed decomposition of peroxide from the dependence of k_{obs}

with [ACT]. However, the k_{CAT} value was obtained in an indirect way, from the inclination of the double-reciprocal graphs (k_{CAT}/k_D) and the average value of k_{obs} obtained in each experiment. In the case of the catalyzed decomposition of 1,2-dioxetanone **2**, it appears that the unimolecular pathway is the predominant one (as indicated by the fact that the observed rate constants do not depend on the activator concentration), therefore the mean k_{obs} values can be used as measure for the unimolecular decomposition rate constant (k_D) of *spiro*-adamantyl-1,2-dioxetanone (Table 60).

Table 60: Singlet quantum yields (Φ_S), infinite quantum yields (Φ_S^{∞}) and kinetic data for the decomposition of *spiro*-adamantyl-1,2-dioxetanone (**2**) using rubrene as a catalyst in pure solvents.

Solv.	η (cP)	$E_T(30)$	k_{obs} / s^{-1} x 10^3	Φ_S (E mol^{-1}) x 10^3 [a]	k_{CAT} / k_D / L mol^{-1} x 10^{-3}	k_{CAT} / L mol^{-1} s^{-1}	Φ_S^{∞} (E mol^{-1}) x 10^3 [b]
TOL	0.56	34	1.7 ± 0.1	2.9 ± 0.1	9.6 ± 0.8	16.61 ± 0.01	1.9 ± 0.7
DPE	2.13	35	2.04 ± 0.01	6.03 ± 0.08	5.6 ± 0.1	11.4 ± 0.1	4.8 ± 11.1
EA	0.45	38.1	1.6 ± 1.2	2.6 ± 0.5	15.5 ± 0.4	24.64 ± 0.01	1.3 ± 1.0
BUT	0.68	38.5	1.6 ± 0.1	3.4 ± 0.3	6.3 ± 0.1	10.14 ± 0.02	1.7 ± 5.0

[rubrene][a] = 0.2 mmol L^{-1} for TOL = toluene, DPE = diphenyl ether; [rubrene][a] = 0.3 mmol L^{-1} for EA = ethyl acetate, BUT = butyl acetate; [rubrene][b] = 0.05 to 0.2 mmol L^{-1} for TOL, DPE and EA; [rubrene][b] = 0.1 to 0.3 mmol L^{-1} for BUT.

In a hypothetical experimental condition, where the concentration of the ACT is infinitely high, every molecule of the peroxide (**2**) will react with the ACT and there will be no contribution of the unimolecular decomposition. This experimental condition can be reached by making double-reciprocal plots of the singlet quantum yields (Φ_S) and the ACT concentration, according to scheme 15. From the intercept of these correlations it is possible to obtain the Φ_S^{∞} values which are equivalent to the Φ_S^{CAT} values obtained for diphenoyl peroxide decomposition.

After having determined the quantum yields for the 1,2-dioxetanone decomposition in pure solvents, some binary solvent mixtures were choosen which possess very similar physicochemical parameters with the exception of the polarity parameter.

Table 61: Chemiluminescence parameters for the rubrene catalyzed decomposition of the *spiro*-adamantyl-1,2-dioxetanone (**2**) in binary solvent mixtures of ethyl acetate and acetonitrile.

%Solvent	$E_T(30)$	Φ_S (E mol^{-1}) x 10^4
acetonitrile	45.6	1.63 ± 0.03
20% ethyl acetate	44.7	1.70 ± 0.04
40% ethyl acetate	43.6	1.72 ± 0.05
60% ethyl acetate	42.3	1.79 ± 0.01
80% ethyl acetate	40.5	1.82 ± 0.02
ethyl acetate	39.38	1.93 ± 0.03

$E_T(30)$ of binary solvent mixture obtained by using Reichardt's dye.

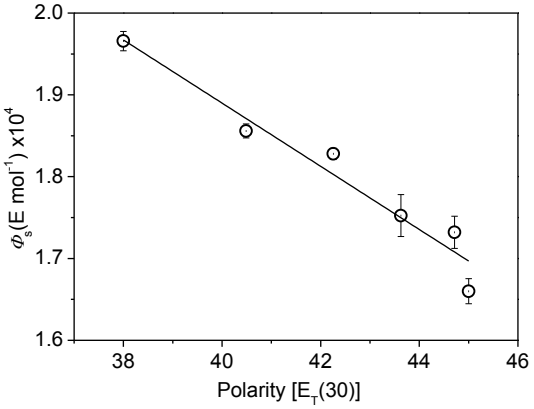

Figure 46: Dependence of the singlet quantum yield (Φ_S) for the rubrene catalyzed decomposition of the *spiro*-adamantyl-1,2-dioxetanone on the solvent polarity constant [$E_T(30)$] using the mixtures of ethyl acetate and acetonitrile at 25 °C.

The solvent system ethyl acetate-acetonitrile possess similar viscosity parameters but completely different polarity parameters [$E_T(30)$] values. For the system ethyl acetate–acetonitrile, the chemiluminescence quantum yields decrease with increasing the polarity of the solvent system; for varying the polarity parameter $E_T(30)$ from $E_T(30)$ = 45.6 (100% ACN) to $E_T(30)$ = 39.38 (100% ethyl acetate) indicated decrease in the quantum yields (Φ_S) by factor of 1.2 (Table 61).

5.3.1. Solvent polarity [$E_T(30)$] and polarizability (π^*) effect on the Φ_S of peroxide (2) using binary solvent mixtures

Surprisingly, the influence of polarity and polarizability parameters has been observed completely different in some solvent systems and showed independent analysis of these factors for the quantum yields. For example the singlet quantum yields increase in the function of polarizability of toluene-acetone and toluene-acetonitrile solvent systems for the intermolecular catalyzed *spiro*-adamantyl α-peroxy lactone (Figuer 47) whereas, the singlet quantum yields decrease in the function of polarity [$E_T(30)$] of toluene-acetone and toluene-acetonitrile solvent systems for the same system (intermolecular catalyzed *spiro*-adamantyl α-peroxy lactone) (Figuer 47).

Table 62a: Chemiluminescence parameters for the rubrene catalyzed decomposition of the *spiro*-adamantyl-1,2-dioxetanone in binary solvent mixtures.

%Solvent	π*	$E_T(30)$	Φ_S (E mol^{-1}) x 10^3
acetone	0.22	42.2	2.6 ± 0.1
20% toluene	0.24	41.6	3.0 ± 0.2
40% toluene	0.25	40.0	3.19 ± 0.04
60% toluene	0.26	38.2	3.36 ± 0.02
80% toluene	0.27	36.2	3.7 ± 0.2
toluene	0.29	33.2	3.8 ± 0.3
ethyl acetate	0.19	39.4	6.43 ± 0.05
20% toluene	0.192	38.6	6.8 ± 0.3
40% toluene	0.202	37.4	6.7 ± 0.4
60% toluene	0.209	36.3	6.7 ± 0.1
80% toluene	0.215	35.6	6.6 ± 0.1
toluene	0.226	33.2	6.8 ± 0.8

$E_T(30)$ and π* of binary solvent mixture obtained by using Reichardt's dye and refractive indices respectively

Table 62b: Chemiluminescence parameters for the rubrene catalyzed decomposition of the *spiro*-adamantyl-1,2-dioxetanone in binary solvent mixtures.

%Solvent	π*	$E_T(30)$	Φ_S (E mol^{-1}) x 10^4
acetonitrile	0.24	45.7	1.22 ± 0.03
20% toluene	0.25	45.0	1.3 ± 0.1
40% toluene	0.26	44.0	1.4 ± 0.3
60% toluene	0.27	43.0	1.6 ± 0.3
80% toluene	0.28	41.4	1.8 ± 0.2
toluene	0.29	34.4	2.1 ± 0.1

$E_T(30)$ and π* of binary solvent mixture obtained by using Reichardt's dye and refractive indices respectively.

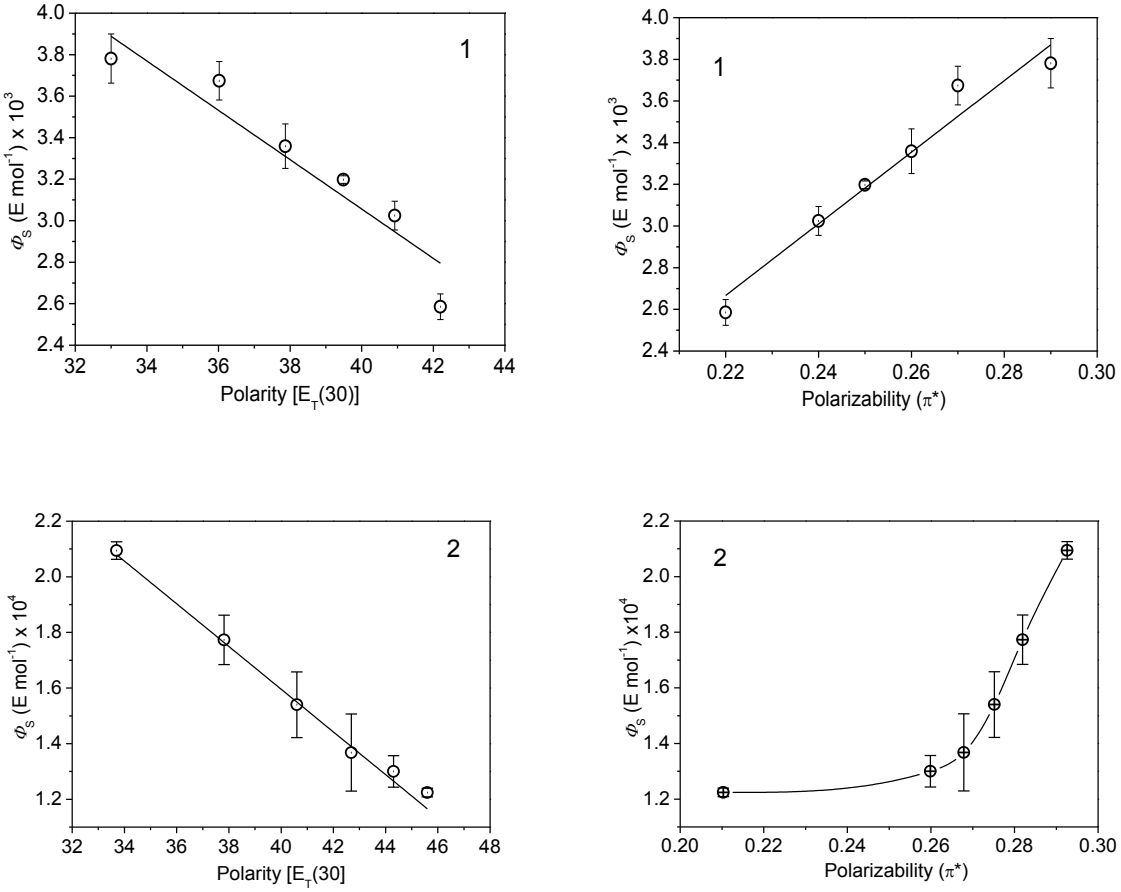

Figure 47: Dependence of the singlet quantum yield (Φ_S) for the rubrene catalyzed decomposition of the *spiro*-adamantyl-1,2-dioxetanone on the solvent polarity parameters: using the binary mixtues of toluene-acetone (1); toluene-acetonitrile (2) at 25 °C.

The experiments were performed in mixtures of toluene and acetone that have similar viscosity parameters (η = 0.56 and 0.42, respectively) but totally distinctive polarity [E_T(30)] and polarizability (π*) parameters. Interestingly, the polarity and polarizability values are conversely for these two solvents, that is, acetone is more polar than toluene, however, toluene is more polarizable as compared to acetone (Table 62a).

The singlet quantum yields increase with increasing solvent polarizability; for varying the polarizability (π*) parameter; from π* = 0.24 (20% toluene) to π* = 0.27 (80%toluene) showed increment in the singlet quantum yields (Φ_S) by a

factor of almost 1.2. Moreover, the singlet quantum yields (Φ_S) increased by a factor of ca. 1.46 from polarizability (π* = 0.29, pure toluene) to polarizability (π* =0.22, pure acetone) (Table 62a).

This experimental data indicate a continuous increase of the singlet quantum yields (Φ_S) with an increasing of the polarizability (π*) of solvent system. However, the effect of $E_T(30)$ values is adverse to polarizability (π*) parameter on the singlet quantum yields (Φ_S) (Figure 47).

The mixtures of toluene and ethyl acetate that have very similar the magnitude of viscosity and different values of $E_T(30)$ parameter. The results got in these studies indicated that the singlet quantum yields (Φ_S) do not enhance with increasing the polarity [$E_T(30)$] parameters of the solvent system (Table 62a).

The experiments also were carried out in the mixtures of toluene and acetonitrile that also have very similar the magnitude of viscosity but entirely different polarizability (π*) as well as $E_T(30)$ values. The quantum yields raise with increasing solvent polarizability (π*); from polarizability (π* = 0.24 100% acetonitrile) to polarizability (π* = 0.29 100% toluene) reflected an increase in singlet quantum yields (Φ_S) by a factor of 1.7 (Table 62b).

The quantum yield starts to decrease with increasing solvent polarity; this behavior indicates higher solvent polarities can lead to the formation of solvent separated ion pairs and individually solvate ions, thereby decreasing chemi-excitation efficiency (Figure47).

5.4. Kinetic study of the induced decomposition of the *spiro*-adamantyl-substituted 1,2-dioxetane (3)

Chemiluminescence reactions usually involve cyclic organic peroxides as energy sources and the reactions are initiated by cleavage of the weak O-O bond and the resulting molecular reorganization liberates enough energy for excited state formation.[46, 103] The oxygen atom in the aryl fragment of dioxetane (**3**) is protected by the electron Withdrawing $SiMe_2Bu$[104] group.

However, the protective group ($SiMe_2Bu$) can be removed by the action of F^- ions, after which the aryl fragment becomes an intramolecular electron donor. This dioxetane is thermally very stable because of the adamantyl fragment.[105, 106] The chemiluminescent decomposition of dioxetane by the attack of F^- ions is initiated by the rate-limiting electron transfer from the phenolate moiety to the antibonding σ^* orbital of the O-O bond in dioxetane (Scheme 16), followed by fast O-O bond cleavage. The dioxetane decomposition finally producing two carbonyl fragments, one of them being possibly formed in its singlet excited state, which decays to the ground state with light emission. The CIEEL emitter, may proceed either directly or by the electron back-transfer (EBT) between the primary solvent-caged radical fragments (Scheme 16).

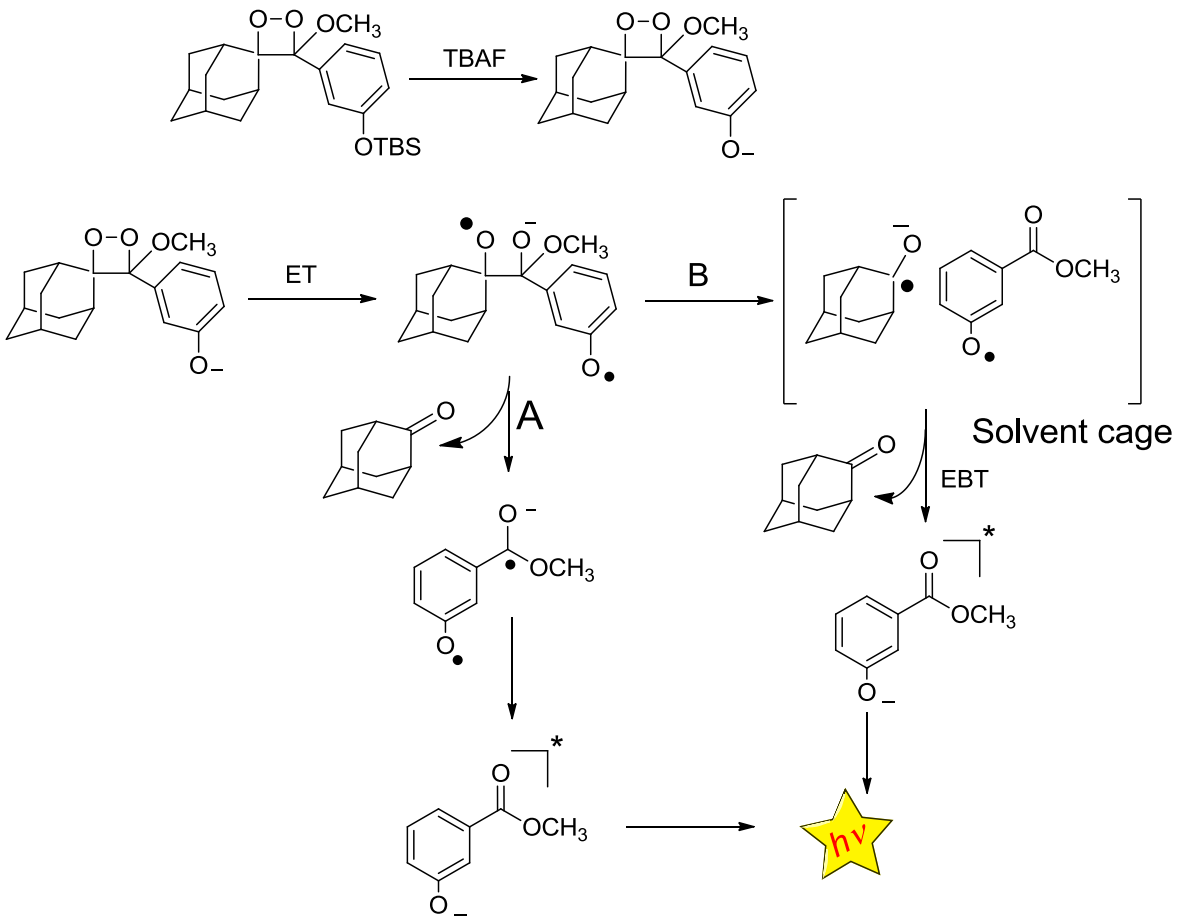

Scheme 16: Mechanism of the induced decomposition of the *spiro*-adamantyl-substituted 1,2-

dioxetane **3**, according to intramolecular CIEEL, indicating the possible occurrence of an intramolecular (A) and intermolecular (B) electron back transfer.[107]

Table 63: Observed rate constants (k_{obs}) and singlet quantum yields (Φ_S) for the decomposition of *spiro*-adamantyl-1,2-dioxetane **3** at 25 °C.

Solvent	ε_r / $E_T(30)$	η (cP)	k_{obs} / s^{-1} x 10^3	Φ_S (E mol^{-1})
ANI	4.45 / 37.1	1.06	4.01 ± 0.02	0.38 ± 0.01
BUTY	5.01 / 38.5	0.69	3.1 ± 0.2	0.25 ± 0.01
EA	6.03 / 38.1	0.42	4.7 ± 0.1	0.44 ± 0.02
THF	7.47 / 37.4	0.46	2.4 ± 0.1	0.54 ± 0.02
ACN	35.94 /45.6	0.37	52.0 ± 4.0	0.43 ± 0.05
DMSO	46.7 / 45.1	1.99	140 ± 10	0.97 ± 0.02

ANI = anisole; BUTY = butyl acetate; EA = ethyl acetate; ACN = acetonitrile; DMSO = dimethyl sulfoxide.

Singlet quantum yields for the decomposition of *spiro*-adamantyl-1,2-dioxetane **3** with fluoride have been determined relative to the luminol standard[43] which increase with increasing the magnitude of dielectric constant (ε_r), $E_T(30)$ as well as viscosity (η). The magnitude of the observed rate constant (k_{obs}) also increases with increasing the magnitude of all the parameters. It is concluded that the effect of dielectric constant (ε_r) and $E_T(30)$ of solvent is significantly observed for the singlet quantum yields (Table 63).

After having determined the quantum yields for the *spiro*-adamantyl-1,2-dioxetane **3** decomposition in pure solvents, some binary solvent mixtures were choosen which possess very similar physicochemical parameters with the exception of the polarity parameter.

5.4.1. Influence of solvent polarity [E_T(30)] and polarizability (π^*) on the Φ_S of 1,2-dioxetane (3) using binary solvent mixtures

Some binary solvent mixtures which have different polarity and polarizability parameters however, with same viscosity parameters, on the other hand, some binary solvent mixtures which have just different polarity parameters but, with same polarizability and viscosity parameters have been used in the case of the induced decomposition of 1,2-dioxetane **3** in order to study the influence of solvent polarity and polarizability on the singlet quantum yields.

Especially, aprotic solvents have been used to avoid formation of hydrogen bonds as happened by protic solvents like water and methanol and also a considerable decrease in the quantum yields obtained.[101] The preliminary choice of solvents was based on the following criteria: (i) probability of no interference occurs in the reaction and the emission process; (ii) to avoid precipitation of the reagent TBAF deprotection as with aromatic and aliphatic hydrocarbons.

Table 64: Observed rate constants (k_{obs}) and singlet quantum yields (Φ_S) for the decomposition of *spiro*-adamantyl-1,2-dioxetane **3** at 25 °C.

Solv.Sys.	% Sol.	$E_T(30)$	π*	k_{obs} / s^{-1} × 10^3	Φ_S (E mol^{-1})
	A	34.2	0.29	3.1 ± 0.2	0.033 ± 0.004
	B	35.5	0.28	1.3 ± 0.2	0.077 ± 0.003
	C	36.0	0.264	1.5 ± 0.3	0.12 ± 0.02
1	D	36.5	0.26	1.8 ± 0.1	0.17 ± 0.01
	E	37.3	0.25	2.01 ± 0.1	0.21 ± 0.01
	F	38.8	0.24	3.2 ± 0.2	0.25 ± 0.01
	G	34.2	0.226	3.1 ± 0.2	0.034 ± 0.004
	H	35.6	0.215	2.0 ± 0.2	0.08 ± 0.01
2	I	36.3	0.209	2.6 ± 0.3	0.16 ± 0.01
	J	37.4	0.202	3.0 ± 0.3	0.30 ± 0.01
	K	38.6	0.192	3.3 ± 0.2	0.37 ± 0.02
	L	39.4	0.190	4.7 ± 0.1	0.44 ± 0.02

Solv. Sys.= solvent systems**; 1** = toluene-butyl acetate system: A = 0% butyl acetate; B = 20% butyl acetate; C =40% butyl acetate; D =60% butyl acetate; E = 80% butyl acetate; F = 100% butyl acetate and **2** = toluene-ethyl acetate system; G = 0% ethyl acetate; H = 20% ethyl acetate; I = 40% ethyl acetate; J = 60% ethyl acetate; K = 80% ethyl acetate; L = 100% ethyl acetate; $E_T(30)$ and π* of binary solvent mixture obtained by using Reichardt's dye and refractive indices respectively.

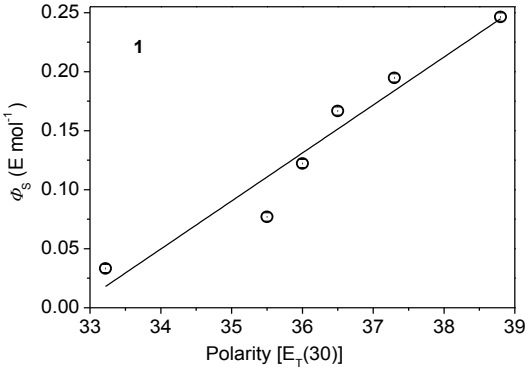

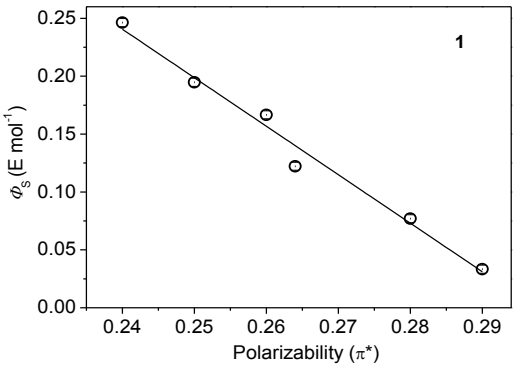

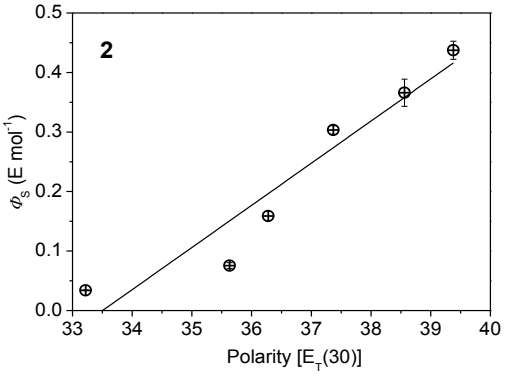

Figure 48: Dependence of the singlet quantum yield (Φ_S) for the decomposition of *spiro*-adamantyl-1,2-dioxetane on the solvent polarity constant [E_T(30)] and polarizability (π*) using binary mixtues of toluene-butyl acetate (1); toluene-ethyl acetate (2) at 25 °C.

The solvent toluene-butyl acetate system (1) consists of very similar the magnitude of viscosity, however, unsimilar the polarity [E_T(30)] and polarizability parameters. The quantum yields raise with raising the values of E_T(30) parameter; the singlet quantum yields increased with increasing the polarity of the solvent system by a factor of 7.5 from E_T(30) = 34.2 (100% toluene) to E_T(30) = 38.8 (100% butyl acetate) (Table 64). On the other hand, the quantum yields declined with increasing the magnitude of polarizability parameter (Table 64). It is concluded that the effect of the polarity [E_T(30)] and polarizability of toluene-butyl acetate system are adversed on the singlet quantum yields (Figure 48).

The solvent toluene-ethyl acetate system (2) consists of very similar the magnitude of viscosity and polarizability however, unsimilar the polarity [E_T(30)] parameters. The singlet quantum yields also increased with increasing the polarity of the solvent system by a factor of 13 from E_T(30) = 34.2 (100% toluene) to E_T(30) = 38.8 (100% ethyl acetate) (Table 64).

Table 65: Observed rate constants (k_{obs}) and singlet quantum yields (Φ_S) for the decomposition of *spiro*-adamantyl-1,2-dioxetane **3** at 25 °C.

Syst.	% Solv.	π *	$E_T(30)$	k_{obs} / s^{-1} × 10^2	Φ_S (E mol^{-1})
	A	0.24	38.8	0.32 ± 0.02	0.08 ± 0.01
	B	0.24	41.26	2.35 ± 0.09	0.17 ± 0.01
	C	0.24	41.86	7.05 ± 0.012	0.236 ± 0.002
1	D	0.24	42.42	11.2 ± 0.3	0.26 ± 0.02
	E	0.24	42.8	16.0 ± 1.0	0.28 ± 0.02
	F	0.24	43.58	21.0 ± 2.0	0.35 ± 0.01
	G	0.29	34.2	0.31 ± 0.02	0.037 ± 0.001
	H	0.283	39.78	1.1 ± 0.1	0.16 ± 0.01
2	I	0.278	40.78	3.4 ± 0.4	0.24 ± 0.01
	J	0.27	41.86	8.2 ± 0.3	0.27 ± 0.01
	K	0.266	42.86	9.3 ± 1.0	0.31 ± 0.03
	L	0.258	43.58	21.0 ± 2.0	0.35 ± 0.03

Solv. Syst.= solvent systems; 1= butyl acetate-*N,N*-dimethyl formamide system; A = 0% *N,N*-dimethyl formamide system; B = 20% *N,N*-dimethyl formamide system; C = 40% *N,N*-dimethyl formamide system; D = 60% *N,N*-dimethyl formamide system; E = 80% *N,N*-dimethyl formamide system; F = 100% *N,N*-dimethyl formamide system and 2 = toluene- *N,N*-dimethyl formamide system; G = 0% *N,N*-dimethyl formamide system; H = 20% *N,N*-dimethyl formamide system; I = 40% *N,N*-dimethyl formamide system; J = 60% *N,N*-dimethyl formamide system; K = 80% *N,N*-dimethyl formamide system; L = 100% *N,N*-dimethyl formamide system; $E_T(30)$ and π* of binary solvent mixture obtained by using Reichardt's dye and refractive indices respectively.

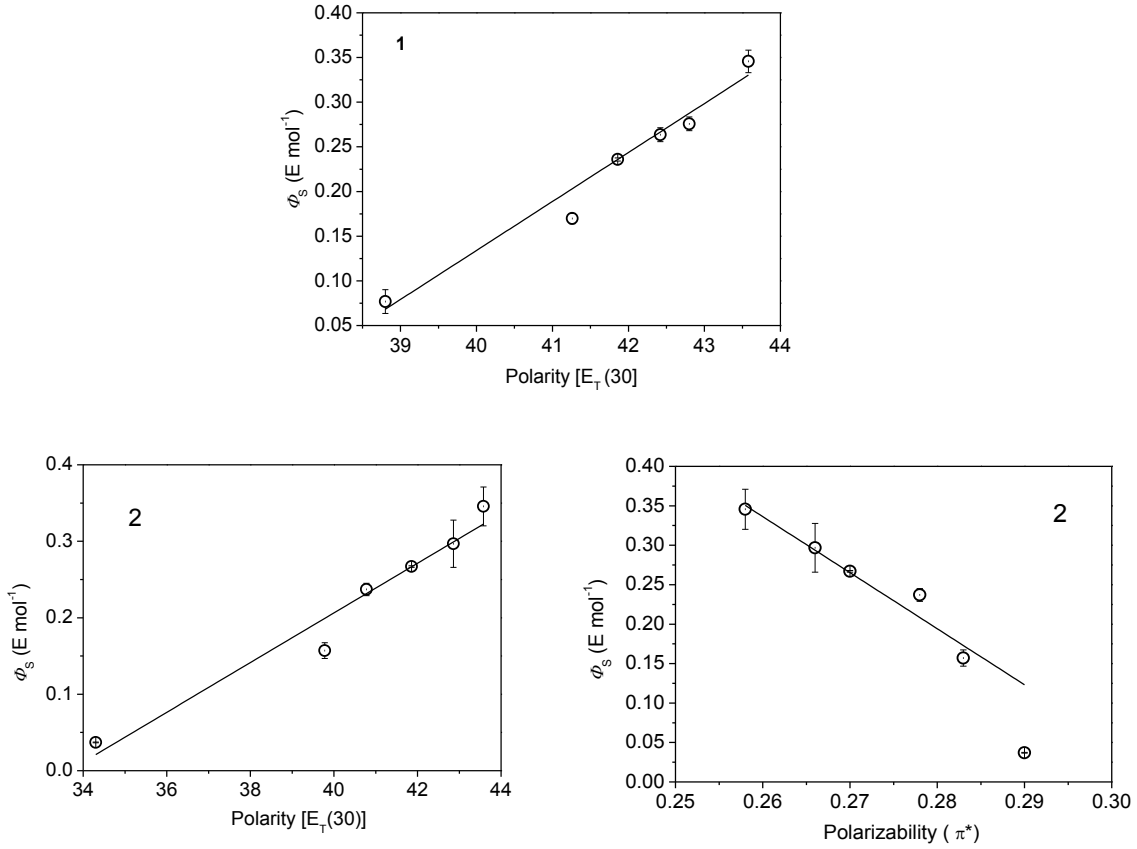

Figure 49: Dependence of the singlet quantum yield (Φ_S) for the decomposition of *spiro*-adamantyl-1,2-dioxetane on the solvent polarity constant [E_T(30)] and polarizability (π*) using binary mixtues of toluene-*N,N*-dimethyl formamide (1); butyl acetate-*N,N*-dimethyl formamide (2) at 25 °C.

The experiments were carried out in mixtures of toluene-*N,N*-dimethyl formamide and butyl acetate-*N,N*-dimethyl formamide. The binary solvent mixture **1** has similar viscosity and polarizability (π*) parameters but completely different polarity [E_T(30)] parameters however, the binary solvent mixture **2** has similar viscosity parameters but completely different polarity [E_T(30)] and polarizability values that are contrarily with each other (Table 65). The singlet quantum yields also increase with increasing the polarity of the solvent system; for varying the polarity parameter E_T(30), from E_T(30) = 5.01 (100% butyl acetate) to E_T(30) = 37.0 (100% *N,N*-dimethyl formamide)

indicated slightly increase in the quantum yields (Φ_S) by a factor of only 4.4 for system 1 (Table 65). The singlet quantum yields increase with increasing the polarity of the binary solvent system (2); for varying the polarity parameter $E_T(30)$, from $E_T(30)$ = 2.43 (100% toluene) to $E_T(30)$ = 37.04 (100% *N,N*-dimethyl formamide) indicated increase in the quantum yields (Φ_S) by a factor of 9.2. In contrast, the quantum yields declined with increasing the magnitude of polarizability parameter for binary solvent system 2 (Figure 49).

Table 66: Observed rate constants (k_{obs}) and singlet quantum yields (Φ_S) for the decomposition of *spiro*-adamantyl-1,2-dioxetane **3** at 25 °C.

Solvent	$E_T(30)$	($\pi*$)	k_{obs} / $s^{-1} \times 10^2$	Φ_S (E mol^{-1})
DPE	35.5	0.30	0.11 ± 0.01	0.32 ± 0.01
20% DMSO	37.8	0.30	3.9 ± 0.1	0.71 ± 0.05
40% DMSO	39.9	0.30	7.0 ± 0.3	0.87 ± 0.02
60% DMSO	42.1	0.30	10.5 ± 0.3	0.93 ± 0.02
80% DMSO	43.6	0.30	12.0 ± 2.0	0.946 ± 0.002
DMSO	45.1	0.30	14.0 ± 1.0	0.97 ± 0.02

DPE = diphenyl ether; DMSO = dimethyl sulfoxide; $E_T(30)$ and π* of binary solvent mixture obtained by using Reichardt's dye and refractive indices respectively.

Table 67: Observed rate constants (k_{obs}) and singlet quantum yields (Φ_S) for the decomposition of *spiro*-adamantyl-1,2-dioxetane **3** at 25 °C.

Solvent	($\pi*$)	$E_T(30)$	k_{obs} / $s^{-1} \times 10^3$	Φ_S (E mol^{-1})
100% THF	0.25	37.7	2.4 ± 0.1	0.54 ± 0.02
20 % acetone	0.24	38.6	3.2 ± 0.2	0.75 ± 0.03
40 % acetone	0.23	39.5	3.6 ± 0.1	0.80 ± 0.05
60 % acetone	0.23	40.4	3.5 ±0.1	0.86 ± 0.04
80 % acetone	0.23	41.3	3.6 ± 0.2	0.92 ± 0.03
100% acetone	0.22	42.2	9.0 ± 3.0	0.96 ± 0.05

$E_T(30)$ and π* of binary solvent mixture obtained by using Reichardt's dye and refractive indices respectively.

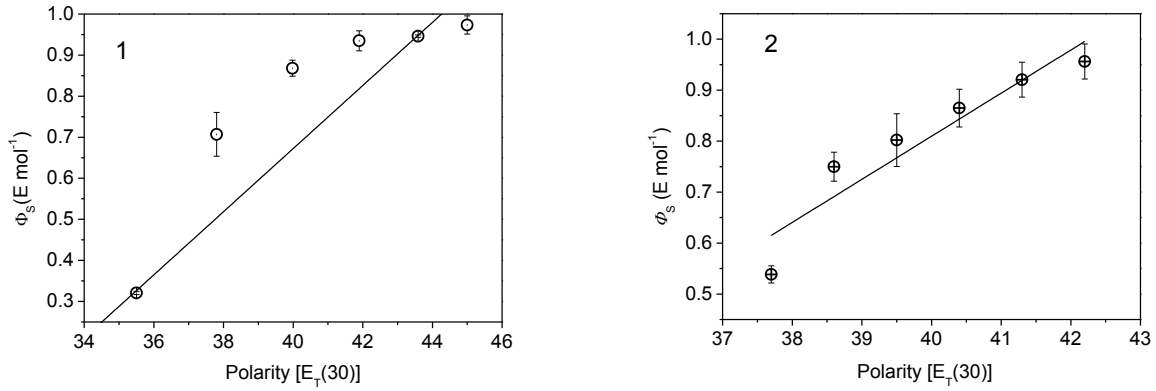

Figure 50: Dependence of the singlet quantum yield (Φ_S) for the decomposition of *spiro*-adamantyl-1,2-dioxetane on the solvent polarity constant [E_T(30)] using binary mixtues of diphenyl ether-DMSO (1); THF-acetone (2) at 25 °C.

The binary diphenyl ether-DMSO system which consists of very similar the magnitude of viscosity and polarizability values, however, unsimilar the polarity [E_T(30)] of solvent. The singlet quantum yields increase with increasing the polarity of the solvent system; the singlet quantum yields (Φ_S) increased by a factor of almost 1.33 from E_T(30) = 37.8 (20% DMSO) to E_T(30) = 42.9 (80% DMSO) (Table 66). Moreover, the singlet quantum yields significantly increased from E_T(30) = 34.5 (100% diphenyl ether) to E_T(30) = 45.1 (100% DMSO) indicated increase in the singlet quantum yields (Φ_S) by a factor of 3 (Table 66).

The perylene catalyzed decomposition of diphenoyl peroxide system has been studied in DMSO solvent but no light observed from this system. Moreover, the singlet quantum yield (Φ_S) for the rubrene catalyzed decomposition of the *spiro*-adamantyl-1,2-dioxetanone has been determined using the binary mixtues of DPE-DMSO. However, no reliable results also obtained from this system.

The solvent system THF-acetone having also similar the magnitude of viscosity and polarizability however, unsimilar the polarity [E_T(30)] values of solvent system. The singlet quantum yields increase with increasing the

polarity of the solvent system; for changing the polarity parameter $E_T(30)$, from $E_T(30)$ = 37.7 (100% THF) to $E_T(30)$ = 42.2 (100% acetone) revealed an increase in the quantum yields (Φ_S) by a factor of almost 1.8 (Table 67).

Table 68: Observed rate constants (k_{obs}) and singlet quantum yields (Φ_S) for the decomposition of *spiro*-adamantyl-1,2-dioxetane **3** with polarity parameter $E_T(30)$ at 25 °C.

% A	% B	$E_T(30)$	k_{obs} / s^{-1} x10^3	Φ_S (E mol^{-1})
100% TOL	0% BUTY	34.2	3.1 ± 0.2	0.033 ± 0.004
80% TOL	20% BUTY	35.5	1.3 ± 0.2	0.077 ± 0.003
80% TOL	20% EA	35.6	2.0 ± 0.2	0.08 ± 0.01
60% TOL	40% BUTY	36.0	1.5 ± 0.3	0.17 ± 0.01
40% TOL	60% EA	37.4	3.0 ± 0.3	0.30 ± 0.01
0% TOL	100% EA	39.4	4.7 ± 0.1	0.44 ± 0.02
40% TOL	60% ACE	40.4	3.5 ± 0.1	0.86 ± 0.03
0% TOL	100% ACE	42.2	1.7 ± 0.1	0.96 ± 0.05
0% TOL	100% DMSO	45.1	14.0 ± 1.0	0.97 ± 0.02

TOL= toluene; BUTY= butyl acetate; EA= ethyl acetate; ACE= acetone; $E_T(30)$ of binary solvent mixture obtained by using Reichardt's dye.

The mixtures of toluene, ethyl acetate, butyl acetate and acetone with different proportionality that have very similar the magnitude of viscosity but fully disparate polarity $E_T(30)$ values. The singlet quantum yields also increased with increasing the polarity of the solvent system; the quantum yields (Φ_S) raised by a factor of 30 from $E_T(30)$ = 34 (100% toluene) to $E_T(30)$ = 42.2 (100% acetone) (Table 68).

From these data, we can conclude that in low polarity binary solvent mixture systems, the quantum yields are relatively low and in the binary high aprotic polar solvents mixtures these values are considerably high, reaching up to 1.0 (Table 68).

Considering the mechanism of induced 1,2-dioxetane decomposition (Scheme 16), increasing solvent polarity must first facilitate the deprotection step by the stabilization of the phenolate ion formed and stabilize the radical ions generated in the sequence of transformation.

In the binary solvent systems, the polarizability parameter sowed to be contrary to the polarity values, therefore, it might appear that an increase of polarizability leads to a decrease in the singlet quantum yields for catalyzed decomposition of diphenoyl peroxide (**1**) and the induced decomposition of **3**, however a increase in the singlet quantum yields for 1,2-dioxetanone (**2**). (Figures 48-50).

Additionally, it appears from our results that, apart from solvent polarity, the polarizability of solvents contribute to modulate electron transfer properties. There are some reports in the literature on solvent polarizability influence on electron transfer reactions[108-110] therefore it appears that this parameter could contribute to the concurrence between ground state and excited state formation in the back-electron transfer step of chemiexcitation (Scheme 16). The elucidation of the solvent polarizability influence on the efficiency of chemiexcitation might be of great interest for the mechanistic interpretation of highly efficient intramolecular transformations as the induced 1,2-dioxetane decomposition and might contribute to explain the difference in efficiency between the inter and intramolecular model systems.

The results obtained from these studies on the solvent polarity and polarizability effect on the quantum efficiency of peroxide **3** would allow to define the exact chemiexcitation mechanisms operating in these transformations and define conditions necessary to obtain highly efficient CL transformations, these obtained results may also lead to new and unexpected applications of chemiluminescence, as shown in Tables 66 and 67.

5.5. Multiple linear regression relationship for inter and intramolecular electron transfer chemiluminescent systems.

In a regression analysis we study the relationship, called the regression function, between one variable y, called the dependent variable, and several others x; called the independent variables. The regression models with more than one independent variable are recognized to as multiple linear regression analysis**.**

General formula:

$$y = \beta_0 + \beta_1 x_1 + \beta_2 x_2 + \beta_3 x_3 + \beta_4 x_4 \qquad \text{Equation 37}$$

In equation 37 the values of β coefficients are found using multiple linear regression and an independent parameters adjusted along x-axis like (viscosity, dielectric constant, polarity or polarizability). The dependent parameter is the singlet quantum yield of systems in each medium along y-axis.

Table 69: The dependent parameters (singlet quantum yield of the intra and intermolecular electron transfer CL systems) and independent parameters (polarity constants and viscosity).

	System 1	**System 2**	**System 3**			
	Φ_S^{CAT} **(E mol^{-1}) x 10^4**	Φ_S **(E mol^{-1}) x10^3**	Φ_S **(E mol^{-1})**	E_T **(30)**	π*	η **(cP)**
A	0.52 ± 0.05	2.9 ± 0.1	0.0395 ± 0.0001	0.04	0.72	0.53
B	0.49 ± 0.04	/	/	0.05	0.71	0.19
C	0.54 ± 0.05	/	/	0.02	0.74	0.26
D	/	6.03 ± 0.08	0.350 ± 0.001	0.15	0.76	0.36
E	1.24 ± 0.04		0.38 ± 0.01	0.08	0.79	0.76
F	1.5 ± 0.5	3.4 ± 0.3	0.25 ± 0.01	0.05	0.83	0.5
G	1.2 ± 0.2	2.6 ± 0.5	0.44 ± 0.02	0.038	0.82	0.49
H	1.6 ± 0.2	/	0.54 ± 0.02	0.04	0.80	0.61
I	1.70 ± 0.04	/	/	0.03	0.90	0.67
J	2.24 ± 0.09	/	/	1.00	0.91	1.00
K	/	0.001 ± 0.001	0.99 ± 0.22	0.15	0.99	0.96
L	/	/	0.43 ± 0.05	0.035	1.00	0.72

A = toluene; B = dibutyl ether; C = diethyl ether; D = diphenyl ether E = anisole; F = butyl acetate; G = ethyl acetate; H = tetrahydrofuran; I = acetone; J = pyrro K = DMSO; L = ACN; normalized values of independent parameters (polarity constants and viscosity) have been correlated to dependent parameters.

Table 70: Values obtained by the correlation between dependent and independent parameters, using multiple linear regression.

Values for	**System 1**	**System 2**	**System 3**
Property analyzed	**values x 10^4**	**values x 10^3**	**values**
Intercept	-4.3 ± 1.3	0.009 ± 0.003	0.97 ± 0.69
Viscosity(η)	0.4 ± 0.4	15.6 ± 0.4	2.0 ± 1.4
Polarity [E_T(30)]	6.5 ± 1.9	-2.6 ± 5.1	1.2 ± 1.0
Polarizability	0.4 ± 0.6	-9.0 ± 2.1	0.47 ± 0.57

The positive values obtained for all of three systems related to the viscosity demonstrate that the singlet quantum yield increase with increase viscosity, nonetheless, high standard deviation were found in the case of system 1. The high value obtained for the correlation with the viscosity of system 2 is surprising and not in agreement with the data obtained from the binary solvent systems.

The correlation with the polarity parameter [E_T(30)] also leads to a positive correlation value for system **1** and **3** showing that the singlet quantum yield increased with increasing polarity, however, this correlation leads to negative values with high standard deviation for system **2**. In the same way, the correlation parameters for systems **1** and **3** showed high standard deviation for the polarizability values, not allowing an interpretation of these data. Moreover, the negative value of the correlation parameter for the polarizability found for system **2** indicates that the singlet quantum yields decrease with increasing polarizability (Table 70).

5.5.1 Multiple linear regression relationship for diphenoyl peroxide system using binary solvent mixtures

The perylene catalyzed decomposition of diphenoyl peroxide has also been studied in binary mixture of ethyl acetate and 1-methyl-2-pyrrolidinone which have different viscosity and different polarity parameters in order to know which parameter acts as a major by using mulitple linear regression function.

Table 71: The dependent parameters (singlet quantum yield of the intermolecular electron transfer CL system) and independent parameters (polarity constant $E_T(30)$ and viscosity).

	Dependent Variables	**Independent Variables**	
Solvent system	**Φ_S (E mol^{-1}) x 10^5**	**η (cP)**	**$E_T(30)$**
ethyl acetate	0.50 ± 0.01	0.03	0.90
20% pyrrolidinone	0.93 ± 0.04	0.22	0.92
40 % pyrrolidinone	1.68 ± 0.02	0.42	0.94
60% pyrrolidinone	2.03 ± 0.04	0.62	0.96
80% pyrrolidinone	2.3 ± 0.03	0.81	0.98
pyrrolidinone	2.41 ± 0.02	1.00	1.00

Table 72: Values obtained by the correlation between dependent and independent parameters, using multiple linear regression.

Property analyzed	**Values**
Intercept	$10 \pm 20 \times 10^{-9}$
viscosity	$2.1 \pm 0.3 \times 10^{-5}$
Polarity [$E_T(30)$]	$5.9 \pm 0.3 \times 10^{-6}$

Adj.R^2 = 0.95

The polarity parameter [$E_T(30)$] and viscosity have positive values, therefore indicating that the singlet quantum yield increases with increasing the both parameter, however, the viscosity influence is greater as compared to the polarity influences on the singlet quantum yields (Table 72).

5.6. Solvent viscosity (η) effect on the inter and intramolecular electron transfer chemiluminescent systems

The study of the influence of solvent viscosity on the quantum yields obtained from diphenoyl peroxide, 1,2-dioxetanone and 1,2-dioxetane systems has been done. The polarity of the solvent system must be kept constant so that should not change in velocity transfer and back-electron transfer processes. To facilitate the formation of ion pairs must be used with considerable polarity solvents, but not so high as to lead to separation of these pairs and consequently, the formation of the products in the ground state and not in the electronically excited state. Furthermore, the use of aprotic solvents should be avoided to preclude the formation of hydrogen bonds, which could lead to reduce yields of chemiluminescence excitation. The solvents utilized in this kind of study should possess different viscosities however should have similar solvent polarity parameters. The solvent systems which have been utilized for this study consist of mixtures of ethyl acetate-dibutyl phthalate, toluene-diphenyl methane and toluene-diphenyl ether etc., which possess similar solvent polarity parameters however, show a wide range of viscosity values.

According to the Marcus theory for electron trasnfer reaction,[32] the free energy for electron transfer (ΔG^*_{EBT}, in this case applied to the EBT reaction is determined by two free-energy parameters: (i) the standard free energy for electron transfer (ΔG_0), which reflects mainly the difference in the redox potential of the involved species; and (ii) the factor ΔG^*_0, the intrinsic activation barrier, which is associated to the change in bond length and to the solvent reorganization energy (Equation 46). This last factor is determined by the dimensions of the electron donor and acceptor (r_D and r_A), as well as, the distance between them (r_{DA}) and the solvent polarity parameters, the refractive index (n) and the relative permittivity [dielectric constant (ε_r)] (Equation 47).

$$\Delta G^{*}_{EBT} = \Delta G^{*}_{0}\left(1+\frac{\Delta G^{0}}{4\Delta G^{*}_{0}}\right)^{2} \qquad \text{Equation 46}$$

$$\Delta G^{*}_{0} = \frac{e^{2}}{4}\left(\frac{1}{2r_{D}}+\frac{1}{2r_{A}}-\frac{1}{r_{DA}}\right)\left(\frac{1}{n^{2}}-\frac{1}{\varepsilon}\right) \qquad \text{Equation 47}$$

In any electron transfer system where the influence of the solvent viscosity is to be verified, the polarity of the solvent has to be maintained constant therefore, the solvent reorganization energy factor (λ_S) should be kept as constant as possible in order to exclude any polarity effects. In this study, λ_S is just expressed by the factor $1/n^2 - 1/\varepsilon$, without specifying the properties of the donor acceptor pair. In order to use uniform values for the polarity parameter all of them have been obtained from the same literature source.

Table 73: Physicochemical parameters of solvents.

# of binary solvent systems	Solvents	ε_r	$E_T(30)$	η
1	TOL	2.4	34.0	0.5
	DPE	2.0	34.5	2.2
2	EA	6.03	39.1	0.42
	DBP	6.44	39.5	9.63
3	DPM	2.6	34.4	2.64
	TOL	2.4	34.0	0.5

TOL = toluene; DPE = diphenyl ether; EA = ethyl acetate; DBP = dibutyl phthalate; DPM = diphenyl methane.

It is interesting to investigate the behavior of the solvent systems on the catalyzed induced decomposition for **1**, **2** and **3**. The solvent systems which have been utilized for this studies shown in Table 73, which retain similar solvent polarity parameters however, show a wide range of viscosity values. The induced decomposition of 1,2-dioxetane by the intramolecular system and dioxetanone and diphenoyl peroxide by the intermolecular system have been studied under catalytic conditions in order to understand the mechanisms

associated with the formation of eclectronic excited states via electron transfer induced decomposition, leading to quantum yields for singlet excitation.

Table 74: The singlet quantum yields (Φ_S) for the decomposition of diphenoyl peroxide using rubrene as a catalyst.

% Solvents	η (cP)	Φ_S (E mol^{-1}) x 10^4
toluene	0.56	2.11 ± 0.06
20% diphenyl methane	0.82	2.20 ± 0.04
40% diphenyl methane	1.05	2.37 ± 0.08
60% diphenyl methane	1.37	2.55 ± 0.06
80% diphenyl methane	2.17	2.71 ± 0.04
89% diphenyl methane	2.57	2.98 ± 0.02
toluene	0.5	1.06 ± 0.01
25% diphenyl ether	0.74	1.19 ± 0.02
50% diphenyl ether	1.1	1.27 ± 0.01
75% diphenyl ether	1.6	1.38 ± 0.06
95% diphenyl ether	2.17	2.26 ± 0.18

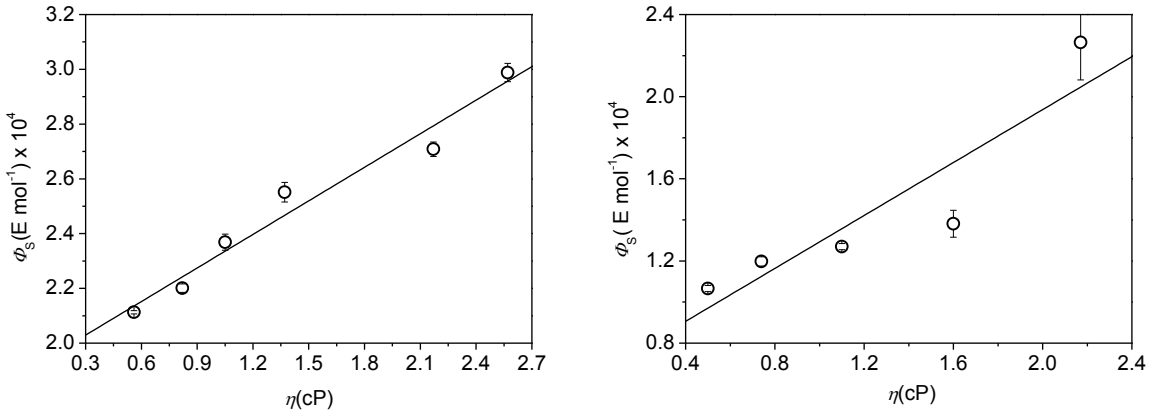

Figure 51: Singlet quantum yields (Φ_S) for the reaction of diphenoyl peroxide (1.0 mmol L^{-1}) with function of medium viscosity (η) using the mixtures of toluene and diphenyl methane (A) and toluene and diphenyl ether (B).

The results of the rubrene catalyzed decomposition of the diphenoyl peroxide indicate that the singlet quantum yields (Φ_S) increased by a factor of almost 1.3 from η = 0.5 cp (100% toluene) to η = 2.57 cP (100% diphenyl methane) (Table 74). The singlet quantum yields (Φ_S) increased by a factor of ca.1.3 from the pure toluene (η = 0.5 cP) to 75% diphenyl ether (η = 1.6 cP) and interestingly, singlet quantum yield in diphenyl ether (η = 2.1 cP) was increased by irregular pattern even the magnitude of viscosity for 75% diphenyl ether is very close to 95%diphenyl ether. This might be because of the preferential solvation of the radical ions in chemiexcitation step for diphenoyl peroxide system (Table 74).

Table 75: The catalyzed singlet quantum yields (Φ_S) for the diphenoyl peroxide using perylene as a catalyst.

% Solvents	**η (cP)**	**Φ_S^{CAT} (E mol^{-1}) x** 10^4
ethyl acetate	0.42	1.0 ± 0.2
20% dibutyl phthalate	0.61	1.13 ± 0.07
40% dibutyl phthalate	0.94	1.4 ± 0.2
60% dibutyl phthalate	1.67	1.48 ± 0.02
80% dibutyl phthalate	3.11	1.7 ± 0.4
di-n-butyl phthalate	9.63	1.8 ± 0.2

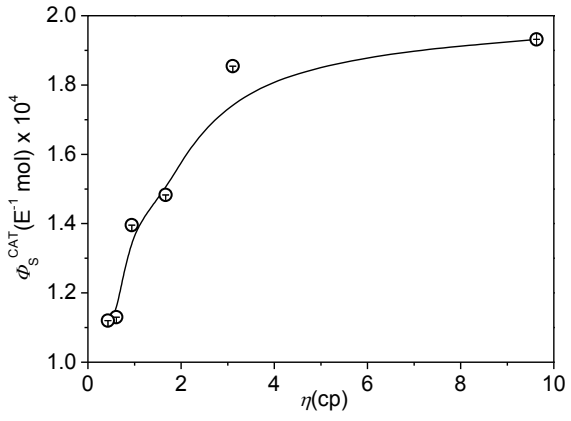

Figure 52: Catalyzed singlet quantum yields (Φ_S^{CAT}) for the reaction of diphenoyl peroxide (1.0 mmol L^{-1}) in the function of medium viscosity (η) using the mixtures of ethyl acetate and dibutyl phthalate .

The catalyzed singlet quantum yields (Φ_S^{CAT}) increase with increasing the viscosity; for varying the viscosity of η = 0.61 cp (20% dibutylphthalate phthalate) to η = 9.63 cP (100% dibutylphthalate) showed slight increase in the catalyzed singlet quantum yields (Φ_S^{CAT}) by a factor of almost 1.6. However, comparing the values for the pure ethyl acetate (η = 0.42 cP) to pure dibutylphthalate (η = 9.63 cP), showed an increase in catalyzed singlet quantum yields (Φ_S^{CAT}) by a factor of ca. 2 (Table 75).

Table 76: Influence of viscosity on the singlet quantum yields of 1,2-dioxetanone **2**

Solvent systems	**η (cP)**	**Φ_S (E mol^{-1}) x10^4**
ethyl acetate	0.42	14.9 ± 0.12
20% dibutyl phthalate	0.61	15.7 ± 0.2
40% dibutyl phthalate	0.94	17.3 ± 0.1
60% dibutyl phthalate	1.67	19.8 ± 0.1
80% dibutyl phthalate	3.11	22.1 ± 0.1
di-n-butyl phthalate	9.63	27.3 ± 0.2
toluene	0.56	0.262 ± 0.002
20% diphenyl methane	0.82	0.401 ± 0.004
40% diphenyl methane	1.05	0.49 ± 0.09
60% diphenyl methane	1.37	0.50 ± 0.04
80% diphenyl methane	2.17	0.54 ± 0.04
89% diphenyl methane	2.57	0.62 ± 0.06
toluene	0.56	5.7 ± 0.1
25% diphenyl ether	0.74	6.6 ± 0.2
50% diphenyl ether	1.1	7.5 ± 0.4
75% diphenyl ether	1.6	8.6 ± 0.1
diphenyl ether	2.1	11.0 ± 1

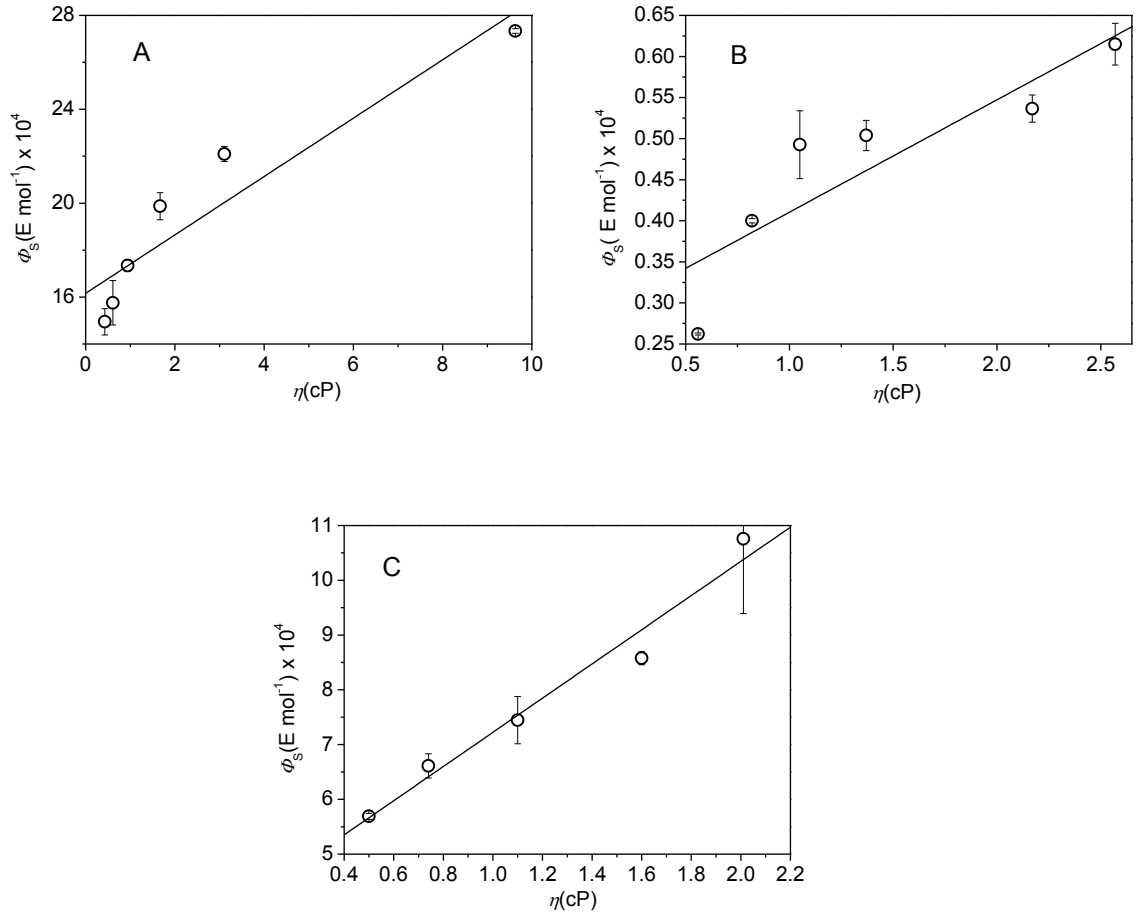

Figure 53: Singlet quantum yields (Φ_S) for the *spiro*-adamantyl-1,2-dioxetanone (0.075 mmol L^{-1}) with rubrene activator in function of medium viscosity (η) using the mixtures of ethyl acetate/dibutyl phthalate (A), toluene / diphenyl methane (B) and toluene / diphenyl ether (C).

The singlet chemiexcitation (Φ_S) increased by a factor of 1.8 from η = 0.61 cp (20% dibutylphthalate phthalate) to η = 9.63 cP (100% dibutylphthalate) and comparing the values for the pure ethyl acetate (η = 0.42 cP) to pure dibutylphthalate(η = 9.63 cP), show the singlet quantum yields increased by a factor of ca. 2 (Table 76).

The results of the rubrene catalyzed decomposition of the *spiro*-adamantyl-1,2-dioxetanone indicate that the singlet quantum yields (Φ_S) increased by a factor of almost 2.3 from η = 0.5 cp (100% toluene) to η = 2.57 cP (100% diphenyl methane) (Table 73).[111] The tendency of increasing singlet quantum yields

obtained with rubrene in toluene and diphenyl methane solvent system is almost same as obtained from the ethyl acetate and dibutylphthalate phthalate solveny system. In both cases slight effect of viscosity was observed on the quantum yields (Table 76). The singlet quantum yields (Φ_S) increased by a factor of almost 2 from η = 0.5 cp (100% toluene) to η = 2.17 cP (100% diphenyl ether) (Table 76). The tendency of increasing singlet quantum yields obtained with rubrene of dioxetanone is almost same as obtained from the decomposition of diphenoyl peroxide. In both cases slight effect of viscosity was observed on the quantum yields (Table 76).

Table 77: The singlet quantum yields (Φ_S) for the decomposition of *spiro*-adamantyl-1,2-dioxetane (**3**) at 36 °C.

% oϕ_2	η(cP)	Φ_S (E mol^{-1})
toluene	0.56	0.040 ± 0.001
20% diphenyl ether	0.64	0.043 ± 0.001
40% diphenyl ether	0.92	0.072 ± 0.001
60% diphenyl ether	1.29	0.14 ± 0.01
80%diphenyl ether	1.80	0.23 ± 0.01
diphenyl ether	2.17	0.35 ± 0.01

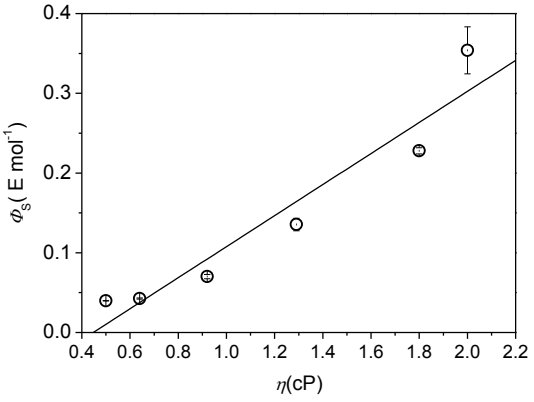

Figure 54: Singlet quantum yields (Φ_S) for the *spiro*-adamantyl-substituted 1,2-dioxetane (0.01 mmol L^{-1}) with tetrabutylammonium fluoride (2.5 mmol L^{-1}) in function of medium viscosity (η) using the mixtures of toluene and diphenyl ether.

The singlet quantum yield obtained for 1,2-dioxetane system in pure toluene is much smaller than the value obtained for a 40% of diphenyl ether, even the magnitude of viscosity for these three mixtures is very close. This result suggests preferential solvation of the radical ions in chemiexcitation step. Furthermore, singlet quantum yields increase in function of viscosity medium. The observed chemiexcitation during the electron transfer chemically and electrochemically produced ion-radical pairs is responsible for the CIEEL processes and EBT mechanism. CIEEL generation should depend on viscosity and its efficiency should be subject to a solvent-cage effect, if it proceeds through EBT processes. EBT mechanism is consistent with our findings because an increase in viscosity results in an increase in the chemiluminescence efficiency.

5.6.1. Free-volume model.

The results obtained from **1**, **2** and **3** systems in binary solvent mixture of (i) toluene-diphenyl ether, (ii) toluene-diphenyl methane and (iii) ethyl acetate-dibutyl phthalate which were interpreted by applying the free-volume as well as collision model.[112-116] The frictional model (is also recognized as a free volume model) has been proposed for the viscosity dependence because of the free volume available in the medium will determine how easily conformational changes by bond rotation and influence the chemiluminescence quantum yields (Φ_S). Doolittle, Cohen and Turnbull proposed this model for representation of the viscosity of solvents.The free volume model is explained by using following equations.

$$\Phi_S = \frac{k_S^{EBT}}{k_{S_0}^{EBT} + k_S^{EBT}} \qquad \text{Equation 37}$$

$$\eta = Aexp\left(\frac{V_0}{V_f}\right) \qquad \text{Equation 38}$$

$$k_{s_0}^{EBT} = k_0\, exp\left(-\alpha \frac{V_0}{V_f}\right) \qquad \text{Equation 39}$$

Substitution of eq 38 into eq 39 gives eq 40 for the viscosity dependence of the rate constant $k_{s_0}^{BET}$.

$$k_{s_0}^{EBT} = k_0 \left(\frac{A}{\eta}\right)^{\alpha} \qquad \text{Equation 40}$$

The combination of eqs 37 and 40 gives eq 52.

$$\frac{k_S^{EBT}}{k_S^{EBT}} = \frac{1-\Phi_S}{\Phi_S} = \frac{k_0}{k_S^{EBT}}\left(\frac{A}{\eta}\right)^{\alpha} \qquad \text{Equation 41}$$

The eq 42 is obtained by the double-logarithmic of eq 41.

$$ln\frac{1-\Phi_S}{\Phi_S} = C - \alpha ln\eta \qquad \text{Equation 42}$$

The most fundamental assumption of this model is that the rate constant of a given free volume dependent process, $k_{s_0}^{EBT}$, will be related to the medium viscosity (η). The free-volume model explaines that a molecule can be moved by rotations and translations way in a liquid medium. The only factor which makes it possible is the availability of sufficient free volume (V_f). For example in those cases where critical volume V_0 is less than the free volume per molecule is proportional to the probability factor [exp(-V_0/V_f)] for the molecular movements in a liquid medium is proportional to viscosity (η) and eq 38 is suitable for the expression of free volume dependence of viscosity, where, proportionality factor is expressed by A. It is quite clear that only a fraction αV_0 (R < 1) of V_0 is required because rotations involve only a fraction of the molecule unlike translational movement of the molecule which involves it as a whole. Therefore, equation 39 is appropriate to express the rate constant $k_{s_0}^{EBT}$ for the ground-state EBT process where k_0 is a pre exponential factor, (the first expression employed to investigate the viscosity dependent photoisomerization

of stilbenes). The linear dependence of Φ_S was predicted by eq 42. The a parameter depends on the nature of the solute and solvent and only indicates the fraction of the free volume cavity of solvent which is necessary for the occurrence of molecular rearrangment (contact between species), essential for chemiexcitation.

5.6.2. Collisional model

The equation 43 indicates the viscosity dependence of the chemiexcitation yield $\Phi_S(\eta)$ and p_{S0}, p_S, and p_T are the partial probabilities of the back electron transfer process at that time when species collide in the solvent cage as a result the ground, excited singlet, and excited triplet states of the CIEEL are produced. The sum of $p_{S0} + p_S + p_T$ indicates the total probability of the back electron transfer process per collision in the solvent cage.

$$\Phi_S(\eta) = \frac{P_S\,\eta}{\left(P_S + P_T + P_{S_0}\right)\eta + A_\eta} \qquad \text{Equation 43}$$

$$\Phi_S^{-1} = \frac{\left(P_S + P_T + P_{S_0}\right)}{P_S} + \frac{A_\eta}{P_S}\eta^{-1} \qquad \text{Equation 44}$$

$$\eta = A_\eta e^{E\eta/RT} \qquad \text{Equation 45}$$

Where, A_η stands for preexponential factor for the viscosity in its Arrhenius form and E_η stands for the energy of activation related to viscosity.

Eqs 46 and 47 show the relation between kinetic rate constants and the probabilistic approach of the chemiexcitation (k_S) and the total (k_{EBT}) EBT processes in the solvent cage.

$$k_S = \tau_C^{-1} P_S \qquad \text{Equation 46}$$

$$k_{EBT} = \tau_C^{-1} P_{EBT} \qquad \text{Equation 47}$$

Where τ_C^{-1} is the mean collision frequency (reciprocal time between Collisions) in the solvent cage and its approximated value is ca. 10^{13} s^{-1}.

When electron back transfer (EBT) pathway prevails in the CIEEL process eq 43 should operate. From the double-reciprocal plots of figures (56) according to eq 44, one may obtain EBT probabilities $p_{S0} + p_S + p_T = p_S$ and p_{EBT} can be obtained according to eq 44, from the double-reciprocal plots of figures (56). As far as the data for p_S is concerned, it is obtained from the slopes A_η/p_S of these plots where the value of A_η (9.9 x10^{-3})cP; the intercepts multiplication ($p_{S0} + p_S + p_T$)/p_S of each plot by p_{S1} grants $p_{EBT} = p_{S0} + p_S + p_T$.

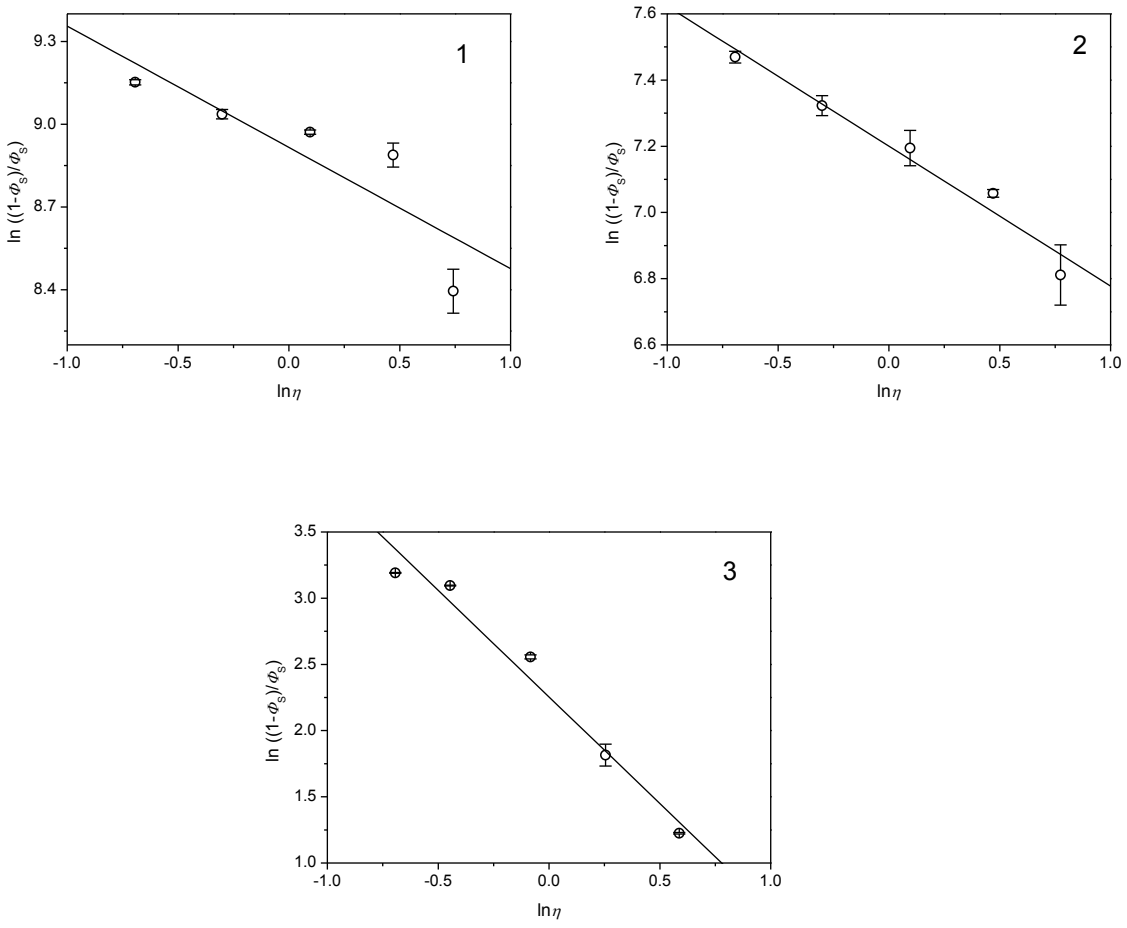

Figure 55: Correlation between ln((1 – Φ_S)/Φ_S) and lnη according to the free volume model for diphenoyl peroxide (**1**), 1,2-dioxetanone (**2**) and 1,2-dioxetane system (**3**).[117]

Table 78: Fitting parameters for the rubrene catalyzed decomposition of diphenoyl peroxide (**1**) and 1,2-dioxetanone **2**, as well as the induced decomposition of phenoxy-substituted 1,2-dioxetane **3**, using free volume model.

	Free volume model		
	$ln\frac{1-\Phi_S}{\Phi_S} = C - \alpha \ln \eta$		
	C	**−α**	**R^2**
1	8.985 ± 0.006	0.24 ± 0.01	0.899
2	7.22 ± 0.01	0.36 ± 0.02	0.994
3	2.278 ± 0.002	1.52 ± 0.01	0.932

Table 79: Fitting parameters for the rubrene catalyzed decomposition of diphenoyl peroxide (**1**) and 1,2-dioxetanone **2,** using free volume model.

		Free volume model		
Solvent systems	Compounds	$ln\frac{1-\Phi_S}{\Phi_S} = C - \alpha \ln \eta$		
		C	**−α**	**R^2**
A	**1**	8.35 ± 0.01	0.22 ± 0.02	0.96
	2	10.11 ± 0.06	0.5 ± 0.1	0.79
B	**1**	8.92 ± 0.04	0.19 ± 0.03	0.88
	2	7.09 ± 0.005	0.197 ± 0.005	0.99

A= diphenyl methane and toluene system; B= dibutyl phthalate and ethyl acetate system.

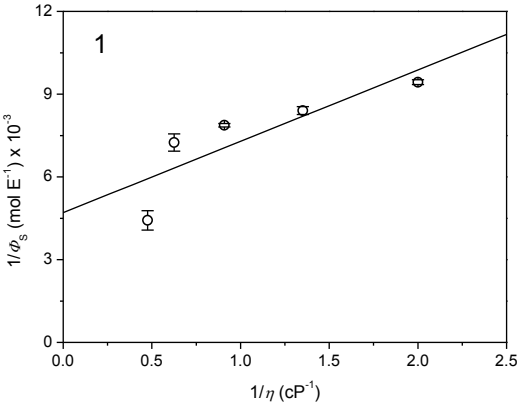

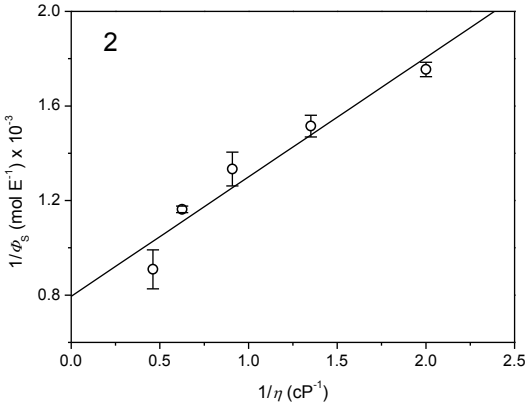

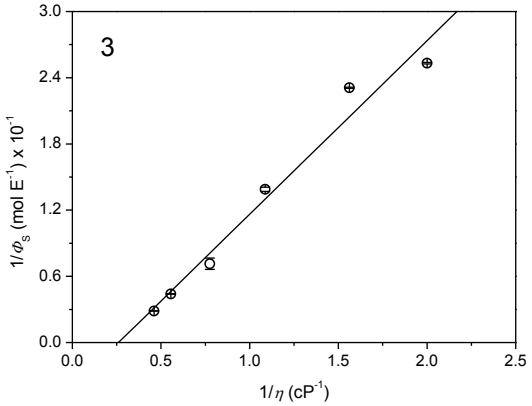

Figure 56: Correlation between $1/\Phi_S$ and $1/\eta$ according to the collisional model for diphenoyl peroxide (**1**), 1,2-dioxetanone (**2**) and 1,2-dioxetane system (**3**).[117]

Table 80: Fitting parameters for the rubrene catalyzed decomposition of diphenoyl peroxide (**1**) and 1,2-dioxetanone **2**, as well as the induced decomposition of phenoxy-substituted 1,2-dioxetane **3**, using the diffusional in toluene-diphenyl ether solvent system.

	Collisional model		
	$\frac{1}{\Phi_S} = B + \frac{A}{\eta}$		
	B	**A**	**R²**
1	6300 ± 130	1600 ± 100	0.823
2	880 ± 20	440 ± 20	0.984
3	–4.60 ± 0.02	16.20 ± 0.03	0.986

Table 81: Fitting parameters for the rubrene catalyzed decomposition of diphenoyl peroxide (**1**) and 1,2-dioxetanone **2,** using diffusional.model.

Solvent systems		**Collisional model**		
	Compounds	$\frac{1}{\Phi_S} = B + \frac{A}{\eta}$		
		B	**A**	**R²**
A	**1**	3200 ± 200	1000 ± 200	0.88
	2	10000 ± 2000	14000 ± 2000	0.89
B	**1**	5197± 352	1829 ± 277	0.89
	2	859 ± 55	275 ± 44	0.89

A= diphenyl methane and toluene system; B= dibutyl phthalate and ethyl acetate system.

The systems 1 and 2 have a linear correlation with adj-$R^2 \approx 0.899$ and 0.99 (Table 83) as well as $R^2 \approx 0.96$,0.88 and 0.79, 0.99 (Table 84) respectively, adj-R^2 values= 0.93 for 3 according to the free-volume model.

The parameters obtained from the correlations for the catalyzed decomposition of **1** and **2** show a poor fitting with respect to collisional model, as indicated by the low adj-R^2 values (Tables 80, 81). The correlation of data from the catalyzed decomposition of **2** and the 1,2-dioxetane **3** decomposition proved to be better described just in toluene-diphenyl ether solvent system (Table 80). However, there is no difference in the quality of fitting for all the cases.

Moreover, according to the free-volume model, the obtained value of a is lower than unity obtained from intermolecular system. It means that the systems 1 and 2 showing that only a part of the molecule is experiencing the solvent viscosity effect (Tables 78,79).

However, the value of a is greater than unity obtained from intramolecular system, which would display the involvement of diffusion of "whole" molecules, which contrary to that expected from the reaction sequences involved (Schemes 11,13 and 15).

5.7. The efficiency of inter and intramolecular electron transfer chemiluminescent systems

The singlet quantum yields (Φ_S) for the three systems studied in different pure solvents have been compiled here in order to compare directly the efficiency of inter and intramolecular electron transfer CL systems.

Table 82: Compilation of singlet quantum yields for inter and intramolecular CIEEL systems.

	System 1	System 2	System 3
Solvents	**Φ_S (E mol^{-1})[a]**	**Φ_S (E mol^{-1})[b]**	**Φ_S (E mol^{-1})**
A	$(2.37 \pm 0.23)10^{-5}$	$(1.78 \pm 0.01)10^{-3}$	0.033 ± 0.004
B	$(2.26 \pm 0.18)\ 10^{-4}$	$(2.77 \pm 0.02)10^{-3}$	0.350 ± 0.001
C	$(5.8 \pm 0.02)10^{-5}$	$(2.39 \pm 0.28)10^{-3}$	0.44 ± 0.02
D	$(4.6 \pm 0.2)10^{-5}$	$(2.6 \pm 0.5)10^{-3}$	0.25 ± 0.01
E	$(1.23 \pm 0.02)10^{-5}$	$(1.6 \pm 0.1)\ 10^{-4}$	0.43 ± 0.05
F	$(2.2 \pm 0.4)10^{-5}$	/	0.35 ± 0.03
G	/	$(5.6 \pm 0.1)\ 10^{-6}$	0.99 ± 0.22

A = toluene; B = diphenyl ether; C = ethyl acetate; D = butyl acetate; E = acetonitrile; F = *N,N*-dimethyl formamide; G = dimethyl sulfoxide; [a]using perylene as activator; [b] using rubrene as activator; system 1 = diphenoyl peroxide; system 2 = *spiro*-adamantyl α-peroxy lactone; system 3 = 1,2-dioxtane;

The singlet quantum yields (Φ_S) are much higher for the intramolecular CIEEL system (induced 1,2-dioxetane decomposition) as compared to the intermolecular systems, showing Φ_S values of up to 100% for the intramolecular system and values lower than 0.1% for the intermolecular systems (Table 82). The mechanisms involved in excited state generation in organic chemiluminescent system evidences the essential importance of electron transfer in the excitation step of several highly efficient CL systems.[31] Furthermore, systems where both, the electron as well as the back-electron transfer occur as intramolecular processes show generally high efficiency for singlet excited state formation. Contrarily, when the electron transfer (or eventually the EBT) occurs in an intermolecular manner efficiency for excited

state formation is drastically diminished.[2,31] These facts are clearly demonstrated by a comparison of the singlet quantum yields obtained in our research work for a series of intra and intermolecular chemiluminescence systems (Table 82).

The catalyzed decomposition of intermolecular chemiluminescent systems occurs with low CL quantum yields which might be due to the following factors: The separation of the ion pairs takes place in the presence of high polar solvents and as a result the excitation quantum yields will be decreased. If these pair of radicals escape from the solvent cage, subsequently, these radical ions will not get a sufficient long lifetime to be able to meet another opposite radical species for back-electron transfer. The chemiexcitation will be "lost" due to these "cage-escaped" radical species.

Summary of most important observations

In this work we have studied the influence of solvent viscosity, polarity and polarizability on the catalyzed decomposition of inter and intramolecular systems. The most important findings are:

(i) The quantum yields increase with increasing solvent viscosity for all the systems, however, the quantum yields for the intermolecular system show a much lower dependence on the medium viscosity as compared to the intramolecular system.[117]

Table 83: Increase of singlet quantum yields with solvent viscosity for inter and intramolecular CIEEL systems.

Solvent systems	Processes	Catalyzed decomposition of:	Φ_S (E mol^{-1}) increased by a factor of:
A	Intermolecular	diphenoyl peroxide	2.2
		1,2-dioxetanone	2.0
B	Intermolecular	diphenoyl peroxide	1.4
		1,2-dioxetanone	2.3
C	Intermolecular	diphenoyl peroxide	2.0
		1,2-dioxetanone	1.8
A	Intramolecular	1,2-dioxetane	10

A = toluene-diphenyl ether; B = toluene-diphenyl methane; C = ethyl acetate-butyl phthalate.

For the intermolecular systems, the singlet quantum yields (Φ_S) increased by a factor of around 2 between the low and high viscosity solvent and all systems show similar behavior. In contrast, the singlet quantum yields (Φ_S) increased by one order of magnitude for 1,2-dioxetane **3** (Table 83).

(ii) The influence of solvent polarity on the quantum yields is studied for inter and intramolecular systems. In low polarity solvents the quantum yields were relatively low and in high aprotic polar solvents these values were higher, reaching up to 1.0 for the intramolecular system. However, for the intermolecular CIEEL systems the polarity dependence of the quantum yields

showed a maximum value at moderately high polarity values and a slight decrease upon further polarity increase (Tables 56-67).

(iii) In the binary solvent systems with different polarities studied, the polarizability parameters showed to be contrary to the polarity parameters (Tables 62-67). Therefore, the singlet quantum yield changes might also be due to the diferent medium polarizability and if this were the case, the singlete quantum yields would decrease with increasing solvent polarizability.

(**iv**) The activators rubrene and perylene were used for the decomposition of diphenoyl peroxide in order to compare the effects of theses activators on the chemiexcitation quantum yields. The results obtained from this comparision studies indicate that singlet quantum yields (Φ_S) and the catalyzed singlet quantum yields (Φ_S^{CAT}) are higher for rubrene as compared to perylene. (Table 56a). This fact is in agreement with the lower oxidation potential of rubrene as compared to perylene.

(**v**) Chemiluminescence parameters of the diphenoyl peroxide (**1**), *spiro*-adamantyl α-peroxy lactone (**2**) and 1,2-dioxtane (**3**) reaction were also studied in pure solvents with different viscosities, polarizabilities and polarities. The obtained singlet quantum yields were correlated with viscosity, polarizability and polarity parameters by multiple linear regression analysis (Tables 71,72).

(**vi**) The obtained singlet quantum yields (Φ_S) are much higher for the intramolecular CIEEL system as compared to the intermolecular systems (Table 82).

Mechanistic discussion for the inter (1 & 2) and intramolecular (3) electron transfer CL systems

The results obtained in this work will be discussed below in the mechanistic context on efficient chemiluminescence transformations and specially concerned with the elucidation of the mechanism of the chemiexcitation step in inter and intramolecular transformation, which are believed to occur by electron transfer sequences similar to the CIEEL mechanism.

The influence of solvent viscosity

To explain the mechanisms of excited state formation and to comprehend the extraordinary effectiveness contrast in the inter and intramolecular systems, the solvent viscosity influence on the quantum efficiency in diverse CL systems has been contemplated in this study.

The solvent cage influence on the catalyzed diphenoyl peroxide and 1,2-dioxetanone decomposition (Schemes 12 and 13) has been compared to the observed effect on the induced 1,2-dioxetane decomposition (Scheme 16).[111,117]

During intermolecular interactions between an ACT and a peroxide (catalyzed diphenoyl peroxide and 1,2-dioxetanone decomposition), a pair of radicals is formed within the solvent cage and possible radical cage escape leading to ground state product formation, therefore, this process might not be highly efficient (Schemes 12 and 13). Conversely, in the induced decomposition of 1,2-dioxetane **3**, after, C-C bond cleavage can happen in two distinct manners: (i) an intramolecular course, where the excited phenolate is produced directly or by a formally intramolecular electron back transfer, expected to lead to highly efficient chemiexcitation; alternatively, (ii) a pair of radicals can be formed within the solvent cage; the now intermolecular electron back transfer can lead to phenolate excited state formation, however this process might not be highly efficient, eventually due to possible radical cage escape leading to ground state product formation (Scheme 16).

Therefore, it would be expected that the intermolecular CIEEL systems should show considerable solvent viscosity effects and the intramolecular system should only show visosity dependence if an intermolecular electron back transfer would be involved in its chemiexcitation. However, the expeimental results show high visocity dependence of the intramolecular system and very low sensitivity to viscosity changes of the intermoelcular transformations.

Consequently, the viscosity dependence of these systems can not be utilized to decide between an inter or intramolecular electron back transfer step in the chemiexcitation of the induced 1,2-dioxetane decomposition. The high viscosity

influence on the quantum yields of **3** can be understood on the basis of an intramolecular electron back transfer step (Scheme 16, pathway(A)), considering that a particular conformation is fundamental for efficient chemiexcitation, as proposed before by our group.[116] The most essential result which validates the conclusion sketched out above on the mechanism of induced 1,2-dioxetane decomposition is the fact that the clearly intermolecular systems (catalyzed diphenoyl peroxide and 1,2-dioxetanone decomposition) demonstrate much lower viscosity dependence.

The low efficient intermolecular CIEEL systems, catalyzed diphenoyl peroxide and 1,2-dioxetanone decomposition, cannot be made much more efficient, although by increasing the solvent viscosity utilizing binary mixture of ethyl acetate and dibutyl phthalate, covering a viscosity range from η = 0.42- 9.63 cP, as a viscosity increment of a variable of 23 leads just to around twofold quantum yield increased in both transformations (Table 75). Hence, these facts show that the low efficiency of these systems is not mainly due to cage escape of the radical pairs. There might be another factor behind the absence of efficiency in these classical CIEEL systems.

One explanation behind this low efficiency might be steric effects for charge-exchange complex development by these peroxides with the ACT, as described somewhere else.[118]

The influence of solvent polarity

The influence of solvent polarity on the chemiexcitation quantum yields as well as the velocity of the electron transfer step was studied, by using polar aprotic solvents with different solvent polarity and polarizability values. however, with similar viscosity values.

On the basis of the mechanisms involved in the chemiluminescent peroxide decomposition, the variation of solvent polarity is expected to have considerable effects on the velocity of the initial rate-limiting electron transfer step of the CIEEL mechanism in its intermolecular as well as intramolecular

version (Schemes 12, 13 and 16). In both cases, an increase in solvent polarity is expected to facilitate charge separation and therefore is supposed to increase the rate of the tranformation. Contrarily, solvent polarity influence on the chemiluminescence emission quantum yields cannot be predicted as easily for the intermolecular as well as intramolecular version.

As outline above, solvent polarity is expected to stabilize the initially formed radical ion pair in the inter as well as intramolecular systems (Schemes 12, 13 and 16). Considering the mechanism of perylene catalyzed decomposition of (**1**) (Scheme 12), increasing solvent polarity must stabilize the radical ions generated in the sequence of the transformation and the observed difference in Φ_S^{CAT} for low polar aprotic solvent, medium polar aprotic solvent and high polar aprotic solvent should be related to the efficiency of the excited state formation in the electron back transfer step (k_{EBT}).

In low polar aprotic solvent the pair of radical ions within the solvent cage, cannot be stabilized and as a result, excited state formation by electron back transfer becomes less efficient and lower quantum yields are obtained. However, in the case of medium polar aprotic solvents, the pair of radical ions within the solvent cage is stabilized by solvents with higher polarity and solvation initially contributes to keep these species together and excited state formation by electron back transfer becomes more efficient. Therefore, in this case the quantum yields obtained are one order of magnitude higher than low polar aprotic solvent. However, using high polar aprotic solvents like acetonitrile (ACN) and *N,N*-dimethyl formamide (DMF), quantum yields started to decrease because high solvent polarity can lead to the separation of the ion pair and consequently to the lowering of the excitation quantum yields (Scheme 12).

A noticeable point here is that chemiexcitation can only occur if the radical ion pair initially formed in the transformation stays together in the same “solvent cage”, allowing excited state formation by electron back transfer

(EBT). If cage-escape of the species has occurred the highly reactive radical species will not have a sufficient long lifetime to be able to meet another opposite radical species for electron back transfer. Therefore, these "cage-escaped" radical species will be "lost" for chemiexcitation, leading to the formation of ground state products only (Scheme 12).

The singlet quantum yields (Φ_S) in the rubrene catalyzed decomposition of *spiro*-adamantyl-1,2-dioxetanone (**2**) in the same medium polar aprotic solvents as used for catalyzed diphenoyl peroxide are insensitive to the solvent polarity. One reason behind the insensitivity of the singlet quantum yields (Φ_S) to the solvent polarity might be that a pair of radical ions within the solvent cage cannot be stabilized because of the hydrophobic part of the radical anion (*spiro*-adamantyl part), consequently, excited state formation by electron back transfer becomes less efficient and therefore, singlet quantum yields (Φ_S) did not change significantly (Scheme 13). Moreover, using high polar aprotic solvents like acetonitrile (ACN) and *N,N*-dimethyl formamide (DMF), quantum yields started to slightly decrease, might be because of the separation of the ion pair due to high solvent polarity effects and consequently, to the lower excitation quantum yields (Table 62).

With the objective to a better understanding of the mechanism involved in the intramolecular electron-transfer initiated 1,2-dioxetane, the influence of aprotic polar solvents and their binary mixtures on the singlet quantum yields (Φ_S) of dioxetane **3** were studied (Tables 63-66). From obtaied results, it is concluded that in low polar aprotic solvents like toluene, the quantum yields are relatively low and in high polar aprotic solvents these values are considerably high.

The quantum yields in the induced decomposition of **3**, are in agreement with occurrence of an intramolecular CIEEL mechanism in this cases. The quantum yields are considerably high in all experimental conditions as compared to most of the intermolecular CIEEL systems.[117]

Considering the mechanism of induced 1,2-dioxetane decomposition (Scheme 16), increasing solvent polarity must first facilitate the deprotection step by the stabilization of the phenolate ion formed and stabilize the radical ions generated in the sequence of transformation and the observed difference in Φ_S for toluene (TOL) and acetonitrile (ACN) (Table 63) indicated the solvent polarity effect on the excited state formation efficiency in the electron back transfer step (k_{EBT}). The carbonyl radical anion, generated after the peroxide cleavage, can be stabilized by high solvent polarity and excited state formation by electron back transfer becomes might be more efficient and high singlet quantum yields are obtained. In toluene as a solvent, this stabilization is not possible, therefore, the obtained quantum yields are one order of magnitude lower than acetonitrile. In this case no decrease in the quantum yields has been observed for solvents with very high polarity, which can be understood by the fact that the whole process is an intramolecular one and no cage-escape of the radical species can occur due to separate ion pair formation (Scheme 16, pathway(A)).

6. Conclusion

(i) In all experimental conditions, the intermolecular CIEEL systems possess very low quantum yields (in the order of 10^{-4} E mol^{-1}), whereas, the intramolecular system shows generally very high quantum yields (close to 1.0 in some cases).

(ii) The singlet quantum yields increase with increasing solvent viscosity for all systems, however, the intermolecular systems show only a slight increase with this solvent parameter (generally a factor of about 2 for a viscosity increase of up to 22 times). Contrarily, the intramolecular system is much more sensitive to medium viscosity, with quantum yields increasing by one order of magnitude in the same mediums.

(iii) The solvent viscosity effects indicate that the low efficient intermolecular CIEEL system cannot be improved by increasing the solvent cage effect and that the highly efficient intramolecular CIEEL system should occur by an entirely intramolecular chemiexcitation pathway, without the participation of an intermolecular electron back transfer step.

(iv) For the intermolecular catalyzed decomposition of diphenoyl peroxide (**1**) and 1,2-dioxetanone **2**, singlet quantum yields increase in function of medium polarity for low polar solvents, reaching maximum values upon increasing polarity and decreasing for high polar solvents. This behavior is in agreement with the stabilization of radical ion pairs by solvation and the formation of solvent separated ion pair (which do not lead to chemiexcitation) by highly polar solvents.

(v) For the induced decomposition of 1,2-dioxetane **3**, the quantum yields increase with increasing solvent polarity also for higly polar solvents, in agreement with the proposal of an entirely intramolecular transformation and the consequent absence of cage escape due to separated ion pair formation.

(vi) Indications were obtained that increasing solvent polarizability could lead to a decrease in the singlet quantum yields, however, this conclusion is only

tentative, as in the binary solvent sytems studied polarizability behaves generally contrarily to polarity, therefore the influence of both parameters cannot be separated.

(vii) Multiple linear regression relationships of the quantum yields with the solvent parameters polarity, polarizability and viscosity for the three systems indicate the positive correlation between the solvent viscosity and the quantum yields, in agreement with the data obtained in binary solvent mixtures. However, the high correlation coefficient obtained for system 2 is contrary to the former results. Polarity and polarizability show positive correlations for systems 1 and 3, however, negative correlation coefficient are obtained for both parameters for system 2; all coeficients have high standard deviations. These observations may indicate that the medium influence on the singlet quantum yields can not be described only by these parameters and specific solvent properties appear to be important for the efficiency of the chemiexcitation for all studied CL systems.

7. References

[1] Campbell A. K., "Chemiluminescence: Principles and Applications in Biology and Medicine", Ellis Horwood Ltd.: Chichester, **1988**.

[2] Baader W. J., Stevani C. V., Bastos E. L., Chemiluminescence of organic peroxides, in: The Chemistry of Peroxides, Zvi Rappaport (Ed.), Wiley–VCH, Chichester, **2006**, pp. 1211–1278.

[3] Wiedemann E., *Ann. Physik & Chemie.*, **1988**, 34, 446-463.

[4] Radiziszewski B., *Ber. Chem. Ges.,* **1877**, 10, 70-75.

[5] Albrecht H. O., *Z. Phys. Chem*., **1928**, 136, 321–330.

[6] Schuster G. B., Schmidt S. P.*, Adv. Phys. Org. Chem*., **1982**, 18, 187–238.

[7] Kopecky K. R., Mumford C., *Can. J. Chem.,* **1969**, 47, 709–711.

[8] Adam W., Liu J. C., *J. Am. Chem. Soc.,* **1972**, 94, 2894–2895.

[9] Suppan P., Chemistry and Light, *R. S. C.,* **1994**.

[10] Hodak J., Harvey D., Valeur B., *Introduction to Fluorescence and Phosphorescence*, **2008**.

[11] Wehry E. L., *Analytical Chemistry*, **1980**, 52, 75–90.

[12] David W. B., Physical Chemistry, 1st Edition *Cleveland State University*, **2003**.

[13] Lakowicz J. R., Principles of Fluorescence Spectroscopy: Introduction to Fluorescence, *springer*. Chapter 1, p. 28, **2006**.

[14] Atkins P., de Paula J., Atkins' Physical Chemistry, Eighth Edition, *Oxford University Press*, **2006**.

[15] Chen G. N., Zhang F., *Fujian Science and Technology Press: Fujian*, **1998**, 4–17.

[16] Lin J. M., *Chemical Industry Press: Beijing*, **2004**, 1–32.

[17] Nery A. L. P., Baader W. J., *Quim. Nova.*, **2001**, 24, 626–636.

[18] Koo J. Y., Schuster G. B., *J. Am. Chem. Soc.*, **1977**, 99, 6107-6109.

[19] Koo J. Y., Schuster G. B., *J. Am. Chem. Soc.*, **1978**, 100, 4496–4503.

[20] Adam W., Cueto O., *J. Am. Chem. Soc.,* **1979**, 101, 6511–6515.

[21] Adam W., Zinner K., Krebs A., Schmalstieg H., *Tetrahedron Lett*., **1981**, 22, 4567-4570.

[22] Adam, W. Baader, W. J., *Angew. Chem. Int. Ed. Engl.,* **1984**, 23, 166–167.

[23] Adam, W. Baader, W. J., *J. Am. Chem. Soc.,* **1985**, 107, 410–416.

[24] Fereja T. H., Hymete A., Gunasekaran1 T., *ISRN Spectroscopy,* **2013**.

[25] Garcıa-Campana A. M., Baeyens W. R. G., *Analysis*, **2000**, 28, 686-698.

[26] Ciscato L. F. M. L., Augusto F. A., Weiss D., Bartoloni F. H., Albrecht S., Brandl H., Zimmermann T., Baader W. J., *ARKIVOC,* **2012** (iii), 391–430.

[27] Franck J., *Trans. Faraday Soc.,* **1926**, 21, 536-542.

[28] Condon E*., Phys. Rev.,* **1926**, 28, 1182–1201.

[29] Condon E., *Phys. Rev.,* **1928**, 32, 858 –872.

[30] Turro N. J., Modern Molecular Photochemistry; University Science Books: *Sausalito*, **1991**.

[31]Bartoloni F. H., Ciscato L. F. M. L., Peixoto, M. M. M., Santos A. P. F., Santos, C. S., Oliveira S., Augusto F. A., Pagano A. P. E., Baader, W. J., *Quim. Nova.*, **2011**, 34, 544–554.

[32] (a) Marcus R. A., *J. Chem. Phys,* **1965**, 43, 2654-2657, (b) Marcus R. A., Siders P., *J. Phys. Chem.,* **1982**, 86, 622–630 (c) Marcus R .A., *Annu. Rev. Phys. Chem.* **1964**, 15,155-196., (d) Marcus R. A., *Electroanal. Chem.,* **2000**, 483, 2-6.

[33] Dodeigne C., Thunus L., Lejeune R., *Talanta.,* **2000**, 51, 415–439.

[34] McCapra F., In Bioluminescence and Chemiluminescence: Molecular Reporting with Photons. (Edited by J. W. Hastings, L. J. Kricka and P. E. Stanley), **1996**, pp.7–15. Wiley & Sons: Chichester.

[35] Turro N. J., Lechtken P., *Pure Appl. Chem.,* **1973**, 33, ,363–388.

[36] O'Neal H. E., Richardson W. H., *J. Am. Chem. Soc.*, **1970**, 92, 6553–6557.

[37] Richardson W. H., O'Neal H. E., *J. Am. Chem. Soc.*, **1972**, 94, 8665–8668.

[38] Richardson W. H., Lovett M. B., Price M. E., Anderegg J. H., *J. Am. Chem. Soc.,* **1979**, 101, 4683–4687.

[39] Richardson W. H., Batinica G., Janotaperret K., Miller T., Shen D. M., *J. Org. Chem.,* **1991**, 56, 6140–6144.

[40] Wilson T., Halpern A. M., *J. Phys. Org. Chem.*, **1995**, 8, 359–363.

[41] Bastos E. L., Baader W. J., *ARKIVOC.,* **2007**, 257–272.

[42. Turro N. J., Devaquet A., *J. Am.Chem. Soc.*, **1975**, 97, 3859–3862.

[43. Augusto F. A., Souza G. A., Souza Jr. S. P., Khalid M., Baader W. J., *Photochem. Photobiol.,* **2013**, 89, 1299-1317.

[44. Miao W., *Chem. Rev.,* **2008**, 108, 2506–2553.

[45. Koo J. Y., Schuster G. B., *J. Am. Chem. Soc.,* **1978**, 100, 4496–4503.

[46. Adam W., Cilento G., *Academic Press, New York,* **1982**, 191–227.

[47. Silva S. M., Wagner K., Weiss D., Beckert R., Stevani C. V., Baader W. J., *Luminescence*, **2002**, 17, 362–369.

[48. Ciscato L. F. M. L., Bartoloni F. H., Bastos E. L., Baader W. J., *J. Org. Chem.*, **2009**, 74, 8974–8979.

[49] Schuster G. B., *Acc. Chem. Res.*, **1979**, 12, 366–373.

[50] Wilson T., *Photochem. Photobiol.,* **1995**, 62, 601–606.

[51] Catalani L. H., Wilson, T., *J. Am. Chem Soc.*, **1989**, 111, 2633–2639.

[52] Schaap A. P., Chen, T. S., Handley R. S., Desilva R., Giri B. P., *Tetrahedron Lett.,* **1987**, 28, 1155–1158.

[53] Adam W., Fell R. T., Schulz M. H., *Tetrahedron Lett.*, **1993**, 49, 2227-2238.

[54] Matsumoto M., Suganuma H., Katao Y., Mutoh H., *J. Chem. Soc. Chem, Commun.*, **1995**, 431–432.

[55] Ciscato L. F. M. L., Bartoloni F. H., Weiss D., Beckert R., Baader W. J., *J. Org.Chem.,* **2010**, 75, 6574–6580.

[56] Beck S., Köster H., *Anal. Chem.,* **1990**, 62, 2258–2270.

[57] Matsumoto M., Suganuma H., Azami M., Aoshima N., Mutoh H., *Heterocycles,* **1995**, 41, 2419-2422.

[58] Nery A. L. P., Weiss D., Catalani L. H., Baader W. J., *Tetrahedron,* **2000**, 56, 5317–5327.

[59] Nery A. L. P., Ropke S., Catalani L. H., Baader W. J., *Tetrahedron Lett.* **1999**, 40, 2443–2446.

[60] Adam W., Bronstein I., Trofimov A. V., Vasil'ev R. F., *J. Am. Chem. Soc.*, **1999**, 121, 958–961.

[61] Armarego, W. L. F., Perrin, D. D., *Purification of Laboratory Chemicals,* Fourth Edition, **1996**.

[62] Ramirez F., Desai M. B., Mitra R. B., *J. Am. Chem. Soc.,* **1961**, 83, 492–492.

[63] Stevani C. V., Silva S. M., Baader, W. J., *Eur. J. Org. Chem.*, **2000**, 4037–4046.

[64] Suzanne F., Dominique L., *J. Chem. Ed. Chem.,* **1999**, 76, 1260-1264.

[65] Adam W., Bronstein I., Vasil'ev R. F., Trofimov A. V., *J. Am. Chem. Soc.,* **1999**, 121, 958–961.

[66] Dimroth, K., Reichardt, C., Siepmann, T., Bohlman, F., *Justus Liebigs Ann. Chem*. **1963**, 661.

[67] Reichardt C., *Chem. Rev.*, **1994**, 94, 2319–2358

[68] https://en.wikipedia.org/wiki/Snell%27s_law

[69] Koppel I. A., Paju A., *J. Reakts. Sposobnost. Org. Soedin*., **1974**, 11, 139

[70] Ramirez F., Desai M. B., Mitra R. B., *J. Am. Chem. Soc.,* **1961**, 83, 492–492.

[71] Ramirez F., Bhatia S. B., Mitra R. B., Hamlet Z., Desai N. B., *J. Am. Chem. Soc.*, **1964**, 86, 4394-4400.

[72] Adam W., Cilento G., *1st ed.; Academic Press: New York, USA,* **1982**, 115–152.

[73] Bastos, E. L., Ciscato, L. F. M. L., Weiss, D., Beckert, R., Baader, W. J., *Synthesis,* **2006**, 1781–1786.

[74] Murov S. L., Carmichael L., Hug G. L., *Handbook of Photochemistry, Second Edition*, section 1, **1993**, 37.

[75] Ware W. R., Baldwin B. A., .*J. Chem. P hys.,* **1964**, 4 0, 1703-1705.

[76] Strickler S. J., Berg. R. A., *J . Chem. Phys.*, **1962**, 37, 814-822.

[77] Birks J. B., Dyson D., *J. Proc. Roy. Soc., A* **1963**, 275, 135-148.

[78] Ramirez F., Desai N. B., Mitra R. B., *J. Am. Chem. Soc.,* **1961**, 83, 492-492.

[79] Ramirez F., Bhatia S. B., Mitra R. B., Hamlet Z., Desai N. B., *J. Am. Chem. Soc.*, **1964**, 86, 4394.

[80] Bartoloni F. H., Oliveira M. A., Augusto F. A., Ciscato L. F. M. L., Bastos E. L., Baader W. J., *J. Braz. Chem. Soc.,* **2012**, 23, 2093–2103.

[81] Bastos E. L., Ciscato L. F. M. L., Weiss D., Beckert R., Baader W. J., *Synthesis,* **2006**, 1781–1786.

[82] Adam W., Cilento G., *Academic Press, New York* **1982**.

[83] Adam W., Cilento G., *Angew. Chem. Int. Ed. Engl.*, **1983**, .22, 529–542.

[84] Schuster G. B., *Acc. Chem. Res.*, **1979**, 12, 366–373.

[85] Adam W., Heil M., Mosandl T., Saha-Möller C.R., *Ed. W. Ando, John Wile & Sons Ltd., Chichester, England,* **1992**, 221–254.

[86] Reichardt C., *Angew. Chem.,* **1979**, 91, 119–131.

[87] Reichardt C., *Angew. Chem.,* **1979**, 18, 98–110.

[88] Reichardt C., *Chem. Rev.,* **1994**, 94, 2319–2358.

[89] Reichardt C., Asharin-Fard S., Blum A., Eschner M., Mehranpour A. M., Milart P., Niem T., Schafer G., Wilk M., *Pure Appl. Chem.,* **1993**, 65, 2593-2601.

[90] Reichardt C., *Green Chem.,* **2005**, 7, 339–351.

[91] Reichardt C., *Chem. Soc. Rev.,* **1992**, 21, 147-153.

[92] Reichardt C., Harbusch-Goernert E., *Liebigs Ann. Chem.,***1983**, 721–743.

[93] Abboud J. L. M., Notario R., *Pure Appl. Chem.*, **1999**, 71, 645-718.

[94] (a) Reichardt C., *Nachr. Chem. Tech. Lab.*, **1997**, 45, 759, (b) Reichardt C., *Angew. Chem.,* **1979**, 18, 98–110.

[95] (a) Kamlet M. J., Abboud J. L. M., Taft R. W., *J. Am. Chem. Soc.*, **1977**, 99, 6027–6038, (b) Kamlet M. J., Abboud J. L. M., *Prog. Phys. Org. Chem.*,

1981, 13, 485-630.

[96] Laurence C., Nicolet P., Dalati M. T., Abboud J. L. M., Notario R., *J. Chem. Phys*., **1994**, 98, 5807-5816.

[97]Chemical Rubber Company Handbook of Chemistry and Physics, 70th Edition, ed.: Lide, D. R., *CRC Press, Boca Raton,* **1998**.

[98] Bastos E. L., Tese de Doutorado, "Mecanismos e Aplicações da Quimiluminescência Orgânica", Instituto de Química, Universidade de São Paulo, **2004**.

[99] Ciscato L. F. M. L., Weiss D., Beckert R., Baader W. J., *J. Photochem. Photobio. A: Chemistry,* **2011**, 218, 41–47.

[100] Oliveira M. A., Bartoloni F. H., Augusto F. A., Ciscato L. F. M., Bastos E. L., Baader W. J., *J. Org. Chem*., **2012**, 77, 10537–10544.

[101] (a) Adam W, Matsumoto M., Trofimov A. V., *J. Org. Chem.,* **2000**, 65, 2078-2082, (b) Adam W, Bronstein I., Trofimov A. V., *J. Phys. Chem. A,* **1998**,102, 5406-5414, (c) Adam W, Bronstein I., Edwards B., Engel T., Reinhardt D., Schneider F. W., Trofimov A. V., Vasil'ev, R. F., *J. Am. Chem. Soc*., **1996**,118, 10400–10407.

[102] Stevani C. V., Tese de Doutorado, Estudo Mecanístico do Sistema Peróxi-Oxalato, Instituto de Química, Universidade de São Paulo, **1997**.

[103] Koo J. Y., Schmidt S. P., Schuster G. B., *Proc. Natl. Acad. Sci., USA,* **1978**, 75, 30–33.

[104] Kazakov V. P., Sharipov G. L., Tolstikov G. A., *Nauka. Moscow,* **1990**.

[105] Turro N. J., Lechtken P. *J. Am. Chem. Soc.,* **1973**, 95, 264-266.

[106] Adam W., Arias L. A., Zinner K., *Chem. Ber.,* **1983**, 116, 839-846

[107] Adam W., Bronstein I., Trofimov A. V., Vasilev R. F., *J. Am. Chem. Soc.,* **1999**, 121, 958-961.

[108] Song X., Marcus R. A., *J. Chem. Phys.,* **1993**, 99, 7768−7773.

[109] Abbott A. P., Rusling J. F., *J. Phys. Chem.,* **1990**, 94, 8910-8912.

[110] Enomoto Y., Kakitani T., Yoshimori A., Hatano Y., *Chem. Phys. Lett.,*

1991, 186, 366-371.

[111] Khalid M., Oliveira M. A., Souza Jr. S. P., Ciscato L. F. M. L., Bartoloni F. H., Baader W. J., *J. Photochem. Photobio. Chemistry A*, **2015**, 312, 81–87.

[112] Adam W., Matsumoto M., Trofimov A. V., *J. Am. Chem. Soc.,* **2000**, 122, 8631-8634.

[113]. Doolitle A. K., *J. Appl. Phys*., **1951**, *22*, 1471-1475.

[114]. Cohen M. H., *J. Chem. Phys.,* **1959**, 31, 1164-1169.

[115]. Gegiou D., Muszkat K. A., Fisher E., *J. Am. Chem. Soc.,* **1968**, 90, 12-18.

[116] Bastos E. L. Silva S. M. Baader W. J., *J. Org. Chem*. **2013**, 78, 4432-4439.

[117] Khalid M., Souza Jr. S. P., Ciscato L. F. M. L., Bartoloni F. H., Baader W. J. *J. Photochem. Photobiol. Sci.,* **2015**, 14, 1296 – 1305.

[118] Bartoloni F. H., Oliveira M. A., Ciscato L. F. M. L., Augusto F. A., Bastos E. L., Baader W. J., *J. Org. Chem.,* **2015**, 80, 3745-3751.

Curriculum Vitae

- Name: Muhammad Khalid
- Date of birth- 29/08/1984

Education

- MS.C. in chemistry B. Z. U. University.
- Ph.D. in chemistry (**Specialization in Physical Chemistry**) São Paulo University.

Distinction, Honors and Awards

- **GRE** Chemistry Subject Test (**ETS, USA**), **74** Percentile, 2010.
- Teaching Assistance **Scholarship** (**USP,** Brazil) 2013.
- Pró-Reitoria de Pós-Graduação **Scholarship** (**USP,** Brazil) 2013.
- Doctorate **Scholarship** (**CAPES,** Brazil) 2011-2015.

Scientific Production

Papers Published in International Journals

- **M. Khalid,** S. P. Souza Jr., L. F. M. L. Ciscato, F. H. Bartoloni and W. J. Baader, Solvent viscosity influence on the chemiexcitation efficiency of inter and intramolecular chemiluminescence systems, *J. Photochem. Photobiol. Sci.* **2015,** 14, 1296 – 1305.
- **M. Khalid**, M. A. Oliveira, S. P. Souza Jr., L. F. M. L. Ciscato, F. H. Bartoloni and W. J. Baader, Efficiency of intermolecular

chemiluminescence systems lacks significant solvent cavity effect in binary toluene/diphenylmethane mixtures, *J. Photochem. Photobiol. A: Chemistry,* **2015,** 312, 81–87.

- A. F. Augusto, A. de Souza, Glalci Souza S. P. Souza Jr., **M. Khalid** and W. J. Baader, Efficiency of Electron Transfer Initiated Chemiluminescence, *J. Photochem. Photobiol.* **2013,** 89, 1299–1317.

International/National Conferences/Workshops/ Attended

- 38ª Reunião Anual da SBQ - Sociedade Brasileira de Química, 25th to 28th May. 2015, Aguas de Lindóia, Brazil.
- 25th National and 13th International Chemistry conference, 20th to 22th Oct. 2014, Institute of Chemistry, University of the Punjab, Panjab, Pakistan.
- 12th International 24th National Chemistry Conference**,** 28th to 30th Oct. 2013, Bahauddin Zakariya University, Multan, Panjab, Pakistan.
- 1st International Conference on Applied Chemistry, 18th to 20th Nov. 2013, Department of Applied Chemistry, G. C. University Faisalabad, Panjab, Pakistan.
- IV Encontro da Pos –Graducao IQ-USP-5th and 6th Set. 2013, Institute of Chemistry, University of the Sao Paulo, Sao Paulo, Brazil.
- Modern Topics in Magnetic resonance Conference 16th and 17th May, 2013, University of the Sao Paulo, Sao Paulo, Brazil.

- Workshop about how to write scientific article, American chemical society, 4th Dec. 2012, the institute of chemistry USP, Sao Paulo, Brazil.
- Workshop de capacitacao para pesquisadores da usp em publicacao cientifica dezembro de 2012, no instituto de quimica (Training Workshop for usp researchers in scientific area, Dec. 2012, the institute of chemistry, Sao Paulo, Brazil).
- Chemistry and Earth Sciences USP Conference 8th and 9th Aug. 2011, University of the Sao Paulo, Sao Paulo, Brazil.

Advanced Courses of Physical Chemistry / Studied

- QFL5620: Chemical Kinetics and Dynamics
- QFL5618: Quantum Chemistry 1
- QFL5630: Photochemistry (Applications in nanometrial systems)
- QFL5953: Synthesis and Applications for Pigments and Dyes
- Introduction to the Theory and Applications of Molecular and Quantum Mechanic